Unclassified

URITY CLASSIFICATION OF THIS PAGE

REPORT DOCUMENTATION PAGE

REPORT SECURITY CLASSIFICATION: Unclassified	1b. RESTRICTIVE MARKINGS:
SECURITY CLASSIFICATION AUTHORITY:	3. DISTRIBUTION/AVAILABILITY OF REPORT: Approved for public release; distribution unlimited
DECLASSIFICATION/DOWNGRADING SCHEDULE:	
PERFORMING ORGANIZATION REPORT NUMBER(S):	5. MONITORING ORGANIZATION REPORT NUMBER(S): AFOSR-TR- 86-0330
6a. NAME OF PERFORMING ORGANIZATION: University of Idaho	6b. OFFICE SYMBOL (If applicable):
7a. NAME OF MONITORING ORGANIZATION: AFOSR/NC	
ADDRESS (City, State and ZIP Code): Mechanical Engineering Department Moscow, ID 83843	7b. ADDRESS (City, State and ZIP Code): Building 410 Bolling Air Force Base 20332
8a. NAME OF FUNDING/SPONSORING ORGANIZATION: AFOSR	8b. OFFICE SYMBOL (If applicable): NC
9. PROCUREMENT INSTRUMENT IDENTIFICATION NUMBER: AFOSR-83-0156	
8c. ADDRESS (City, State and ZIP Code): Building 410 Bolling Air Force Base 20332	10. SOURCE OF FUNDING NOS.

PROGRAM ELEMENT NO.	PROJECT NO.	TASK NO.	WORK UNIT NO.
61102F	2303	A3	

11. TITLE (Include Security Classification): Improvement and Optimization of Internal Damping in Fiber Reinforced Composite Materials

12. PERSONAL AUTHOR(S): R.F. Gibson

13a. TYPE OF REPORT	13b. TIME COVERED	14. DATE OF REPORT (Yr., Mo., Day)	15. PAGE COUNT
Final	FROM June 83 TO Nov 85	March 3, 1986	225

16. SUPPLEMENTARY NOTATION: See summary

17. COSATI CODES			18. SUBJECT TERMS (Continue on reverse if necessary and identify by block number)
FIELD	GROUP	SUB. GR.	Damping, Stiffness, Optimization, Composites, Polymer Matrix

19. ABSTRACT (Continue on reverse if necessary and identify by block number)

The objectives of this research were to study the effects of such parameters as fiber aspect ratio, fiber orientation and fiber/matrix properties on damping in fiber reinforced polymer composites. These objectives were to be met by using both experimental and analytical approaches. The development of improved techniques for fabrication and testing of specimens and the development of relatively simple design equations for prediction of damping were desirable goals which were also met.

(Continued)

20. DISTRIBUTION/AVAILABILITY OF ABSTRACT	21. ABSTRACT SECURITY CLASSIFICATION
UNCLASSIFIED/UNLIMITED ☒ SAME AS RPT ☒ DTIC USERS ☐	Unclassified

22a. NAME OF RESPONSIBLE INDIVIDUAL	22b. TELEPHONE NUMBER (Include Area Code)	22c. OFFICE SYMBOL
Dr. Donald Ulrich	202-767-4963	

DD FORM 1473, 83 APR — EDITION OF 1 JAN 73 IS OBSOLETE.

Unclassified

SECURITY CLASSIFICATION OF THIS PAGE

(19. Continued from page 1)

Two new computer-aided testing techniques based on the impulse frequency response approach were developed. Small beam specimens were excited in either flexural or extensional vibration by an electromagnetic hammer with a force transducer, while specimen response was measured with an eddy current displacement transducer or an accelerometer. A desktop computer/Fast Fourier Transform analyzer system was then used for rapid data acquisition and computation of the complex modulus by curve-fitting to the frequency response function. Specimens of graphite/epoxy, boron/epoxy and Kevlar aramid/epoxy were fabricated by using an autoclave-style press cure which was developed specifically for this program.

Although a number of parameters were studied, the emphasis was on the influence of fiber length, fiber orientation and fiber material on damping of polymer composites. The experimental results show that, as predicted, very low fiber aspect ratios are required to produce significant improvements in damping. Of the three fiber types tested, the Kevlar aramid fiber composite was found to have much better damping than graphite or boron fiber composites. Measurements and predictions also indicate that the control of fiber orientation in a continuous fiber reinforced laminate may be a better approach to the improvement of damping than the control of fiber aspect ratio.

IMPROVEMENT AND OPTIMIZATION OF INTERNAL DAMPING IN FIBER REINFORCED COMPOSITE MATERIALS

by

R.F. Gibson and S.A. Suarez

Mechanical Engineering Department

University of Idaho

Moscow, ID 83843

FEBRUARY 1986

FINAL REPORT ON GRANT NO. AFOSR-83-0156

for

Air Force Office of Scientific Research
AFOSR/NC
Bolling AFB, D.C. 20332

ABSTRACT

This report describes two new techniques for characterization of damping in fiber reinforced composite materials and the application of these techniques to the study of improvement and optimization of damping. Flexural and extensional vibration tests are used for determination of complex moduli of aligned discontinuous fiber composite and off-axis fiber composite specimens, respectively. The results from tests on graphite/epoxy, Kevlar/epoxy and boron/epoxy composites are then compared with theoretical predictions from micromechanics models based on a single fiber. The analytical model is fitted to the experimental results by varying certain parameters that have uncertainties associated with them. It is shown that improved damping can be obtained with very low fiber aspect ratios, and that even better damping properties are possible with off-axis fibers.

TABLE OF CONTENTS

TABLE OF CONTENTS (continuation)

TABLE OF CONTENTS (continuation)

TABLE OF CONTENTS (continuation)

LIST OF TABLES

LIST OF TABLES (continuation)

LIST OF FIGURES

LIST OF FIGURES (continuation)

LIST OF FIGURES (continuation)

LIST OF FIGURES (continuation)

LIST OF FIGURES (continuation)

LIST OF FIGURES (continuation)

LIST OF FIGURES (continuation)

LIST OF FIGURES (continuation)

LIST OF SYMBOLS

a	- geometrical dimension defined in Fig. 2.9
$a(x_o)$	- displacement amplitude at location of probe
a_i	- amplitude of the input
a_r	- amplitude of the response
$\ddot{a}_b$	- base acceleration amplitude of beam
A	- cross sectional area of the beam
b	- geometrical dimension defined in Fig. 2.9
c_f	- final crucible weight
c_i	- initial crucible weight
C_n	- constant depending on resonant mode number n
d	- diameter of the fiber
D	- energy dissipated per cycle
E^*	- complex moduli
E', E''	- storage and loss moduli
E_f^*	- complex extensional modulus for the fiber
E_{fT}^*	- complex transverse modulus for the fiber
E^*_L	- composite extensional complex modulus
E^*_m	- complex modulus for the matrix
E^*_T	- composite transverse complex modulus
E^*_x	- composite complex modulus along the x axis
E_f', E_f''	- extensional storage and loss moduli for the fiber
E'_{fT}, E''_{fT}	- transverse storage and loss moduli for the fiber

LIST OF SYMBOLS (continuation)

E_L', E_L'' - extensional storage and loss moduli for the composite

E_m', E_m'' - storage and loss moduli for the matrix

E_T', E_T'' - transverse storage and loss moduli for the composite

E_x', E_x'' - composite storage and loss moduli along the x axis

f - frequency

f_a - frequency above resonance where the real part of the compliance reaches a peak (Fig. 2.6)

f_b - frequency below resonance where the real part of the compliance reaches a peak of opposite sign (Fig. 2.6)

f_n - resonant frequency of mode n

f_1, f_2 - frequencies at each end of the diameter parallel to the real axes in the Nyquist plot

G_f - shear modulus for the isotropic fiber

G_{fLT} - in-plane shear modulus for the anisotropic fiber

G_{LT} - in-plane shear modulus for the composite

G^*_{fLT} - complex in-plane shear modulus for the anisotropic fiber

G^*_{LT} - complex in-plane shear modulus for the composite

G^*_m - complex shear modulus for the matrix

LIST OF SYMBOLS (continuation)

G_f', G_f'' - real and imaginary components of the shear modulus for the isotropic fiber

G'_{fLT} G''_{fLT} - real and imaginary components of the shear modulus for the anisotropic fiber

G_{LT}', G_{LT}'' - real and imaginary components of the in-plane shear modulus for the composite

G_m', G_m'' - real and imaginary components of the shear modulus for the matrix

$G_x(f)$ - power spectrum of the excitation

$G_{xy}(f)$ - cross power spectrum of the excitation

$G_y(f)$ - power spectrum of the response

I - area moment of inertia of the beam about the neutral axes

K - bulk modulus

K_f - fiber bulk modulus

K_m - matrix bulk modulus

ℓ - fiber length

(ℓ/d) - fiber aspect ratio

$(\ell/d)_{eff}$ - effective fiber aspect ratio

L - subscript denoting longitudinal direction along the fiber

M - corresponding composite modulus: E_T or G_{LT}

M_f - corresponding fiber modulus E_f or G_f

M_m - corresponding matrix modulus E_m or G_m

LIST OF SYMBOLS (continuation)

M_1, M_2 - masses at each end of the free-free beam

n - mode number (1, 2, 3, ...)

Q - amplification factor

r_o - radial distance from center of the fiber

r - fiber radius

R - radius of representative volume element, or one half of center-to-center fiber spacing

s - Laplace plane

S - span of the beam

t - time

T - subscript denoting transverse direction, perpendicular to the fiber

u - displacement of the beam in the x direction

U - stored energy per unit volume

v_c - composite volume fraction

v_f - fiber volume fraction

v_m - matrix volume fraction

v_v - void volume fraction

w_c - composite weight

w_d - dry composite weight

w_f - fiber weight

w_m - matrix weight

w_w - wet weight of composite

LIST OF SYMBOLS (continuation)

W_f - strain energy stored in a volume v of fiber

W_m - strain energy stored in a volume v of matrix

x - distance along span of beam

x_n - amplitude after n cycles have elapsed in free vibration decay

x_o - first amplitude considered in free vibration decay

$x(t)$ - excitation time history

$\bar{X}(f)$ - Fourier transform of excitation time history

$X(s)$ - Laplace transform of excitaiton time history

$X(f)$ - complex conjugate of X(f)

y - deflection of the beam

$y(t)$ - response time history

$Y(f)$ - Fourier transform of response time history

$Y(s)$ - Laplace transform of response time history

z - curve fitting parameter

α - parameter defined in Eq. 2.10

β - parameter defined in Eq. 2.7

γ_c - specific weight of composite

γ_f - specific weight of fiber

γ_m - specific weight of matrix

δ - logarithmic decrement

ε - unit strain

LIST OF SYMBOLS (continuation)

ε_L - extensional strain

ε_T - transverse strain

ζ - damping factor

η - loss factor

η_f - fiber loss factor

$\eta_h, \eta_{h1}, \eta_{h2}$ - parameters defined in Eqs. 2.24, 2.29 and 2.30, respectively

η_m - matrix loss factor

θ - angle of the fibers with respect to the direction of the applied load

λ_n - eigenvalue for the nth mode

ν - Poisson ratio

ν_f - fiber Poisson ratio

ν^*_{LT} - composite complex major Poisson ratio

ν'_{LT}, ν''_{LT} - real and imaginary components of the composite major Poisson ratio

ξ, ξ_1, ξ_2 - Halpin-Tsai parameters

ρ - density of specimen

ρ_a - density of air

ρ_c - density of composite

ρ_w - density of water

σ - applied stress

σ_f - fiber extensional stress

$\bar{\sigma}_f$ - average extensional stress in the fiber

LIST OF SYMBOLS (continuation)

$\bar{\sigma}_L$ - average extensional stress in the composite

$\bar{\sigma}_m$ - average extensional stress in the matrix

τ - interfacial shear stress

ϕ - mode shape function

$\phi_n(X_o), \phi_n(S)$ - mode shape functions of the nth mode at location of the probe or at the end of the beam length, respectively

ω - angular frequency

ω_n - angular resonant frequency of mode n

1.0 INTRODUCTION

"A composite material is a material system composed of a mixture or combination of two or more macroconstituents differing in form and/or material composition that are essentially insoluble in each other" [1][1]. One of the constituents is a continuous phase known as the matrix and the other(s) is discontinuous and usually stronger and harder than the continuous phase. It is called the reinforcement or reinforcing material [2]. Matrix materials vary from very soft organic foams to glasses, ceramics and metallic matrices. Reinforcing agents range from elastomers and cotton to extremely hard intermetallic whiskers with shapes varying from very small, round or angular particles to continuous, very long fibers. The composite materials exhibit the best qualities of their constituents.

Composite materials can be of two types: fiber reinforced or particle reinforced. The fiber reinforced composite materials can be single layered laminae or multilayered laminates. The layers can have continuous or discontinuous fiber reinforcement with preferred orientation (off-axis) or unidirectional fibers (aligned). Hybrid composites having either mixed fiber materials or mixed continuous/discontinuous fibers are also common.

---

[1]The numbers in square brackets denote entries in the list of References.

Advanced fiber reinforced composite materials [3] with fibers such as boron or graphite brought improvements in strength and stiffness. Organic fiber reinforcements such as aramid improves damping characteristics, which means even more versatility for composite materials. The use of advanced composite materials is greatly increasing day by day. The range of applications goes from aerospace/aircraft/automotive structures to printed circuit boards, prosthetic devices, golf clubs, and tennis racquets [4].

Widespread use of composite materials is possible because they allow the designer to use their anisotropy to tailor the properties to reach specific requirements of the final product. This includes high strength applications, high stiffness applications, low thermal conductivity and thermal expansion applications, corrosion-resistant and dent-resistant applications, and designs where weight reductions or part consolidation are required.

A lot of work has been done on improvement and optimization of the strength and stiffness of composite materials [1,2,5], but many of the applications already outlined also require good vibration damping properties [4,6,7].

Damping is a measure of the total energy dissipated in any vibrating structure, so it is important to mention the primary sources of energy dissipation in fiber reinforced polymeric matrix materials.

It appears that the viscoelastic behavior of the bulk matrix and the interface, and the friction at the interface caused by relative motion between matrix and fiber are the primary sources for the good damping characteristics of these materials. Both effects are significant in discontinuous fiber composites, since high shear stresses are developed at the fiber matrix interface when the material is subjected to a cyclic strain. The matrix near the end of the short fibers undergoes a high cyclic shear strain that produces a significant viscoelastic energy loss.

The shear stress concentration may induce plastic effects as well as partial debonding at the fiber matrix interface that could result in slip between fiber and matrix with corresponding frictional losses. It is desirable to have a strong interfacial bond such that slip at the interface can be avoided, since this adversely affects the strength and stiffness of the composite.

In conclusion, the most viable mechanisms of enhanced energy dissipation appears to be the shear deformation in the matrix caused by shear stress concentration near the fiber ends [6], and the shear stress due to off-axis coupling effects, as the experimental results show.

Based on the stress transfer mechanism between fiber and the matrix, internal damping can be improved and optimized by varying several parameters: fiber aspect ratio (length/diameter), fiber matrix modulus ratio E'_f/E'_m , fiber

volume fraction, v_f, and fiber direction. Even more, random fiber orientation and hybridization appear to cause interlaminar shear stresses that may be additional sources of energy dissipation [8,9,10].

The damping properties of continuous fiber reinforced composites have been studied by several authors [11,12,13,14], but, as mentioned earlier, the possibility of improving and even optimizing the damping characteristics of composites using short reinforcing fibers [6,15,16], the lack of valid data on damping and the interest and support of the U.S. Air Force Office of Scientific Research, gave the author the motivation for this research.

The research described here is constrained to the improvement and optimization of internal damping of fiber reinforced composite materials by variation of fiber aspect ratio, type of fiber reinforcement and fiber direction. The present dissertation includes the development of techniques for fabrication of composite material laminated plates by using an autoclave style press cure and the development of a faster and more accurate damping measurement technique using an impulsive force, as described in Chapter 3.

The measured static and dynamic properties of bare resin specimens that are used in the micromechanical model of a single round fiber surrounded by a cylindrical matrix, as explained in Chapter 2, are included in Chapter 4.

The experimental data and corresponding correlation with the theoretical model for three advanced composite materials: graphite/epoxy, Kevlar[1]/epoxy and boron/epoxy in aligned continuous and discontinuous fiber configurations are given in Chapter 5.

Finally, results from tests done on off-axis fiber specimens of graphite/epoxy and Kevlar/epoxy are compared with predictions in Chapter 6.

---

[1]Kevlar is a proprietary aramid fiber produced by E.I. duPont de Nemours, Inc., Wilmington, Delaware.

2.0 BACKGROUND

This chapter is written with the objective of reviewing the theory involved in the development of the present research.

2.1 PREDICTION OF COMPLEX MODULI FOR COMPARISON WITH DAMPING MEASUREMENTS

The purpose of this section is to present a theoretical approach to the prediction of the composite complex moduli from those of the constituent materials (matrix and fibers) for comparison, in later chapters, with measured composite properties. The analysis of internal damping and dynamic stiffness for aligned discontinuous fiber reinforced composite materials was based on the complex moduli as established in [6].

The complex modulus of a viscoelastic material can be defined in terms of the storage and loss moduli [17].

$$E^* = E' + iE'' \tag{2.1}$$

Where the storage modulus, E', is related to the stored energy per unit volume, U, by Eq. 2.2,

$$U = \frac{1}{2} \epsilon^2 E' \tag{2.2}$$

and the loss modulus, E" is related to the specific damping energy, D, by Eq. 2.3.

$$D = \pi\epsilon^2 E'' \tag{2.3}$$

The damping property, or loss factor, of materials is defined by the ratio of the energy dissipated per cycle or damping energy to strain energy, Eq. 2.4.

$$\eta = \frac{D}{2\pi U} = \frac{\pi\epsilon^2 E''}{2\pi(\epsilon^2 E'/2)} = \frac{E''}{E'} \tag{2.4}$$

The complex modulus generally depends on frequency. The real part, or elastic modulus, is generally less frequency dependent than is the imaginary part [18,19]. Experimental results shown in Chapter 4 for neat resin specimens, and in Chapter 5 for the composite material specimens tested, verify this prediction. In the same way, the complex modulus is temperature dependent [20] and care was taken in performing all the experimental work at the same ambient conditions.

The analytical model was based on the Cox stress distribution [21] which assumes:

a.- A round fiber surrounded by a cylindrical matrix under extensional load, (Fig. 2.1).

b.- Fiber and matrix are isotropic. In order to fit the experimental data to the analytical model, this assumption had

to be modified as shown later in this chapter, so that the fibers are considered to be anisotropic.

c.- A perfect bond exists between the fiber and the matrix.

d.- There is no load transfer through the ends of the fiber, and,

e.- The transfer of load from the matrix to the fiber depends upon the difference between the actual displacement at a point on the interface and the displacement that would exist if the fiber were absent [22,23,24].

The interfacial shear stress, τ , and longitudinal fiber stress, σ_f, obtained by Cox were used by Gibson, et.al [6] as a starting point to find the solution for the complex modulus by two approaches, the Energy Method and the Force-Balance method.

The shear stress is:

$$\tau = \frac{r_0^2 E_f' \epsilon \beta}{2r} \frac{\sinh[\beta(\ell/2 - x)]}{\cosh(\beta\ell/2)} \qquad (2.5)$$

And the longitudinal stress is:

$$\sigma_f = \epsilon E_f' \left\{1 - \frac{\cosh[\beta(\ell/2 - x)]}{\cosh(\beta\ell/2)}\right\} \qquad (2.6)$$

Where β is:

$$\beta^2 = \frac{G_m'}{E_f'} \frac{2}{r_0^2 \, \mathrm{Ln}(R/r_0)} \qquad (2.7)$$

2.1.1 ENERGY APPROACH

For the first approach, the stresses from Eqs. 2.5 and 2.6 are used to find the energy stored in the matrix and fiber and the resulting longitudinal complex modulus in terms of its component storage and loss moduli [17].

It is assumed that the matrix is linearly viscoelastic and that the interface has the same viscoelastic properties as that of the bulk matrix. It is stated that the strain energy is stored in both constituent materials but the dissipation of energy takes place only in the matrix, (i.e., $\eta_f = 0$). Thus,

$$\eta = \frac{\eta_f W_f + \eta_m W_m}{W_f + W_m}$$

Since $\eta_f = 0$, then:

$$\eta = \frac{\eta_m W_m}{W_f + W_m} \tag{2.8}$$

After some manipulation [6], the longitudinal storage modulus is given by:

$$\frac{E'_L}{E'_m} = \frac{E'_f}{E'_m} v_f + v_m + \frac{E'_f}{E'_m}\left\{\frac{v_f}{\beta\ell} - \frac{v_m}{\beta\ell[(R^2/r_o^2) - 1]}\right\}\left[\frac{\alpha\sinh(\beta\ell) + \beta\ell}{1 + \cosh\beta\ell}\right] \tag{2.9}$$

Where

$$\alpha = \frac{1 - v_f(3R^2/r_o^2 - 2)}{v_f(R^2/r_o^2) - 1} \tag{2.10}$$

and the longitudinal loss modulus is given by

$$\frac{E''_L}{E''_m} = v_m \left\{\frac{E'_f}{E'_m} \frac{1}{2[(R^2/r_o^2) - 1]} \left[\frac{\tanh(\beta\ell/2)}{\beta\ell/2} - \frac{1}{\cosh^2(\beta\ell/2)}\right] + 1\right\} \tag{2.11}$$

The ratio R/r_o may be expressed in terms of the fiber volume fraction for a specified packing array.

For a hexagonal array:

$$\left(\frac{R}{r_o}\right)^2 = \frac{\pi}{2\sqrt{3}\, v_f} \tag{2.12}$$

For a square array:

$$\left(\frac{R}{r_o}\right)^2 = \frac{\pi}{4\, v_f} \tag{2.13}$$

2.1.2 FORCE-BALANCE APPROACH

In this approach, static equilibrium, geometric compatibility, and the elastic-viscoelastic correspondence principle [18] are used to obtain the complex moduli. In this derivation, the fibers are assumed to contribute to the energy dissipation and the fiber loss factor is non-zero.

Based on the fiber stress distribution (Eq. 2.6) the average fiber stress can be written as:

$$\bar{\sigma}_f = \frac{1}{\ell/2} \int_0^{\ell/2} \sigma_f d_x = \varepsilon E_f' \left[1 - \frac{\tanh(\beta\ell/2)}{\beta\ell/2} \right] \tag{2.14}$$

Considering static equilibrium, the total longitudinal stress applied to the composite is:

$$\bar{\sigma}_L = E_L' \varepsilon = \bar{\sigma}_f v_f + \bar{\sigma}_m v_m \tag{2.15}$$

The extensional strain for composite, fiber and matrix are assumed to be equal. The longitudinal storage modulus and loss modulus are then:

$$E_L' = E_f' v_f \left[1 - \frac{\tanh(\beta\ell/2)}{(\beta\ell/2)} \right] - \frac{E_f'' v_f}{2} (\eta_{Gm} - \eta_f) \left[\frac{\tanh(\beta\ell/2)}{(\beta\ell/2)} - \frac{1}{\cosh^2(\beta\ell/2)} \right] + E_m' v_m \tag{2.16}$$

and

$$E''_L = E''_f v_f \left[1 - \frac{\tanh(\beta\ell/2)}{(\beta\ell/2)}\right] + \frac{E'_f v_f}{2}(\eta_{Gm} - \eta_f)$$

$$\left[\frac{\tanhn(\beta\ell/2)}{(\beta\ell/2)} - \frac{1}{\cosh^2(\beta\ell/2)}\right] + E''_m v_m \qquad (2.17)$$

From these equations it can be seen that when the fiber loss factor is equal to zero, Eqs. 2.16 and 2.17 will be similar to Eqs. 2.9 and 2.11 obtained with the energy method. The force balance approach was used for the analysis of damping of composite materials as explained later in chapters 5 and 6.

Both analytical methods predict an optimum fiber aspect ratio (ratio of the length to diameter of the fiber) for maximum damping [6]. This prediction was one of the main reasons for this research, because this analytical result had to be checked against experimental values.

2.2 OFF-AXIS ANALYSIS

The previous analysis was used for the optimization of internal damping of fiber reinforced polymer composite materials when the applied load is parallel to the fiber direction. The following analysis will consider the variation and possible optimization of internal damping when the applied load is not parallel to the fiber direction.

Again the Force-Balance approach [6] and the elastic-viscoelastic correspondence principle [18] are used to obtain the equation for storage modulus, loss factor and loss modulus along the fiber direction [25].

The stress-strain relations for a lamina of arbitrary orientation under constant environmental conditions are given by

$$\{\varepsilon\}_{xy} = [\bar{S}]\{\sigma\}_{xy} \tag{2.18}$$

Where

$$[\bar{S}] = [T]^{T}[S][T] \tag{2.19}$$

is the off-axis compliance matrix, [S] is the compliance matrix along the fiber direction, and

$$[T] = \begin{bmatrix} \cos^2\theta & \sin^2\theta & 2\cos\theta\sin\theta \\ \sin^2\theta & \cos^2\theta & -2\cos\theta\sin\theta \\ -\sin\theta\cos\theta & \sin\theta\cos\theta & \cos^2\theta-\sin^2\theta \end{bmatrix} \tag{2.20}$$

is the matrix that accounts for the tensor transformation of stresses and strains from the x axis to the principal axes (Fig. 2.2).

$[T]^T$ is the matrix transpose of [T].

Each of the terms S_{ij} of the compliance matrix is a function of the engineering constants [3]. For the case of isotropic materials there are two such constants, the elastic modulus E and Poisson's ratio . For an orthotropic material in plane stress there are four independent material properties: the longitudinal modulus, E_L , the transverse modulus, E_T, the in-plane shear modulus, G_{LT} , and the major Poisson's ratio, ν_{LT} .

The apparent modulus, E_x , along the direction of the applied stress is given in Eq. 2.21 as a function of the four independent properties already given and the angle of direction of the fibers with respect to the direction of the applied load, θ , [3].

$$\frac{1}{E_x} = \frac{1}{E_L}\cos^4\theta + \left(\frac{1}{G_{LT}} - \frac{2\nu_{LT}}{E_L}\right)\sin^2\theta\cos^2\theta + \frac{1}{E_T}\sin^4\theta \qquad (2.21)$$

By using either of the models described in the previous section, the longitudinal modulus can be written as:

$$E_L = E_f\left[1 - \frac{\tanh(\beta\ell/2)}{(\beta\ell/2)}\right]v_f + E_m v_m \qquad (2.22)$$

Where β is given by equation (2.7).

The transverse modulus and the in-plane shear modulus can be obtained empirically by using the Halpin-Tsai equations [3], which are approximate representations of more complicated

micromechanics results and can be equally applied to fiber, ribbon or particulate composites:

$$\frac{M}{M_m} = \frac{1 + \xi \eta_h V_f}{1 - \eta_h V_f} \tag{2.23}$$

Where

$$\eta_h = \frac{(M_f/M_m) - 1}{(M_f/M_m) + \xi} \tag{2.24}$$

ξ is a measure of fiber reinforcement which depends on the fiber geometry, packing array and load conditions. For circular fibers in a square array, good results were obtained using $\xi = 2$ for the transverse modulus and $\xi = 1$ for the in-plane shear modulus [3].

The major Poisson's ratio can be obtained by using the rule of mixtures [3]:

$$\nu_{LT} = \nu_f V_f + \nu_m V_m \tag{2.25}$$

At this point, the elastic-viscoelastic correspondence principle [26] can be used to transform the elastic constants to viscoelastic constants:

$$E_x^* = E_x' + iE_x''$$

$$E_f^* = E_f' + iE_f''$$

$$E_m^* = E_m' + iE_m''$$

$$E_L^* = E_L' + iE_L''$$

$$E_T^* + E_T' + iE_T''$$

$$G_f^* = G_f' + iG_f''$$

$$G_m^* = G_m' + iG_m'' \qquad (2.26)$$

$$G_{LT}^* = G_{LT}' + iG_{LT}''$$

$$\nu_{LT}^* = \nu_{LT}' + i\nu_{LT}''$$

After introducing the complex elastic constants in Eq. 2.21, the off-axis composite storage moduli and the loss moduli can be obtained by separating the real and imaginary parts and neglecting higher order terms in the loss factor (since $\eta << 1$). These equations are very long, so only the general form is presented here. The complete mathematical manipulation is given in Appendix A of Reference [53].

In general terms,

$$\text{(a)} \quad \frac{E_x'}{E_m'} = \phi_1 \left[E_f', E_m', \nu_f, \nu_v, (\ell/d), \eta_f, \eta_m, \nu_f, \nu_m, \theta, \text{packing array}\right]$$

$$\text{(b)} \quad \eta = \phi_2 \left[E_f', E_m', \nu_f, \nu_v, (\ell/d), \eta_f, \eta_m, \nu_f, \nu_m, \theta, \text{packing array}\right] \qquad (2.27)$$

$$\text{(c)} \quad \frac{E_x''}{E_m''} = \phi_3 \left[E_f', E_m', \nu_f, \nu_v, (\ell/d), \eta_f, \eta_m, \nu_f, \nu_m, \theta, \text{packing array}\right]$$

The analysis up to this point is based on the assumption that matrix and fibers are each isotropic, so the properties of the fiber are the same in all directions and the shear modulus can be obtained using the well known elastic relation given by Eq. 2.28 [27].

$$G_f' = \frac{E_f'}{2(1 + \nu_f)} \tag{2.28}$$

In the present research, graphite, Kevlar and boron fibers were used in the experimental part. These fibers are essentially anisotropic [26,28] which means that the elastic properties vary with direction. Whitney [29] showed that by treating the fiber as an orthotropic, transversely isotropic material, the micromechanics equations can be adapted easily to take care of its anisotropy. Thus, the composite transverse modulus is given by

$$E_T = E_m \left[\frac{1 + \xi \eta_{h1} v_f}{1 - \eta_{h1} v_f}\right] \tag{2.29}$$

Where:

$$\eta_{h1} = \frac{(E_{fT}/E_m) - 1}{(E_{fT}/E_m) + \xi_1}$$

and the in-plane shear modulus is given by

$$G_{LT} = G_m \left[\frac{1 + \xi_2 \eta_{h2} v_f}{1 - \eta_{h2} v_f}\right] \tag{2.30}$$

Where:

$$\eta_{h2} = \frac{(G_{fLT}/G_m) - 1}{(G_{fLT}/G_m) + \xi_2}$$

2.3 VIBRATION OF A CONTINUOUS SYSTEM

For the development of the experimental technique, small cantilever beam specimens were used for transverse modes, and free-free with masses attached at both ends for longitudinal modes.

Cantilever beam specimens of aligned discontinuous fiber reinforced composites were used for the fiber/length studies. Under flexural vibration, no mixed coupling effects are present and the complex moduli can be obtained from measured resonant frequencies and the frequency equation for a cantilever beam. Since the laminate properties do not vary through the thickness, the measured flexural modulus is equal to the extensional modulus.

For the case of off-axis tests used for fiber direction studies, the flexural vibration technique cannot be used, since flexural-torsional coupling effects exist. These specimens were therefore tested in longitudinal vibration with masses attached at both ends. The masses were needed in order to adjust the resonant frequency of the first mode to the range of interest for this research. Again the complex modulus was obtained from

the measured resonant frequency and the corresponding frequency equation for a mass-mass beam.

2.3.1 TRANSVERSE VIBRATION OF A CONTINUOUS BEAM

The elastic moduli of aligned discontinuous fiber composites were found, as mentioned in the previous section, from cantilever beam specimens by exciting the flexural or transverse modes and measuring the modal frequencies.

The equation of motion for the cantilever beam of Fig. 2.3 is given by Eq. 2.31

$$EI \frac{\partial^4 y}{\partial x^4} + \rho A \frac{\partial^2 y}{\partial t^2} = 0 \tag{2.31}$$

The boundary conditions for a cantilever beam are:

At the free end

$$\frac{\partial^2 y}{\partial x^2} = \frac{\partial^3 y}{\partial x^3} = 0 \tag{2.32}$$

At the clamped end

$$y = \frac{\partial y}{\partial x} = 0 \tag{2.33}$$

Using Eqs. 2.31, 2.32 and 2.33 the resonant frequencies for each mode are found to be:

$$f_n = \frac{\lambda_n^2}{2\pi S^2} \left(\frac{EI}{\rho A}\right)^{1/2} \tag{2.34}$$

Where n = 1,2,3,....

The eigenvalues λ_n for the cantilever beam are found by solving the transcendental Equation 2.35

$$\cos\lambda_n \cosh\lambda_n + 1 = 0 \tag{2.35}$$

Values of the eigenvalues for all the modes are given in [30].

2.3.2 LONGITUDINAL VIBRATION OF A CONTINUOUS BEAM

The free-free beam with masses attached at its ends (Fig. 2.4), was used to obtain the elastic moduli under longitudinal vibrations.

The differential equation of motion is given in Eq. 2.36 [31].

$$\frac{\partial^2 u}{\partial x^2} = \frac{\rho}{E} \frac{\partial^2 u}{\partial t^2} \tag{2.36}$$

The boundary conditions are:

At x = 0

$$AE \left(\frac{\partial u}{\partial x}\right) = M_1 \left(\frac{\partial^2 u}{\partial t^2}\right) \tag{2.37}$$

At x = S

$$AE \left(\frac{\partial u}{\partial x}\right) = -M_2 \left(\frac{\partial^2 u}{\partial t^2}\right) \tag{2.38}$$

The natural frequencies are given by Eq. 2.39

$$f_n = \frac{\lambda_n}{2\pi S} \left(\frac{E}{\rho}\right)^{1/2} \tag{2.39}$$

Where n = 1,2,3,....

The eigenvalues λ_n are obtained from the following transcendental equation:

$$\tan\lambda_n = \frac{(M_1 + M_2)\, AS\rho\lambda_n}{M_1 M_2 \lambda_n^2 - (A\rho S)^2} \tag{2.40}$$

The complete mathematical development of the equations for the transverse and longitudinal vibrations are given in Appendix B of Reference [53].

2.4 MODAL ANALYSIS

The principal objective of this research was to experimentally characterize the dynamic properties of composite materials. The use of modal analysis helps by identifying the modes of vibration. Each mode of vibration has a specific

natural frequency, damping factor and mode shape that can be identified from any point of the structure [32].

Modal analysis is useful for the following reasons:

a.- It allows verification and/or changes in the mathematical model that describe the structure under testing.

b.- It helps to identify the weak points of the structure.

c.- It provides information about unwanted noise or vibration.

2.4.1 FREQUENCY RESPONSE TRANSFER FUNCTION

Modal analysis is based on the measurement of the frequency response function, or transfer function.

There are six useful forms of the transfer function. These are:

a.- Compliance (displacement/force)

b.- Dynamic or apparent stiffness (force/displacement)

c.- Mobility (velocity/force)

d.- Impedance (force/velocity)

e.- Inertance (acceleration/force)

f.- Dynamic or apparent mass (force/acceleration)

Computing techniques like the Fast Fourier Transform in combination with powerful instruments like Digital Fourier Analyzers provide fast and accurate determination of the frequency spectrum of a time-domain signal. In order to facilitate the implementation of modal analysis on a Digital Fourier

Analyzer, the relationships between the time, frequency and Laplace domain are greatly used. The mathematical tools are the Fourier and Laplace transforms.

In the time domain the system behavior may be determined in terms of the system impulse response h(t) using the convolution integral [33,34].

$$y(t) = \int_0^t x(\tau)h(t - \tau)d\tau \tag{2.41}$$

The transfer function that relates the impulse to the output is expressed in the Laplace domain by:

$$H(s) = \frac{Y(s)}{X(s)} \tag{2.42}$$

Where:

$$X(s) = \int_0^\infty e^{-st}x(t)dt \tag{2.43}$$

$$Y(s) = \int_0^\infty e^{-st}y(t)dt \tag{2.44}$$

$$H(s) = \int_0^\infty e^{-st}h(t)dt \tag{2.45}$$

The s-plane is complex and the magnitude of any function such as the transfer function H(s) can be plotted as a three

dimensional surface above the complex s-plane [32] . The transfer function evaluated along the frequency axes ($s=i\omega$) is the Fourier Transform, or the system frequency response function.

Since these variables cannot be measured in the Laplace domain, the Fourier transform is of great importance for computation [35] .The frequency domain transfer function is:

$$H(f) = \frac{Y(f)}{X(f)} = \frac{Y(f)\bar{X}(f)}{|X(f)|^2} \tag{2.46}$$

Where:

$$H(f) = \int_{-\infty}^{\infty} h(t)e^{-i2\pi ft}dt \tag{2.47}$$

$$X(f) = \int_{-\infty}^{\infty} x(t)e^{-i2\pi ft}dt \tag{2.48}$$

$$Y(f) = \int_{-\infty}^{\infty} y(t)e^{-i2\pi ft}dt \tag{2.49}$$

and $\bar{X}(f)$ is the complex conjugate of $X(f)$.

The expanded numerator and denominator of Eq. 2.46 are called the cross spectrum between the input and output, $G_{xy}(f)$, and the power spectrum of the excitation or input, $G_x(f)$, respectively.

$$Y(f)\bar{X}(f) = G_{xy}(f) \tag{2.50}$$

$$X(f)\bar{X}(f) = |X(f)|^2 = G_x(f) \tag{2.51}$$

There is an inherent bias error in measuring the cross spectrum. The magnitude of the bias error is inversely proportional to the number of averages made in the computation. The greater the noise, the greater the number of averages that should be done in order to approximate the value of the cross spectrum [35].

One of the most important advantages in computing the cross spectrum is that magnitude and phase can be computed at the same time, since both pieces of information are contained in it. Another advantage is that by using this formulation, any wave form that is Fourier transformable can be used, so it is not limited to just sinusoidal signals.

2.4.2 COHERENCE FUNCTION

Another advantage of computing the cross spectrum is that it allows the computation of the coherence function between the input and output signals, defined by Eq. 2.52

$$\gamma^2_{xy}(f) = \frac{|G_{xy}(f)|^2}{G_x(f)G_y(f)} \tag{2.52}$$

The coherence function will be 1 if there is no noise in the measurements and if the system is linear. It will be 0 when there is no correlation between the two signals. The coherence

function is a good check of the influence of noise in the signals. It is the monitor of the quality of the transfer function.

2.4.3 MEASUREMENT OF DAMPING

Damping is a measure of the total energy dissipated in any vibrating structure. Its value is of great importance when designing dynamic structures. This section is written with the objective of reviewing the most commonly used methods of damping measurements. Most of the methods are based on the single-degree-of-freedom analysis of a single mode. This is appropriate, since analytical modal analysis shows that a continuous system can be modeled as an infinite number of single degree of freedom systems [34].

The damping properties in resonance are related to the amplification factor Q as follows:

$$Q = \frac{1}{2\zeta} \tag{2.53}$$

The loss factor η is the inverse of the amplification factor. This is the parameter that will be used for the characterization of damping in this research.

$$\eta = \frac{1}{Q} \tag{2.54}$$

The loss factor can be measured from the frequency response function by several methods and some of the most popular are described below [36].

a.- Ratio of the static compliance to the compliance magnitude at the natural frequency.

$$\eta = \frac{\text{static compliance}}{\text{compliance magnitude at the natural frequency}} \tag{2.55}$$

b.- Bandwidth technique (See Fig. 2.5).

$$\eta = \frac{\Delta f}{f_n} \tag{2.56}$$

c.- From the real component of the transfer function (see Fig. 2.6).

$$\eta = \frac{(f_a/f_b)^2 - 1}{(f_a/f_b)^2 + 1} \tag{2.57}$$

d.- Coincident-quadrature or Nyquist plot (See Fig. 2.7).

$$\eta = \frac{f_2 - f_1}{f_n} \tag{2.58}$$

e.- Curve fitting based on a model of a single-degree-of-freedom or a multidegree-of-freedom system. In the first case the model is given by Eq. 2.59, where the variable for curve-fitting is the damping factor ζ.

$$y(t) = \frac{x(t)}{\{[1 - (\omega/\omega_n)^2]^2 + [2\zeta(\omega/\omega_n)]^2\}^{1/2}} \qquad (2.59)$$

For a multidegree of freedom model, several modes are considered at the same time and exponential equations, polynomial equations or other equations can be used to fit the transfer function of the system.

There are other methods to obtain damping which are not based on the frequency transfer function.The most popular are:

a.- Free vibration decay, based on the decay of the oscillation in the time domain (See Fig. 2.8).

The loss factor is:

$$\eta = \frac{\delta}{\pi} \qquad (2.60)$$

Where the logarithmic decrement is:

$$\delta = \frac{1}{n} \operatorname{Ln} \frac{x_0}{x_n} \qquad (2.61)$$

b.- Resonant dwell, which is based on the ratio of the amplitude of the input ,a_i, to the amplitude of the response ,a_r , at resonance under sinusoidal excitation.

$$\eta = K \frac{a_i}{a_r} \qquad (2.62)$$

Where K is a factor which depends on boundary conditions and mode number.

c.- Hysteresis loop in a force-displacement curve (see Fig. 2.9) [38].

$$= \frac{D}{2\pi U} = \frac{a}{b} \qquad (2.63)$$

The choice of the technique depends on the properties of the material to be tested, the ranges of frequency and stress of interest, the type of excitation available (forced-sinusoidal, random or impulsive force), and apparatus available. In all cases, parasitic losses such as support friction and air drag must be minimized, since erroneous measurements of damping can be obtained.

3.0 EXPERIMENTAL TECHNIQUE

From References [6,38,39] it can be concluded that, theoretically, discontinuous fiber reinforcement can be used to improve internal damping in fiber reinforced polymer composite materials. As shown in Reference 6 , there is a theoretical optimum value for the fiber aspect ratio for which the loss modulus is maximum, but this is only obtained with very low fiber aspect ratios. In addition, theoretical optimum off-axis angles are shown in [25].

In this research, specimens with fiber length ranging from continuous to 1/16" (1.588 mm) were tested in order to verify predicted trends at low fiber aspect ratios, while continuous and 1/4" (6.35 mm) fiber length specimens were tested for different fiber orientations. The effects of the elastic modulus ratio (E'_f/E'_m) also were considered in these tests by using different kinds of fiber reinforcement: graphite, boron and Kevlar.

This chapter will cover the fabrication procedure, the development of the experimental technique for damping measurements, the experimental procedures for determination of fiber and void volume fraction and the Poisson's ratio for the different composite materials used.

3.1 FABRICATION OF THE SPECIMENS

The specimens used were small cantilever beams with global dimensions of 3/4" (19.05 mm) wide by 8" (203.2 mm) to 11" (279.4 mm) long. The thickness depended on the type of composite material under consideration, but twelve plies were used to fabricate all the specimens. The specimens were fabricated in the laboratories of the Mechanical Engineering Department at the University of Idaho. The procedure was similar to that reported in reference [6], except that only 12 plies were used and the autoclave curing process was simulated in a laminating press.

The composite materials are available in prepreg tape rolls of different width. For this research, three different composite materials were used:

a.- Fiberite Hy-E1034C graphite/epoxy pre-preg[1] with non-woven continuous T300 graphite filament and Fiberite 934 resin in a roll of 12" (304.8 mm) width.

b.- Fiberite Hy-E1734A2 aramid/epoxy pre-preg with non-woven continuous Kevlar 49 filament and Fiberite 934 resin in a roll of 12" (304.8 mm) width.

---

[1] Fiberite Corporation, 501 W. 3rd St., Winona, Minnesota 55987

c.- AVCO 5505/4 boron/epoxy pre-preg[1] with continuous boron 4 mil filament and 5505 resin in a roll with three separated strips of 1" (25.4 mm) wide each.

As stated previously, References [6,38] predict that internal damping of composite materials can be improved with reinforcement having low fiber aspect ratio (ratio of fiber length to diameter of the fiber). Since the objective of this research is the optimization of internal damping of fiber reinforced composite materials, it was necessary to develop a suitable technique for the fabrication of plates of various fiber length. This includes cutting the pre-preg, curing the plates and machining the specimens to the actual size. Plates of graphite/epoxy, Kevlar/epoxy and boron/epoxy with fiber length ranging from continuous to 1/16" (1.588 mm) were fabricated with excellent results.

It was decided that the number of plies used to fabricate the plates were to be 12 after preliminary tests done by the author using 3M Scotchply Sp 322 T300 graphite/epoxy pre-preg tape. The thickness of the plate with 12 plies after curing gives the specimens enough rigidity for the tests to be done and the frequencies for the principal modes fall inside the range of interest for the present work (10-1000 Hz for flexural vibration, and up to 1300 Hz for longitudinal vibration).

---

[1] AVCO, Specialty Materials Division, 2 Industrial Ave., Lowell, MA 01851

3.1.1 CUTTING THE PREPREG TAPE

Two techniques were developed to cut the pre-preg tape at the desired fiber length. The first one was used on graphite/epoxy and Kevlar/epoxy while the second technique was used on boron/epoxy prepreg tape [39,40].

A.- Graphite/Epoxy and Kevlar/Epoxy

These materials were cut in laminae having dimensions of 12" (304.8 mm) x 12" (304.8 mm) from a roll previously stored at 0 °F (-18 °C) with a standard utility knife with stainless steel blades. After warming up to room temperature, the tacky surface was pressed against a urethane surface that holds the ply to be cut in strips at the desired fiber length, while leaving the backing paper attached to the free surface. The measurements for the required fiber length were marked on the backing paper by using a pair of dividers. All the strips were sliced across the fibers beginning and ending within the edges of the pre-preg tape (Fig. 3.1) to prevent the edge fibers from being pulled out of the pre-preg. A contact paper was attached to the backing paper tape so that the strips would be aligned end-to-end. The single ply then was moved to the uncured laminate (Fig. 3.2). The alternating plies were layed up such that the fiber ends were staggered, with a final uncured laminate of

12" (304.8 mm) x 12" (304.8 mm). The contact and backing papers were removed from each ply either as one piece or separately.

The maximum number of specimens to be tested for each fiber aspect ratio was decided to be six, so, only laminated plates of 6" (152.4 mm) wide were required. Two laminated plates of 6" (152.4 mm) wide, each one of different fiber length, were placed side by side for curing purposes, since the aluminum mold was designed for plates of dimensions 12" (304.8 mm) x 12" (304.8 mm).

B.- Boron/Epoxy

For boron/epoxy composite a different technique was used. After allowing the pre-preg to warm up to room temperature, the tape was arranged into a 3" (76.2 mm) wide strip and then it was cut in 12" (304. mm) lengths. The boron fibers were then sandwiched between the backing paper and a transparent contact paper previously marked at the desired fiber length on a thin strip of white paper. The 3" (76.2 mm) x 12" (304.8 mm) ply was then fractured at each mark using a guillotine device with a 3" (76.2 mm) carbide blade as shown in Fig. 3.3 The fibers were sheared against a urethane cutting surface. Two of these plies were placed side by side in order to increase ply width to 6" (152.4 mm). The backing paper was removed and the ply was pressed against the uncured laminate. The alternating plies were layed up such that the fiber ends were staggered. Then the

contact paper was carefully removed. Two of these uncured laminates, each one of 12 plies and dimensions 6" (152.4 mm) x 12" (304.8 mm)were finally placed side by side in the mold for the cure process.

3.1.2 CURE PROCESS

Two different processes [39,40] were followed; one for curing the composite plates with specific variations for each one of the materials used, and the second process to cure neat resin plates. Specimens of pure matrix had to be tested in order to obtain properties that were applied in the micromechanics model.

A.- Composite material cure process

The 12" (304.8 mm) x 12" (304.8 mm) laminated plates were cured using an autoclave style press cure with a specially designed vacuum mold as shown in Fig. 3.4 . Table 3.1 shows a listing of the components used in the lay-up of the mold. Fig 3.5 shows the general set-up for the curing process.

The general procedure is as follows:

a.- Spray the mold, pressure plate, vacuum bag, rubber dam and

spacer plate with release agent Frekote 33[1]. It requires at least 15 minutes to set.

b.- Place the rubber dam and the uncured laminated plate (which was previously warmed up to room temperature) in the mold.

c.- Place the porous release fabric and two layers of bleeder cloth (cut to oversized dimensions) over the uncured laminate.

d.- Place the pressure plate in the mold.

e.- Fold the excess bleeder cloth over the rubber dam and press into the manifold along each edge.

f.- Start the vacuum pump and place the vacuum bag over the top of the mold. Press along the edge of the mount to seal O-ring against mold.

g.- Put the spacer plate over the pressure plate with the vacuum bag between them, then place the mold in the laminating press.

h.- Set and start the data acquisition system for temperature recording with a thermocouple located in a small hole just below the vacuum fitting.

i.- Follow the cure cycle as described in Table 3.2 or 3.3, depending on material used.

The quality of the plate obtained using the process just described is comparable to that obtained from an autoclave. Two

---

[1]Frekote Inc, 170 W. Spanish River Blvd, Boca Raton, FL 33431

identical 12 ply unidirectional continuous fiber laminates were layed up using Fiberite Hy-E1034C graphite/epoxy pre-preg. One plate was cured in a laboratory autoclave at the University of Florida and the other was cured by the autoclave style press cure at the University of Idaho. The density, fiber and void volume fractions were determined using the process described later in this chapter from four locations in each plate . The two plates were nearly identical, as seen in Table 3.4.

Micrograph sections of the cured laminates also show the good quality and low void content of the composite materials obtained using the autoclave style press cure. Micrographs of graphite/epoxy composite obtained from an autoclave, and graphite/epoxy, Kevlar/epoxy and boron/epoxy composites produced by an autoclave style press cure may be seen in Figs. 3.6, 3.7, 3.8 and 3.9, respectively.

B.- Resin Cure Process

Resin castings of Fiberite 934 and AVCO 5505 having dimensions 12" (304.8 mm) x 12" (304.8 mm) x 1/8" (3.18 mm) were produced in an aluminum mold following the cure cycles outlined in Tables 3.5 and 3.6, respectively 40 . The mold and the equipment required to produce neat resin plates are shown in Figs. 3.10 and 3.11, respectively. These specimens were needed since the micromechanics model required input data on the dynamic properties of the matrix material [6].

3.1.3 MACHINING OF THE SPECIMENS

The specimens were machined in the Machine Shop of the Mechanical Engineering Department using a precision reciprocating grinder. The cured laminated plate was fixed with double sided tape on 1" (25.4 mm) thick styrofoam, then placed on the working table of the grinder. Graphite/epoxy and Kevlar/epoxy laminated plates were cut with an abrasive cut-off wheel while the boron/epoxy plates were cut with a diamond cut-off wheel Fig. 3.12.

The machining of the graphite/epoxy and boron/epoxy specimens did not give any major complications, but the machining of Kevlar/epoxy specimens was problematic since delamination occurred at the edges of the specimens. Water was used as lubricant to machine this material. More recently, Kevlar/epoxy plates were machined with an electric band saw at high speed with the saw blade mounted backward (Fig. 3.13), followed by a trimming process in a vertical rotor with an opposed helix router tool.

In addition to the specimens for the vibration tests, small specimens of 1.5" (38.1 mm) x 3/4" (19.05 mm) were machined for determination of material density and fiber volume fraction. In order to minimize the effect due to delamination in Kevlar/Epoxy specimens, the length was increased to 2" (50.8 mm). Four specimens were machined for each fiber length plate for these type of tests.

The total number of plates fabricated were:

a.- 13 plates (118 small beam specimens) of graphite/epoxy,

b.- 8 plates (66 small beam specimens) of Kevlar/epoxy,

c.- 4 plates (42 small beam specimens) of boron/epoxy,

d.- 4 plates (6 small beam specimens) of neat Fiberite 934 resin, and,

e.- 2 plates (6 small beam specimens) of AVCO 5505 neat resin.

3.2 DIGESTION TEST

This test was performed with the objective to determine the fiber volume fraction and void volume fraction of the cured laminated plates by digestion of the matrix resin in a liquid medium which does not attack the fibers excessively. It is also necessary to obtain the density of each plate.

The specimens used in these tests were of 3/4" (19.05 mm) x 1.5" (38.1 mm) for graphite/epoxy and boron/epoxy specimens and 3/4" (19.05 mm) x 2" (50.8 mm) for Kevlar/epoxy as specified previously.

3.2.1 DENSITY DETERMINATION

The American Society for Testing and Materials (ASTM) Standard Test Method for Specific Gravity and Density of Plastics by Displacement, D-792-66, was used to determine the density of the laminated plates. Room temperature and pressure

at the time of the tests were recorded. The weight of the specimens in the air and in the water then were used in Eq. 3.1 to determine the required density value. The procedure followed is outlined in Table 3.7 [39].

The equipment needed includes an analytical balance, beaker, thermometer, and a metal clip suspended by a nylon wire from a glass rod (Fig. 3.14). The density of the specimen is:

$$\rho_c = \frac{w_c(\rho_w - \rho_a)}{w_c - w_w} \tag{3.1}$$

3.2.2 FIBER AND VOID VOLUME FRACTION DETERMINATION

The American Society for Testing and Materials (ASTM) Standard Test Method for Fiber Content of Reinforced Resin Composites, D3171-76, Procedure A, was used with graphite/epoxy. For Kevlar/epoxy composite material specimens, the same standard was slightly modified. The digestion was obtained using nitric acid assay 70.6 % at 167 °F (75 °C) for 5 hours for graphite/epoxy and 1 hour for Kevlar/epoxy The temperature was obtained with water and a circulating pump heater as shown in Fig. 3.15 [39].

It was noted that bare Kevlar fibers digested for 1 hour increased their weight by approximately 2.5 %. The fiber weight in the composite was then corrected for this value in the respective calculations.

The digestion for boron/epoxy was based on the procedure outlined in reference [41]. The digestion was carried out using sulfuric acid assay 96.3 % at 400 °F (204.4 °C) for 16 hours. This temperature was reached with a hot plate (Fig. 3.16).

The calculations for all materials were based on the equation of the rule of mixtures for specific weight [2].

$$\gamma_c = \gamma_f v_f + \gamma_m v_m \tag{3.2}$$

The fiber volume fraction is:

$$v_f = \frac{w_f}{\rho_f}\frac{\rho_c}{w_c} \tag{3.3}$$

and the void volume fraction is:

$$v_v = 1 - \frac{w_f \rho_c}{w_c \rho_f} - \frac{w_m \rho_c}{w_c \rho_m} \tag{3.4}$$

The calculations were done using the HP 9836 desk computer. The detailed procedure is given in Table 3.8 for graphite/epoxy and Kevlar/epoxy composite materials and in Table 3.9 for boron/epoxy.

3.3 DEVELOPMENT OF THE TECHNIQUE FOR DAMPING MEASUREMENTS

The number of tests to be done and the lack of valid data on internal damping of composite materials motivated the author to find an accurate and fast damping measurement technique that was easy to use and had the potential for making in-situ measurements for non destructive testing [42].

Gibson and Plunkett [43] developed a forced sinusoidal vibration technique for measuring damping and stiffness in composite materials, which was improved later by Gibson, et al [44]. The block diagram for this technique is shown in Fig. 3.17. This technique has been used succesfully on numerous composite materials [19,20]. This technique was not used in the present research because it is too slow. Only one frequency can be excited at a time, and tuning the resonant frequency to obtain the Lissajous pattern on an oscilloscope is not easy. The other techniques described here excite all the modes at the same time, under random or impulsive excitation, and the transfer function in the frequency domain is generated in real time. The sinusoidal technique was used for comparison of results during the development of the new technique.

A 2024-T351 aluminum alloy specimen was used for calibration tests since the Zener Thermoelastic theory is quite accurate in predicting damping for structural metals under flexural vibration [43,45,46]. That is, experimental damping

values were compared with well-accepted values from thermoelastic theory.

Unreinforced epoxy resin specimens and composite material specimens such as continuous fiber graphite/epoxy (12 plies) and short fiber E-glass/polyester were also used during calibration tests. These materials were selected to give a range of damping from low (aluminum) to intermediate (composite) to high (epoxy).

3.3.1 RANDOM TECHNIQUE

Fig. 3.18 shows the block diagram for this technique. This diagram is similar to the one used for the forced sinusoidal technique, except for the shaker input. The transfer function in the frequency domain is obtained with the Fast Fourier Transform (FFT) analyzer while the specimen is continuously excited with an electromagnetic shaker with a random input. The random signal (actually pseudo-random) is generated by the noise source of the FFT analyzer. This type of signal minimizes the leakage effects of a non periodic signal [47], which is the energy from the non periodic part that leaks on to the periodic part giving less accurate results.

The pseudo-random waveform provides the fastest means for finding statistically accurate transfer functions, which then are used to determine the internal damping of the material by means of the half-power bandwidth method as described later. A

typical transfer function showing several resonant peaks is shown in Fig. 3.19. Use of the zoom feature of the FFT analyzer makes it possible to analyze the peaks more accurately, as shown in Fig. 3.20.

The specimen used is a double cantilever beam, which is the same as that used for the forced sinusoidal technique 44 (Fig. 3.21). The specimen response is sensed by a non contacting eddy current proximity transducer, whose calibration curve is shown in Fig. 3.22. The input is measured with a piezoelectric accelerometer.

Excitation and response signals are fed into the FFT analyzer and the desired transfer function on the desired frequency span is displayed on the screen in real time.

The principal characteristics of this excitation method are [47]:

a._ The force level is easily controlled (noise source knob and power amplifier knob).

b._ The transfer function spectrum can easily be shaped at resonant peaks with ensemble averaging, which removes extraneous noises, nonlinearities and distortion effects (RMS averaging and Hanning window function).

c._ No leakage errors are present

d._ A well designed fixture and exciter system are required. This means that this technique may not be suitable for in-situ testing of engineering structures.

3.3.2 IMPULSE TECHNIQUE

In this case, the transfer function for the specimen is found by tapping the specimen with a hammer which has a force transducer attached at its head. Two specimens were used in this technique. A cantilever beam specimen (same as Fig. 3.21) was fixed in a vise at the resin shoulder. A free-free beam specimen was supported at the nodal points for the fundamental mode with nylon wire (Fig. 3.23).

The signals from the force transducer and from the motion transducer (non-contacting proximity probe) were fed into the FFT analyzer, which displayed the desired transfer function. The block diagram for this technique is shown in Fig. 3.24.

The principal characteristics of the impulse technique are [47]:

a._ The force level cannot be accurately controlled.

b._ The transfer function can be shaped with small difficulty at resonant peaks using ensemble averaging which removes extraneous noises and, to some degree, nonlinearities and distortion effects (RMS averaging and uniform window function).

c._ Leakage errors may be present.

d._ A special fixture and exciter system are not required, so that in-situ testing of engineering structures is possible.

For both random and impulse techniques, care must be taken to avoid measurement of response near nodal points for the modes to be tested. Such measurements would consist primarily of noise, since the actual response is very small near nodal points. In addition, the amplitude of vibration for the response must be kept smaller than the thickness of the specimen in order to minimize air damping and support friction damping.

Since the frequency response function is in terms of the cross- spectrum [35], the coherence function, which is the ratio of the response power caused by the applied input to the measured response power [32], can be computed at the same time. The value of the coherence function is equal to 1 when the measured response is caused totally by the measured input. The coherence value is less than 1 when the measured response is greater than that due to the measured input, which means that extraneous noise or nonlinearities are contributing to the output power. Every transfer function should be accompanied by a coherence check.

3.3.3 DATA REDUCTION

A.- Forced Sinusoidal Vibration Technique

The forced sinusoidal technique was used to check the results from the new techniques. Data reduction for this test was carried out by using the HP-85 micro-computer.

The basic equations used to find the loss factor and the storage modulus are based on the ratio of the base to tip amplitudes at resonance [48] and on the frequency equation for a cantilever beam vibrating in its nth mode [30,49], respectively:

The flexural loss factor is found from [48,50]:

$$\eta = \frac{C_n \phi_n(x_o) \ddot{a}_b}{\phi_n(S) \omega_n^2 a(x_o)} \tag{3.5}$$

The flexural storage modulus is;

$$E' = \frac{4\pi^2 S^4 A \rho f_n^2}{\lambda_n^4 I} \tag{3.6}$$

The flexural loss modulus is then:

$$E'' = \eta E' \tag{3.7}$$

B.- Random and Impulse Techniques

The loss factor at resonant frequency f_n is obtained with the half-power bandwidth technique:

$$\eta = \frac{\Delta f}{f_n} \tag{3.8}$$

The half power points are found at 3 dB below the peak value of the transfer function for a specific mode when a logarithmic scale is used, or at 0.707 of this peak value when a linear scale is used. The data reduction is carried out by using a Hewlett Packard HP-85 microcomputer which is connected to the FFT analyzer using the HP-IB interface. After the desired number of ensemble averages, the desired transfer function is displayed on the screen of the FFT. The computer program "DAMP" (Reference [53]) reads the binary values from the memory of the FFT, makes the corresponding transformations to the current scale, finds the points on either side of the half-power points, and finds the half-power points by interpolation. The resonant frequency and the half-power bandwidth are then used in Eq. 3.8 to find the loss factor, while the flexural storage modulus and loss modulus are obtained using Eqs. 3.6 and 3.7 respectively. A different frequency equation is required for extensional vibration, however. The coherence value at resonance is recorded in each measurement.

3.3.4 RESULTS

The descriptions of the specimens used in developing the technique are given in Table 3.10. Double cantilever beam specimens of aluminum, graphite/epoxy[1] (12 plies, continuous), chopped glass fiber reinforced polyester[2] and unreinforced epoxy[3] were used for the three techniques. Free-free beam specimens of aluminum (lowest loss factor) and glass/polyester (high loss factor) were used to perform another variation of the impulse technique.

The results are presented in figures for each one of the materials used. Fig. 3.25 shows the variation of loss factor of the aluminum cantilever specimen at four resonant frequencies for the three techniques compared with the theoretical curve of the Zener thermoelastic theory. This is a severe test of the apparatus, since composite damping is much greater than that of aluminum. In all three techniques, acceptable values for the first three modes were obtained, and this reinforces the validity of the forced sinusoidal technique as reference. In the fourth mode, the values are consistently greater than the predicted values, which probably means that another physical mechanism is present in addition to the thermoelastic mech-

---

[1] Sp 322 T300. Manufactured by 3M Company, 3M Center, St. Paul, Minnesota 55101.

[2] PPG-SMC-R65. Manufactured by PPG Industries, Fiber Glass Division, Pittsburg, PA 15222

[3] Epoxy for 3M Sp 322 graphite/epoxy prepreg tape, manufactured by 3M Company.

anism. Other possible mechanisms are grain boundary viscosity, point defect relaxations, eddy current effects, stress-induced ordering, and electron effects [17].

In Figs. 3.26, 3.27 and 3.28, the results for the forced sinusoidal, random and impulse techniques for glass/polyester, graphite/epoxy and unreinforced epoxy specimens, respectively are shown. The values obtained for each mode are comparable between the three techniques with acceptable data scatter.

Additional data were obtained by testing aluminum and glass/polyester free-free beam specimens using the impulse technique (Fig. 3.29). For very low damping (aluminum), the results are not acceptable. Experimental values, which are high with respect to the predicted values, indicate the presence of nonlinearities (probably from the nylon wires). For high material damping, this technique gives reasonable values with the additional advantage that it can be used to analyze more than five modes.

The coherence values recorded after ensemble averages for the random and impulse techniques had a large scatter, going from as low as 0.4 to 1 depending on the mode analyzed and the material of the specimen tested. The low modes generally had lower coherence compared with higher modes. In the same way, low damping materials had lower coherence than the high damping materials. Since the damping values so obtained show good agreement with those obtained using the technique of reference,

the relationship between the value of the coherence function and validity of the damping measurements is not very clear.

3.3.5 CONCLUSIONS ON CALIBRATION TESTS

a.- The new random and impulse techniques give acceptable experimental results based on comparison with the previously developed sinusoidal technique.

b.- Both new techniques are faster and easier to use than the previously developed sinusoidal technique.

c.- The random technique requires equipment that may not be available for in-situ tests of structures, whereas the impulse technique can be easily used for such tests.

d.- The amplitude of vibration must be kept below the thickness of the specimen in order to minimize air damping and support damping. This is more easily accomplished by using the impulse technique than by using either the random or forced sinusoidal techniques.

e.- All things considered, the impulse technique with cantilever beam specimens was selected for the following tests of this research.

3.3.6 ADDITIONAL IMPROVEMENTS ON THE IMPULSE TECHNIQUE

a.- The hand-held hammer used to excite the specimen produced some variability in successive measurements. This problem

was solved by replacing the hand-held hammer with a solenoid-type electromagnetic exciter (Fig. 3.30), which gives a more reproducible impulse, while the nonlinearities and extraneous noises were minimized (the coherence value was improved).

b.- The amplitudes of vibration were sufficiently low with the electromagnetic exciter that the epoxy shoulders on the single cantilever beams or in the double cantilever beams specimens were not necessary. The results of the experimental values obtained using specimens with and without shoulders are shown in Fig. 3.31.

c.- The input using the electromagnetic-hammer is nearly constant so that the response spectrum is nearly the same for repeated tests. The shape of the transfer function spectrum after ensemble averaging tends to approach that of the single test response spectrum in the vicinity of the resonant peaks. In addition, the loss factors obtained using the bandwidth method on the response spectrum do not vary with respect to those values obtained using the transfer function (Fig. 3.32). The advantages of using the response spectrum can be summarized as follows:

1.- Data scatter is reduced, and,

2.- The experimental procedure is faster, since it is not necessary to perform ensemble averages at all.

3.3.7 GENERAL TEST PROCEDURE FOR DAMPING MEASUREMENTS

The impulse technique as described previously was extended for extensional vibration tests for the off-axis fiber composite specimens.

Under transverse or flexural vibration, the beam flexes perpendicular to its own axis to alternately store potential energy in the elastic bending of the beam and then release it into the kinetic energy of transverse motion [30]. The normal stress parallel to the beam axis is the only stress acting on the beam. When the specimens used are aligned fiber composite materials, complex moduli can be determined directly from this test. In the case of the off-axis specimens, the normal stress can induce both normal and shear strain and correction for various coupling effects, such as flexural-torsional effects, would be necessary before comparing with theoretical prediction. Thus the isolation of damping due only to flexural deformation appeared to be very difficult. Extensional vibrations eliminate flexure-torsion coupling effects, but both normal and shear strains are still present. The tensor transformations in the theoretical off-axis analysis in Section 2.2 take this into account, however. Thus, the complex moduli obtained by this method can be compared directly with predicted values.

The following two sections describe the general procedure for each one of these techniques as they were used in this research.

A.- Flexural vibration tests

The block diagram of the flexural vibration apparatus is shown in Fig. 3.33. Small beam specimens were tested under transverse vibration. An aluminum foil target of 3/8" (9.53 mm) diameter was placed on each specimen at a distance equivalent to 70% of the effective length of the specimen from the clamped end. The effective length in a cantilever beam is the length from the clamp to the free end. The aluminum target is needed because the eddy current probe used to sense the response works only with metallic surfaces.

The signals from the response transducer and the force transducer attached to the tip of the electromagnetic hammer are fed into the FFT Analyzer as explained previously in this chapter. The computer program "DAMP" (Reference [53]), was used for data acquisition and reduction. The input data to run this program are the length, width and thickness of the specimen, the density obtained from the ASTM standard test D-792-66, the temperature at the time of the test, and the fiber and void volume fraction. The next step is to set the front panel of the FFT Analyzer for the impulse technique: sensitivity of channels

A and B, frequency mode, frequency span, type of spectrum, window function and scale.

After the frequencies for the first four modes were determined, the zoom feature of the FFT Analyzer was used to isolate each mode one by one. Three to four measurements were done for each mode of every specimen. The computer program makes the corresponding calculations and the hard copy of the output shows the resonant frequency, the loss factor, and the storage and loss modulus. The coherence function is printed only if tne transfer function is used to calculate the loss factor. The storage modulus is calculated by using the resonant frequency for the mode under consideration and the frequency equation (Eq. 3.6) for a cantilever beam.

The set up used for this test is shown in Fig. 3.34.

B.- Extensional vibration tests

The block diagram of the extensional vibration apparatus for longitudinal vibrations is shown in Fig. 3.35. Small beam specimens with masses attached at each end were used with this technique (Fig. 2.4). Changes of length of the beam and the masses are necessary in order to maintain the frequency of the first mode inside the range of interest for this research. This is accomplished with the help of a computer program written in BASIC for the Hewlett Packard HP-85 micro-computer. This program calculates the eigenvalue for the mode of interest, and

by varying the masses or the length of the beam, the estimated value for the resonant frequency is obtained. This calculation is repeated until the estimated value is close to the pre-defined resonant frequency to be used in the tests.

This technique was used for characterization of damping as a function of fiber orientation. The impulse technique was used again but the beam-mass assembly was suspended from a steel bracket with nylon wires attached at each concentrated mass. The specimens were excited longitudinally with the electromagnetic hammer, while the response was measured with a piezoelectric accelerometer.

Data acquisition and reduction were the same as for the flexural vibration, except that Eq. 3.9 was used to calculate the apparent storage modulus along the axis of the beam, and the values for each one of the masses were part of the input for the program "DAMP".

$$E' = \frac{4\pi^2 S^2 \rho f_n^2}{\lambda_n^2} \tag{3.9}$$

The set-up of the equipment used in this test is shown in Fig. 3.36.

3.4 POISSON RATIO DETERMINATION

The Poisson's ratios for the matrix and the composite materials are needed for the micromechanics model used for comparison with the experimental results.

Poisson's ratios for the bare resin specimens and for the composite materials were obtained by static loading the same small beam specimens of dimensions 8" (203.2 mm) long x 0.75" (19.05 mm) wide and 12 plies thick for the composite materials or 1/8" (3.175 mm) for the resin specimens.

SR-4 strain gages type FAET-12A-12513L[1] were installed on the specimens in two quarter Wheatstone bridge circuits. A Hounsfield tensometer was used to apply load to the specimens. A HP 3947A data acquisition system interfaced with a HP 9836 desk-computer was used to sense the imbalance in the bridges when the load was applied. Using a computer program, the longitudinal and transverse strains were obtained and Poisson's ratio was calculated from the slope of the line formed by plotting longitudinal versus transverse strains.

Equation 3.10 is the mathematical expression for Poisson's ratio [27] which is the negative of the ratio of the transverse to the longitudinal strains.

$$\nu = -\frac{\varepsilon_T}{\varepsilon_L} \tag{3.10}$$

---

[1] Fabricated by BLH Electronics, 42 Fourth Av., Waltham, Mass 02154

The results are plotted in Fig. 3.37 for Fiberite 934 resin, Fig. 3.38 for AVCO 5505 resin, Fig. 3.39 for graphite/epoxy composite, Fig. 3.40 for Kevlar/epoxy composite and in Fig. 3.41 for boron/epoxy composite.

4.0 TESTS ON NEAT RESIN SPECIMENS

The dynamic properties of neat resin are needed, as stated before, as input data for the micromechanics model used to predict the dynamic properties of composite materials. The matrix is assumed to be linearly viscoelastic in shear but linearly elastic in dilatation, thus the bulk modulus is real, non-dissipative and frequency-independent while the shear modulus is complex, dissipative and frequency-dependent [49]. Under these assumptions, the complex modulus for the matrix as a function of frequency was needed for the analysis of composite specimens at different resonant frequencies.

Two types of epoxy resin are used in the pre-preg tapes used in the fabrication of the composite specimens. Fiberite 934 resin is a component of the graphite/epoxy and kevlar/epoxy pre-preg tapes and 5505 AVCO resin is in the boron/epoxy pre-preg tape. Resin castings were produced as described in section 3.1.

Six small cantilever beam specimens for each r[illegible]ere tested under flexural vibration, as explained in section 3.3.7 part A. The geometric and physical properties of the specimens are given in Table 4.1, where each dimension is the average value of all specimens of the same group and material.

With the flexural test, dynamic properties of the resin for the first four modes were obtained. The resonant frequency

for the fourth mode had a maximum value of 900 Hz, which was enough for analysis of the aligned fiber composites. The resonant frequencies for the first modes in the tests done with off-axis fiber composite specimens under extensional vibration, were larger than 900 Hz, so the dynamic properties of the matrix in this range were also needed. Extensional vibration tests, as described in section 3.3.7 part B, were used with Fiberite 934 resin specimens (Table 4.2), since graphite/epoxy and Kevlar/epoxy are the only off-axis composite specimens tested.

Since the resin is highly hygroscopic, the tests were done as soon as the specimens were fabricated with the least possible time between operations (curing, cutting and testing). Thus, moisture absorption should have no effect on the results.

4.1 FIBERITE 934 RESIN CASTING

The tests were done at an average temperature of 70° F $\pm$ 2 °F (21 °C $\pm$ 1 °C) and a humidity of 40% $\pm$ 2%. Sample outputs of the tests are included in Appendix C of Reference [53].

Figs. 4.1 and 4.2 show the variation of storage modulus and loss factor with frequency and the respective curve-fitting done using the computer program "CURVE" from the standard pack of the HP-85 micro-computer. The experimental data for the storage modulus were fitted with a linear regression given by Eq. 4.1:

$$E'_m = 571252.737 + 55.647 \times f \text{ (psi)} \qquad (4.1)$$

Where f is the frequency in cycles per second (Hz).

For high frequencies, care must be taken since the small beam specimens show a drop in the effective storage modulus due to the presence of shear deformation. The analysis leading to the frequency equation in section 2.3 neglects shear, however.

The logarithmic regression found for the loss factor is given by Eq. 4.2.

$$\eta_m = 0.004 + 0.006 \times \text{Ln } (f) \qquad (4.2)$$

The loss factor as seen in Fig. 4.2 shows a large rate of change for low frequencies followed by a small rate of change up to the largest frequency of the test, 1400 Hz.

It is important to point out that both tests used with this resin: (flexural and extensional vibrations) show consistent results due to the overlap obtained with storage modulus and loss factor data in Figs. 4.1 and 4.2, respectively.

4.2 AVCO 5?05 RESIN CASTING

Only the flexural vibration was performed to find the dynamic properties for this resin. Six specimens (Table 4.1) were tested at an average temperature of 72° F (22 °C) and a humidity of 41% following the same procedure as for the Fiberite 934 resin castings.

Sample output of the data for these tests is given in Reference [53]. Figs. 4.3 and 4.4 show the experimental data for storage modulus and loss factor with its respective curve-fit.

The curve fitting of the data with "CURVE" gives a linear equation for the storage modulus, Eq. 4.3 and an exponential equation for the loss factor, Eq. 4.4.

$$E'_m = 570140.406 + 14.943 \times f \text{ (psi)} \tag{4.3}$$

$$\eta_m = 0.019 \times f^{0.096} \tag{4.4}$$

Where f is the frequency in cycles per second (Hz)

5.0 TESTS ON DISCONTINUOUS ALIGNED FIBER REINFORCED COMPOSITES

In this chapter, the experimental results will be presented and compared with predictions from the micromechanics analysis [5,14] as shown in Chapter 2. Flexural vibration of small cantilever beam specimens (Fig. 3.33) was the technique used to test the discontinuous aligned fiber reinforced composites of three types: graphite/epoxy, Kevlar/epoxy and boron/epoxy. The geometry and physical properties for the specimens tested are given in Table 4.1. Data reduction was carried out using the computer program "DAMP", while for comparison purposes and curve fitting needed to find the best agreement between the experimental results and the predicted curves, the computer program "OFFTRI" was used (Reference [53]).

5.1 EXPERIMENTAL RESULTS

Three tests were done for each mode on every specimen. Six specimens for each fiber aspect ratio (fiber length/fiber diameter) for each composite material: graphite/epoxy, Kevlar/epoxy and boron/epoxy were tested under a room temperature fo 70° F $\pm$ 2 °F (21 °C $\pm$ 1 °C) and humidity of 40% $\pm$ 2%. Sample outputs for each test are shown in Appendix C of Reference [53].

Tables 5.1, 5.2 and 5.3 give the experimental results for the first three flexural modes for graphite/epoxy, Kevlar/epoxy

and boron/epoxy, respectively. Each value in this table is the average of 18 data values (6 specimens and 3 tests done on each one).

In Figs. 5.1, 5.2 and 5.3 the storage modulus for each composite material is plotted against frequency while in Figs. 5.4, 5.5 and 5.6 the loss factors vs frequency are presented.

For comparison with experimental data, Eqs. 2.16 and 2.17 are used to generate the predicted curves. As predicted [6,51] the storage modulus is essentially independent of frequency, while it decreases with decreasing fiber length. The loss factor increases with increasing frequency and decreasing fiber length.

The experimental data for the first resonant frequency was manipulated in order to present dimensionless ratios of the composite storage modulus E'_L to the matrix storage modulus E'_m and the composite loss modulus E''_L to the matrix loss modulus E''_m. Respective data scatter is also shown in Tables 5.4, 5.5 and 5.6. The matrix properties are estimated from Eqs. 4.1 and 4.2 for the case of graphite/epoxy and Kevlar/epoxy and from Eqs. 4.3 and 4.4 for the case of boron/epoxy. The frequencies used for these calculations correspond to the average of all first resonant frequencies of the specimens tested.

Figs. 5.7, 5.8 and 5.9 show the variation of the ratio E'_L/E'_m with fiber aspect ratio experimentally and theoretically.

Figs. 5.10, 5.11 and 5.12 show the variation of loss factor with fiber aspect ratio experimentally and theoretically.

Figs. 5.13, 5.14 and 5.15 show the variation of the estimated values of E''_L / E''_m obtained experimentally with respect to fiber aspect ratio in comparison with the predicted theoretical curves.

The predicted curves were plotted using, as stated before, the computer program "OFFTRI" with the following input:

a.- Type of resin:

Fiberite 934 resin for graphite/epoxy and Kevlar/epoxy

AVCO 5505 resin for boron/epoxy

b.- Frequency of the first resonant frequency:

54 Hz for graphite/epoxy

38.75 Hz for Kevlar/epoxy

51.62 Hz for boron/epoxy

c.- Type of fiber packing array considered:

Square array for all cases. As shown in [6], there is almost no difference in the predicted results using square or hexagonal packing array.

d.- Storage modulus for the fiber (values given by the manufacturers):

For T300 graphite filament: 33 x 10 psi (227.37 GPa)

For Kevlar filament: 18 x 10 psi (124.02 GPa)

For boron filament: 58 x 10 psi (399.62 GPa)

e.- Bulk modulus for matrix. These values are real and frequency independent [49,52].

$$K_m = \frac{E_m}{3(1 - 2\nu_m)} \tag{5.1}$$

Where: K_m = bulk modulus for matrix

E_m = Static elastic modulus for matrix

ν_m = Poisson ratio for matrix

First Eq. 5.1 was used to find the real and frequency independent bulk modulus for the matrix using the elastic modulus and Poisson's ratio at zero frequency (static properties). Eqs. 4.1 or 4.3 (Fiberite 934 or AVCO 5505 resins), were used for a frequency of 0 Hz. The Poisson's ratio is obtained using the rule of mixtures with the experimental values from chapter 3. Secondly, the frequency-dependent properties as ν_m and G'_m were found using again E' from Eq. 4.1 or Eq. 4.3 at the resonant frequency of interest and Eq. 5.1, for the case of the Poisson's ratio. G'_m was found from Eq. 5.2.

$$G'_m = \frac{3K_m E'_m}{9K_m - E'_m} \tag{5.2}$$

The complete mathematical manipulation is given in Appendix A of Reference [53].

The values were:

For graphite/epoxy composite:

$$E'_m = 5.713 \times 10^5 \text{ psi } (3.936 \text{ GPa}) \text{ (dynamic value)}$$

ν_f = 0.16 (static value)

ν_m = 0.345 (static value)

k_m = 6.143 x 10^5 psi (4.233 GPa) (static value)

For Kevlar/epoxy composite:

E'_m = 5.713 x 10^5 psi (3.936 GPa) (dynamic value)

ν_f = 0.376 (static value)

ν_m = 0.345 (static value)

k_m = 6.143 x 10^5 psi (4.233 GPa) (static value)

For boron/epoxy composite:

E'_m = 5.701 x 10^5 psi (3.928 GPa) (dynamic value)

ν_f = 0.21 (static value)

ν_m = 0.318 (static value)

k_m = 5.221 x 10^5 psi (3.597 GPa) (static value)

f.- Fiber and void volume fraction (v_f, v_v)

graphite/epoxy: 0.654, 0.0036

Kevlar/epoxy: 0.661, 0.0302

boron/epoxy: 0.607, 0.003

The fiber and void volume fractions shown above are the average values of the experimental results obtained by digestion tests of the cured laminate plates fabricated for each composite material (Chapter 3).

g.- Fiber loss factor equal to zero for all three composites since no information about this factor is available (this will be used as a curve-fitting parameter as shown later, however).

As can be seen in Figs. 5.7 through 5.15, the experimental values do not fit the predicted curves. While the experimental values for E'_L/E'_m are smaller and shifted to the right, the experimental values for the loss factor are greater and again shifted to the right.

The next step in the analysis is to find the necessary parameters to best fit the predicted curves to the experimental values.

5.2 CURVE-FITTING

The parameters which had the greatest uncertainties associated with them were used as curve-fitting parameters. For example, due to uncertainties in the values for the elastic modulus of the fiber given by the manufacturers, this parameter was used as a curve-fitting parameter. The values given by the manufacturers are based on bare fibers and apparently there is a reduction in the fiber properties in the pre-preg material. This parameter shifts the curves in Figs. 5.7 to 5.9 up and down.

The fibers do contribute damping, but, since no information on fiber loss factors is available, this is another parameter used for curve-fitting. The fiber loss factor was assumed to be independent of frequency, however. Variation of the fiber loss factor shifts the curves in Figs. 5.10 to 5.12 up and down.

The Force-balance model is based on a single fiber 6 . However, the influence of contiguous fibers in fiber bundles is not known, so an "effective fiber aspect ratio", $(1/d)_{eff}$, is introduced as given in Eq. 5.3.

$$(\ell/d)_{eff.} = (\ell/d)Z \tag{5.3}$$

Where Z is a curve fitting parameter that shifts the curves from Figs. 5.7 through 5.12 to the left or to the right.

Varying these parameters one at a time and using the computer program "OFFTRI" a good fit was obtained with the following values:

For graphite/epoxy composite:

$E'_f = 25.51 \times 10^6$ psi (175.76 GPa)

Manufacturer's value: 33×10^6 psi (227.36 GPa)

$\eta_f = 0.0015$

$Z = 0.03$

For Kevlar/epoxy composite:

$E'_f = 14.48 \times 10^6$ psi (99.767 GPa)

Manufacturer's value: 18×10^6 psi (124.02 GPa)

$\eta_f = 0.011$

$Z = 0.03$

For boron/epoxy composite:

$E'_f = 55.43 \times 10^6$ psi (381.913 GPa)

Manufacturer's value: 58×10^6 psi (399.62 GPa)

$\eta_f = 0.0019$

$Z = 0.4$

Where the values for E_f' were obtained by using the rule of mixtures with the experimental results of composite and matrix storage modulus for a continuous fiber [6].

The curves generated by using these values are shown in Figs. 5.16 through 5.27.

Figs. 5.25, 5.26 and 5.27 are the theoretical tridimensional plots for E_L'/E_m', loss factor and E_L''/E_m'' as function of fiber aspect ratio and frequency for graphite/epoxy. These curves are presented for an overall view of the results obtained with these tests.

The predicted loss factor had an optimum value for a very low fiber aspect ratio based on a single fiber (See Figs. 5.19, 5.20 and 5.21), which is not attainable in practice by using discontinuous fibers. Microfibers and whiskers may be in this range, presenting interesting perspectives on optimization of damping. The predicted loss factor increases asymptotically with increasing frequency.

The predicted stiffness is practically frequency independent but decreases with decreasing fiber aspect ratio.

The estimated loss modulus (product of storage modulus and loss factor) has a maximum value at an optimum fiber aspect ratio.

These results should have interesting implications, especially in structures subjected to high frequency vibrations.

The combination of low fiber aspect ratio and high frequencies produces large increases in the damping properties and a comparatively small reduction in stiffness.

Even though good agreement was obtained between the experimental data and the predicted curves after curve fitting, some of the limitations of the model should be mentioned. The model does not consider fiber interaction, since it is based on a single fiber. In addition, it does not consider interface effects that can have substantial influence on the shear strains.

6.0 TESTS ON OFF-AXIS FIBER REINFORCED COMPOSITES

These tests were done in order to prove whether, as predicted [25], there is maximum damping for an optimum fiber direction.

Flexural vibration was not used to characterize damping in off axis fiber specimens since mixed modes would have been present due to coupling of torsional and shear deformation and extensional deformation due to flexure. Shear deformation has a substantial effect on the natural frequency of the beam, and, of course on the damping [30]. In addition, the isolation of damping due only to the flexural deformation appeared to be very difficult. The solution chosen was to excite the longitudinal modes with an impulsive force at one end of a free-free beam with masses attached at each end, as described in section 3.3.7, part B.

In Ref. [25] it is predicted that for fiber aspect ratios greater than 100, the damping of the off-axis composite becomes independent of the fiber aspect ratio, except for angles below 15 . The lowest fiber aspect ratio,(based on a single fiber) practically attainable from a pre-preg tape of aligned fibers was 226.45 for graphite/epoxy and 132.98 for Kevlar/epoxy. In order to check the prediction above, it was decided to test specimens of 0°, 2.5°, 7.5°, 12.5°, 20°, 45°, 60°, 75° and 90° for two different fiber lengths (continuous and 1/4" (6.35 mm))

using graphite/epoxy composite. Continuous fiber Kevlar/epoxy composite was also tested, since this material had the best damping characteristics (Chapter 5). The geometry and physical properties for the specimens tested are shown in Table 4.2.

The computer program "DAMP" was used for data reduction while the program "OFFTRI" was used to generate the predicted curves.

6.1 EXPERIMENTAL RESULTS

Three tests were done on every specimen under room temperature of 66 ° F $\pm$ 2 °F (18 ° C $\pm$ 1 °C) and humidity of 46% $\pm$ 2%. Sample outputs for each test are shown in Reference [53].

Tables 6.1, 6.2 and 6.3 show the experimental results as functions of the direction of the fibers and the first resonant frequency. The storage modulus was obtained using Eqs. 2.39 and 2.40, the loss factor as explained in chapter 3, using the halfpower points and the bandwidth technique, and the loss modulus by simple multiplication of the storage modulus and the loss factor.

For comparison with the predicted curves, the dimensionless ratio of E'_x / E'_m, the loss factor and the dimensionless ratio of E''_x / E''_m are plotted against direction of the fibers in Figs. 6.1 through 6.9 for continuous and discontinuous fiber graphite/epoxy and continuous fiber Kevlar/epoxy specimens.

The predicted curves are plotted using the real and imaginary parts of Eq. 2.21 (Reference [53]) and the computer program "OFFTRI" with the following input:

a.- Type of resin: Fiberite 934 resin

b.- Frequency of the tests:

Graphite/epoxy: continuous fiber 1152.5 Hz

Discontinuous fiber 1206.15 Hz

Kevlar/epoxy: 895.1 Hz

c.- Type of fiber packing array: Square array in all cases

d.- Storage modulus for the fiber:

For T300 graphite filament: 33×10^6 psi (227.37 GPA)

For Kevlar filament: 18×10^6 psi (124.02 GPa)

e.- Bulk modulus for matrix:

Graphite/epoxy composite: $K_m = 6.143 \times 10^5$ psi (4.233 GPa)

Kevlar/epoxy composite: $K_m = 6.143 \times 10^5$ psi (4.233 GPa)

f.- Fiber and Void volume fraction (v_f , v_v)

Graphite/epoxy composite: continuous fiber 0.675, 0.002

Discontinuous fiber 0.678, 0.0067

Kevlar/epoxy composite 0.715, 0.0138

g.- Fiber loss factor equal to zero in all cases

h.- Halpin-Tsai parameters:

2 for the transverse modulus

1 for the shear modulus [3]

i.- Fiber aspect ratio:

Graphite/epoxy continuous fiber: 10,870 corresponding to 3" (76.2 mm) fiber length.

Graphite/epoxy discontinuous fiber: 905.8 corresponding to 1/4" (6.35 mm) fiber length.

Kevlar/epoxy continuous fiber: 3191.5 corresponding to 1.5" (38.1 mm) fiber length.

j.- Parameter that changes the fiber aspect ratio: Z=1

As seen in Figs. 6.1 through 6.9, the experimental values do not fit the predicted curves. For E'_x /E'_m the experimental values are smaller and shifted to the left. The loss factors are smaller from 90° down to 5° where they cross over the predicted curves. The necessity of using parameters that can be varied until the predicted curves fit with the experimental values is evident.

6.2 CURVE-FITTING

The first parameters introduced were those that best fit the predicted curves in the previous case of aligned discontinuous fiber (fiber angle θ= 0°) as given in Chapter 5. These values are:

a.- Fiber storage modulus:

For graphite/epoxy: 25.51 x10^6 psi (175.76 GPa)

For Kevlar/epoxy: 14.48 x 10^6 psi (99.767 GPa)

b.- Fiber loss factor:

For T300 Graphite filaments: 0.0015

For Kevlar filaments: 0.011

c.- Parameter for the effective fiber aspect ratio, Z equal to 0.03 for both composite materials.

These parameters corrected the curves for the 0 fiber direction. The remainder of this section deals with curve-fitting for other fiber angles up to 90°.

Up to this point the fibers have been considered to be isotropic. The next step was to consider the anisotropy of the fibers by introducing the transverse and shear moduli for the fiber as parameters for curve-fitting [29], as shown in Eqs. 2.29 and 2.30. That is, the fiber is assumed to be orthotropic and transversely isotropic. In the same way, the Halpin-Tsai parameters may be varied independently until a good fit can be obtained.

The final values obtained were:

a.- Transverse modulus for the fiber:

T300 graphite filament: 2×10^6 psi (13.78 GPa)

Kevlar filament: 1×10^6 psi (6.89 GPa)

b.- Shear modulus for the fiber:

T300 graphite filament: 4×10^6 psi (27.56 GPa)

Kevlar filament: 2×10^6 psi (13.78 GPa)

c.- Halpin-Tsai parameters:

Graphite/epoxy: 2 for transverse modulus and
4 for shear modulus

Kevlar/Epoxy: 2 for transverse modulus and
1 for shear modulus.

It has to be mentioned that when fiber anisotropy was introduced, the transverse loss modulus of the fiber was obtained by the product of the transverse storage moduli of the fiber and the extensional fiber loss factor. More research has to be done in this area since the transverse loss factor for the fiber should be different from the extensional loss factor.

Figs. 6.10 through 6.18 show the experimental values with the best predicted curves. It is interesting to note that the stiffness is maximum at 0 ° and continuously goes down, rapidly up to about 30 ° and then slowly up to 90°. The loss factor increases up to a maximum for an optimum fiber direction of approximately 30 ° then decreases slowly with increasing fiber direction. The loss modulus has a maximum between 10° to 15°. These results verify the predictions from [25] in the cases of graphite/epoxy composite, continuous and discontinuous fiber. For Kevlar/epoxy specimens, the same trend for the curves were obtained, but the results showed a higher damping and lower stiffness than expected. These results may be related to the poor machinability of the specimens that produced delamination along the edges, and, an unexpected variation on the cure cycle for the laminate used for the specimens of 75 ° and 90 ° fiber direction.

These results showed that the influence of off-axis fiber orientation on damping were greater than that of the fiber length.

These results can be better visualized with the tridimensional plots of E'_x / E'_m, loss factor and E''_x / E''_m as functions of fiber direction and fiber aspect ratio for graphite/epoxy, continuous fiber that are shown in Figs. 6.19, 6.20 and 6.21, respectively.

7.0 CONCLUSIONS

This chapter summarizes the principal conclusions obtained during this research. They are separated into three sections: conclusions on the fabrication of the specimens, conclusions on the experimental techniques, and finally, conclusions on the analytical model and the results.

7.1 CONCLUSIONS ON FABRICATION OF THE SPECIMENS

1.- The technique used for cutting the pre-preg tape worked well. For graphite/epoxy and Kevlar/epoxy, fiber lengths as low as 1/16" (1.588 mm) were obtained using a utility knife with stainless steel blades. Boron/epoxy pre-preg tape was fractured with a guillotine device with carbide blade.

2.- The autoclave style-press cure yielded quality plates comparable to those obtained from an autoclave. The density, fiber and void volume fraction, and even loss factor and storage modulus were almost the same for both plates.

3.- Machining of graphite/epoxy and boron/epoxy were done without difficulties, using abrasive and diamond cut-off wheels, respectively. Machining of Kevlar/epoxy specimens had complications since delamination was present at the specimen edges. The use of an electric band saw at high

speed with the saw blade mounted backward gave the best results with this material.

4.- The digestion test was the step with more complications. First of all, there was not enough literature on the subject, so a great amount of time was expended in experimentation. For graphite/epoxy, the ASTM Standard D 3171-76, Procedure A was followed without problems. The same procedure with modifications was used for Kevlar/epoxy. It was noted that Kevlar filaments reacted with the acid and increased their weight, so, the fiber weight in the composite had to be corrected. More complications were experienced with the boron/epoxy composite, since its digestion took over 16 hours for completion.

7.2 CONCLUSIONS ON THE EXPERIMENTAL TECHNIQUE

a.- The impulse technique using the electromagnetic hammer gave reliable loss factor measurements. The reason is because of the nearly constant input that minimizes nonlinearities and extraneous noises. The data scatter was reduced.

2.- The impulse technique is faster than the previously used techniques because of the use of the response spectrum. This eliminates the need for a large number of ensemble averages, as was the case when the transfer function was used for loss factor determination.

3.- Air damping, support damping and friction losses from the apparatus were minimized since the impulse from the electromagnetic hammer kept the maximum amplitude below the thickness of the specimen. This conclusion was also verified by the good results obtained for calibration tests done with aluminum specimens. This was a severe test for the apparatus, since damping of composite materials is much larger than that for aluminum.

4.- The results obtained from the flexural and extensional vibration tests showed good agreement since overlap was obtained.

7.3 CONCLUSIONS ON THE ANALYTICAL MODEL AND EXPERIMENTAL RESULTS

1.- The analytical model is based on a single fiber. The experimental results showed that there may be an influence of fiber bundle effects, since an "effective fiber length" had to be introduced as curve-fitting parameter. Fiber interaction may also contribute to this disagreement between experiment and theory.

2.- In the original analytical model, the fiber and matrix were assumed to be isotropic. The experimental results for off-axis composites showed that the fibers are anisotropic. The transverse modulus and shear modulus for the fiber had to be used as curve-fitting parameters.

3.- Experimental results showed that fibers do contribute to damping. The fiber loss factor had to be treated as a curve-fitting parameter, since data on loss factors of fibers are not available.

4.- The analytical model does not consider interface effects, which may be partly responsible for the "fiber damping".

5.- As predicted in [6], discontinuous fiber composite materials give optimum damping for very low fiber aspect ratios (based on a single fiber) not attainable in this research. These aspect ratios are in the range of whiskers and microfibers, however.

6.- The results showed, as predicted in [25], that even better damping can be obtained with off-axis fiber orientation, at the expense of reduced stiffness.

7.- The results showed that the Kevlar/epoxy composite has the best damping properties, while the boron/epoxy composite has the best stiffness properties.

Much work has to be done, and there are still questions that have to be answered. For example, the analytical model should account for fiber interaction and interface effects. In any case, the results obtained from this research verify the excellent properties and unlimited versatility of fiber reinforced composite materials.

REFERENCES

[1] Schwartz, M.M., Composite Materials Handbook, Mc Graw-Hill Inc,1984.

[2] Agarwal, B.D. and Broutman, L.J., Analysis and Performance of Fiber Composites, John Wiley Sons, Inc, 1980.

[3] Jones, R.M., Mechanics of Composite Materials, Scripta Book Company, 1975.

[4] ASTM Standardization News, December 1983.

[5] Short Fiber Reinforced Composite Materials, ASTM Special Technical Publication 772, American Society for Testing and Materials, Philadelphia, Pa., 1982.

[6] Gibson, R.F., Chaturvedi, S.K. and Sun, C.T., "Complex Moduli of Aligned Discontinuous Fibre-Reinforced Polymer Composites", Journal of Materials Science, 17, 1982, pp. 3499-3509.

[7] Gibson, R.F., "Recent Research on Dynamic Mechanical Properties of Fiber Reinforced Composite Materials and Structures", The Shock and Vibration Digest, 15 (2), February 1983.

[8] Puppo, A.H. and Evensen, H.A., "Interlaminar Shear in Laminated Composites Under Generalized Plane Stress", Journal of Composite Materials, 4, 1970, pp. 204-220.

[9] Pipes, R.B. and Pagano, N.J., "Interlaminar Stresses in Composite Laminates-An Approximate Elasticity Solution", Journal of Applied Mechanics, 41, 1974, pp. 668-672.

[10] Schultz, A.B. and Tsai, S.W., "Measurements of Complex Dynamic Moduli for Laminated Fiber-Reinforced Composites", Journal of Composite Materials, 3, July 1969, pp. 434-443.

[11] Bert, C.W. and Clary, R.R., Composite Materials: Testing and Design (3rd Conference), ASTM STP 546, The American Society for Testing and Materials, Philadelphia, 1974, pp. 250-265.

[12] Gibson, R.F. and Plunkett, R., "Dynamic Stiffness and Damping of Fiber-Reinforced Composite Materials", Shock and Vibration Digest, 9 (2), February 1977, pp. 9-17.

REFERENCES (continuation)

[13] Gibson, R.F. and Wilson, D.G., "Dynamic Mechanical Properties of Fiber-Reinforced Composite Material", Shock and Vibration Digest, 11 (10), October 1979.

[14] Bert, C.W., Damping Applications for Vibration Control, ASME AMD-38, American Society of Mechanical Engineers, New York 1980, pp. 53-63.

[15] Gibson, R.F. and Yau, A., "Complex Moduli of Chopped Fiber and Continuous Fiber Composites: Comparison of Measurements with Estimated Bounds", Journal of Composite Materials, 14, April 1980, pp. 155-167.

[16] McLean, D. and Read, B.E., "Storage and Loss Moduli in Discontinuous Composites", Journal of Materials Science, 10, 1975, pp. 481-492.

[17] Lazan, B.J., Damping of Materials and Members in Structural Mechanics, Pergamon Press, Oxford, England, 1968

[18] Hashin, Z., "Complex Moduli of Viscoelastic Composites. I. General Theory and Application to Particulate Composites", Int. Journal of Solids Structures, 6, 1970, pp. 539-552

[19] Gibson, R.F., Yau, A. and Riegner, D.A., "Vibration Characteristics of Automotive Composite Materials", Short Fiber Reinforced Composite Materials, ASTM STP 772, B.A. Sanders, Ed., American Society for Testing and Materials, 1982, pp. 133-150.

[20] Gibson, R.F., Yau, A., Mende, E.W. and Osborn, W.E., "The Influence of Environment Conditions on the Vibration Characteristics of Chopped Fiber Reinforced Composite Materials", Journal of Reinforced Plastics and Composites, 1 (3), July 1982, pp. 225-241

[21] Cox, M.A.,"The Elasticity and Strength of Paper and other Fibrous Materials", British Journal of Applied Physics, Vol. 3, 1952, pp. 72-79

[22] Holister, G.S. and Thomas, C., Fibre Reinforced Materials, Elsevier, England, 1st ed.,1966.

[23] Kelly, A., Strong Solids, Oxford University Press, 1st ed.,1966

[24] Chamis, C.C., "Mechanics of Load Transfer at the Interface", Composite Materials, 6, Academic Press, New York, 1974

REFERENCES (continuation)

[25] Sun, C.T., Gibson, R.F. and Chaturvedi, S.K., "Internal Material Damping of Polymer Matrix Composites under Off-Axis Loading", Journal of Materials Science, in print.

[26] Hashin, Z., "Analysis of Properties of Fiber Composites with Anisotropic Constituents", Journal of Applied Mechanics, 46, September 1979, pp. 543-550

[27] Dally, J.W. and Riley, W.F., Experimental Stress Analysis, McGraw-Hill Book Company, 1965

[28] Kriz, R.D. and Stinchcomb, W.W., "Elastic Moduli of Transversely Isotropic Graphite Fibers and their Components", Experimental Mechanics, 19, 1979, pp. 41-49

[29] Whitney, J.M., "Elastic Moduli of Unidirectional Composites with Anisotropic Filaments", Journal of Composite Materials, 1, 1967, pp. 188-193

[30] Blevins, R.D., Formulas for Natural Frequency and Mode Shapes, Van Nostrand Reinhold Company Inc, New York, 1979, pp. 101-200

[31] Seto, W., Theory and Problems of Mechanical Vibrations, Shaum Publishing c.o., New York, 1964

[32] Ramsey, K.A., "Effective Measurements for Structural Dynamics Testing, Part 1", Sound and Vibration, 9 (11), November 1975, pp. 24-35

[33] Thomson, W.T., Theory of Vibrations With Applications, Prentice Hall, Inc., Englewood, Cliffs, N.J.,1981

[34] Meirovitch, L., Elements of Vibration Analysis, McGraw-Hill, Inc, 1975.

[35] Halvorsen, W.G. and Brown, D.L., "Impulse Technique for Structural Frequency Response Testing", Sound and Vibration, April 1976, pp. 8-21

[36] Lang, G.L., "Understanding Vibration Measurements", Nicolet Scientific Corporation, Application Note 9, December 1978

[37] Gibson, R.F., "Vibration Damping Characteristics of Graphite/Epoxy Composites for Large Space Structures", Large Space Systems Technology-1981, NASA Conference Publication 2215 Part 1, pp. 123-132

REFERENCES (continuation)

[38] Gibson, R.F., "Development of Damping Composite Materials", 1983 Advances in Aerospace Structures, Materials and Dynamics, AD-06, American Society of Mechanical Engineers, 1983.

[39] Decbald, L.R., Gibson, R.F. and Suarez, S.A., "Techniques for Fabrication and Volume Fraction Determination of Fiber Reinforced Polymer Composite Materials", Internal Report, Mechanical Engineering Department, University of Idaho, May 1984.

[40] Gibson, R.F, Deobald, L.R. and Suarez, S.A., "Laboratory Production of Discontinuous-Aligned Fiber Composite Plates Using an Autoclave-Style Press Cure", Submitted to Composites Technology Review, July 1984.

[41] McDonnell Douglas, "Process Specification", P.S. 21332, March 19, 1975, PP. 5.

[42] Suarez, S.A., Gibson, R.F. and Deobald, L.R., "Development of Experimental Techniques for Measurement of Damping in Composite Materials", SESA, 1983 Fall Meeting Procedings, November 1983, pp 55-60.

[43] Gibson, R.F. and Plunkett, R., "A Forced Vibration Technique for Measurement of Material Damping", Experimental Mechanics, 11 (8), August 1977, pp 297-302.

[44] Gibson, R.F., Yau, A. and Riegner, D.A., "An Improved Forced- Vibration Technique for Measurement of Material Damping" Experimental Techniques, 6 (2), April 1982, pp 10-14.

[45] Granick, N. and Stern, J.E., Material Damping of Aluminum by a Resonant Dwell Technique, NASA TN-D-1467, 1965.

[46] Crandall, S.H., On Scaling Laws for Material Damping, NASA TN-D-1467, 1962.

[47] Ramsey., K.A., Effective Measurements for Structural Dynamic Testing, Part II", Sound and Vibration, of, 10 (4), April 1976, pp. 18-31.

[48] Yau, A., Experimental Techniques for Measuring Dynamic Mechanical Behavior of Composite Materials, M.Sc. Thesis, University of Idaho, July 1980.

REFERENCES (continuation)

[49] Gibson. R.F. and Plunkett, R., "Dynamical Mechanical Behavior of Fiber-Reinforced Composites: Measurement and Analysis", Journal of Composite Materials, 10, October 1976, pp. 325-341.

[50] Bishop, R.E.D. and Johnson, D.C., The Mechanics of Vibration, Cambridge University Press, 1960.

[51] Bert, C.W., "Composite Materials: a Survey of the Damping Capacity of Fiber Reinforced Composites", Damping Applications for Vibration Control, AMD-Vol. 38, The American Society of Mechanical Engineers, 1978, pp. 53-63.

[52] Mazza, L.T., Paxson, E.B. and Rodgers, R.L., "Measurement of Damping Coefficients and Dynamic Modulus of Fiber Composites", VSAAVLABS Technical Note 2, U.S. Army Aviation Material Laboratories, Fort Eusties, Virginia, February 1970.

[53] Suarez, S. A., "Optimization of Internal Damping in Fiber Reinforced Composite Materials", Ph.D. Dissertation, University of Idaho, October, 1984.

TABLE 3.1

List of layup materials used in the vacuum mold

Material	Trade Name
Bleeder cloth (polyester breather)	Air Weave N-4
Release fabric (porous teflon-coated fiberglass, 0.003" thick)	Release Ease 234 TFP
Vacuum bag (nylon, 0.002" thick)	Wrightlon 7400.002
Rubber Dam	Air Pad[1]
Releasing agent	Frekote 33[2]
Prepreg graphite/epoxy	Fiberite Hy-E1034C[3]
Prepreg Kevlar/epoxy	Fiberite Hy-E1734A2[3]
Prepreg boron/epoxy	AVCO 5505[4]

[1] Airtech International, 2452 E. Del Amo Blvd., P.O. Box 6207. Carson, CA 90749
[2] Frekote Inc., 170 W. Spanish River Blvd., Boca Raton, FL 33431
[3] Fiberite Corporation, 501 W. 3rd St., Winona, MN 55987
[4] AVCO Specialty Materials Division, 2 Industrial Ave., Lowell, MA 01851

TABLE 3.2

Cure cycle for Fiberite Hy-E1034C (graphite/epoxy) and Hy-E1734A2 (Kevlar/epoxy) prepregs. Resin system: Fiberite 934.

1.- Apply vacuum to mold-bag assembly

2.- Heat to 245 °F with a rate of 3 -5°F/minute

3.- Hold 15 minutes at 245 °F.

4.- Apply 100 psi pressure.

5.- Hold 45 minutes.

6.- Heat to 350 °F at a rate of 3 -5°F/minute.

7.- Hold at 350 °F for 2 hours.

8.- Cool to 150 °F under vacuum and pressure for graphite/epoxy (release vacuum and pressure before cooling for Kevlar/epoxy).

TABLE 3.3

Cure cycle for AVCO 5505 boron/epoxy prepreg

1.- Apply vacuum to mold-bag assembly.

2.- Heat to 245 °F at a rate of 4 -6°F/minute.

3.- Hold 30 minutes at 245 °F.

4.- Apply 50 psi pressure.

5.- Heat to 350 °F at a rate of 4 -6°F/minute.

6.- Hold at 350 °F for 2 hours.

7.- Cool to room temperature under vacuum and pressure.

8.- Oven post-cure at 375 °F for 4 hours.

TABLE 3.4

Comparison of volume fractions and density between autoclave and autoclave style press cure for graphite/epoxy composites.

	Autoclave style press cure			Autoclave Cure		
	Density (g/cc)	v_f (%)	v_v (%)	Density (g/cc)	v_f (%)	v_v (%)
1	1.588	65.9	0.12	1.588	67.0	0.28
2	1.587	66.3	0.15	1.565	62.0	0.38
3	1.573	65.1	0.84	1.593	67.1	0.03
4	1.590	66.7	0.03	1.589	68.3	0.64
AVG.	1.585	66.0	0.28	1.584	66.1	0.33

Note.- Graphite/epoxy fabricated from Fiberite Hy-E1034C prepreg.

v_f = fiber volume fraction

v_v = void volume fraction

TABLE 3.5

Cure cycle for Fiberite 934 Resin 350 ° F (177 °C) Cure

1.- Let resin warm overnight to room temperature.

2.- Heat in oven at 80 °C for 1 hour, then pour into vacuum flask.

3.- Apply vacuum while maintaining 80 °C temperature until resin has outgassed.

4.- Preheat mold to 125 °C, then pour resin into mold.

5.- Cure at 100 °C for 16 hours, then at 177 °C for 2 hours.

6.- Removed cured resin plate from mold and allow to cool to room temperature.

TABLE 3.6

Cure cycle for AVCO 5505 Resin 350 °F (177 °C) Cure

1.- Let resin warm overnight to room temperature.

2.- Heat in oven at 125 °C for 30 minutes, then pour into vacuum flask.

3.- Apply vacuum while maintaining 95 °C temperature until resin has outgassed.

4.- Preheat mold to 150 °C, then pour resin into mold.

5.- Cure at 100 °C for 16 hours, then at 177 °C for 2 hours.

6.- Removed cured resin plate from mold and allow to cool to room temperature.

TABLE 3.7

Density determination procedure

American Society for Testing and Materials (ASTM) Standard Test Methods for Specific Gravity and Density of Plastics by Displacement, D-792-66.

Procedure:

1.- Zero analytical balance.

2.- Weigh specimen in air to nearest mg.

3.- Fill 600 ml beaker with distilled water such that clip will be totally submerged.

4.- Weigh glass rod/clip assembly with clip submerged in water (do not allow it to touch side).

5.- Prewet composite specimen then place it in clip. Slowly lower specimen in water as to avoid air bubbles. Use wire to remove air bubbles.

6.- Weigh glass rod/clip/composite assembly.

7.- Record room temperature and pressure.

8.- Use tables to determine ρ_w and ρ_a.

9.- Make the corresponding calculations.

TABLE 3.8

Fiber and void volume fraction determination for graphite/epoxy and Kevlar/epoxy composite specimen.

American Society for Testing and Materials (ASTM) Standard Test Methods for Fiber Content of Reinforced Resin Composites, D 3171-76.

Procedure A:

1.- Determine density by ASTM Standard D 792-66.

2.- Zero analytical balance.

3.- Weigh specimen and crucible to nearest mg.

4.- Place composite specimen in beaker containing 40 ml of 70% nitric acid.

5.- After 5 hours digestion at 75 °C (167 °F) filter complete contents into crucible.

6.- To obtain proper vacuum, let drain tube fill with water by pinching the end.

7.- Rinse beaker into crucible with 20 ml nitric acid and filter a second time.

8.- Rinse 3 times with distilled water and twice with acetone. Rinse beaker each time.

9.- Place crucible on screen in core oven for 1 hour at 100 °C (212 °F).

10.- Cool crucible in desiccator, then weigh.

11.- Make the corresponding calculations.

TABLE 3.9

Fiber and void volume fraction determination for boron/epoxy composite specimen.

Procedure:

1.- Determine density by ASTM Standard D 792-66.

2.- Zero analytical balance.

3.- Weigh specimen and crucible to nearest mg.

4.- Heat 40 ml of concentrated sulfuric acid up to 204 C (400 F) using a hot plate.

5.- Place the specimen in beaker an digest it for 16 hours.

6.- Remove beaker and heat an additional 40 ml of sulfuric acid for rinsing.

7.- Partially fill the vacuum flask with cold water. Pour the contents of the beaker into the crucible and filter the excess acid.

8.- Rinse beaker with the hot sulfuric acid and pour into the crucible for a second rinse.

9.- Let the crucible to cool off for 10 minutes and drain the contents of the vacuum flask. Rinse 3 times with hot distilled water and twice with acetone. Rinse beaker each time.

10.- Place crucible on screen in core oven for 1 hour at 100° C (212 °F).

11.- Cool crucible in dessicator, then weigh.

12.- Make the corresponding calculations.

TABLE 3.10

Description of specimens used for calibration tests.

Specimen	Length in	Length mm	Thickness in	Thickness mm	Density lb/in^3	Density g/cc
Aluminum (cantilever beam)	10.00	254.00	0.125	3.175	0.098	2.718
Aluminum (Free-free beam)	20.00	508.00	0.125	3.175	0.098	2.718
3M SP-322 Graphite/epoxy (Cantilever)	8.00	203.20	0.0655	1.664	0.0536	1.487
PPG-SMC R65 E-glass/polyester (Cantilever beam)	7.75	196.85	0.135	3.429	0.067	1.858
PPG-SMC R65 E-glass/polyester (Free-free beam)	16.00	406.4	0.135	3.429	0.067	1.858
Unreinforced epoxy [1] (Cantilever beam)	8.25	209.55	0.125	3.175	0.0456	1.265

Note.- The aluminum foil targets for the composite materials and unreinforced epoxy cantilever beam specimens are located at 7.375 in (187.3 mm).
Width for all specimens: 0.75 in (19.05 mm)
[1] Resin for 3M SP-322 graphite/epoxy.

TABLE 4.1

Description of discontinuous aligned specimens tested with flexural vibration

No	Fiber Length (in)	(mm)	Width (in)	(mm)	Thickness (in)	(mm)	Density (lb/in^3)	(g/cc)	Vf (%)
				FIBERITE 934 RESIN CASTING					
6	N/A		0.744	18.898	0.123	3.134	0.0469	1.298	N/A
				AVCO 5505 RESIN CASTING					
6	N/A		0.753	19.126	0.119	3.023	0.0445	1.232	N/A
				GRAPHITE / EPOXY					
6	7.5	190.5	0.746	18.948	0.062	1.575	0.0571	1.584	66
6	1/2	12.7	0.76	19.304	0.0588	1.494	0.0571	1.584	66.5
6	1/4	6.35	0.733	18.618	0.06	1.523	0.0572	1.586	66.6
6	1/8	3.175	0.749	19.025	0.061	1.554	0.0568	1.574	64.7
6	1/16	1.588	0.753	19.126	0.0625	1.588	0.0567	1.574	63.2
				KEVLAR / EPOXY					
5	7.5	190.5	0.755	19.177	0.0528	1.341	0.0492	1.362	65.8
5	1/2	12.7	0.755	19.177	0.0542	1.377	0.0487	1.348	68.1
6	1/4	6.35	0.74	18.796	0.0521	1.323	0.0477	1.323	66.7
6	1/8	3.175	0.749	19.025	0.053	1.346	0.049	1.357	67.1
6	1/16	1.588	0.746	18.948	0.0553	1.405	0.0498	1.382	63
				BORON / EPOXY					
6	7.5	190.5	0.745	18.923	0.0459	1.167	0.0743	2.061	63.4
6	2	50.8	0.746	18.923	0.0481	1.221	0.0732	2.031	62.9
6	1	25.4	0.749	19.012	0.0551	1.399	0.0724	2.009	60.4
6	1/2	12.7	0.748	18.991	0.0532	1.351	0.073	2.024	60.2
6	1/4	6.35	0.751	19.075	0.0487	1.237	0.0751	2.084	62
6	1/8	3.175	0.75	19.05	0.0504	1.279	0.0734	2.037	60.3
6	1/16	1.588	0.751	19.075	0.0541	1.373	0.0704	1.954	56

Note.- The length for all the specimens is 7.5 in (190.5 mm)
Vf = Fiber volume fraction

TABLE 4.2

Description of off-axis fiber specimens tested with extensional vibration

No	Fiber angle	Length (in)	Length (mm)	Width (in)	Width (mm)	Thickness (in)	Thickness (mm)	Mass 1 (lb)	Mass 1 (kg)	Mass 2 (lb)	Mass 2 (kg)
					FIBERITE 934 RESIN CASTING						
1	N/A	8.344	211.938	0.745	18.923	0.124	3.150	0.627	0.285	0.6316	0.287
1	N/A	5.563	141.3	0.746	18.948	0.126	3.2	0.627	0.285	0.6316	0.287
1	N/A	1.875	47.625	0.746	18.948	0.126	3.2	0.627	0.285	0.6316	0.287
1	N/A	0.875	22.225	0.746	18.948	0.126	3.2	0.627	0.285	0.6316	0.287
					GRAPHITE / EPOXY CONTINUOUS FIBER						
6	0	8.375	212.725	0.746	18.948	0.062	1.575	1.2615	0.573	1.2686	0.577
5	2.5	8.556	217.322	0.741	18.821	0.060	1.524	1.2615	0.573	1.2686	0.577
5	7.5	8.25	209.550	0.729	18.517	0.062	1.575	1.2615	0.573	1.2686	0.577
6	12.5	7.896	200.558	0.73	18.542	0.060	1.524	0.946	0.43	0.9514	0.432
5	20	7.422	188.519	0.728	18.491	0.060	1.524	0.627	0.285	0.6316	0.287
6	45	5.037	127.94	0.731	18.567	0.060	1.524	0.305	0.139	0.3076	0.14
6	60	4.060	103.124	0.729	18.517	0.060	1.524	0.305	0.139	0.3076	0.14
6	75	3.058	77.673	0.729	18.517	0.061	1.549	0.305	0.139	0.3076	0.14
6	90	3.037	77.140	0.729	18.517	0.061	1.549	0.305	0.139	0.3076	0.14
					GRAPHITE / EPOXY DISCONTINUOUS FIBER						
6	0	8.125	206.375	0.733	18.618	0.060	1.524	1.2615	0.573	1.2686	0.577
5	2.5	9.307	236.398	0.73	18.542	0.062	1.575	0.946	0.43	0.9514	0.432
5	7.5	8.863	225.120	0.729	18.517	0.061	1.549	0.946	0.43	0.9514	0.432
6	12.5	6.933	176.098	0.731	18.567	0.061	1.549	0.946	0.43	0.9514	0.432
5	20	5.938	150.825	0.729	18.517	0.063	1.600	0.627	0.285	0.6316	0.287
6	45	4.537	115.240	0.722	18.339	0.061	1.549	0.305	0.139	0.3076	0.14
6	60	3.542	89.963	0.732	18.593	0.062	1.575	0.305	0.139	0.3076	0.14
5	75	3.063	77.788	0.725	18.415	0.062	1.575	0.305	0.139	0.3076	0.14
5	90	3.057	77.648	0.724	18.390	0.063	1.600	0.305	0.139	0.3076	0.14

Note.- Density 0.0469 lb/in^3 (1.298 g/cc)

Note.- Density 0.0573 lb/in^3 (1.589 g/cc)
Fiber volume fraction 67.5 %
Void volume fraction 0.2 %

Note.- The fiber length for these specimens is 1/4 in (6.35 mm),
Density 0.0573 lb/in^3 (1.589 g/cc), and
Fiber volume fraction 67.8 %
Void volume fraction 0.67 %

TABLE 4.2 (continuation)

Description of off-axis fiber specimens tested with extensional vibration

No	Fiber angle	Length (in)	Length (mm)	Width (in)	Width (mm)	Thickness (in)	Thickness (mm)	Mass 1 (lb)	Mass 1 (kg)	Mass 2 (lb)	Mass 2 (kg)
					KEVLAR / EPOXY CONTINUOUS FIBER						
4	0	8.375	212.725	0.755	19.177	0.053	1.346	1.2615	0.573	1.2686	0.577
4	2.5	7.914	201.016	0.733	18.618	0.053	1.346	1.2615	0.573	1.2686	0.577
4	7.5	7.899	200.635	0.734	18.644	0.054	1.372	0.946	0.43	0.9514	0.432
5	12.5	6.938	176.225	0.742	18.847	0.053	1.346	0.627	0.285	0.6316	0.287
3	20	4.464	113.386	0.753	19.126	0.054	1.372	0.627	0.285	0.6316	0.287
6	45	3.072	78.029	0.75	19.05	0.054	1.372	0.305	0.139	0.3076	0.14
4	60	2.089	53.061	0.742	18.847	0.054	1.372	0.305	0.139	0.3076	0.14
4	75	1.553	39.446	0.75	19.05	0.057	1.448	0.305	0.139	0.3076	0.14
4	90	1.442	36.627	0.762	19.355	0.055	1.397	0.305	0.139	0.3076	0.14

Note.- Density 0.05 lb/in^3 (1.387 g/cc)
Fiber volume fraction 71.5 %
Void volume fraction 1.38 %

TABLE 5.1

Experimental data for the first three modes in flexural vibration for graphite/epoxy specimens

Fiber length in	(mm)	Mode	f (Hz)	E' Mpsi	E' GPa	E'' Kpsi	E'' MPa	η_3 10^3	V_f (%)	V_v (%)
Continuous		1	60.145	16.88	116.3	37.08	255.48	2.197	66.0	0.284
		2	376.35	16.83	115.96	43.32	298.47	2.574		
		3	1053.23	16.81	115.82	47.75	329	2.84		
1/2	12.7	1	54.125	15.17	104.52	45.43	313.01	2.995	66.5	0.42
		2	340.83	15.32	105.55	58.54	403.34	3.821		
		3	951.5	15.25	105.07	65.25	449.57	4.279		
1/4	6.35	1	54.194	14.86	102.39	47.91	330.1	3.224	66.6	0.38
		2	368.688	14.76	101.70	74.27	511.72	5.032		
		3	951.13	14.84	102.25	88.48	609.63	5.962		
1/8	3.175	1	53.354	13.76	94.81	57.74	397.83	4.196	64.7	0.52
		2	334.235	13.76	94.81	80.84	556.99	5.875		
		3	934.73	13.73	94.6	101.97	702.57	7.427		
1/16	1.588	1	48.397	10.69	73.65	69.6	479.54	6.511	63.2	0.20
		2	308.815	11.07	76.27	97.75	673.50	8.83		
		3	870.85	11.22	77.31	111.99	771.61	9.981		

TABLE 5.2

Experimental data for the first three modes in flexural vibration for Kevlar/epoxy specimens

Fiber length in (mm)	Mode	f (Hz)	E' Mpsi	E' GPa	E'' Kpsi	E'' MPa	η_3 10^{-3}	V_f (%)	V_v (%)
Continuous	1	41.54	9.746	67.15	111.8	770.3	1.115		
	2	259.84	9.697	66.81	128.8	887.43	1.341	65.8	2.38
	3	722.48	9.565	65.90	140.7	969.42	1.500		
1/2 12.7	1	40.5	8.436	58.12	98.3	677.29	1.18		
	2	255.33	8.538	58.83	115.4	795.11	1.355	68.1	3.16
	3	713.3	8.498	58.55	106.30	732.41	1.252		
1/4 6.35	1	39.15	8.47	58.36	119.50	823.36	1.335		
	2	244.380	8.40	57.88	125.70	866.07	1.468	66.7	5.7
	3	683.55	8.38	57.74	130.60	899.83	1.536		
1/8 3.175	1	37.19	7.598	52.35	104.10	717.25	1.371		
	2	234.5	7.657	52.76	122.40	843.34	1.594	67.1	3.1
	3	659.23	7.751	53.40	132.00	909.48	1.708		
1/16 1.588	1	35.35	6.33	43.61	97.8	673.84	1.547		
	2	220.32	6.265	43.17	114.6	789.59	1.836	63.0	0.743
	3	624.75	6.429	44.3	132.20	910.86	2.069		

TABLE 5.3

Experimental data for the first three modes in flexural vibration for boron/epoxy specimens

Fiber in	length (mm)	Mode	f (Hz)	E' Mpsi	E' GPa	E'' Kpsi	E'' MPa	η_3 10^3	V_f (%)	V_v (%)
Continuous		1	55.613	33.87	233.36	73.94	509.45	2.182		
		2	343.00	32.81	226.06	245.36	1690.53	7.466	63.4	0.50
		3	961.845	32.91	226.75	111.80	770.3	3.400		
2	50.8	1	56.872	32.21	221.93	100.49	692.38	3.134		
		2	353.801	31.75	218.76	181.27	1248.95	5.815	62.9	0.67
		3	992.353	31.85	219.45	129.03	889.02	4.589		
1	25.4	1	58.38	25.58	176.25	91.30	629.06	3.416		
		2	355.922	24.45	168.46	158.71	1093.51	6.614	60.4	0.64
		3	1012.66	24.97	172.04	125.11	862.01	5.086		
1/2	12.7	1	55.421	24.94	171.84	97.79	673.77	3.967		
		2	346.221	24.81	170.94	111.82	770.44	4.364	60.2	0
		3	967.16	24.67	169.98	118.02	813.16	4.643		
1/4	6.35	1	50.888	25.74	177.35	111.68	769.48	4.368		
		2	313.849	24.93	171.77	133.90	922.57	5.420	62.0	0
		3	879.14	24.94	171.84	141.37	974.04	5.722		
1/8	3.175	1	46.24	19.47	134.15	130.4	898.46	6.746		
		2	289.785	19.47	134.15	178.3	1228.49	9.225	60.3	0
		3	812.661	19.52	134.49	187.78	1293.80	9.783		
1/16	1.588	1	37.926	10.90	75.10	131.15	903.62	12.05		
		2	238.917	11.01	75.86	159.70	1100.33	14.522	56.0	0.3
		3	670.834	11.07	76.27	182.82	1259.63	16.535		

TABLE 5.4

Experimental results of the first resonant frequency for graphite/epoxy specimens, as used for comparison with the analytical model

Data scatter	(ℓ/d)	E'/E'	E''/E''	Loss factor 10^3
Upper limit		30.38	3.46	3.432
Mean value	27174.00	29.39	2.314	2.197
Lower limit		28.02	1.49	1.403
Upper limit		30.51	3.16	3.681
Mean value	1811.59	26.41	2.835	2.995
Lower limit		22.67	2.42	2.259
Upper limit		30.12	3.33	3.994
Mean value	905.80	25.87	2.99	3.224
Lower limit		20.46	2.56	2.603
Upper limit		25.81	3.95	4.416
Mean value	452.90	23.96	3.604	4.196
Lower limit		19.83	3.13	3.960
Upper limit		20.20	4.75	7.488
Mean value	226.45	18.61	4.344	6.511
Lower limit		15.28	3.57	5.843

Note.- Average frequency for the first mode: 54.00 Hz
Average fiber volume fraction: 65.4%
Average void volume fraction: 0.36%
Fiber diameter: 0.000276" (0.00701 mm)

TABLE 5.5

Experimental results of the first resonant frequency for Kevlar/epoxy specimens, as used for comparison with the analytical model

Data scatter	(ℓ/d)	E'/E'	E''/E''	Loss factor 10^2
Upper limit		17.88	9.04	1.401
Mean value	15957.45	17.00	7.53	1.155
Lower limit		15.38	5.27	0.7641
Upper limit		15.41	7.58	1.350
Mean value	1063.83	14.71	6.62	1.180
Lower limit		13.83	5.45	0.9164
Upper limit		16.06	8.26	1.375
Mean value	531.91	14.77	8.05	1.335
Lower limit		12.90	6.85	1.311
Upper limit		14.17	7.46	1.390
Mean value	265.96	13.25	7.01	1.371
Lower limit		11.81	6.27	1.349
Upper limit		12.08	7.04	1.605
Mean value	132.98	11.04	6.59	1.547
Lower limit		9.67	6.01	1.477

Note.- Average frequency for the first mode: 38.75 Hz
Average fiber volume fraction: 66.1%
Average void volume fraction: 3.02%
Fiber diameter: 0.00047" (0.011938 mm)

TABLE 5.6

Experimental results of the first resonant frequency for boron/epoxy specimens, as used for comparison with the analytical model

Data scatter	(ℓ/d)	E'/E'	E''/E''	Loss factor 10^3
Upper limit	1875.00	61.30	5.22	2.357
Mean value		59.32	4.67	2.182
Lower limit		58.23	4.21	1.99
Upper limit	500.00	58.90	7.49	4.032
Mean value		56.41	6.35	3.134
Lower limit		51.45	5.20	3.013
Upper limit	250.00	48.49	10.37	6.434
Mean value		44.80	5.77	3.416
Lower limit		40.09	3.96	2.349
Upper limit	125.00	47.53	7.66	5.196
Mean value		43.68	6.18	3.967
Lower limit		37.57	5.09	3.296
Upper limit	62.50	49.21	8.66	5.768
Mean value		45.08	7.06	4.368
Lower limit		41.59	6.50	3.819
Upper limit	31.25	37.20	9.42	7.780
Mean value		34.10	8.24	6.746
Lower limit		27.22	7.44	5.924
Upper limit	15.625	21.44	9.28	13.390
Mean value		19.09	8.29	12.050
Lower limit		17.99	7.23	11.140

Note.- Average frequency for the first mode: 51.62 Hz
Average fiber volume fraction: 60.7%
Average void volume fraction: 0.30%
Fiber diameter: 0.004" (0.1016 mm)

TABLE 6.1

Experimental results of the first resonant frequency for graphite/epoxy continuous fiber specimens tested with extensional vibration, as used for comparison with the analytical model.

Data scatter	angle (deg)	f (Hz)	E' Mpsi	E' GPa	E" Kpsi	E" MPa	Loss factor 10^3	E'/E'	E"/E"
Upper limit							3.701	30.02	2.40
Mean value	0.0	1256.94	18.555	127.84	54.77	377.00	2.947	29.22	1.86
Lower limit							2.045	28.55	1.26
Upper limit							5.956	27.89	3.54
Mean value	2.5	1170.24	17.052	117.49	85.49	589.00	5.027	26.85	2.91
Lower limit							3.755	25.61	2.26
Upper limit							9.732	23.12	4.60
Mean value	7.5	1094.74	14.176	97.67	112.85	778.00	8.006	22.32	3.84
Lower limit							6.223	21.01	3.11
Upper limit							13.980	16.87	5.02
Mean value	12.5	1091.93	10.438	71.92	139.68	962.00	13.412	16.44	4.75
Lower limit							11.990	15.26	4.35
Upper limit							19.390	11.32	4.32
Mean value	20.0	1114.27	6.804	46.88	124.98	861.00	18.398	10.71	4.25
Lower limit							17.660	10.04	4.16
Upper limit							22.890	4.00	1.93
Mean value	45.0	1161.70	2.432	16.76	53.76	370.00	22.048	3.83	1.83
Lower limit							20.930	3.68	1.75
Upper limit							23.680	2.91	1.47
Mean value	60.0	1108.70	1.799	12.40	37.98	262.00	21.113	2.83	1.29
Lower limit							19.280	2.74	1.19
Upper limit							24.360	2.54	1.24
Mean value	75.0	1199.92	1.563	10.77	30.26	208.00	19.410	2.46	1.03
Lower limit							17.620	2.36	0.97
Upper limit							21.200	2.47	1.01
Mean value	90.0	1174.18	1.489	10.26	28.33	195.00	19.080	2.34	0.96
Lower limit							17.250	2.22	0.92

Note.- Average frequency for the first mode: 1152.5 Hz
Average fiber volume fraction: 67.5%
Average void volume fraction: 0.20%
Fiber aspect ratio: 10870

TABLE 6.2

Experimental results of the first resonant frequency for graphite/epoxy discontinuous fiber specimens tested with extensional vibration, as used for comparison with the analytical model.

Data scatter	angle (deg)	f (Hz)	E' Mpsi	E' GPa	E'' Kpsi	E'' MPa	Loss factor 10^3	E'/E'	E''/E''
Upper limit							5.486	26.32	3.32
Mean value	0.0	1189.92	16.295	112.27	74.18	511.00	4.570	25.51	2.49
Lower limit							3.016	24.72	1.70
Upper limit							5.757	25.57	3.05
Mean value	2.5	1259.45	15.990	110.17	78.49	541.00	4.915	25.04	2.64
Lower limit							3.391	24.69	1.83
Upper limit							10.340	21.84	4.47
Mean value	7.5	1180.63	13.602	93.72	114.28	787.00	8.431	21.30	3.84
Lower limit							7.393	20.17	3.42
Upper limit							14.780	16.88	5.24
Mean value	12.5	1189.19	10.700	73.72	127.00	875.00	11.872	16.75	4.27
Lower limit							10.780	16.53	3.90
Upper limit							19.580	10.41	4.01
Mean value	20.0	1236.77	6.409	44.16	112.54	775.00	17.584	10.03	3.78
Lower limit							16.630	9.55	3.57
Upper limit							24.800	3.95	2.02
Mean value	45.0	1233.80	2.457	16.93	57.44	396.00	23.388	3.85	1.93
Lower limit							22.520	3.75	1.86
Upper limit							25.750	2.87	1.48
Mean value	60.0	1192.43	1.756	12.10	37.86	261.00	21.592	2.75	1.27
Lower limit							19.920	2.68	1.21
Upper limit							19.470	2.53	1.05
Mean value	75.0	1204.11	1.545	10.65	29.34	202.00	18.996	2.42	0.99
Lower limit							18.150	2.28	0.95
Upper limit							19.610	2.33	0.94
Mean value	90.0	1169.05	1.435	9.89	27.21	187.00	18.974	2.25	0.91
Lower limit							17.560	2.19	0.88

Note.- Average frequency for the first mode: 1206.15 Hz
Average fiber volume fraction: 67.8%
Average void volume fraction: 0.67%
Fiber aspect ratio: 905.8

TABLE 6.3

Experimental results of the first resonant frequency for Kevlar/epoxy continuous fiber specimens tested with extensional vibration, as used for comparison with the analytical model.

Data scatter	angle (deg)	f (Hz)	E' Mpsi	E' GPa	E" Kpsi	E" GPa	Loss factor 10^2	E'/E'	E"/E"
Upper limit	0.0	920.7	11.550	79.58	148.50	1.023	1.422	18.82	5.75
Mean value							1.287	18.60	5.34
Lower limit							1.237	18.10	5.17
Upper limit	2.5	872.5	10.130	69.80	145.60	1.003	1.618	17.16	5.66
Mean value							1.444	16.31	5.24
Lower limit							1.163	15.38	4.46
Upper limit	7.5	866.27	7.331	50.51	126.66	0.872	1.857	12.16	4.75
Mean value							1.729	11.80	4.55
Lower limit							1.610	11.45	4.35
Upper limit	12.5	947.95	5.137	35.39	91.56	0.631	1.859	8.41	3.44
Mean value							1.783	8.27	3.29
Lower limit							1.687	8.22	3.17
Upper limit	20.0	908.40	2.912	20.06	83.07	0.572	3.450	5.15	3.50
Mean value							2.897	4.69	2.99
Lower limit							1.960	4.38	2.25
Upper limit	45.0	844.81	0.852	5.87	29.93	0.206	4.963	1.47	1.47
Mean value							3.544	1.37	1.08
Lower limit							2.569	1.23	0.84
Upper limit	60.0	923.16	0.694	4.78	22.55	0.155	3.911	1.15	0.98
Mean value							3.246	1.12	0.81
Lower limit							2.913	1.09	0.84
Upper limit	75.0	896.87	0.451	3.11	15.65	0.108	4.763	0.77	0.70
Mean value							3.521	0.73	0.56
Lower limit							2.739	0.66	0.71
Upper limit	90.0	875.28	0.415	2.86	21.41	0.148	6.954	0.77	1.01
Mean value							4.423	0.67	0.77
Lower limit							3.114	0.60	0.44

Note.- Average frequency for the first mode: 895.1 Hz
Average fiber volume fraction: 71.5%
Average void volume fraction: 1.38%
Fiber aspect ratio: 3191.5

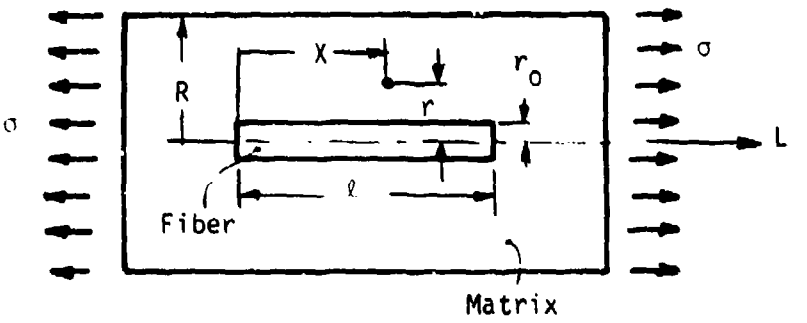

Figure 2.1 Representative Volume Element for Single Aligned Fiber

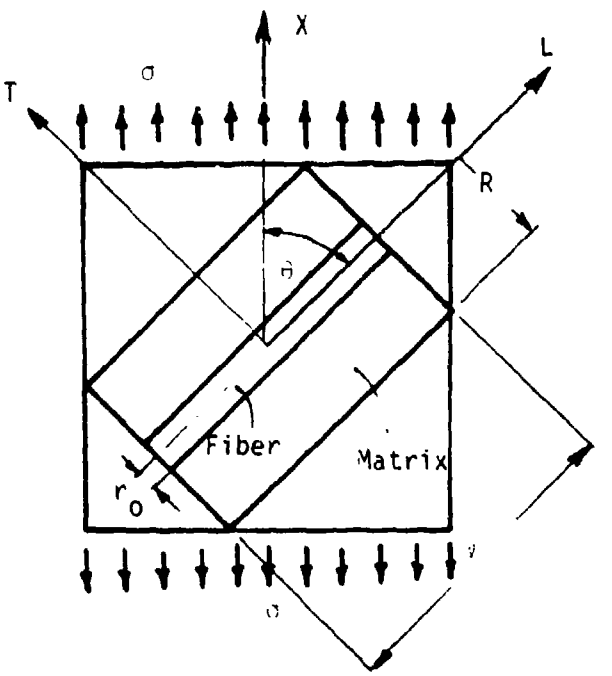

Figure 2.2 Representative Volume Element for a Single Off-Axis Fiber

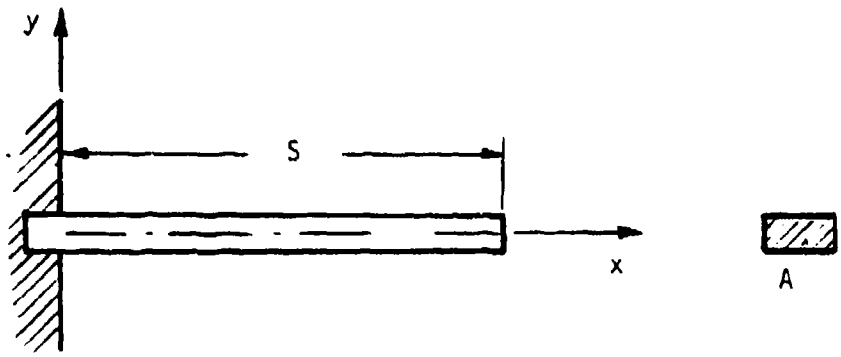

Figure 2.3 Cantilever beam specimen

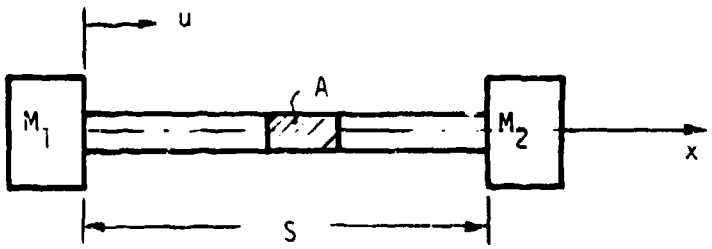

Figure 2.4 Mass-mass beam specimen

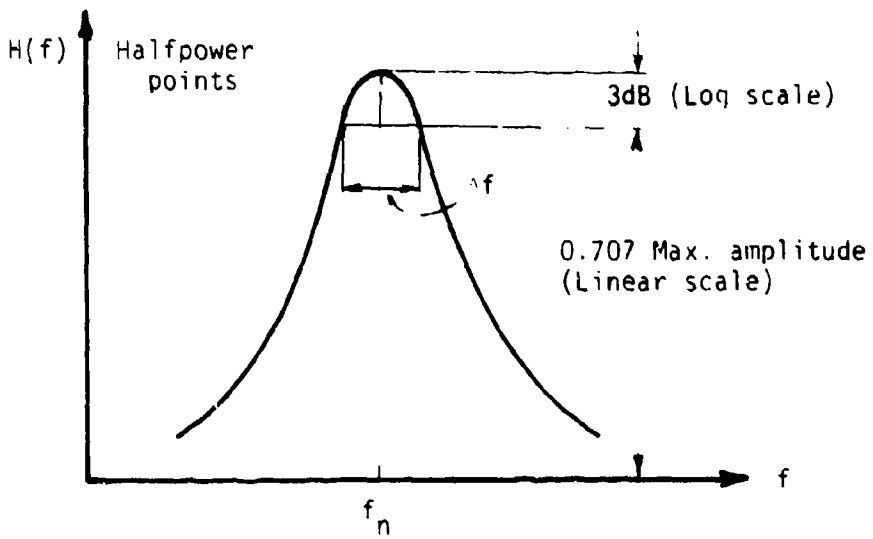

Figure 2.5 Transfer function vs frequency

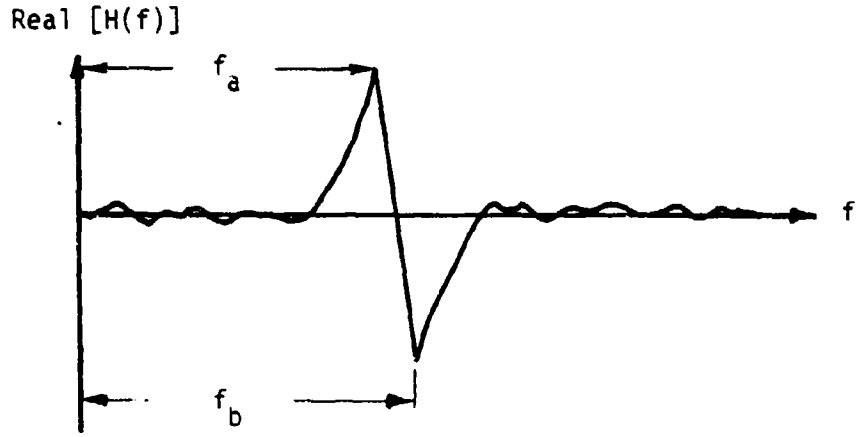

Figure 2.6 Real component of the transfer function vs frequency

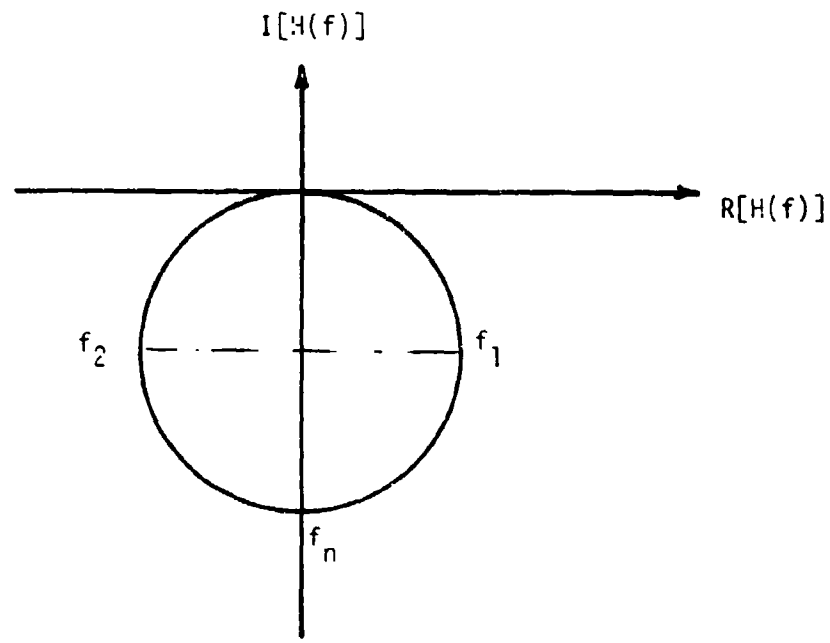

Figure 2.7 Nyquist plot

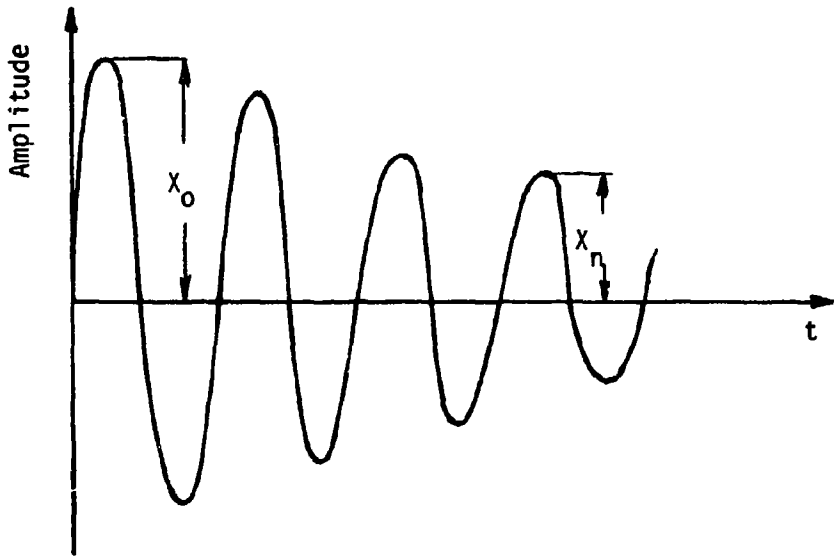

Figure 2.8 Free vibration decay

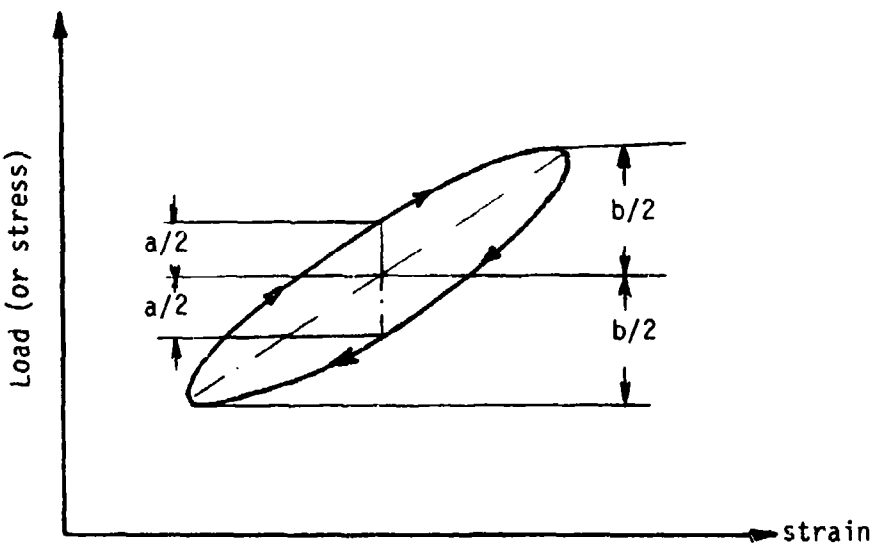

Figure 2.9 Hysteresis loop in a force-displacement curve

Figure 3.1. Slicing graphite/epoxy prepreg tape to produce discontinuous fibers.

Figure 3.2. Transferring single sliced ply to the uncured laminate.

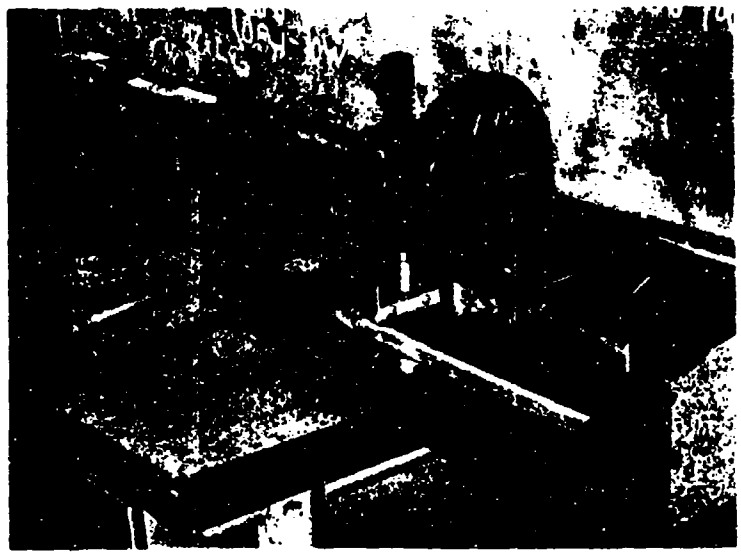

Figure 3.3. Set-up for cutting boron/epoxy prepreg tape.

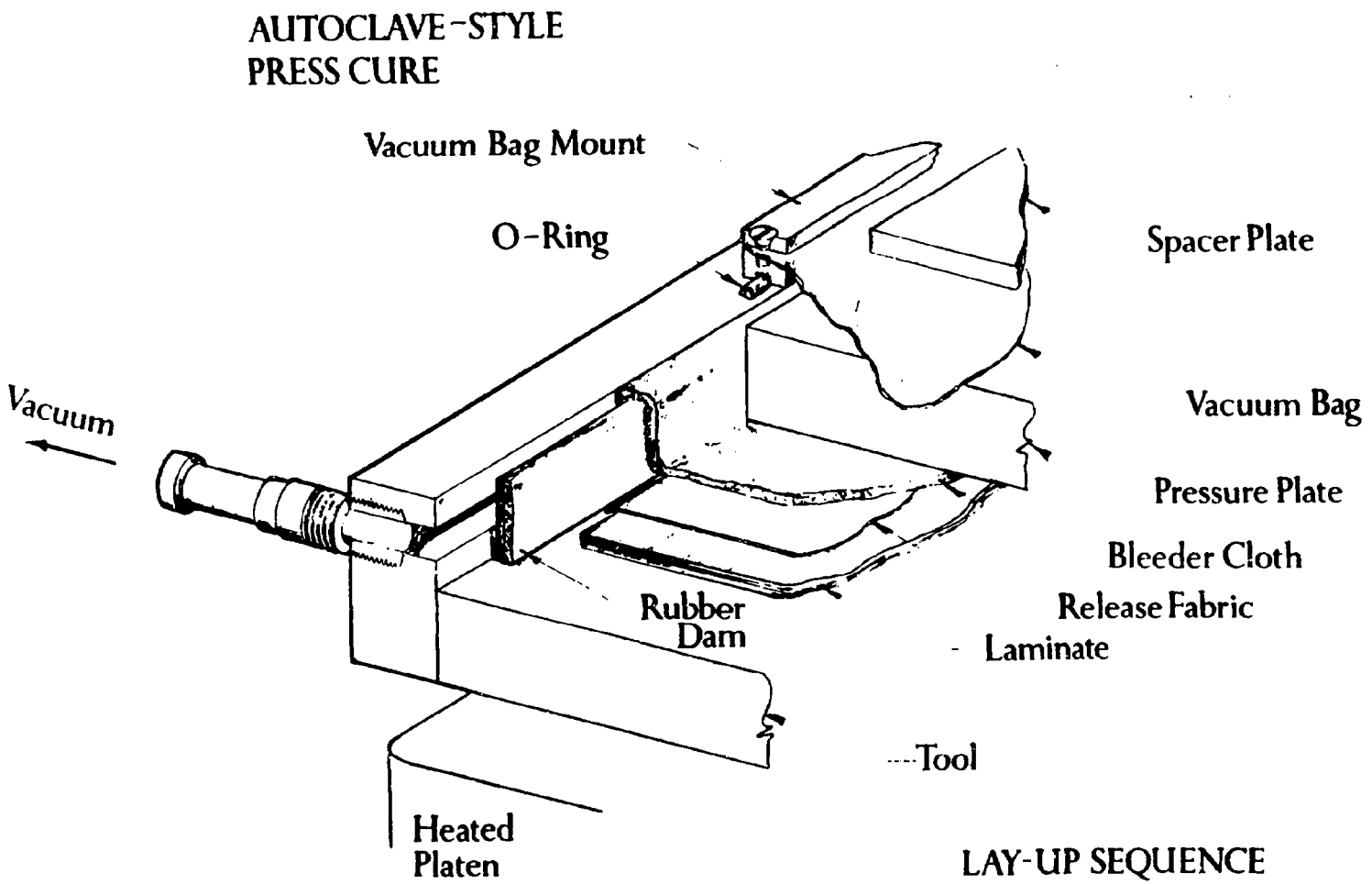

Figure 3.4. Cutaway view of autoclave-style press cure system.

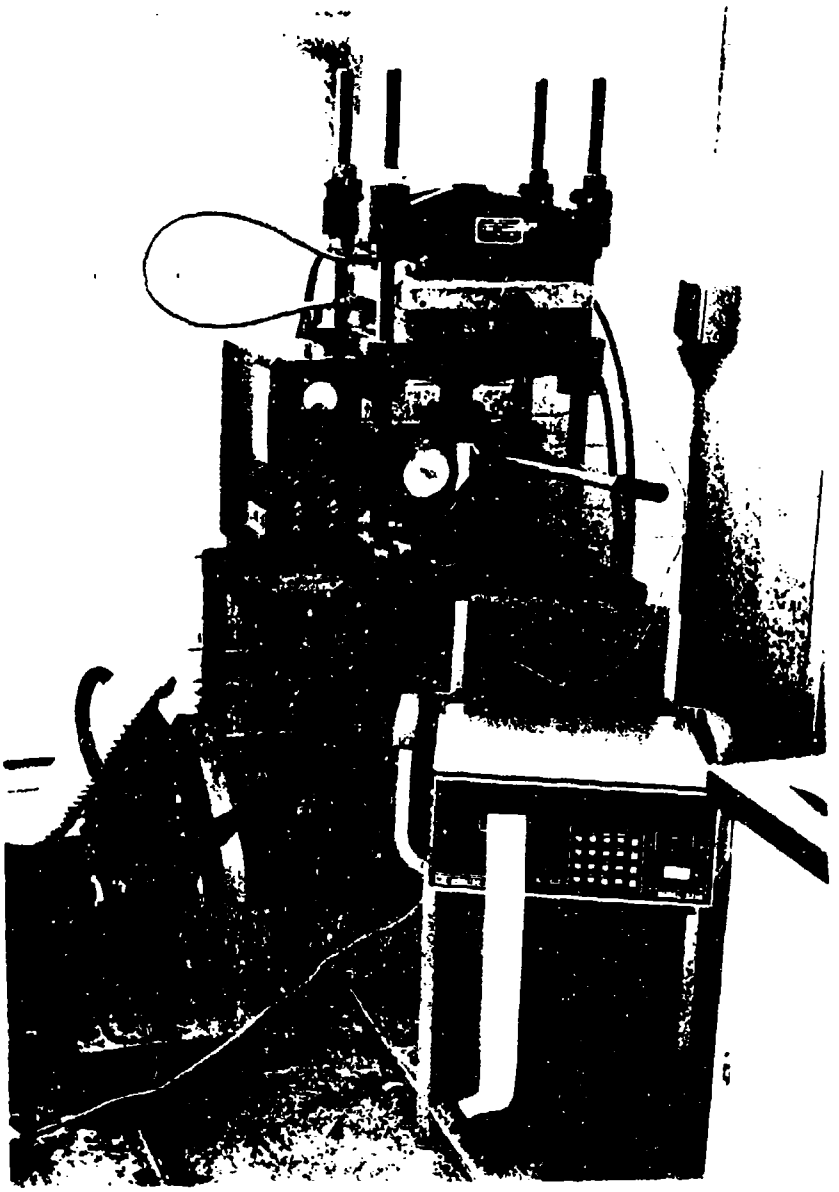

Figure 3.5. Set-up for autoclave sytle press cure.

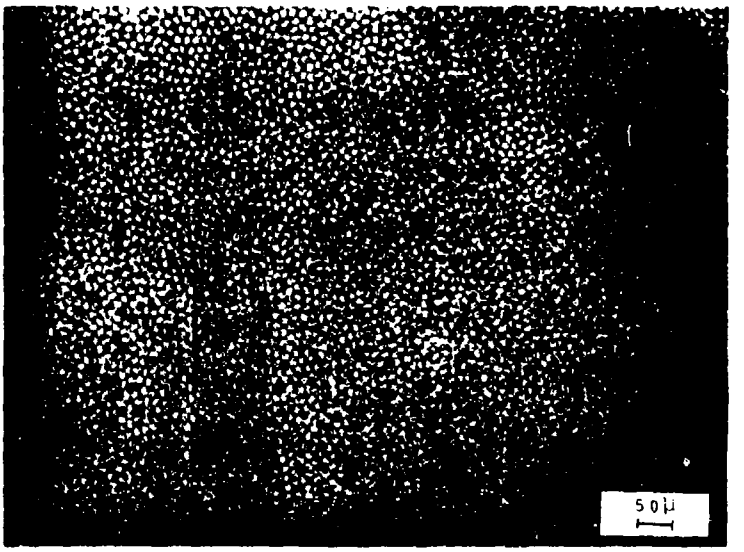

Figure 3.6. Graphite/epoxy composite produced by autoclave (scale 200:1).

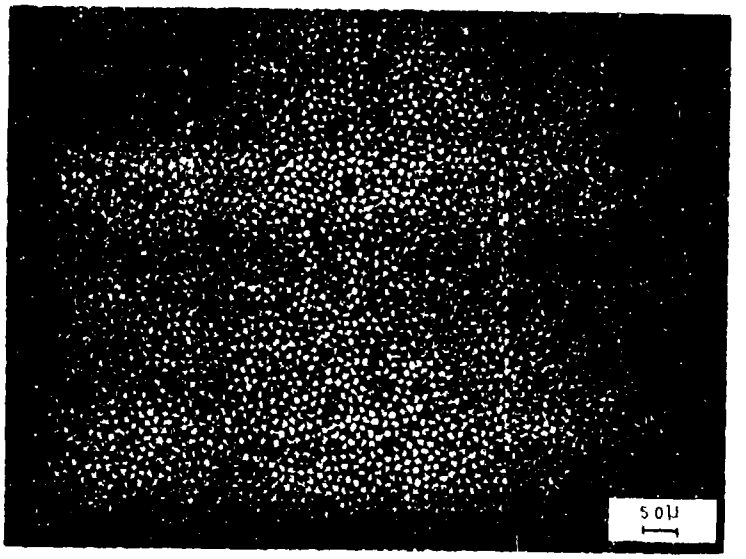

Figure 3.7. Graphite/epoxy composite produced by autoclave style press cure (scale 200:1).

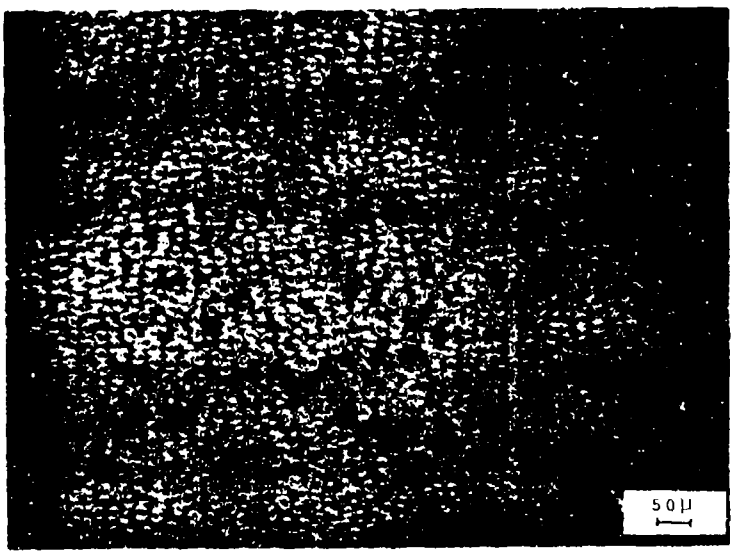

Figure 3.8. Kevlar/epoxy composite produced by autoclave style press cure (scale 200:1).

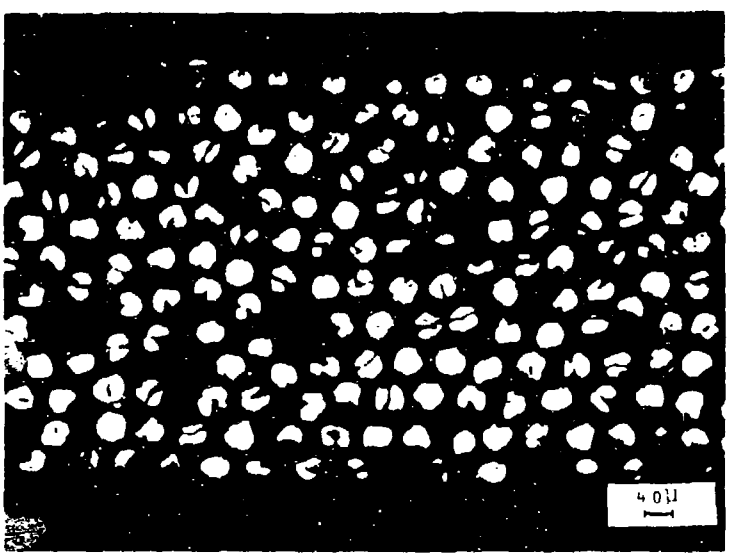

Figure 3.9. Boron/epoxy composite produced by autoclave style press cure (scale 40:1).

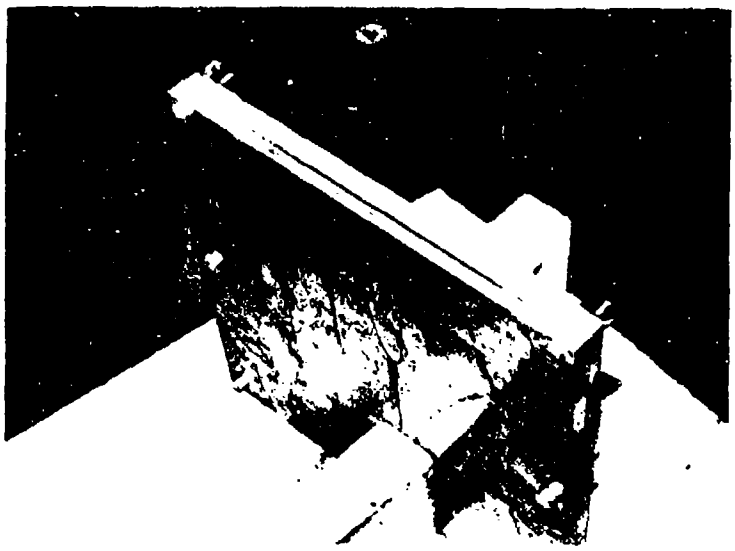

Figure 3.10. Mold to cast neat resin plates.

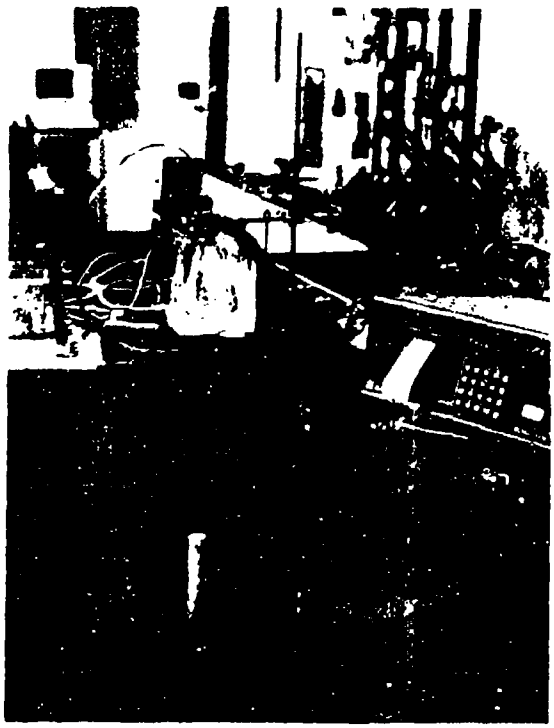

Figure 3.11. Equipment required to produce neat resin plates.

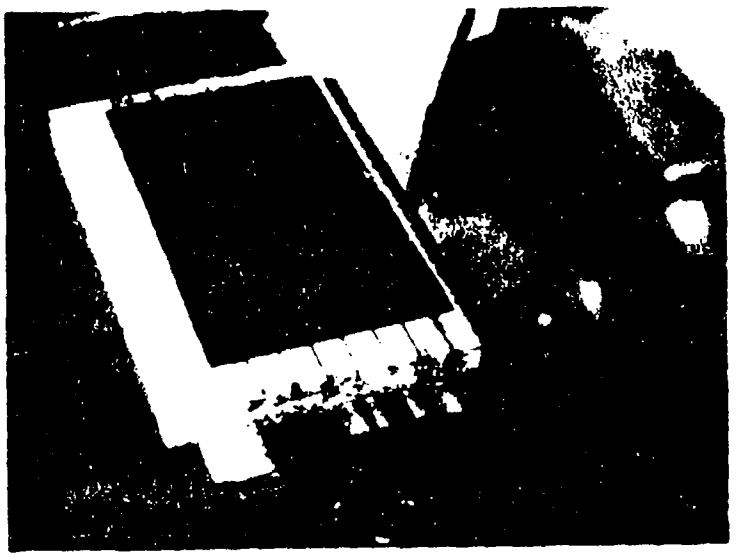

Figure 3.12. Precision reciprocating grinder used to machine graphite/epoxy and boron/epoxy composite specimens.

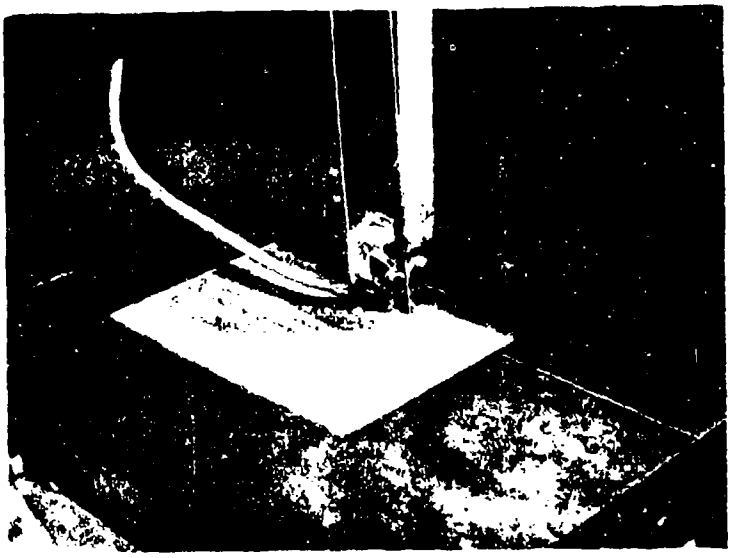

Figure 3.13. Electric band saw used to machine Kevlar/epoxy composite specimens.

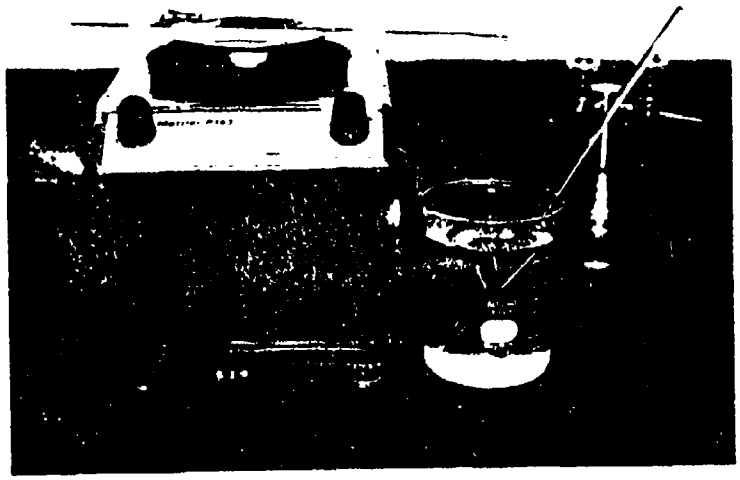

Figure 3.14. Equipment required to measure composite density.

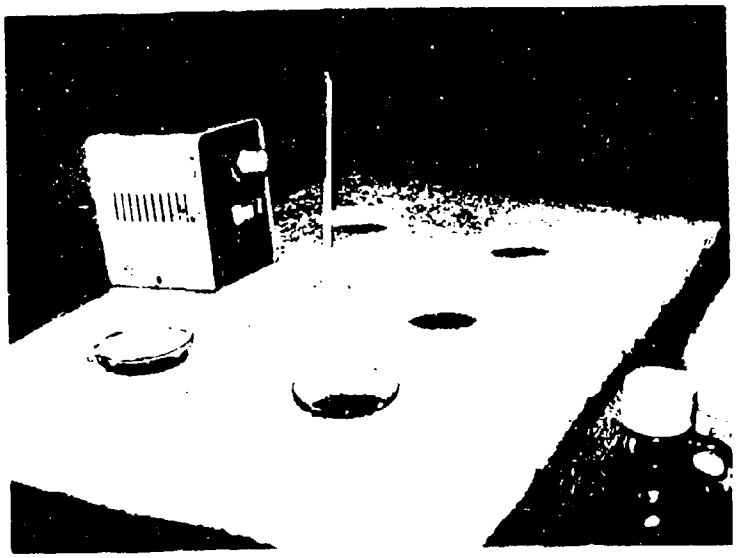

Figure 3.15. Water bath used for volume fraction determination of graphite/epoxy and Kevlar/epoxy composites.

Figure 3.16. Hot plate used for the digestion of boron/epoxy composite.

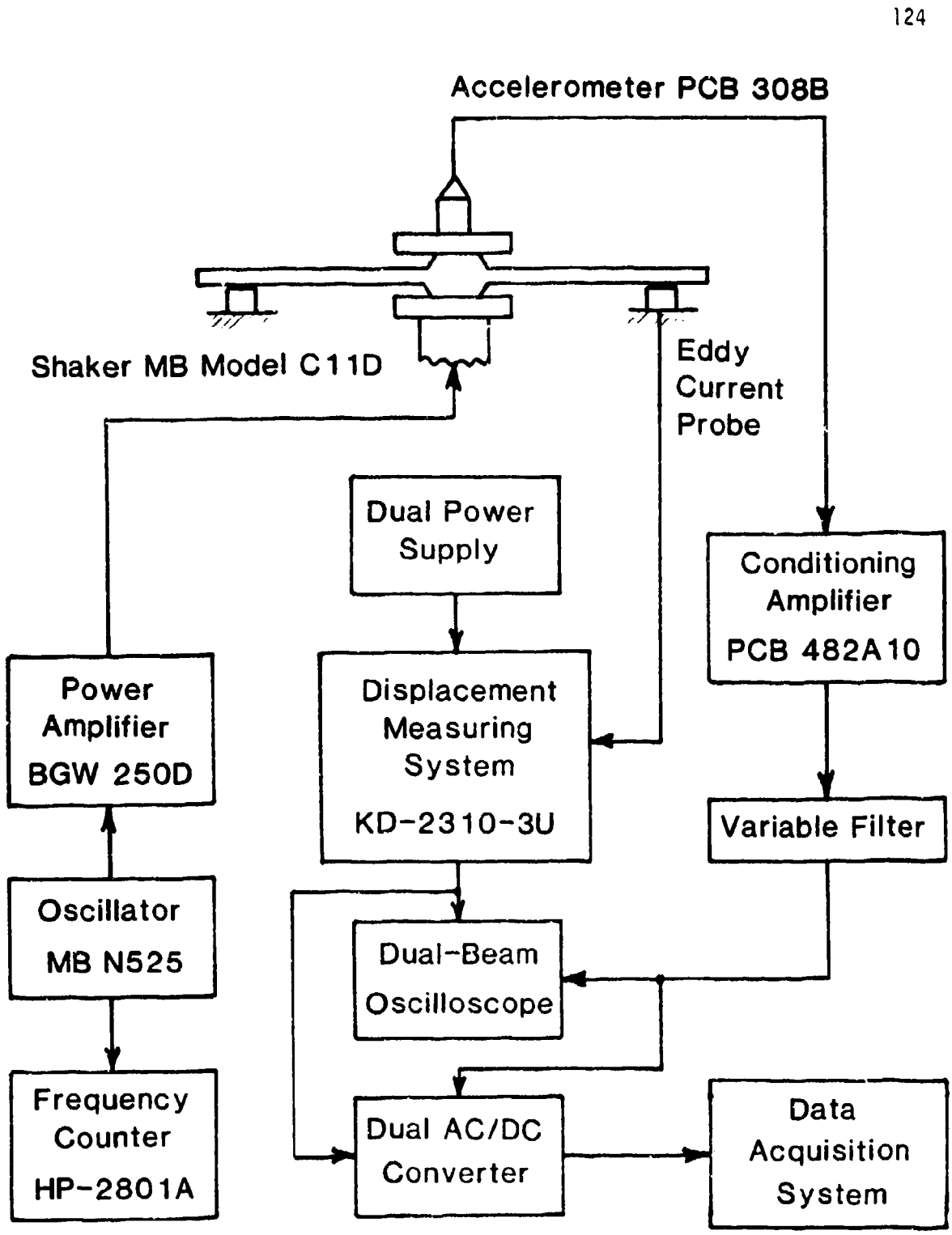

Figure 3.17. Block diagram of instrumentation for the forced sinusoidal vibration technique.

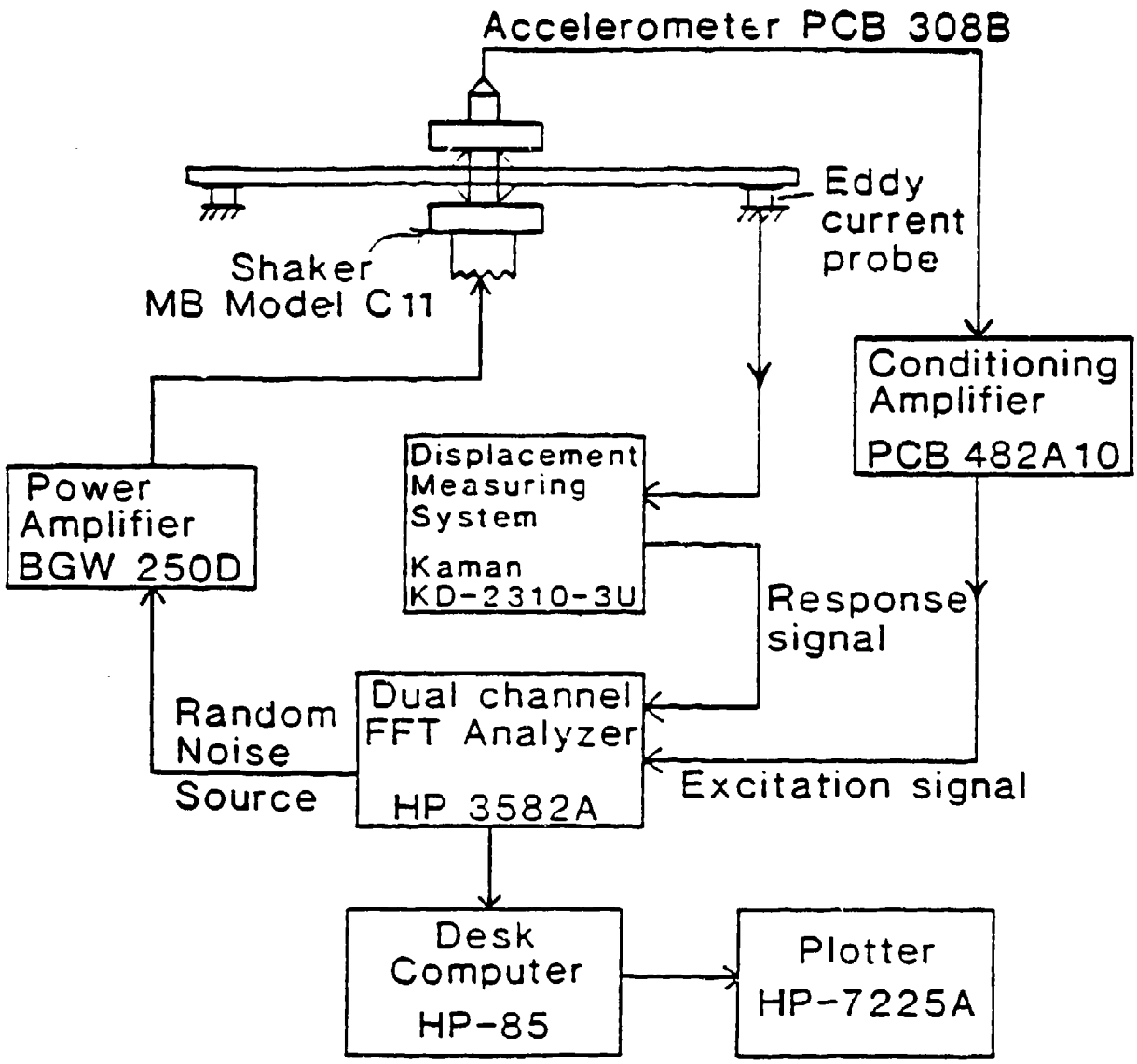

Figure 3.18. Block diagram of instrumentation for the random technique.

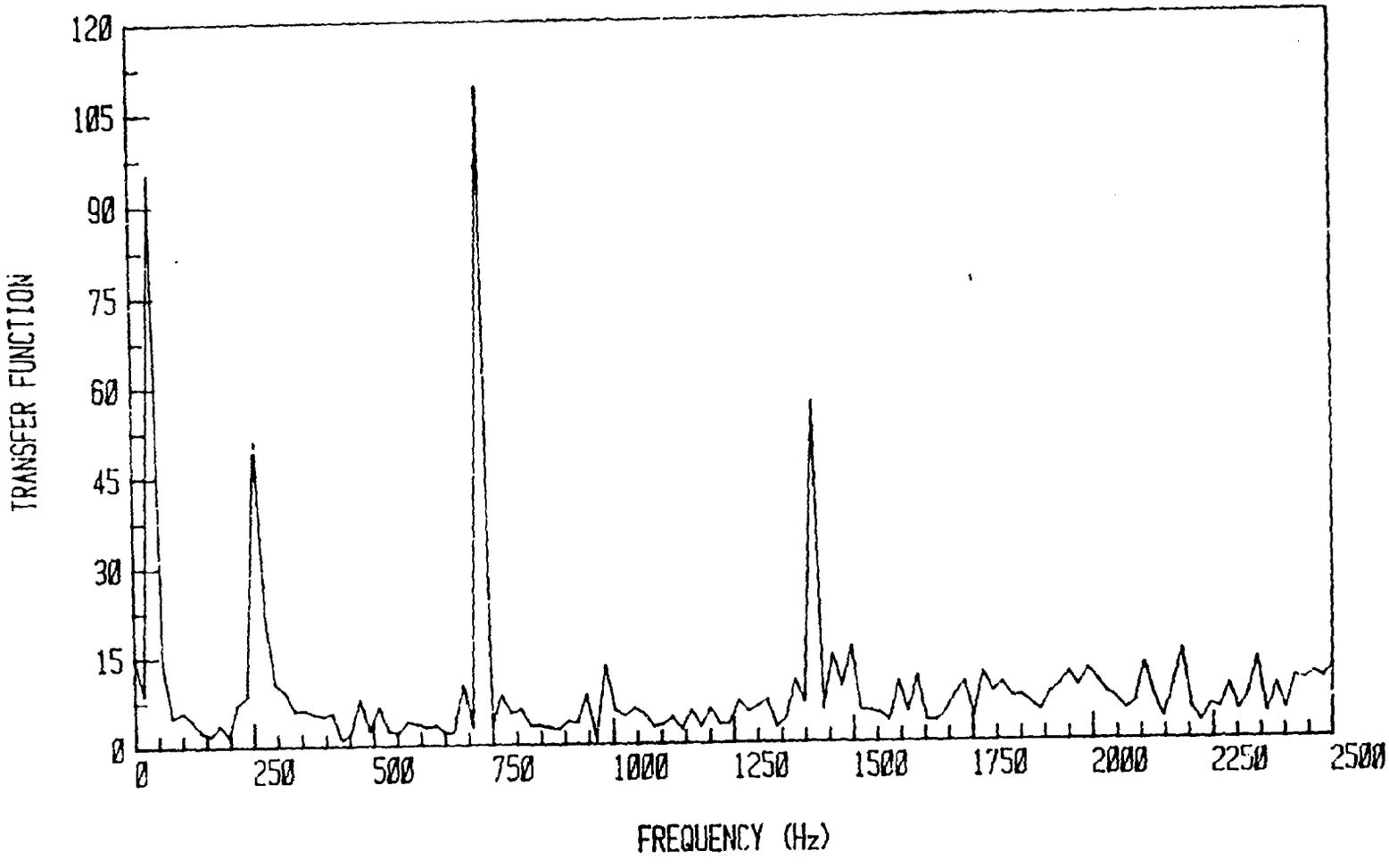

Figure 3.19. Typical transfer function trace on screen of FFT Analyzer.

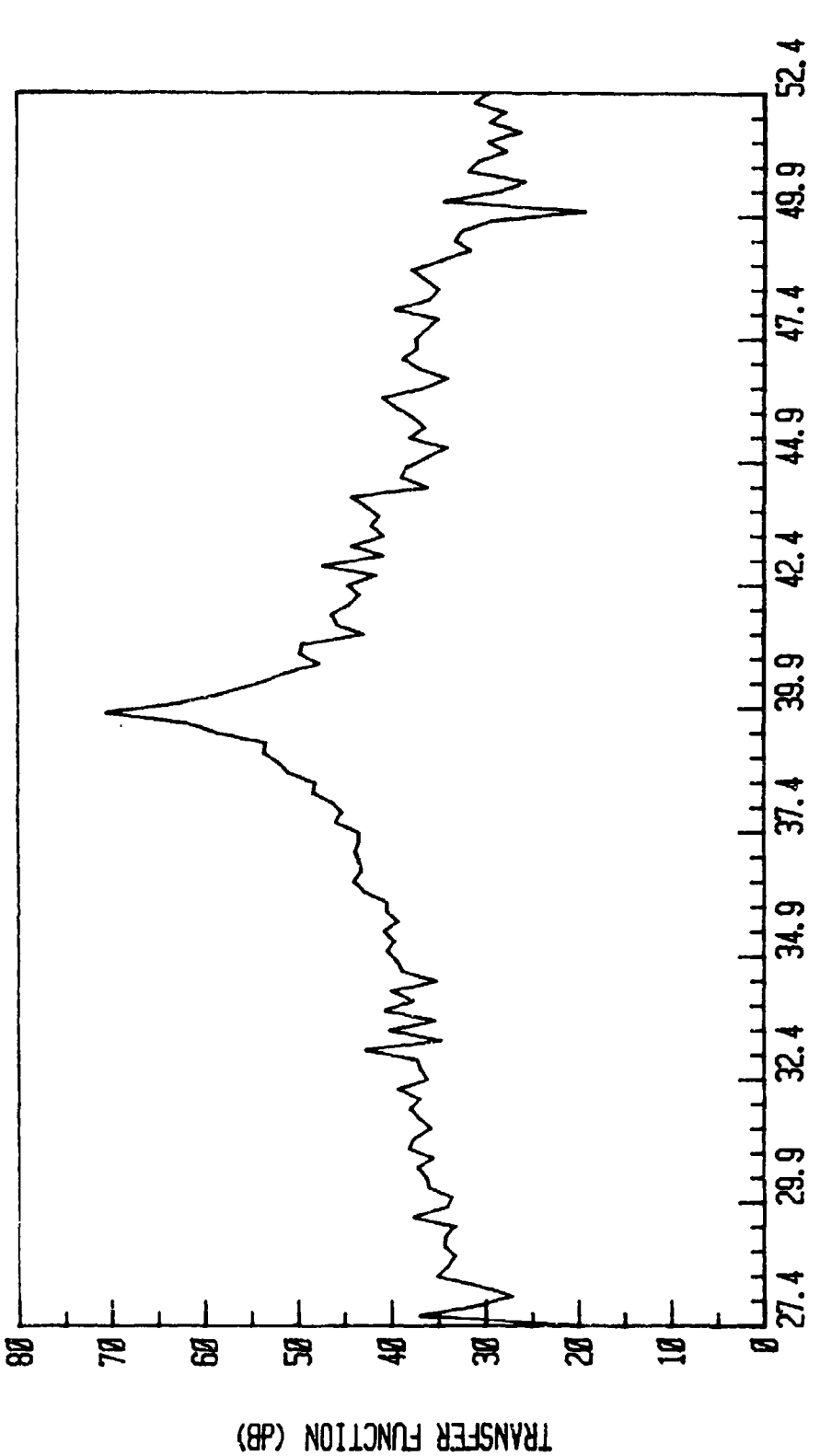

Figure 3.20. Peak of transfer function at one mode using zoom feature on FFT Analyzer.

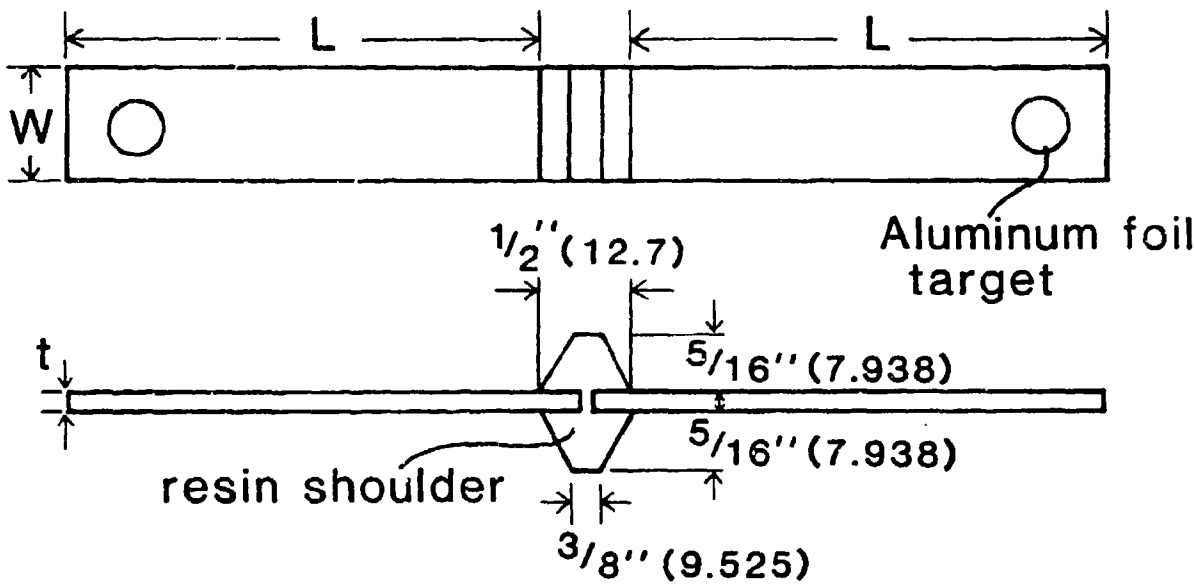

Figure 3.21. Double cantilever beam specimen.

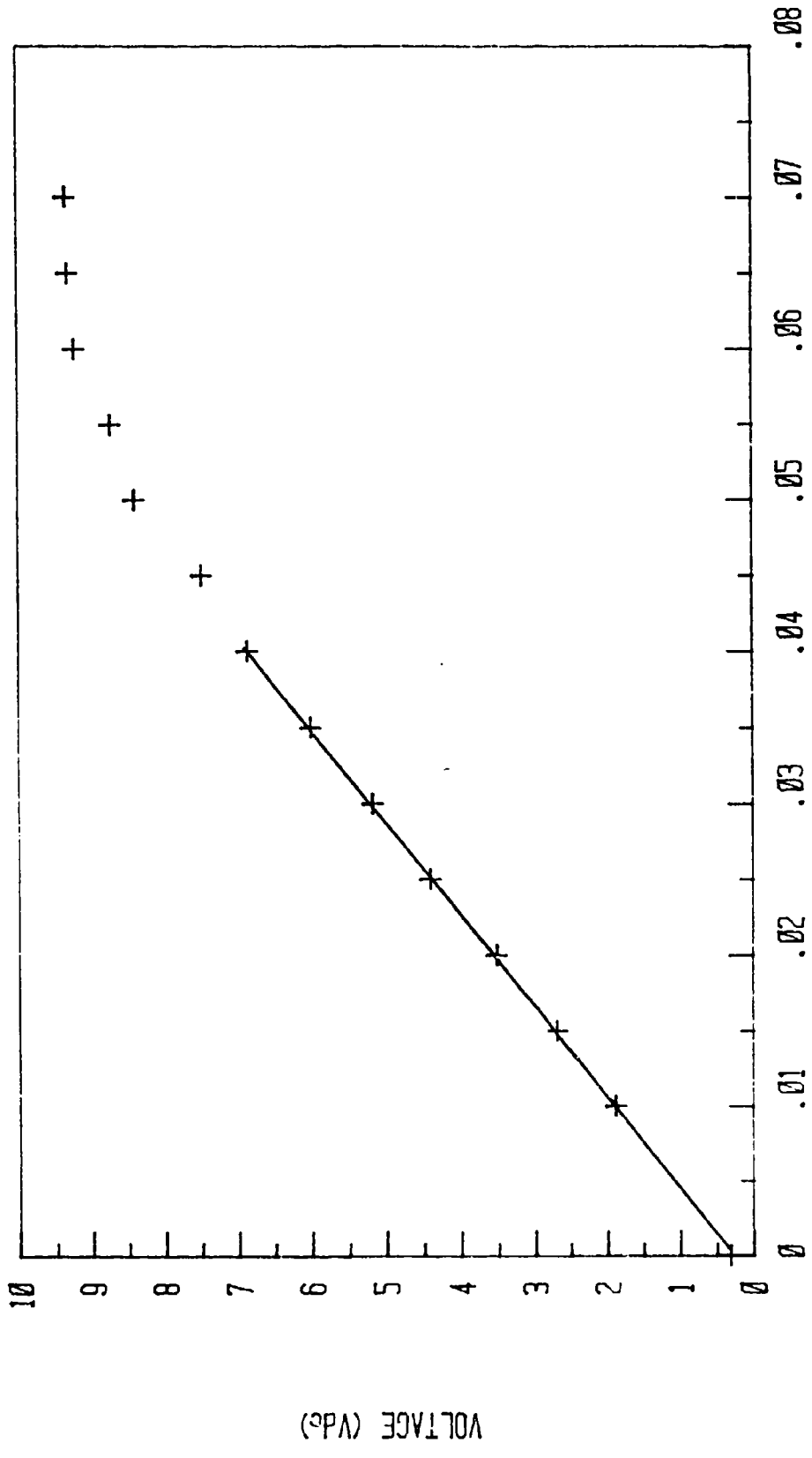

Figure 3.22. Calibration curve for a non contacting probe.

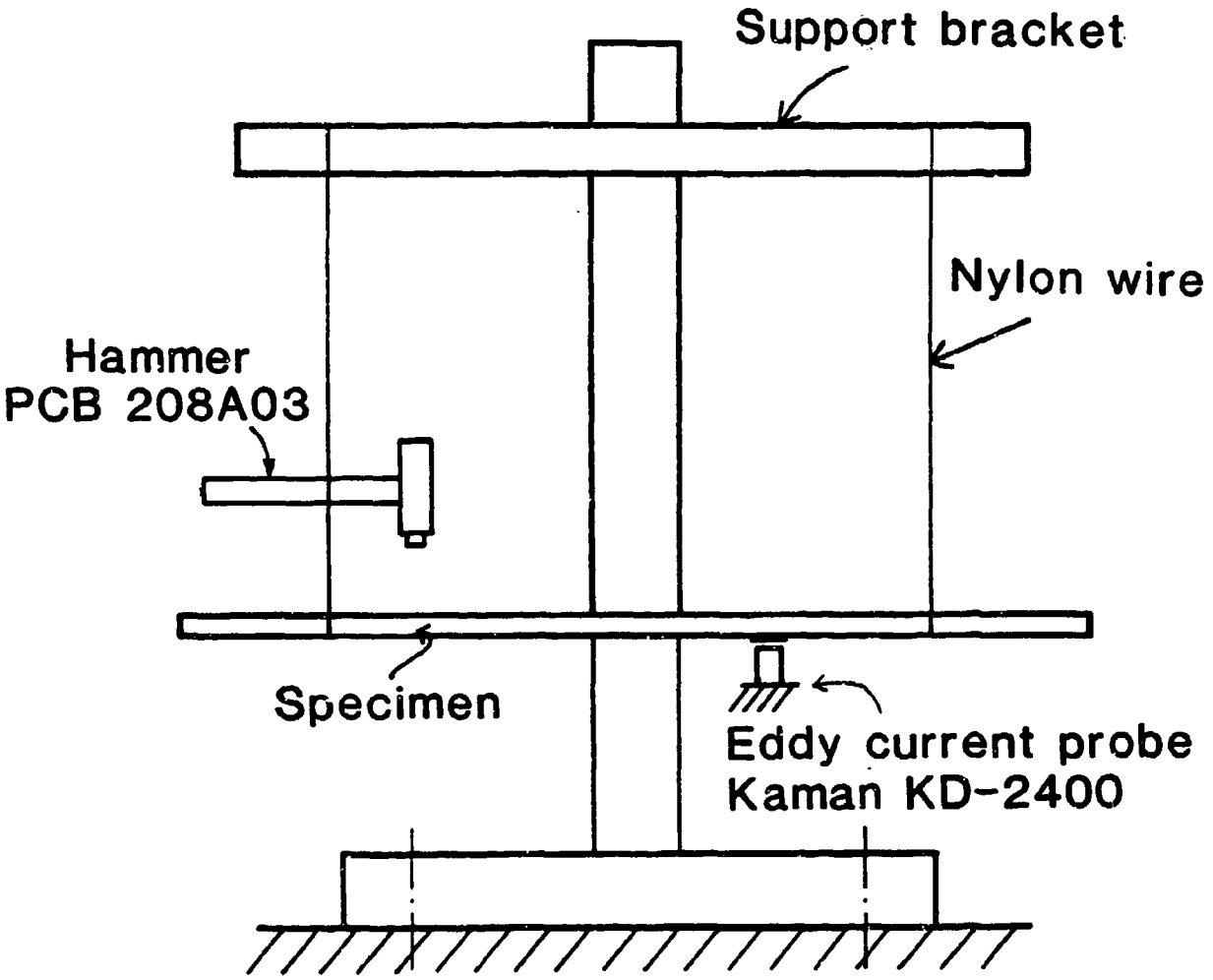

Figure 3.23. Free-free beam apparatus

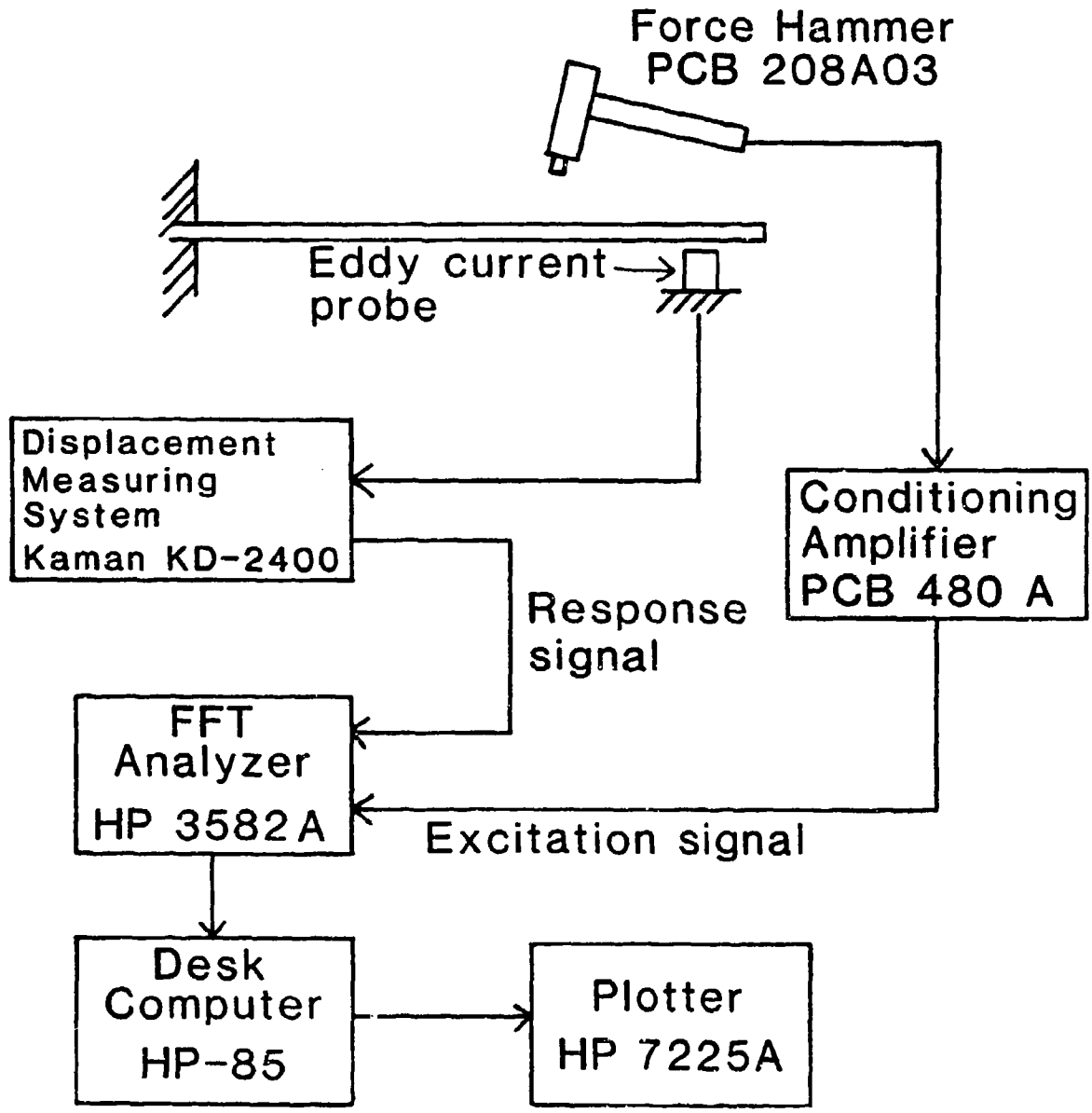

Figure 3.24. Block diagram of instrumentation for impulse technique.

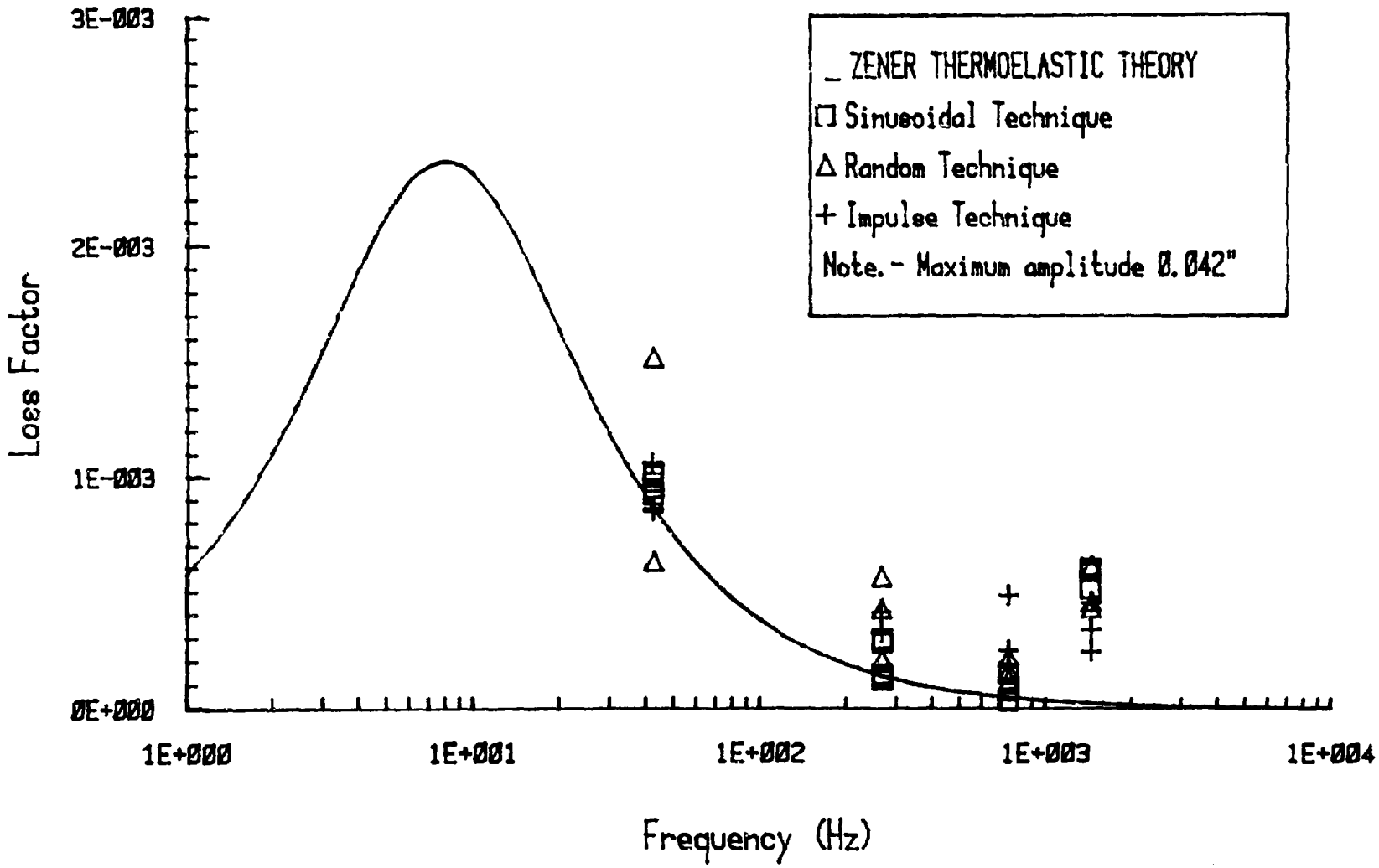

Figure 3.25. Variation of loss factor with frequency for aluminum cantilever beam specimens.

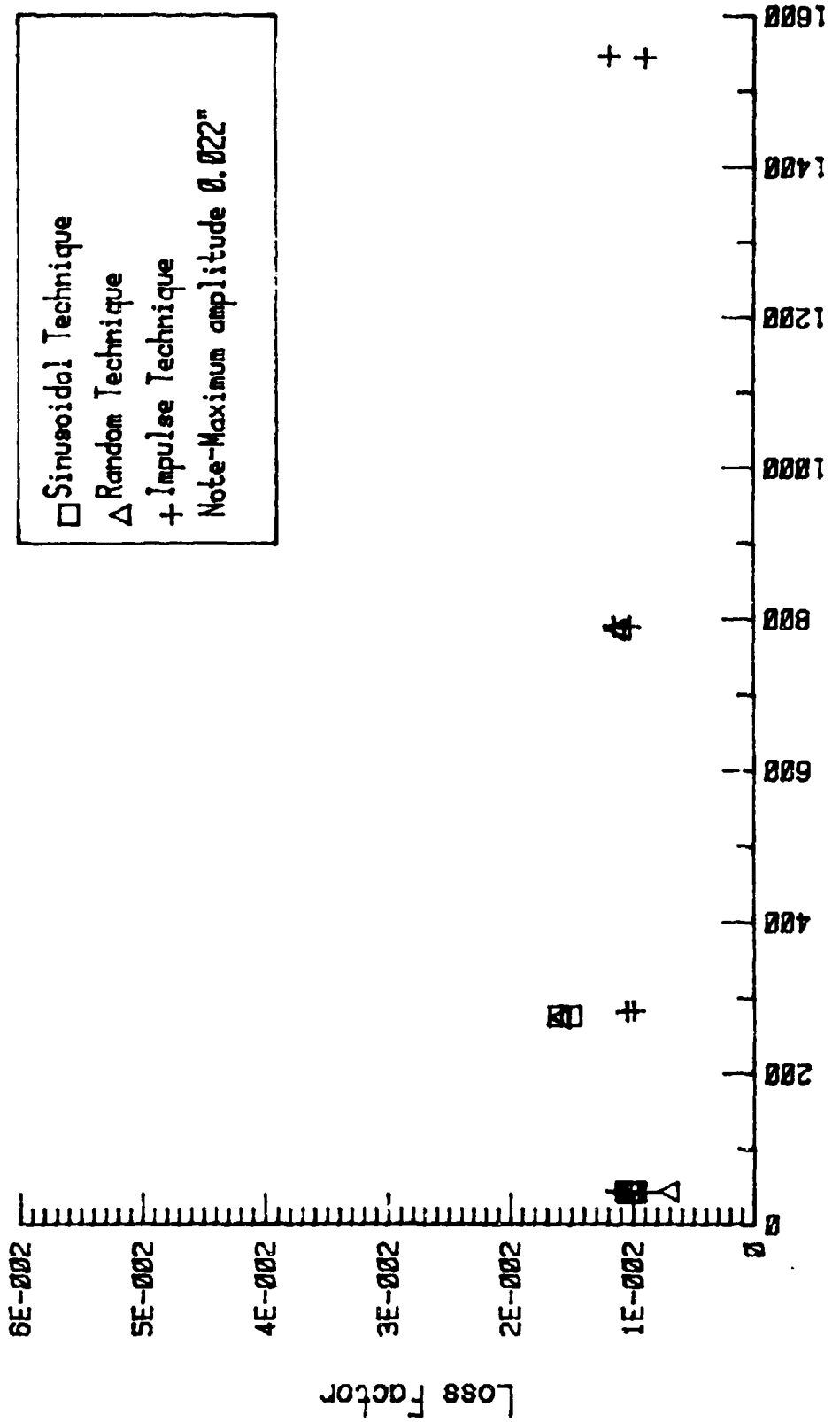

Figure 3.26. Variation of loss factor with frequency for E-glass/polyester cantilever beam specimens.

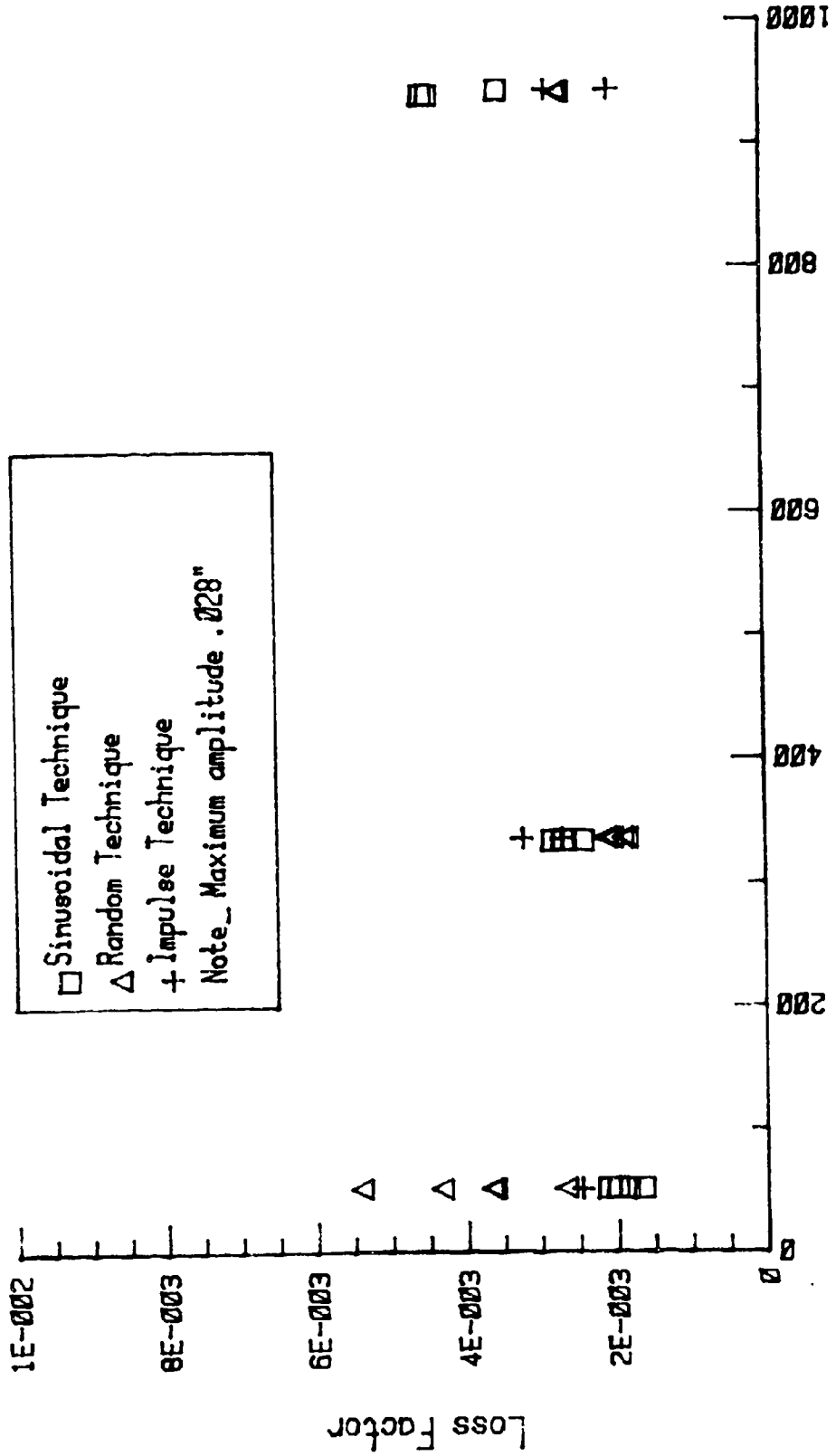

Figure 3.27. Variation of loss factor with frequency for graphite/epoxy cantilever beam specimens.

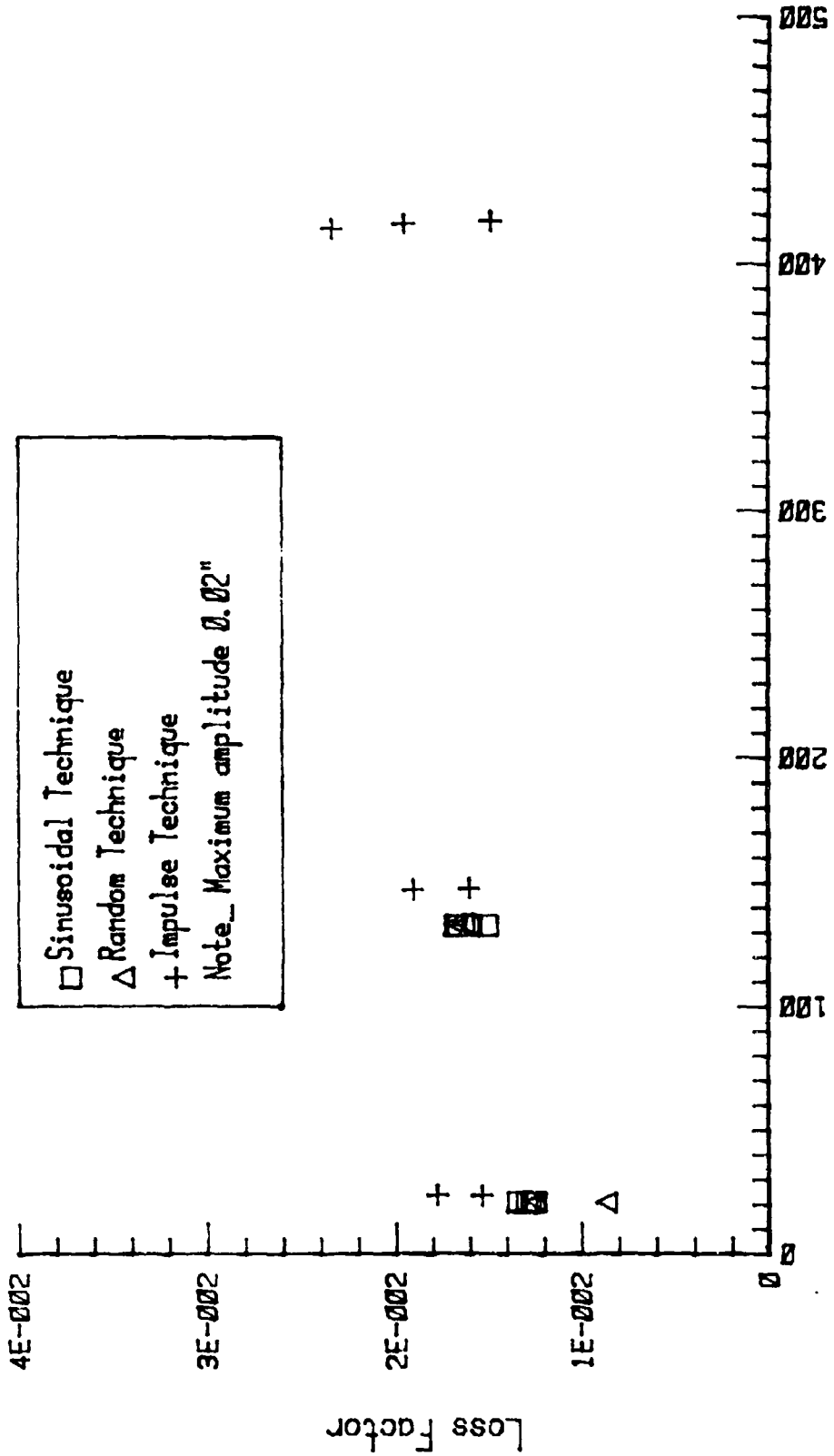

Figure 3.28. Variation loss factor with frequency for epoxy cantilever beam specimens.

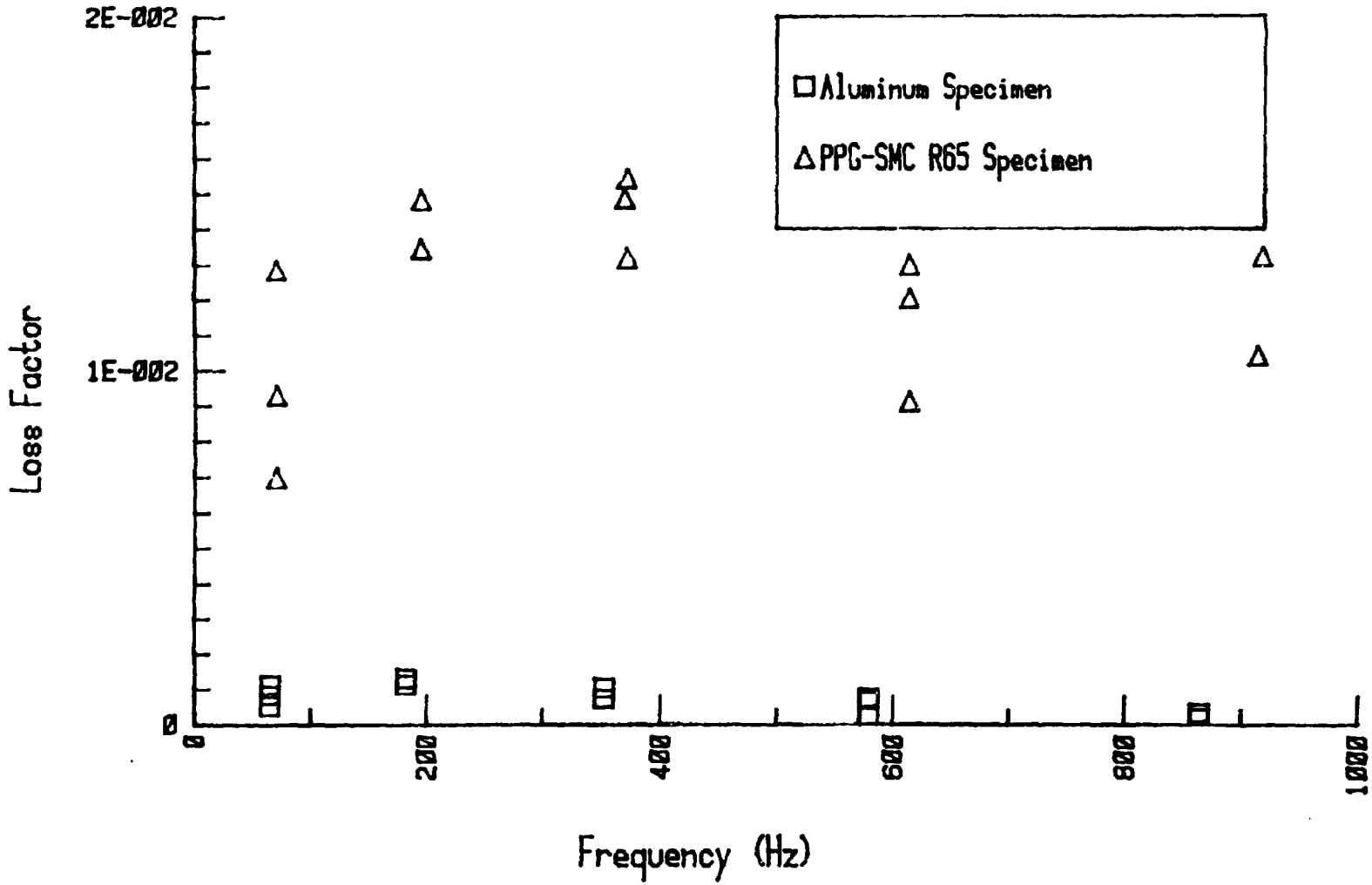

Figure 3.29. Variation of loss factor with frequency for aluminum and E-glass/epoxy polyester free-free beam specimens.

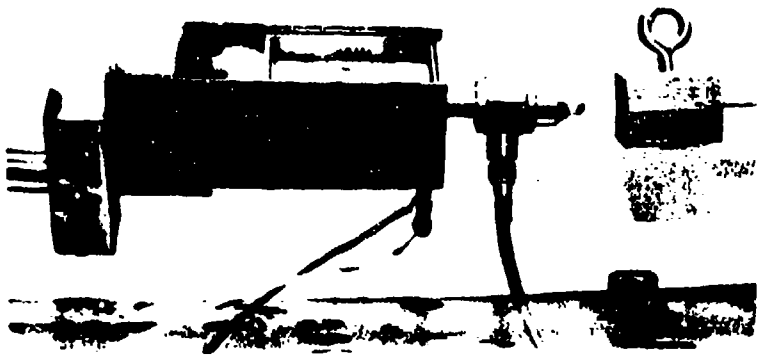

Figure 3.30. Solenoid-type electromagnetic exciter.

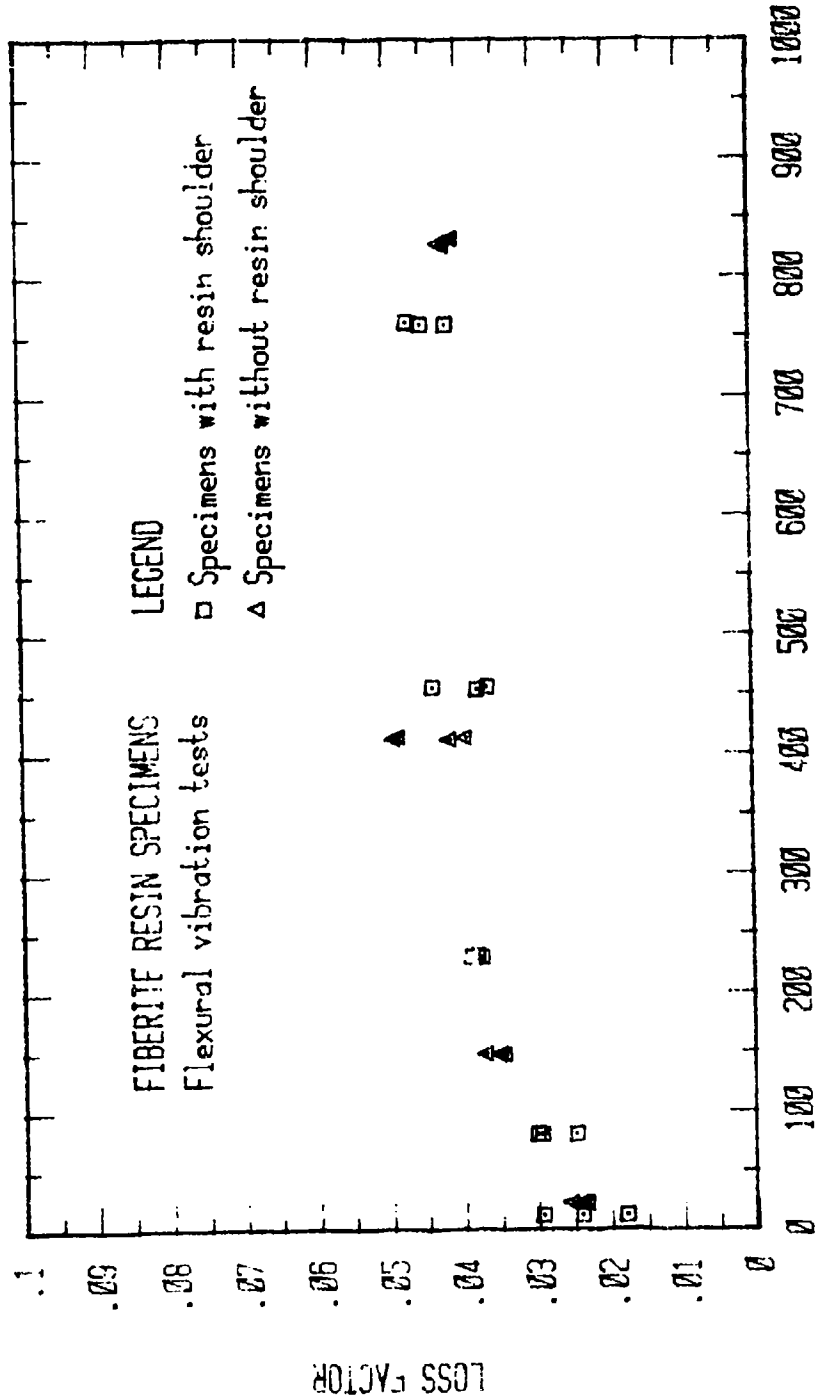

Figure 3.31. Comparison of loss factors using the specimens with and without shoulders.

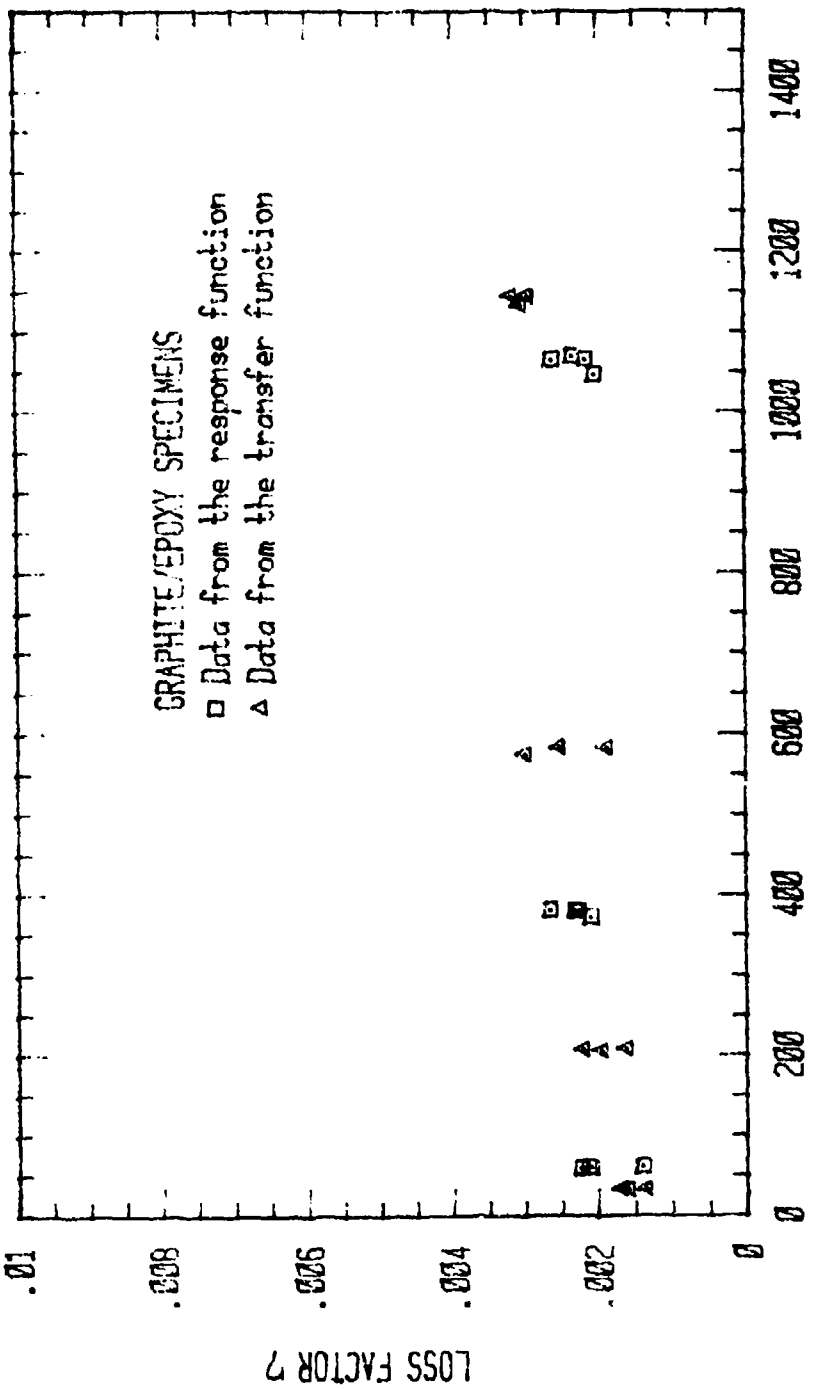

Figure 3.32. Comparison of loss factors using the response and the transfer functions.

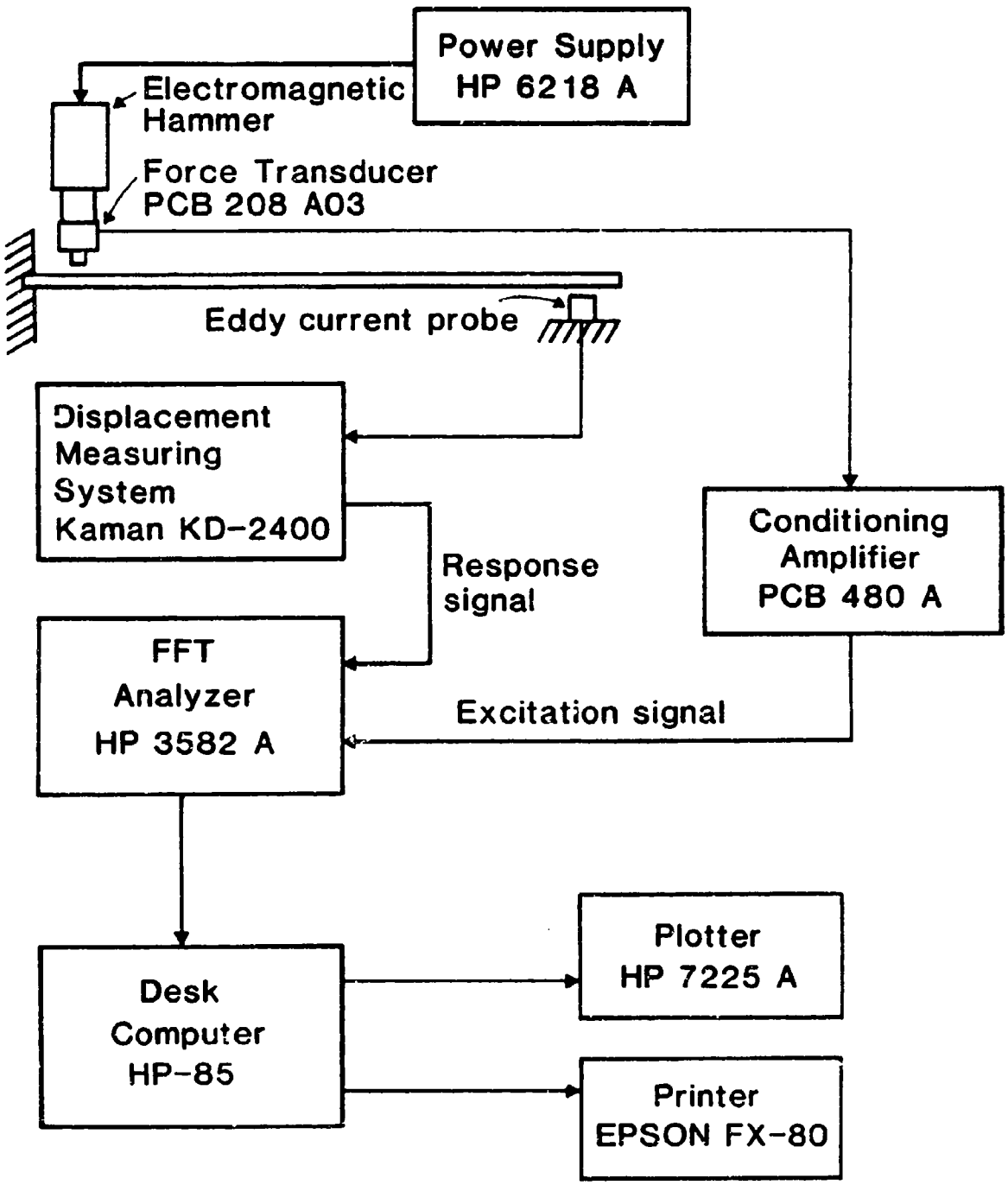

Figure 3.33. Block diagram of instrumentation for flexural vibration tests.

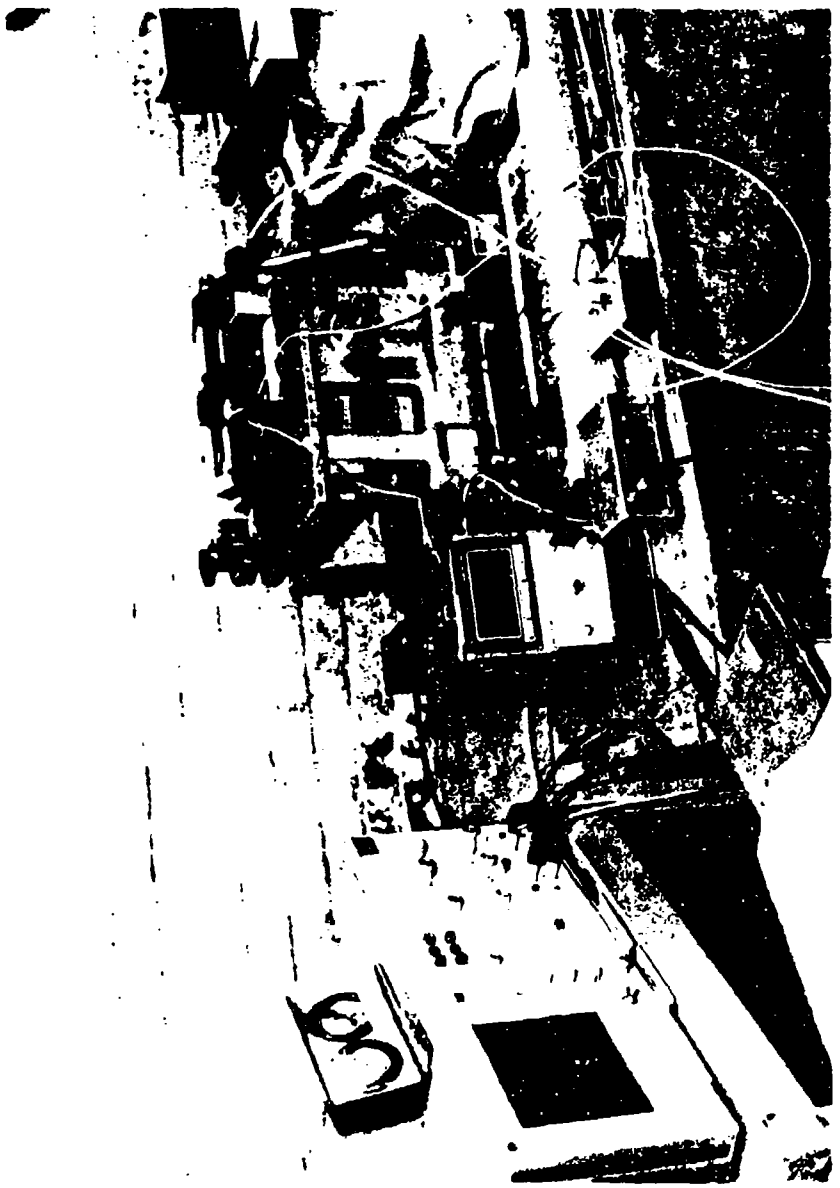

Figure 3.34. Equipment used with the flexural vibration tests.

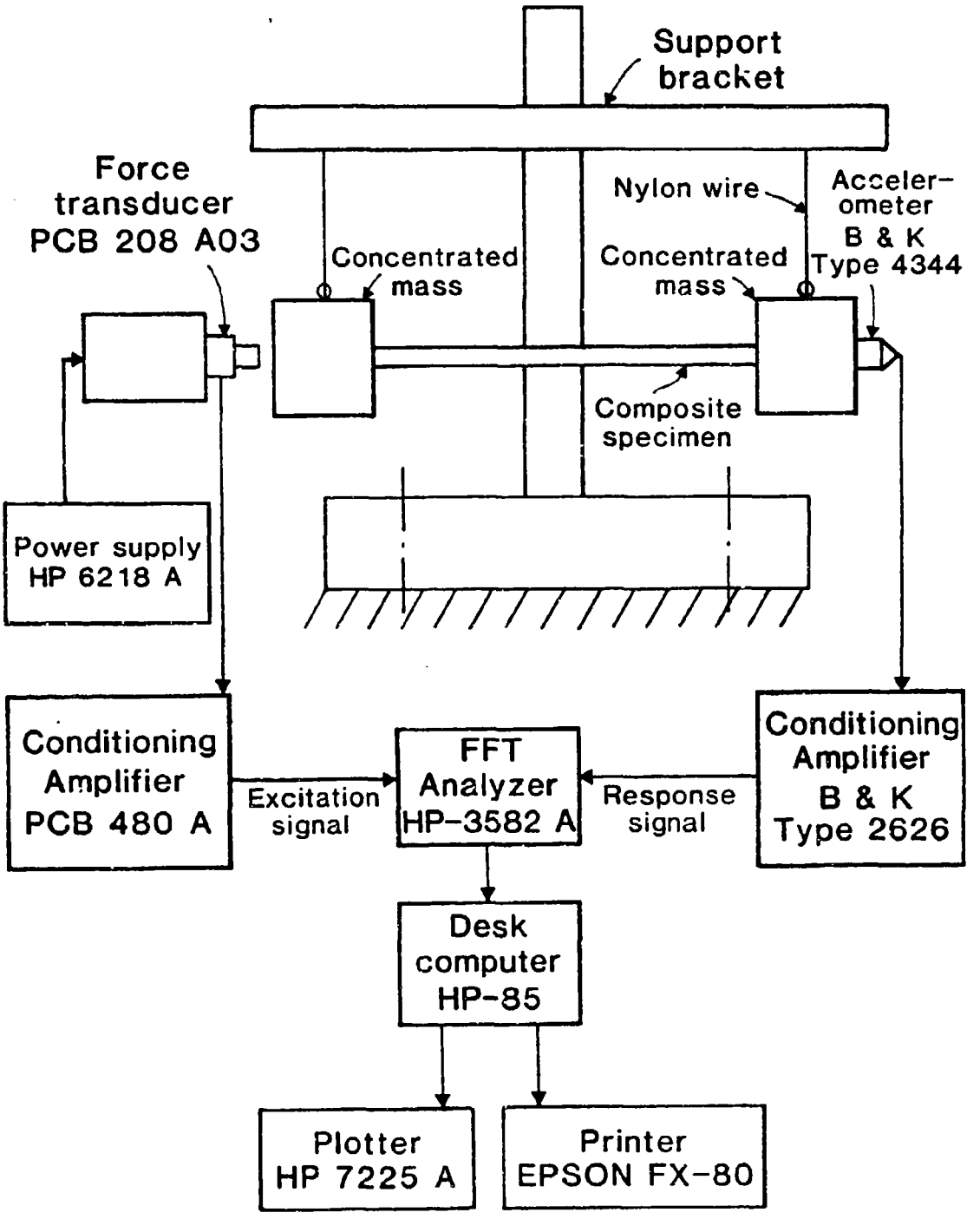

Figure 3.35. Block diagram of instrumentation for extensional vibration tests.

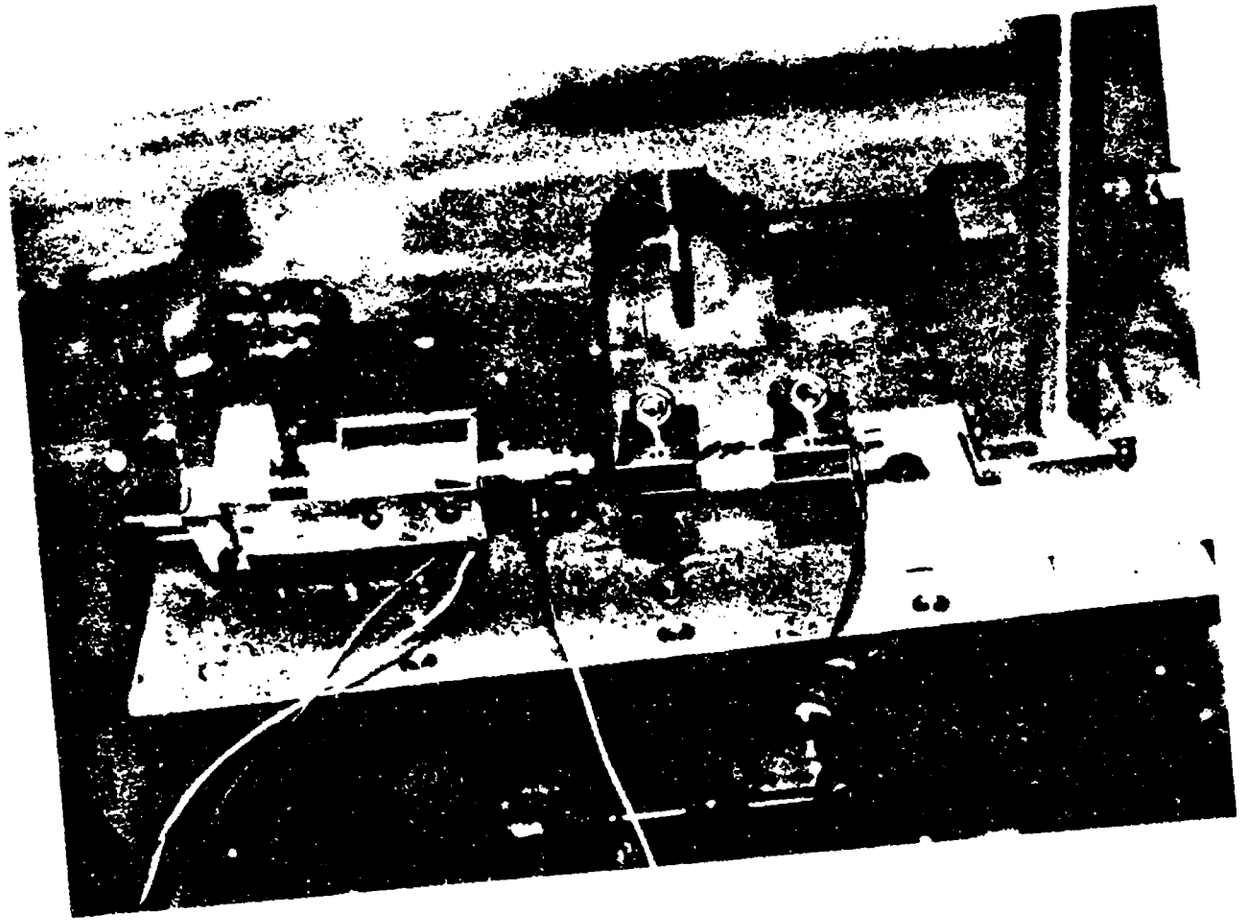

Figure 3.36. Equipment used with the extensional vibration tests.

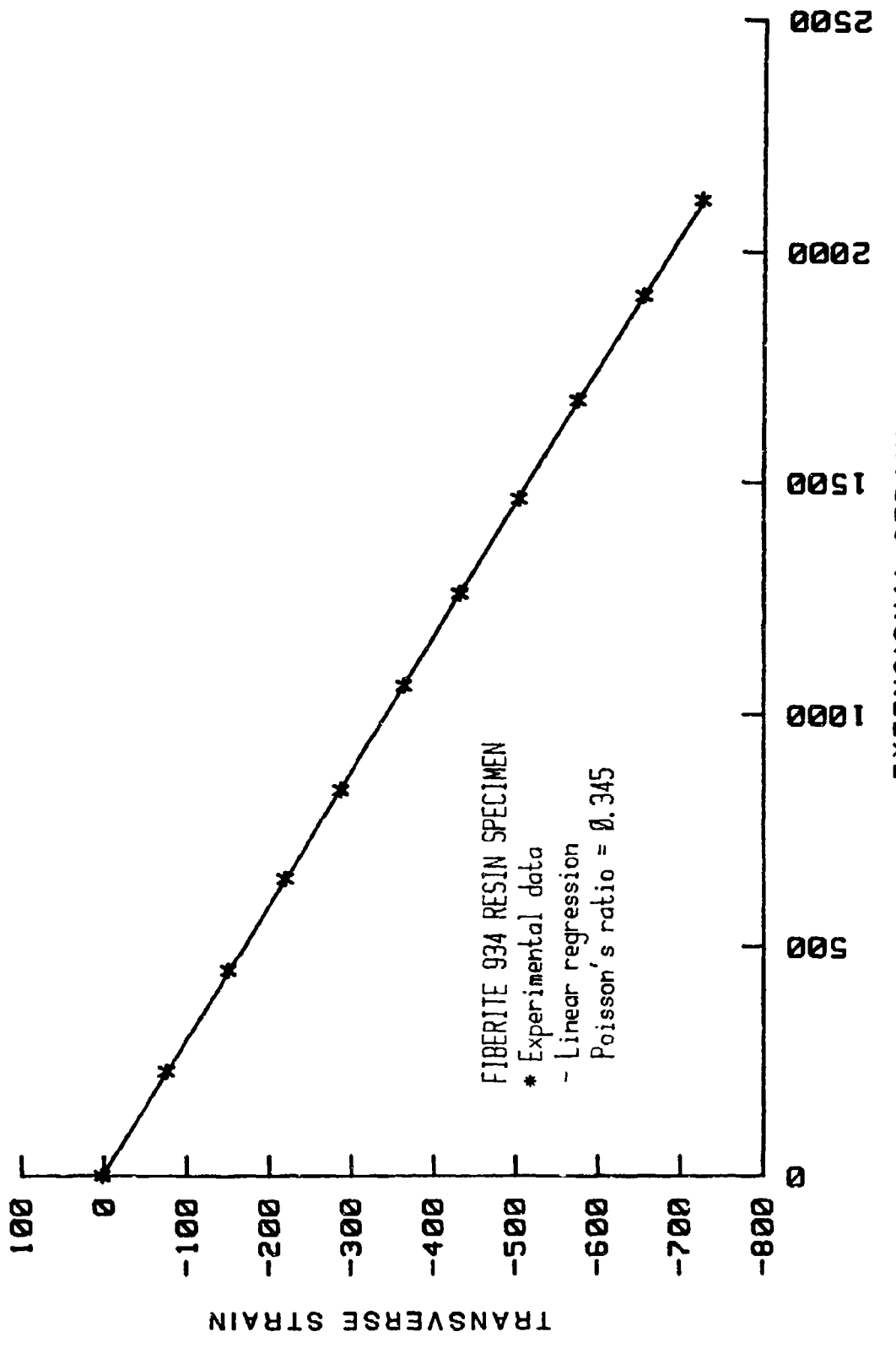

Figure 3.37. Poisson's ratio for Fiberite 934 resin.

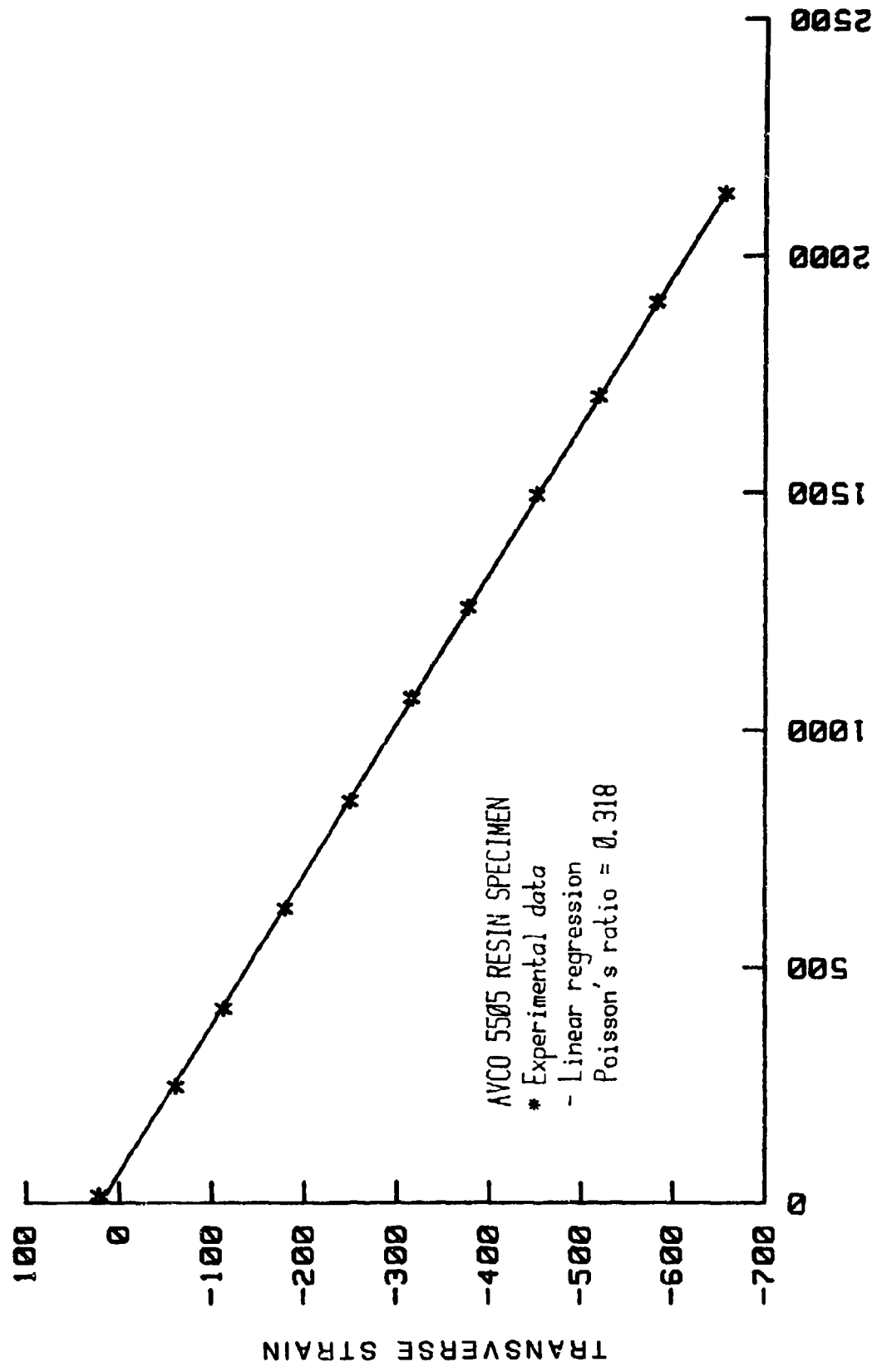

Figure 3.38. Poisson's ratio for AVCO 5505 resin.

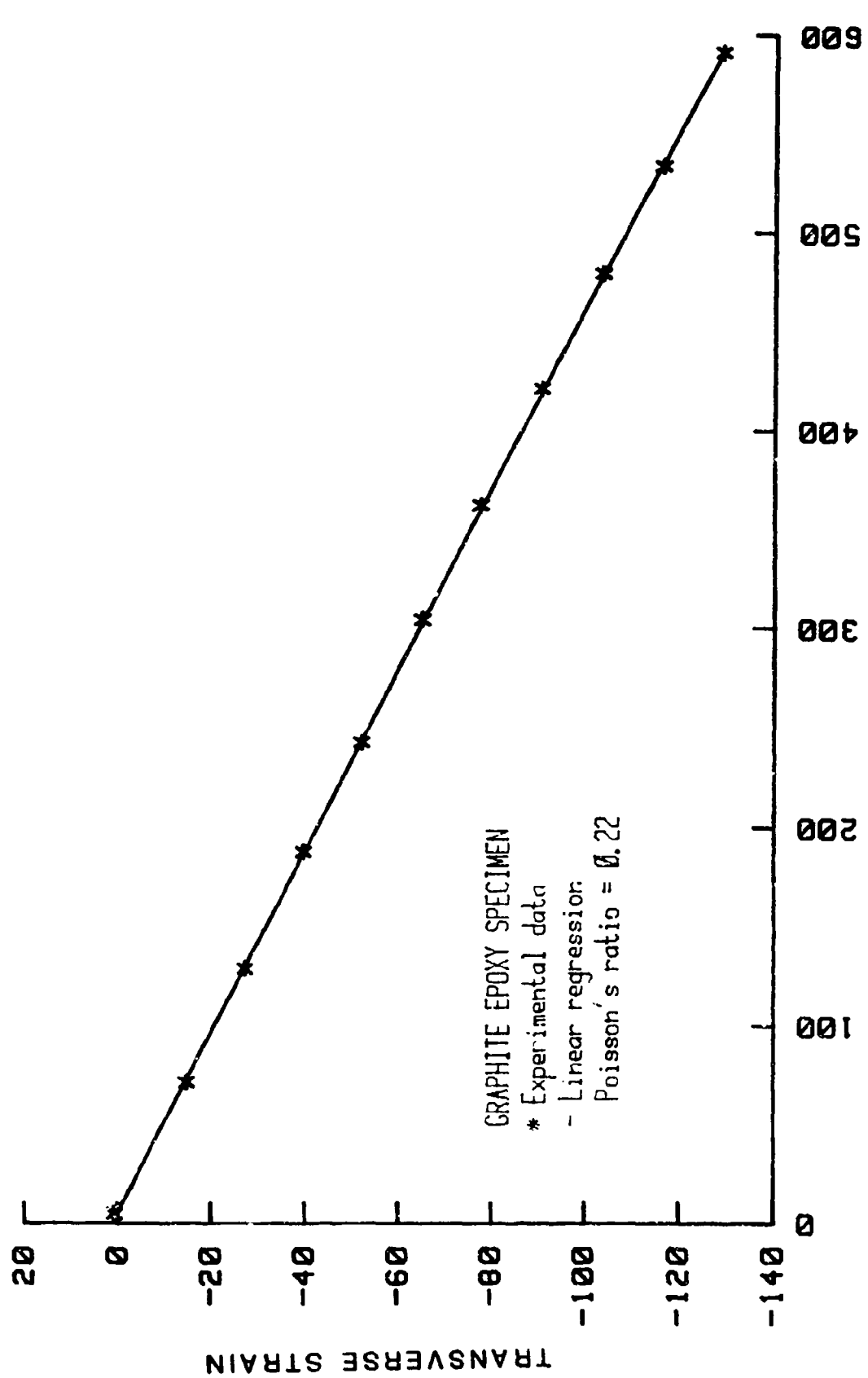

Figure 3.39. Poisson's ratio for graphite/epoxy composite.

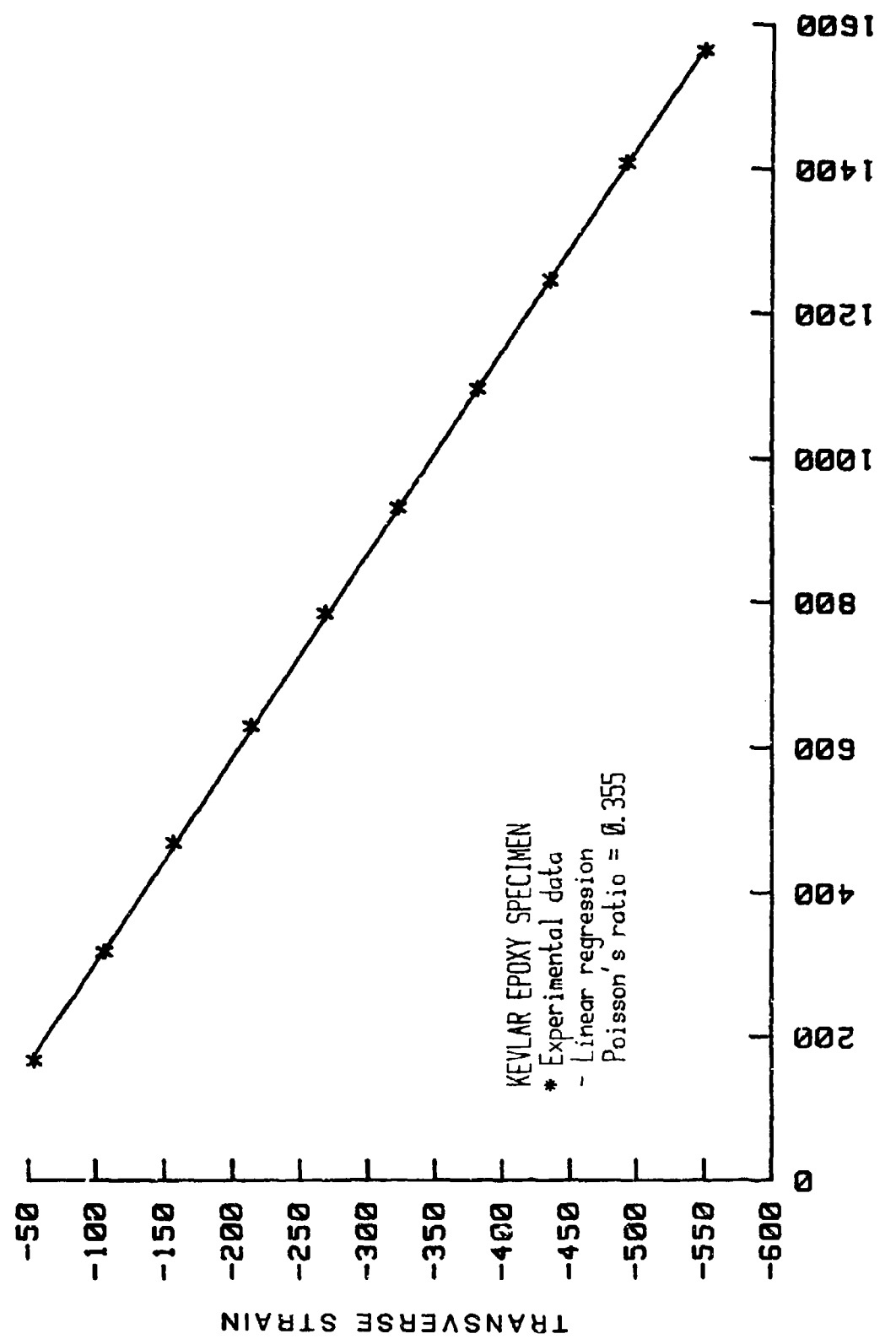

Figure 3.40. Poisson's ratio for Kevlar/epoxy composite.

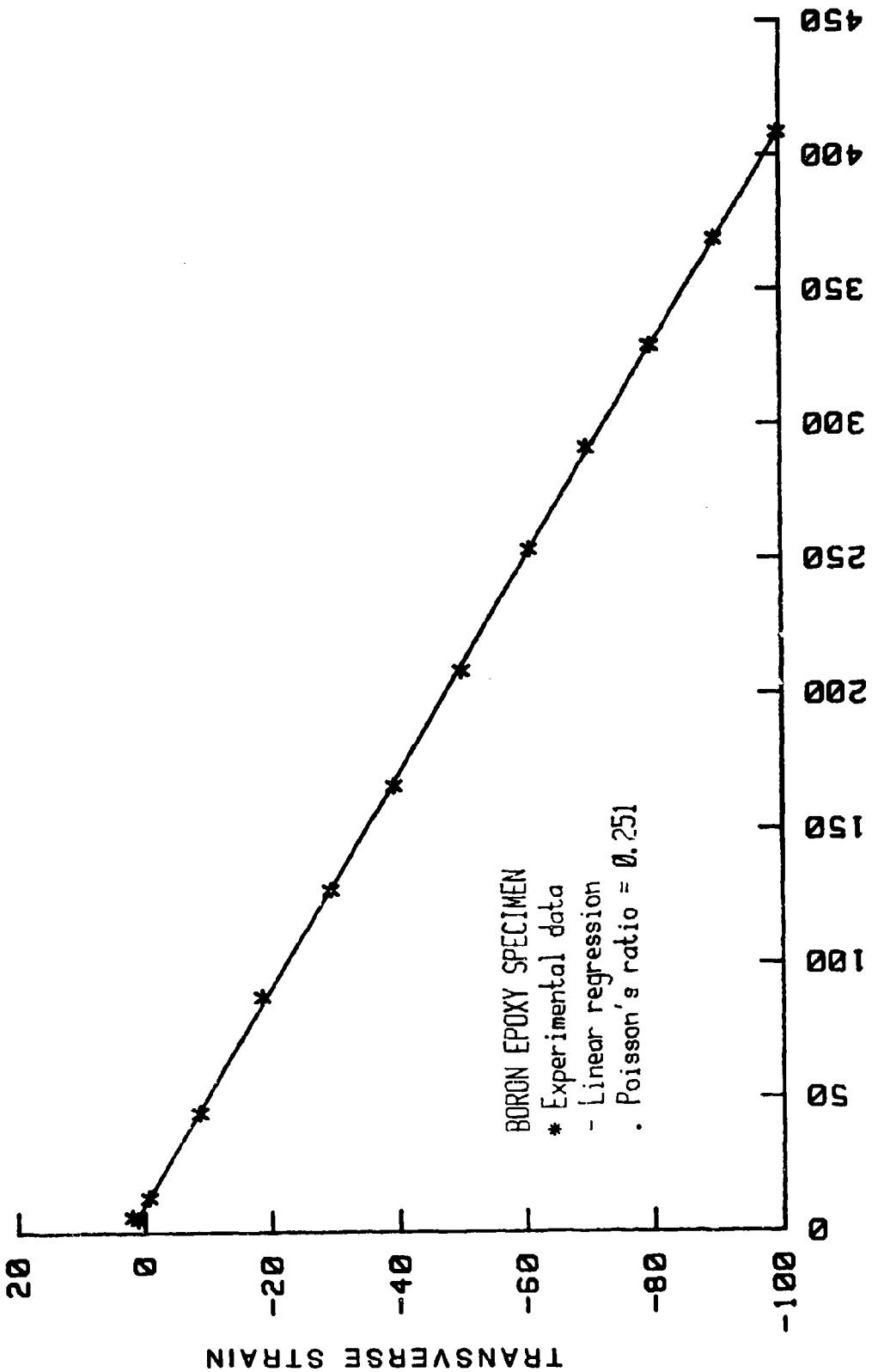

Figure 3.41. Poisson's ratio for boron/epoxy composite.

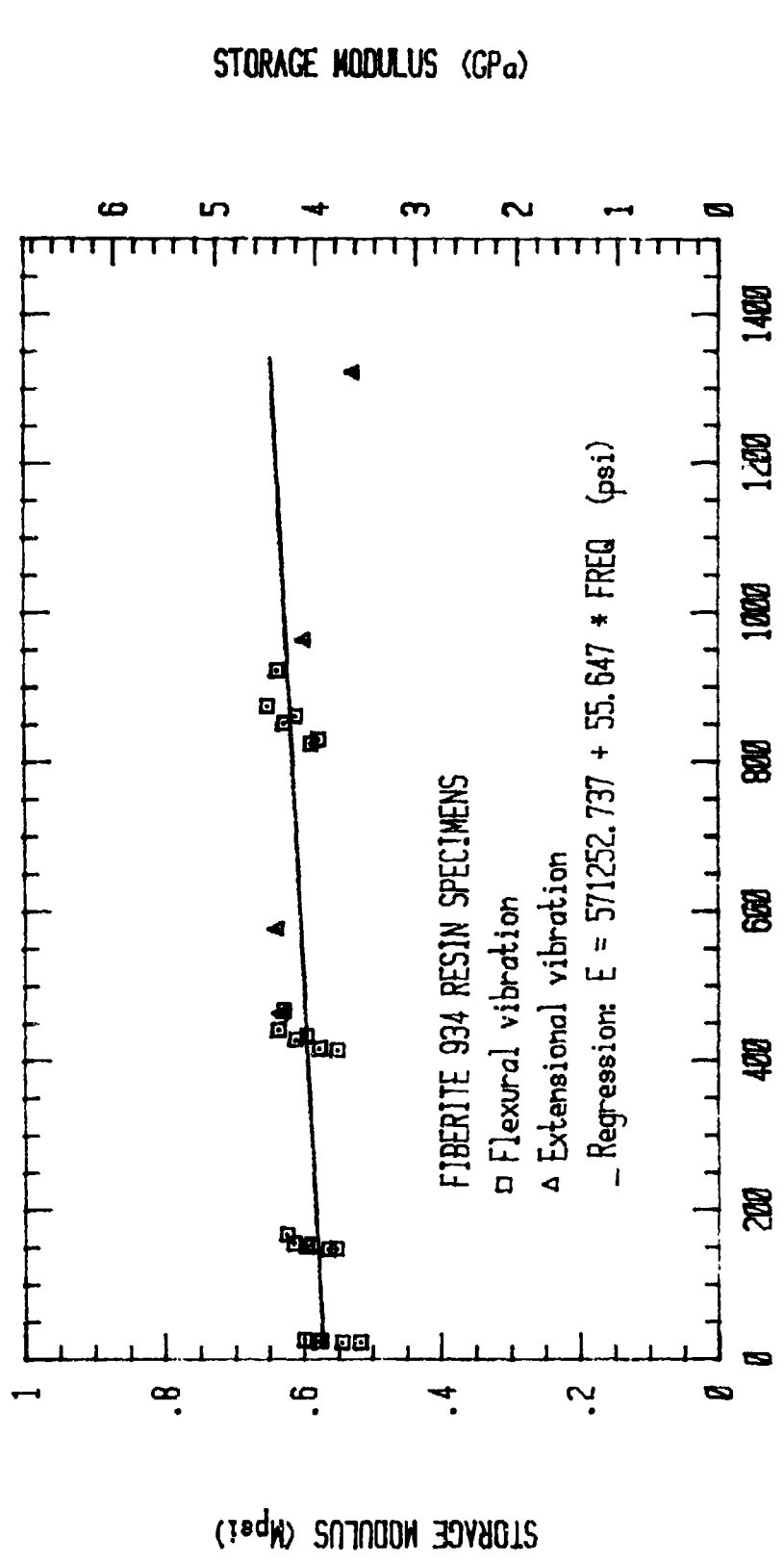

Figure 4.1. Variation of storage moduli with frequency for Fiberite 934 resin casting.

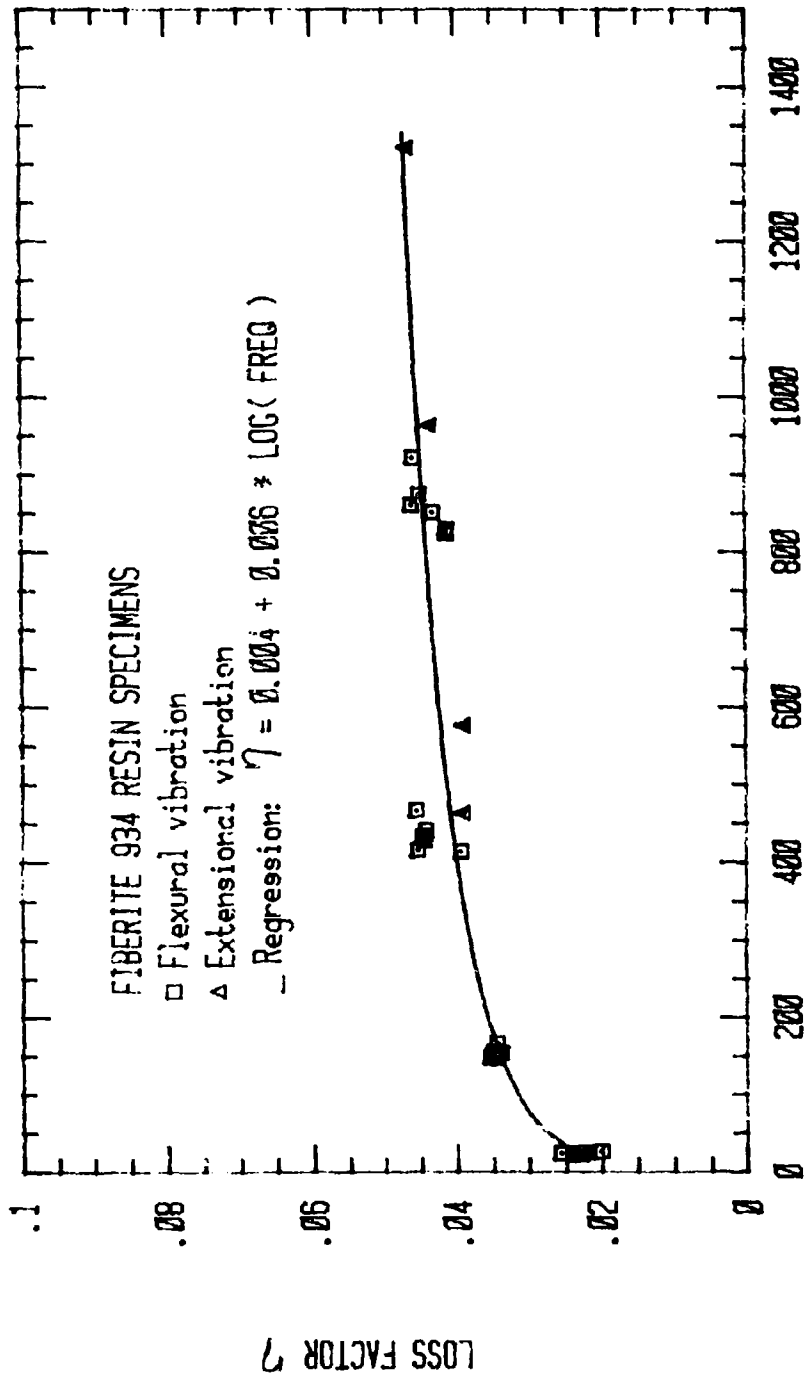

Figure 4.2. Variation of loss factor with frequency for Fiberite 934 resin casting.

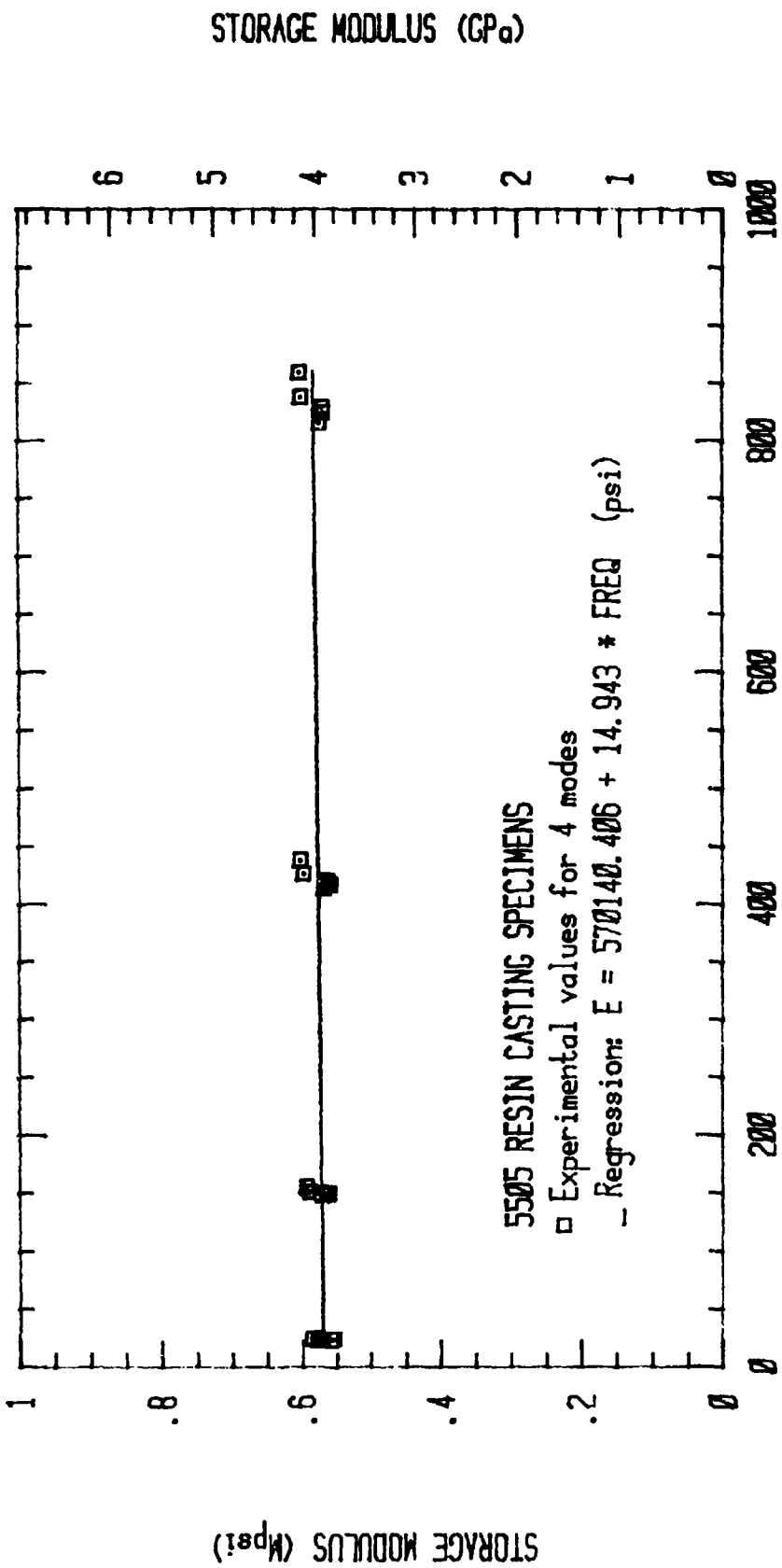

Figure 4.3. Variation of storage modulus with frequency for AVCO 5505 resin casting.

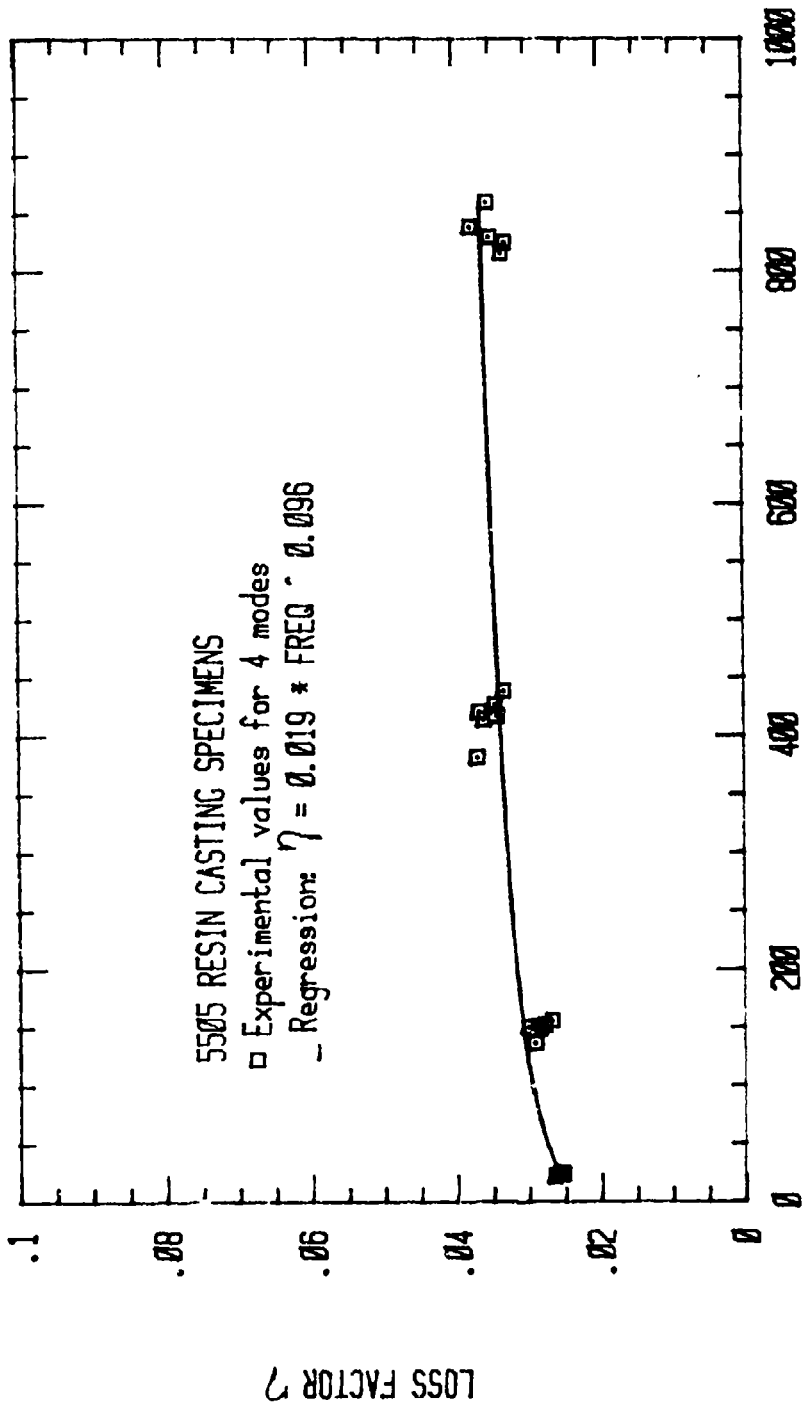

Figure 4.4. Variation of loss factor with frequency for AVCO 5505 resin casting.

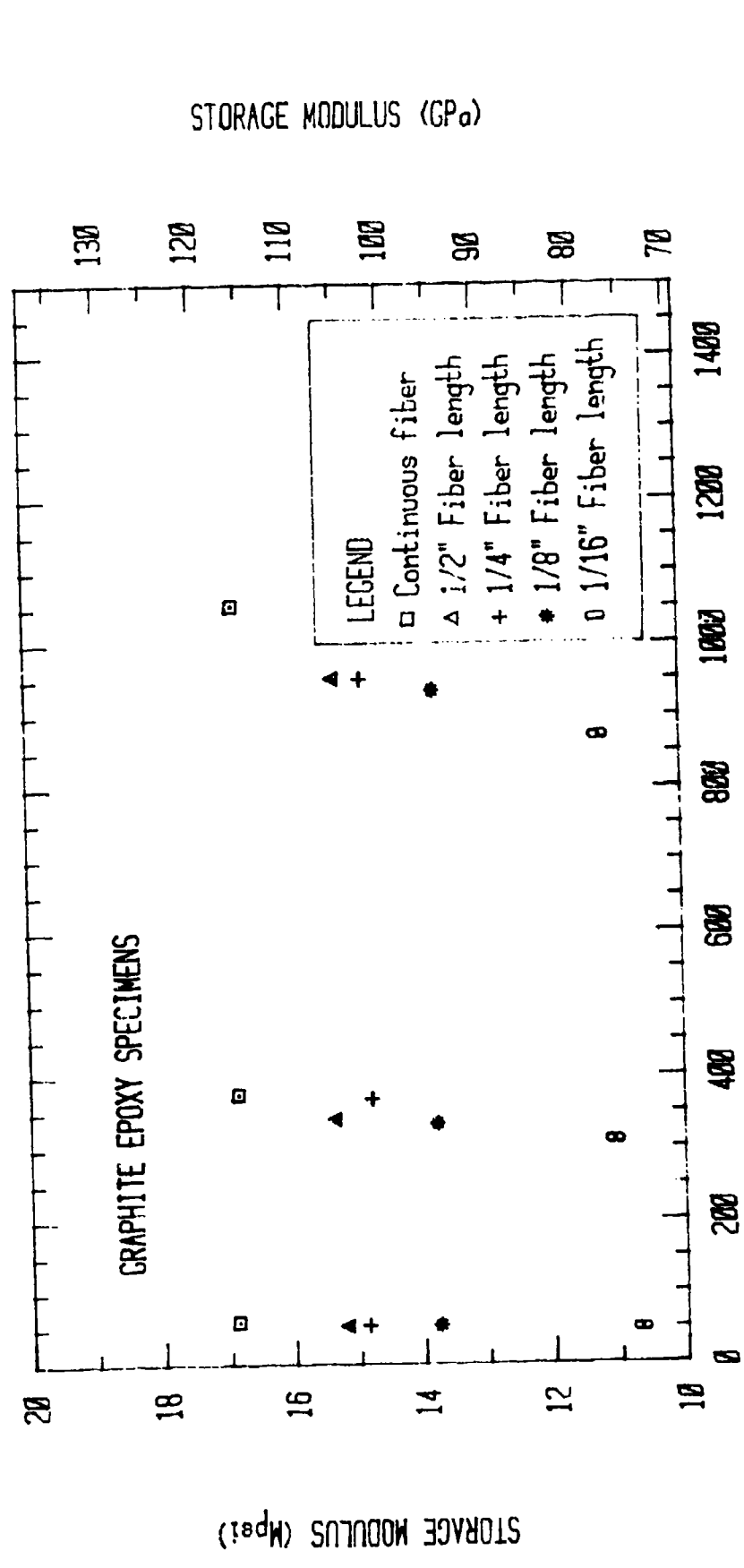

Figure 5.1. Variation of storage modulus with frequency for graphite/epoxy specimens.

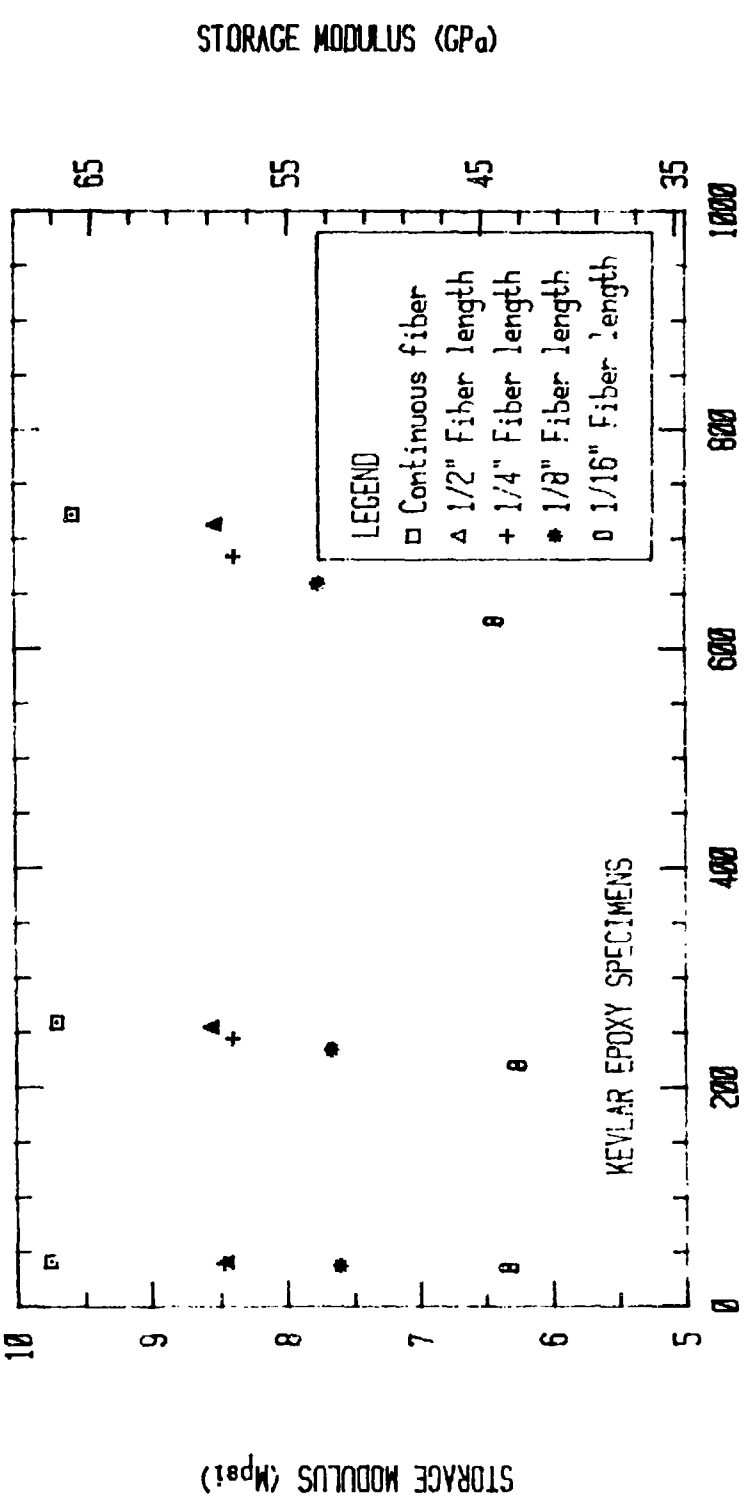

Figure 5.2. Variation of storage modulus with frequency for Kevlar/epoxy specimens.

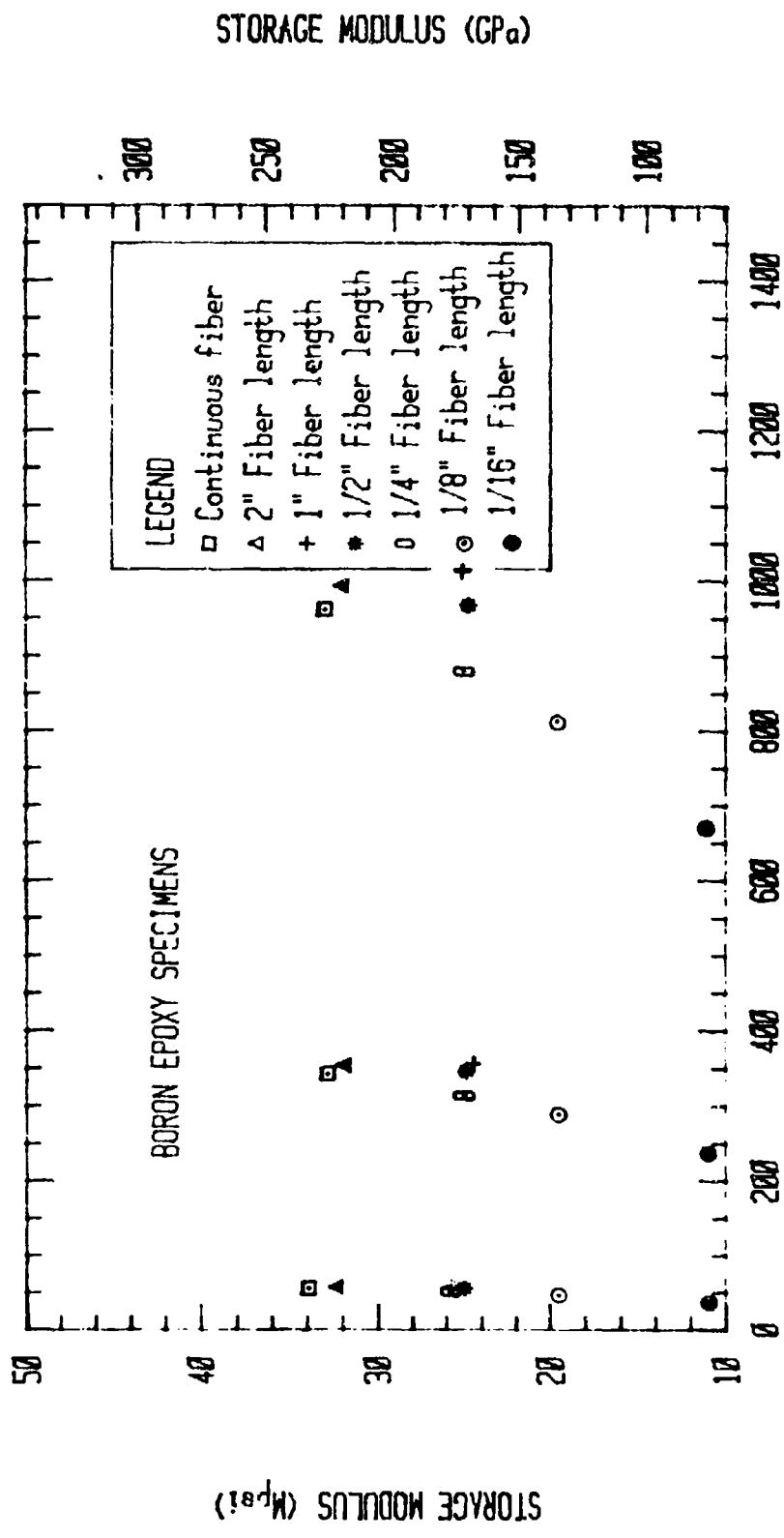

Figure 5.3. Variation of storage modulus with frequency for boron/epoxy specimens.

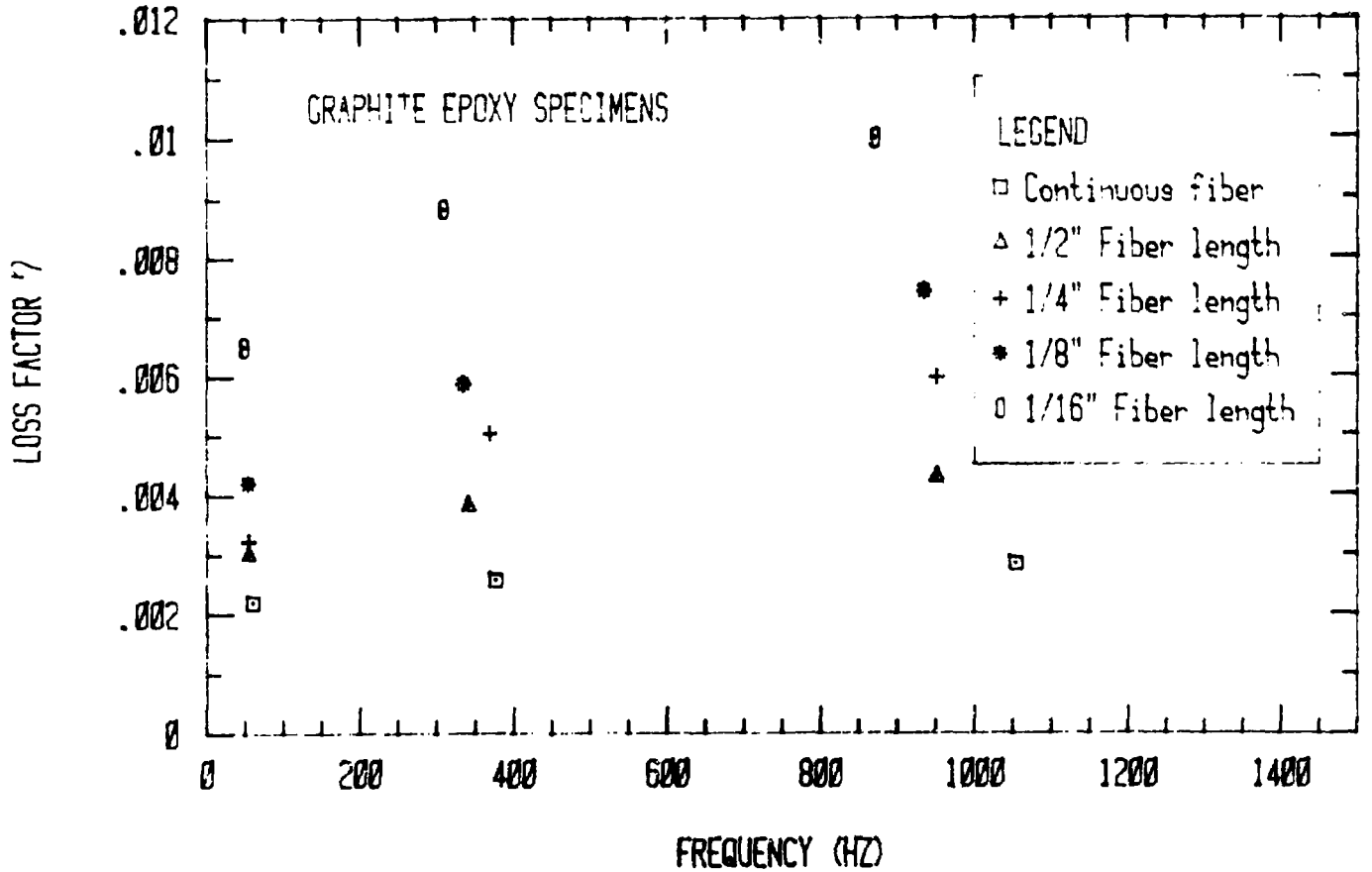

Figure 5.4. Variation of loss factor with frequency for graphite/epoxy specimens.

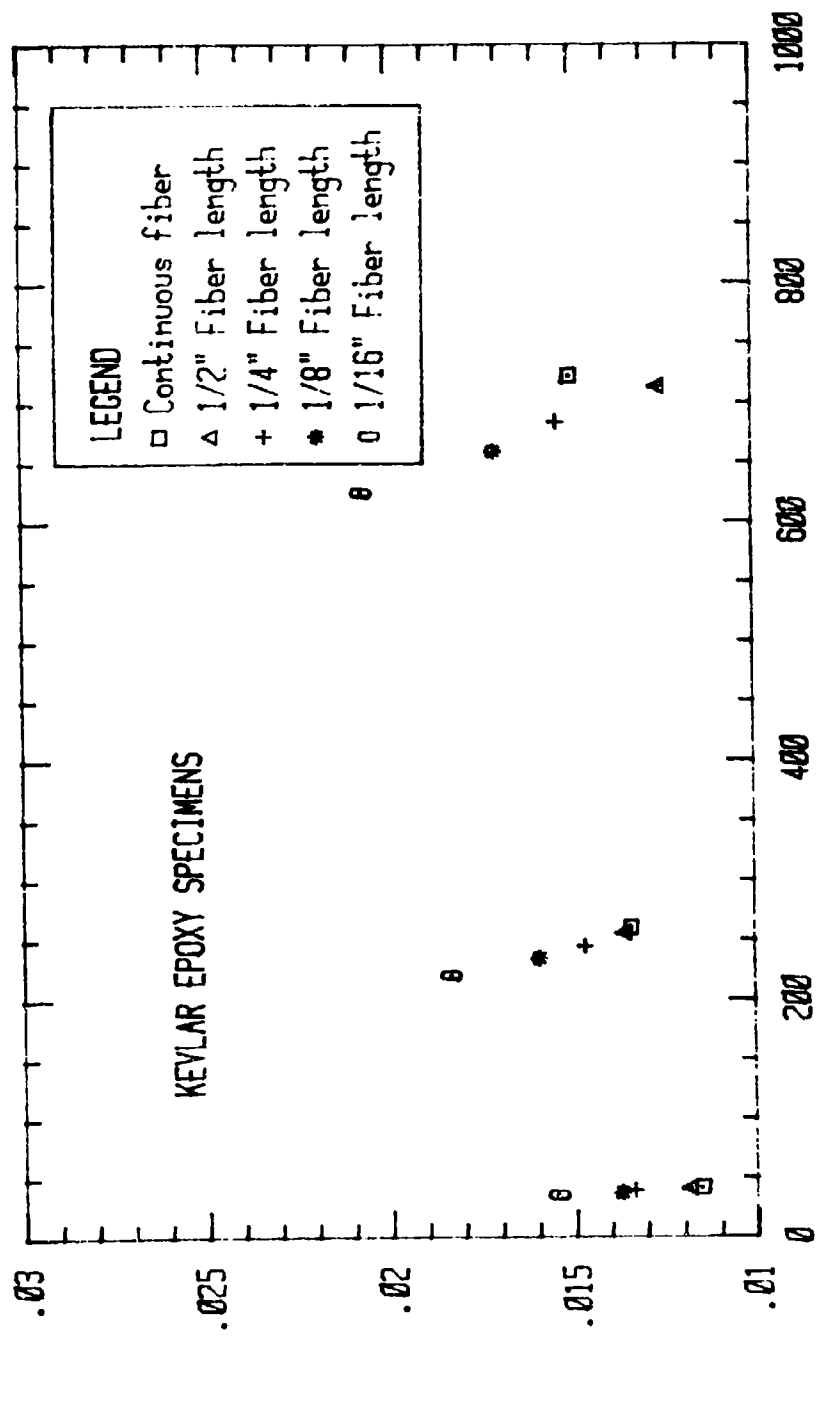

Figure 5.5. Variation of loss factor with frequency for Kevlar/epoxy specimens.

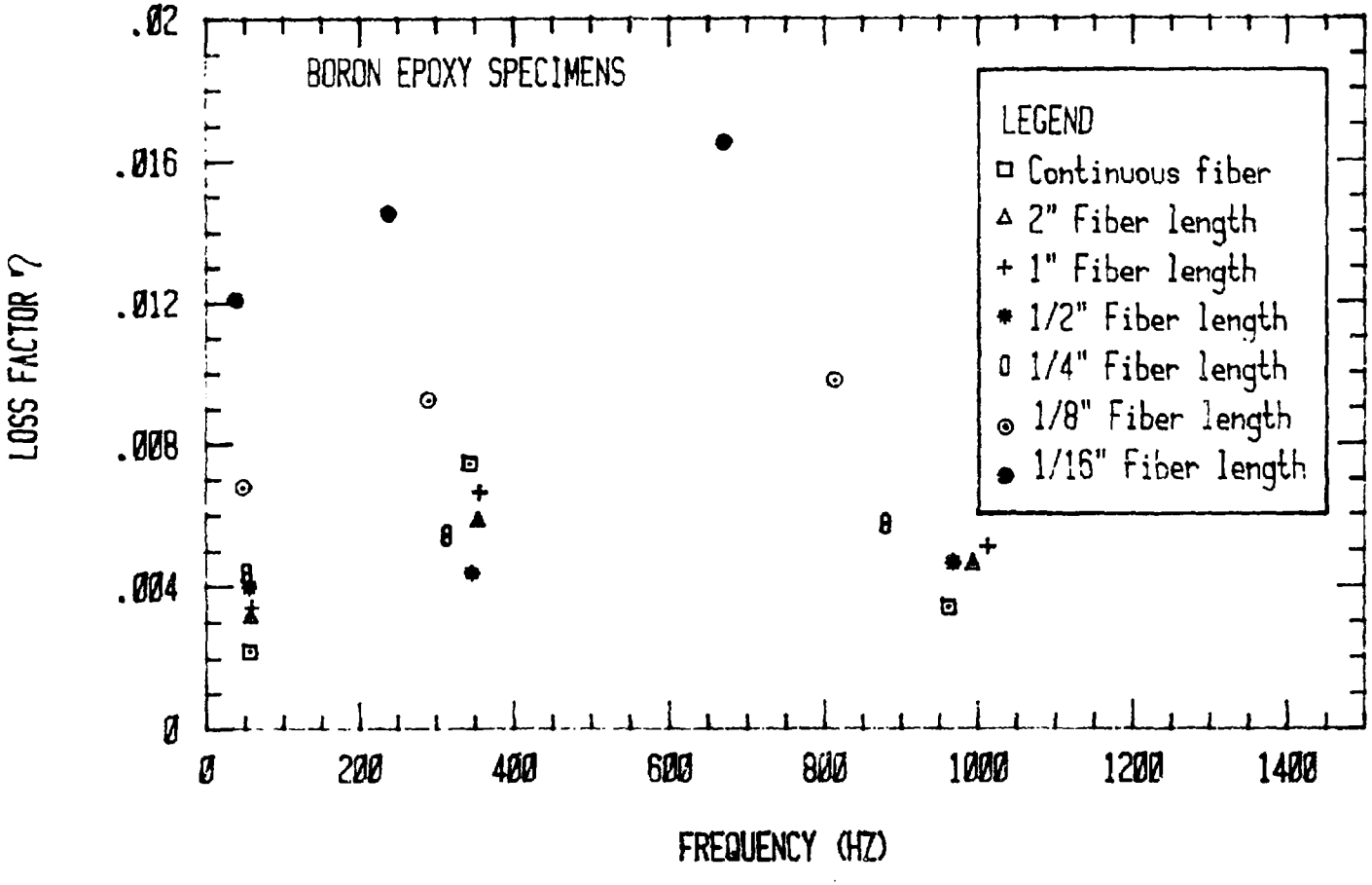

Figure 5.6. Variation of loss factor with frequency for boron/epoxy specimens.

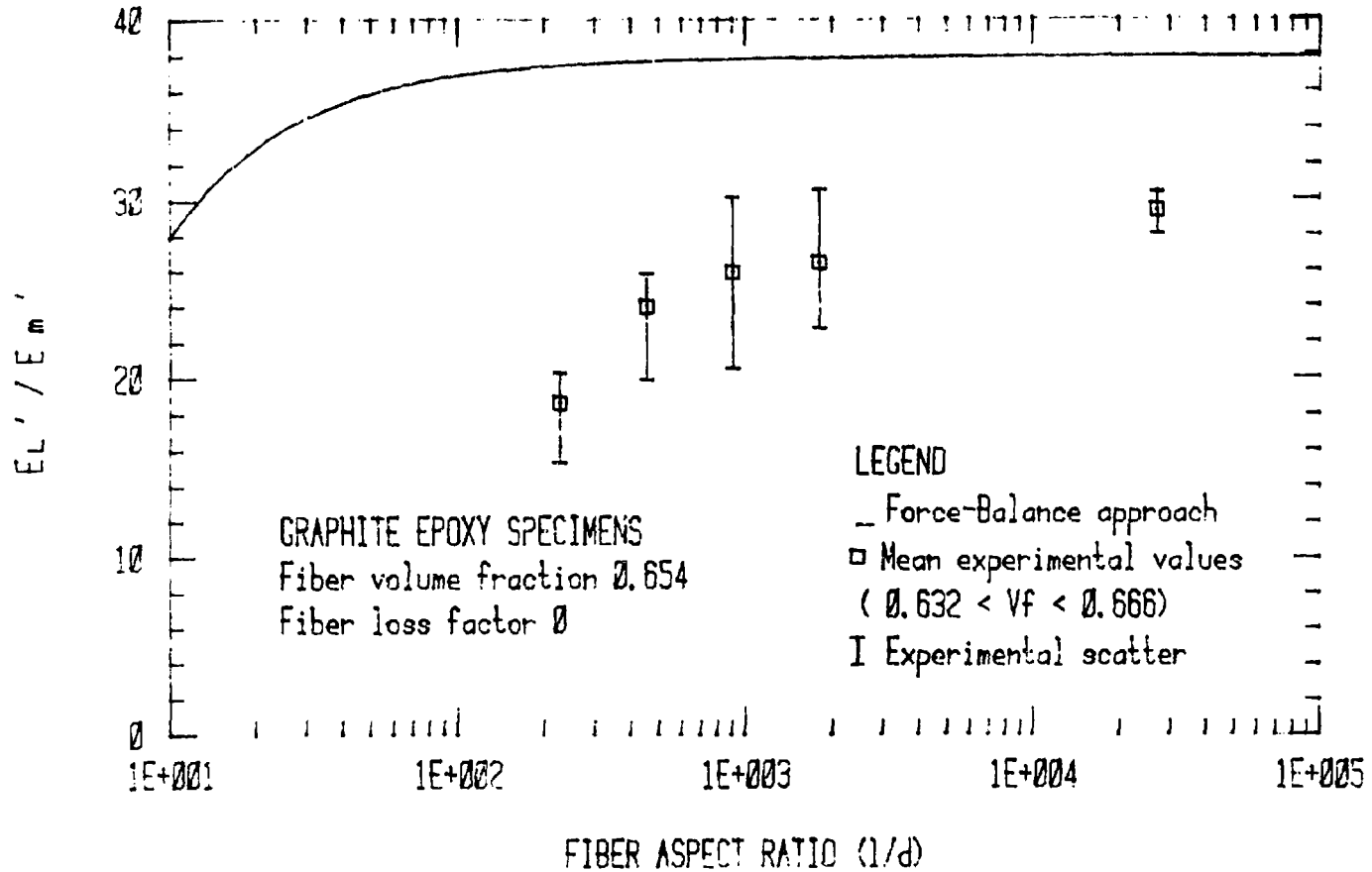

Figure 5.7. E_L'/E_m' vs. fiber aspect ratio for graphite/epoxy without curve fitting [E_f' = 33.10^6 psi (227.38 GPa), Z=1, f=54 Hz].

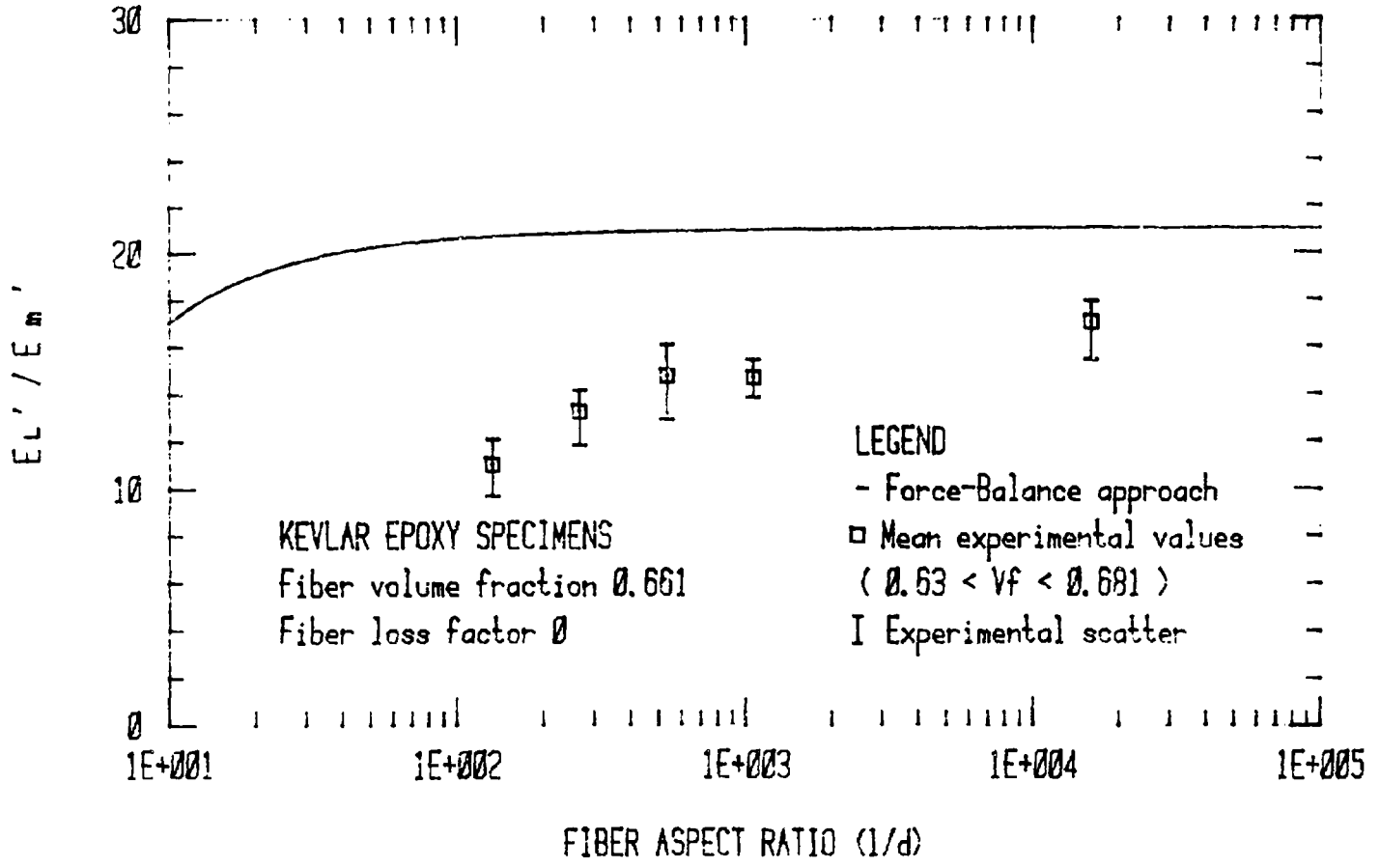

Figure 5.8. E_L'/E_m' vs. fiber aspect ratio for Kevlar/epoxy without curve fitting [E_f' = 18 x 10^6 psi (124.02 GPa), Z=1, f=54 Hz].

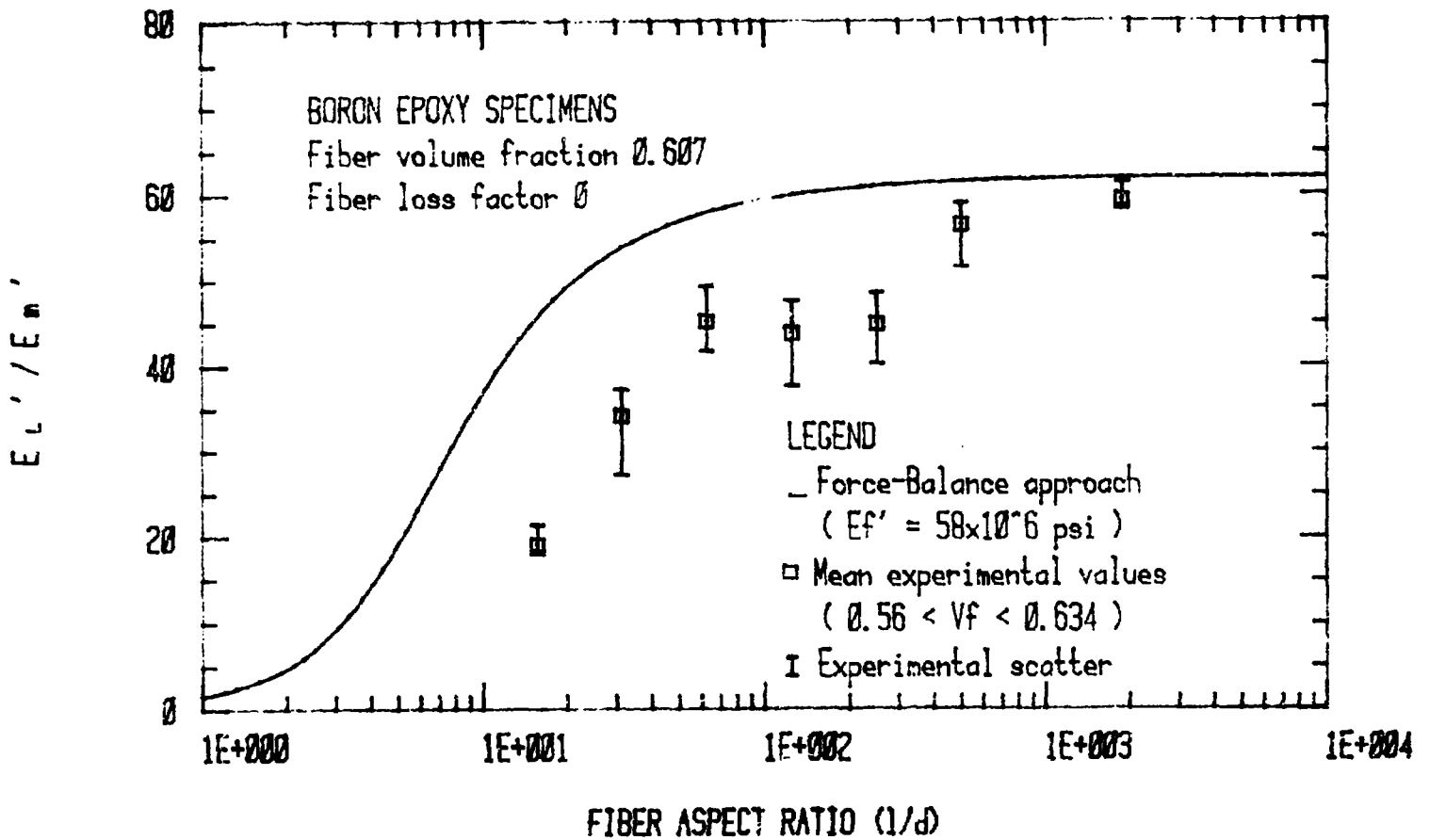

Figure 5.9. E_L'/E_m' vs. fiber aspect ratio for boron/epoxy without curve fitting [E_f' = 58 x 10^6 psi (399.62 GPa), Z=1, f=51.62 Hz].

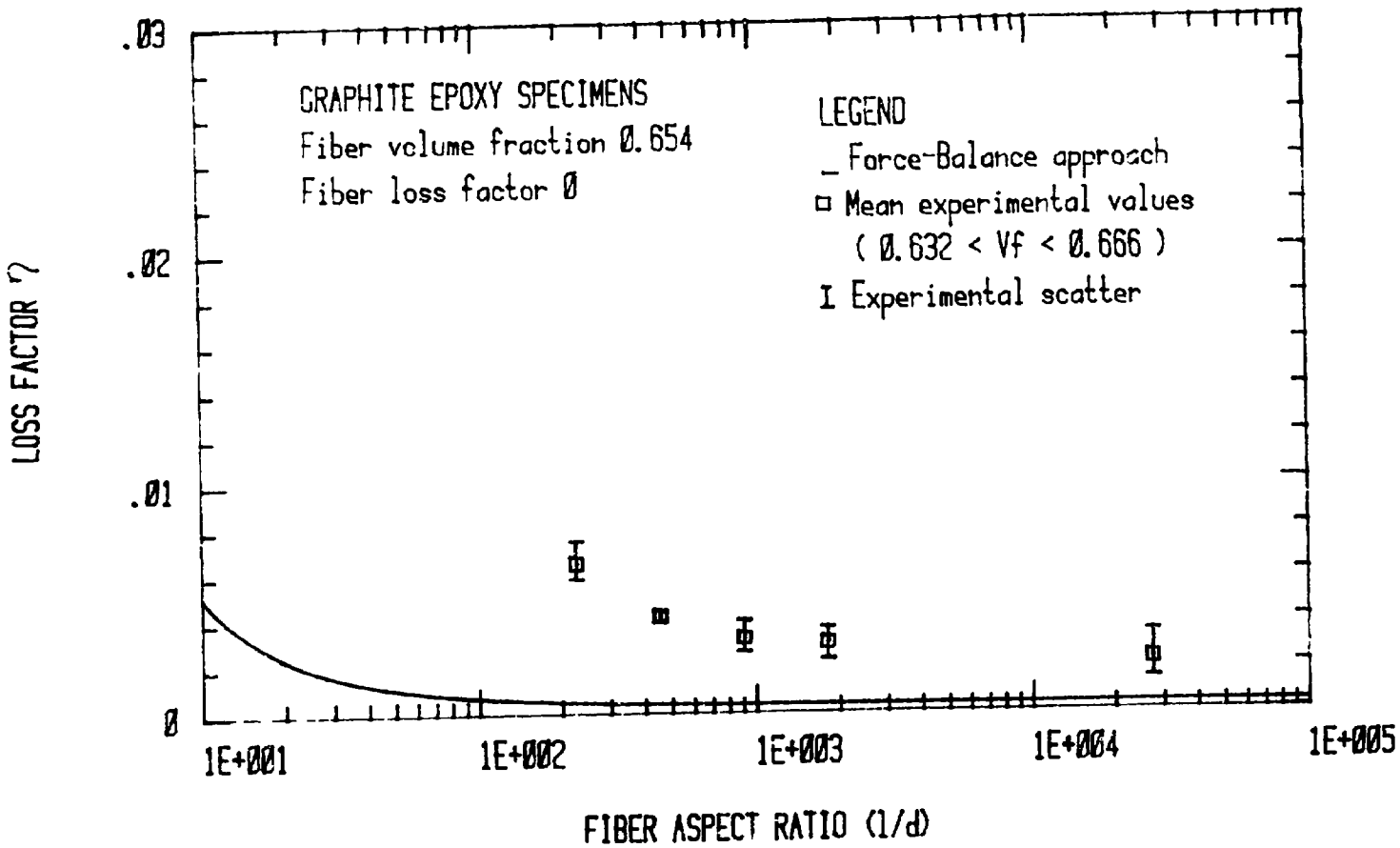

Figure 5.10. Loss factor vs. fiber aspect ratio for graphite/epoxy without curve fitting [E_f' = 33 x 10^6 psi (227.38 GPa), Z=1, f=54 Hz].

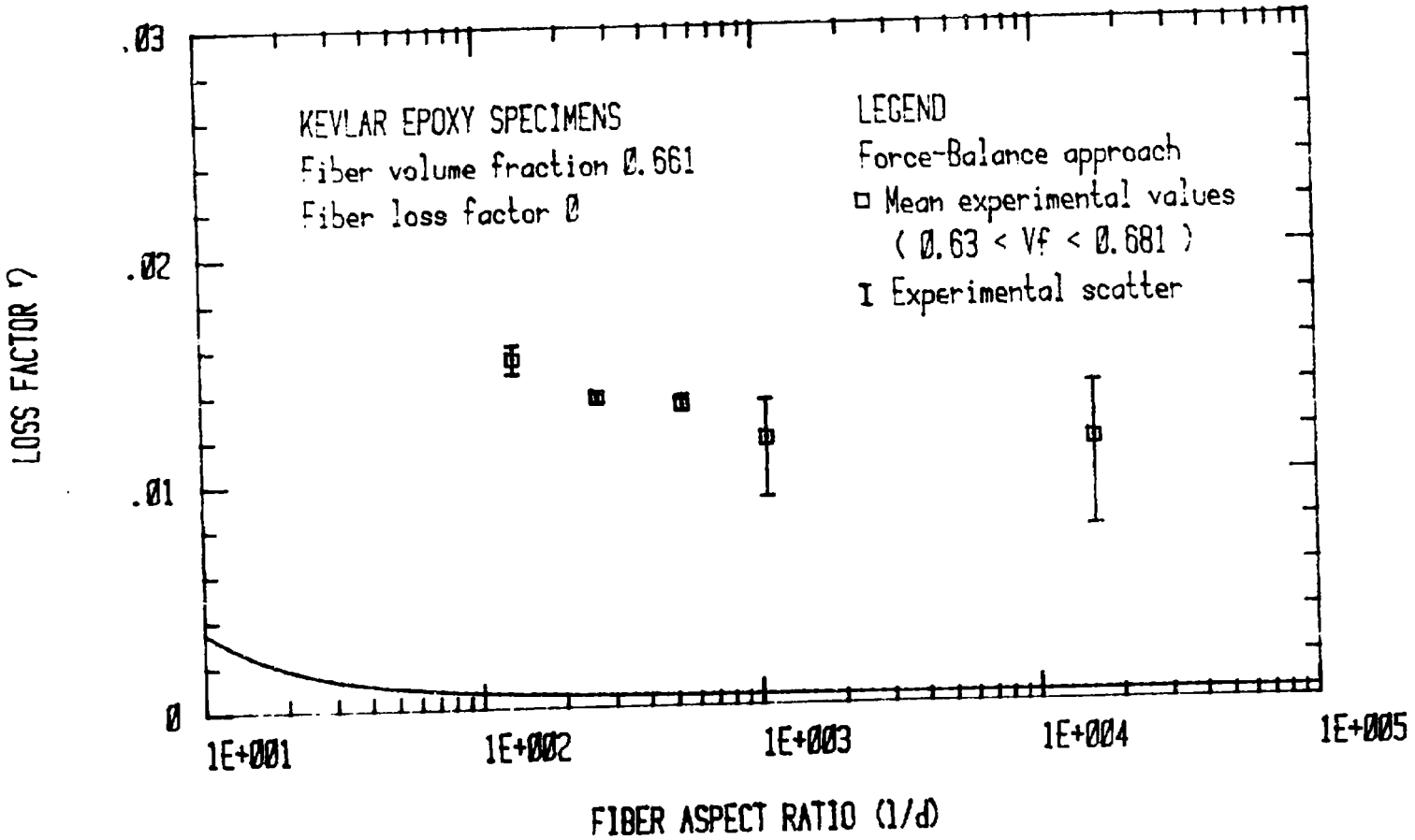

Figure 5.11. Loss factor vs. fiber aspect ratio for Kevlar/epoxy without curve fitting [E_f^1 = 18 x 10^6 psi (124.02 GPa), Z=1, f=38.75 Hz].

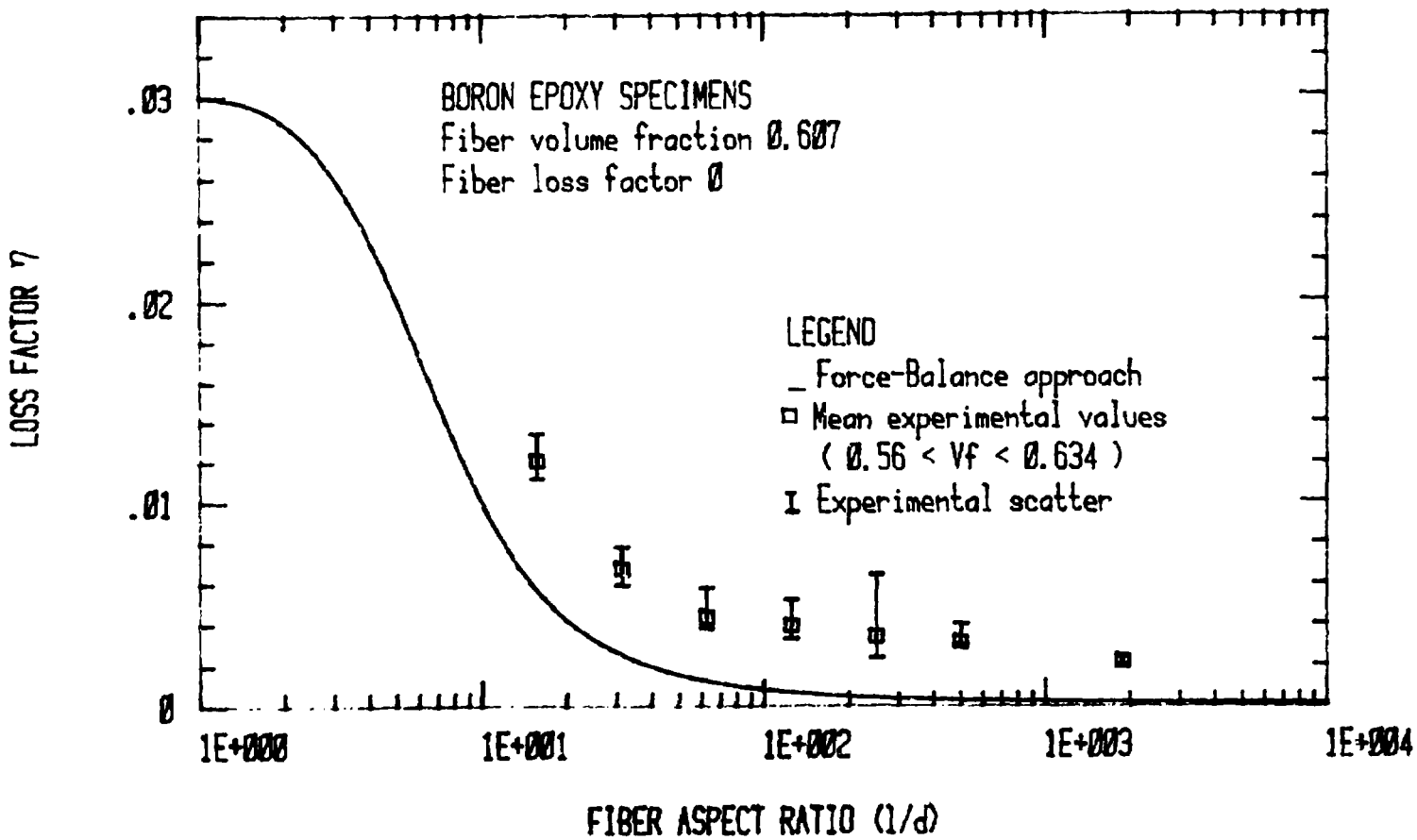

Figure 5.12. Loss factor vs. fiber aspect ratio for boron/epoxy without curve fitting [E_f' = 58 x 10^6 psi (399.62 GPa), Z=1, f=51.62 Hz].

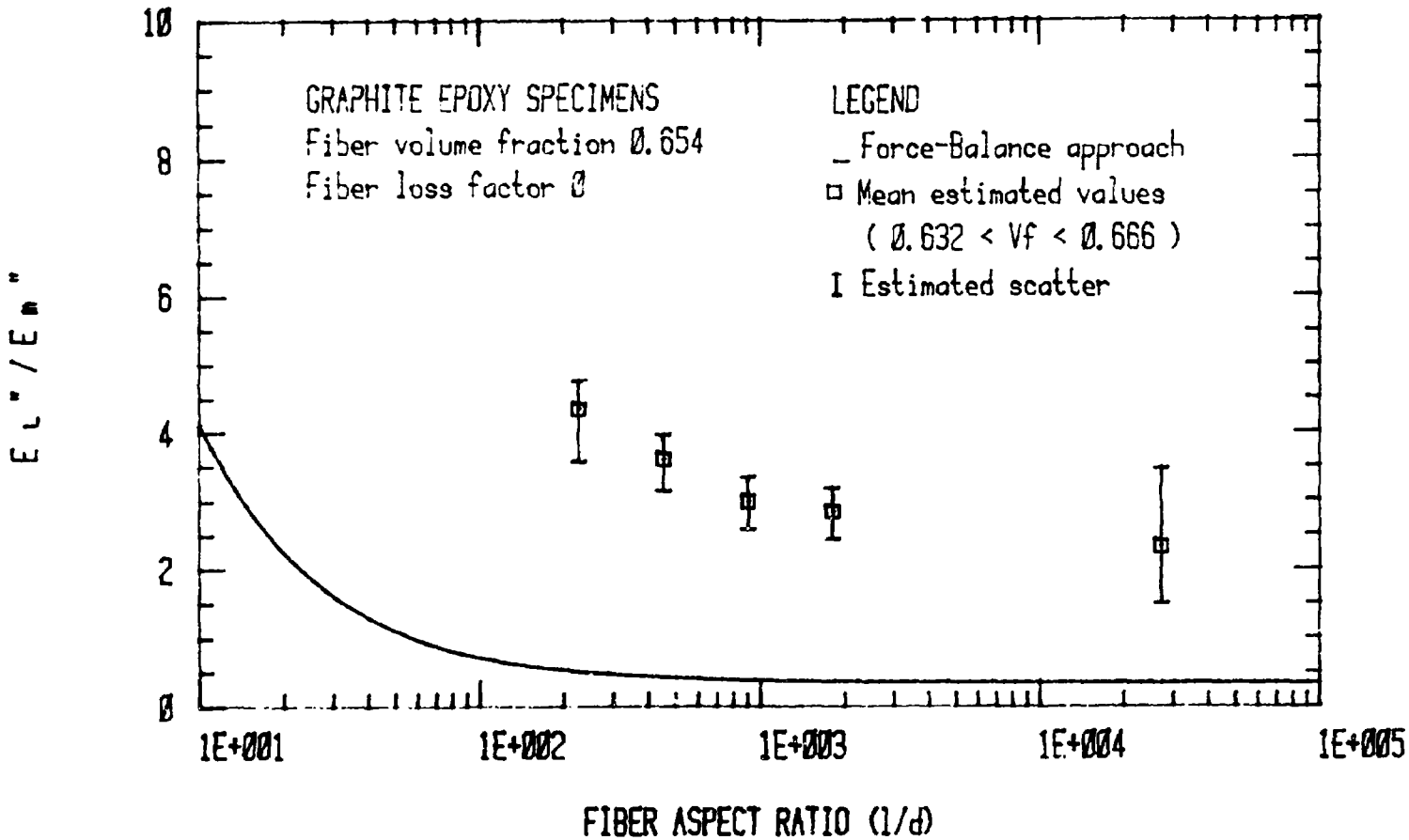

Figure 5.13. E''_L/E''_m vs. fiber aspect ratio for graphite/epoxy without curve fitting [E'_f = 33 x 10^6 psi (... .38 GPa), Z=1, f=54 Hz.]

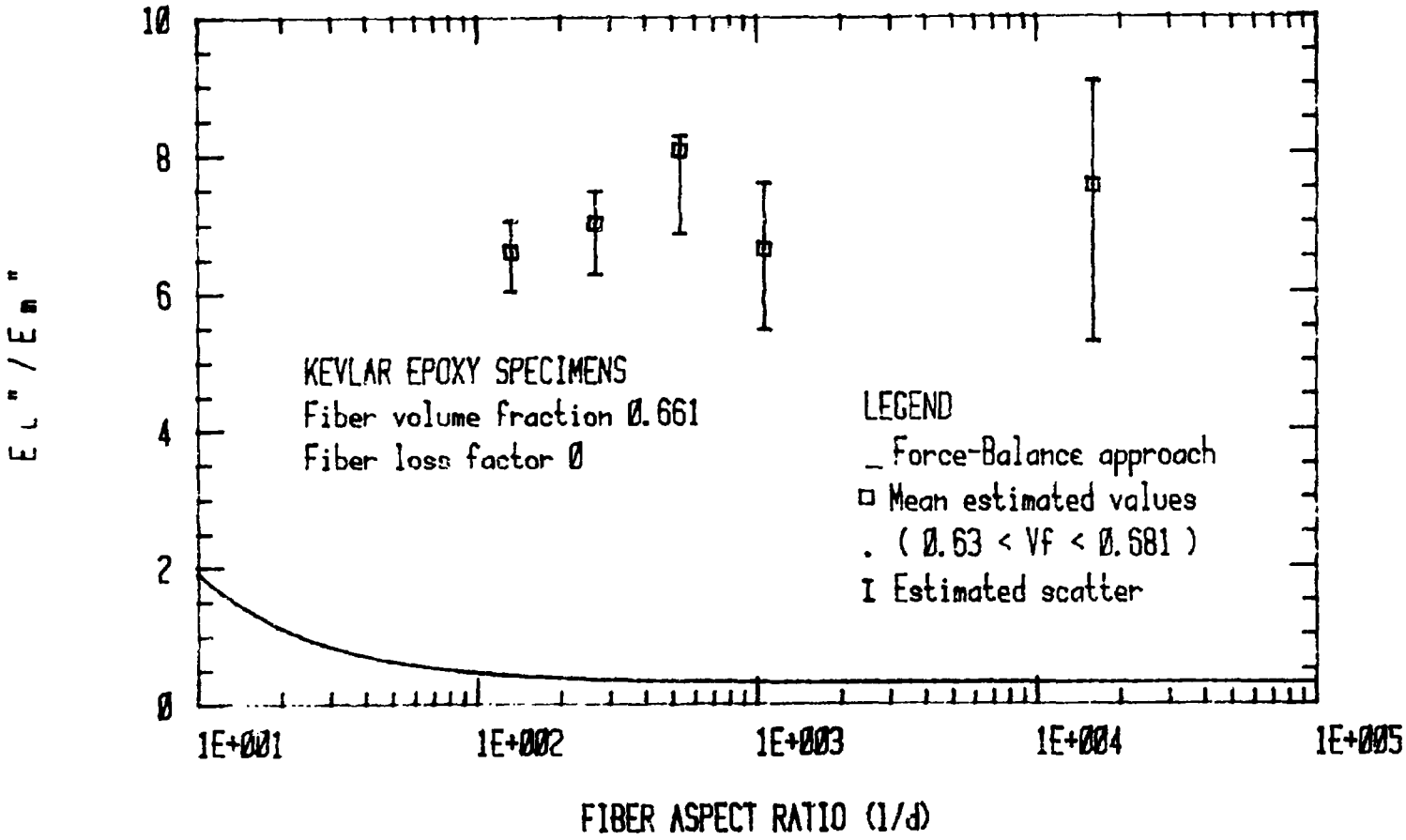

Figure 5.14. E'_L/E''_m vs. fiber aspect ratio for kevlar/epoxy without curve fitting [E'_f = 18 x 10^6 psi (124.02 GPa), Z=1, f=38.75 Hz].

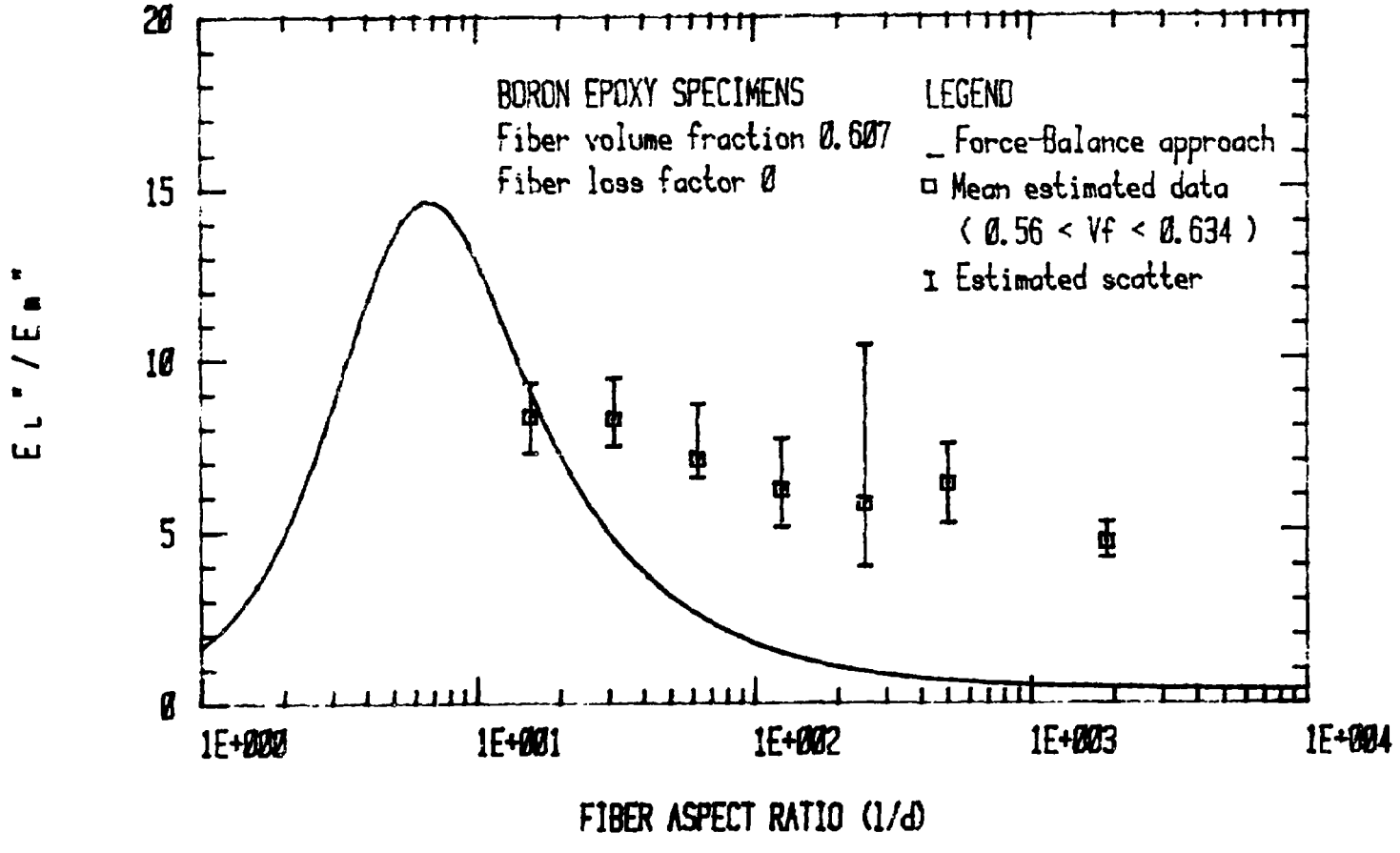

Figure 5.15. E''_L/E''_m vs. fiber aspect ratio for boron/epoxy without curve fitting [E'_f = 58 x 10^6 psi (399.62 GPa), Z=1, f=51.62 Hz].

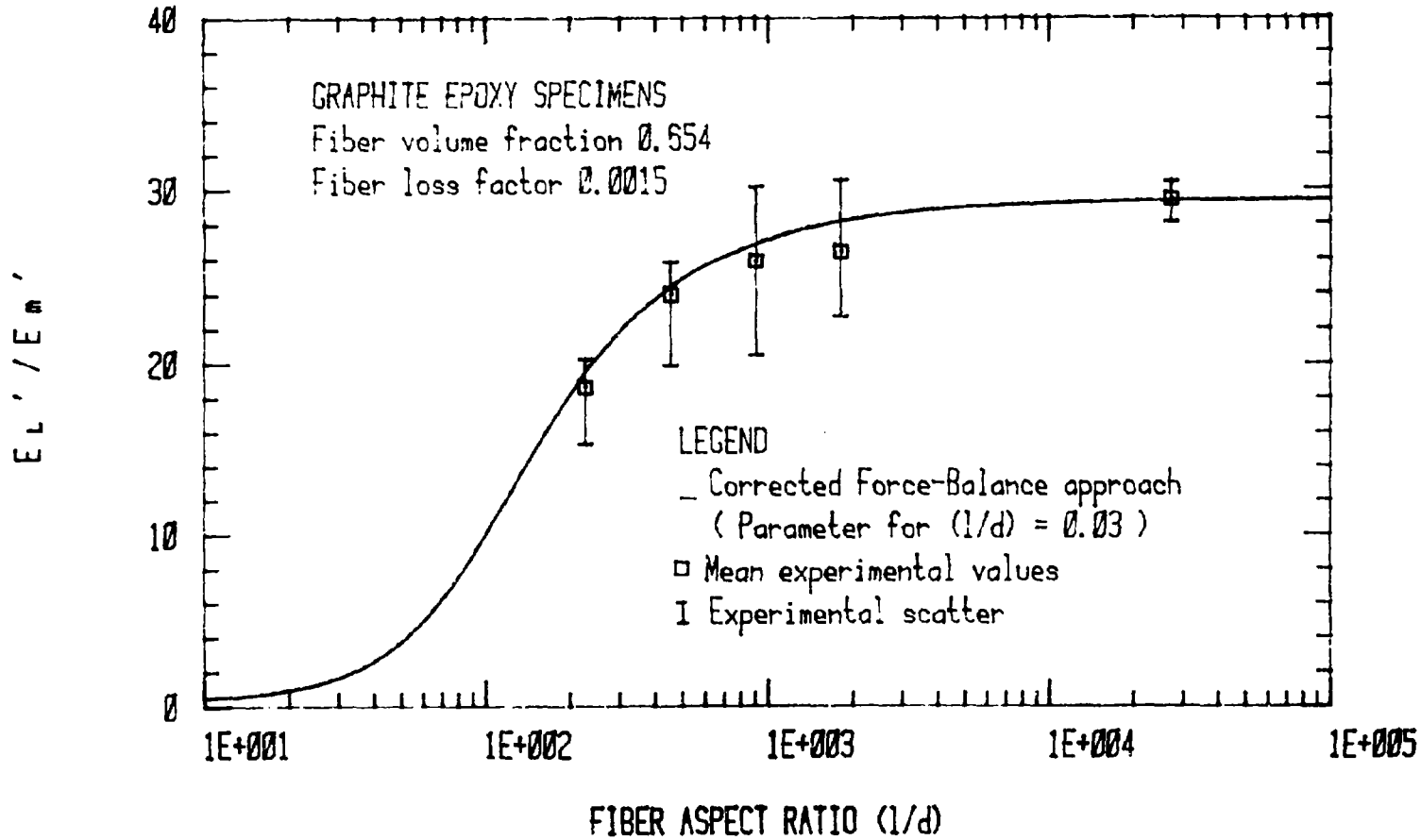

Figure 5.16. E_L'/E_m' vs. fiber aspect ratio for graphite/epoxy with curve fitting [E_f' = 25.51 x 10^6 psi (175.76 GPa), Z=0.03, f=54 Hz].

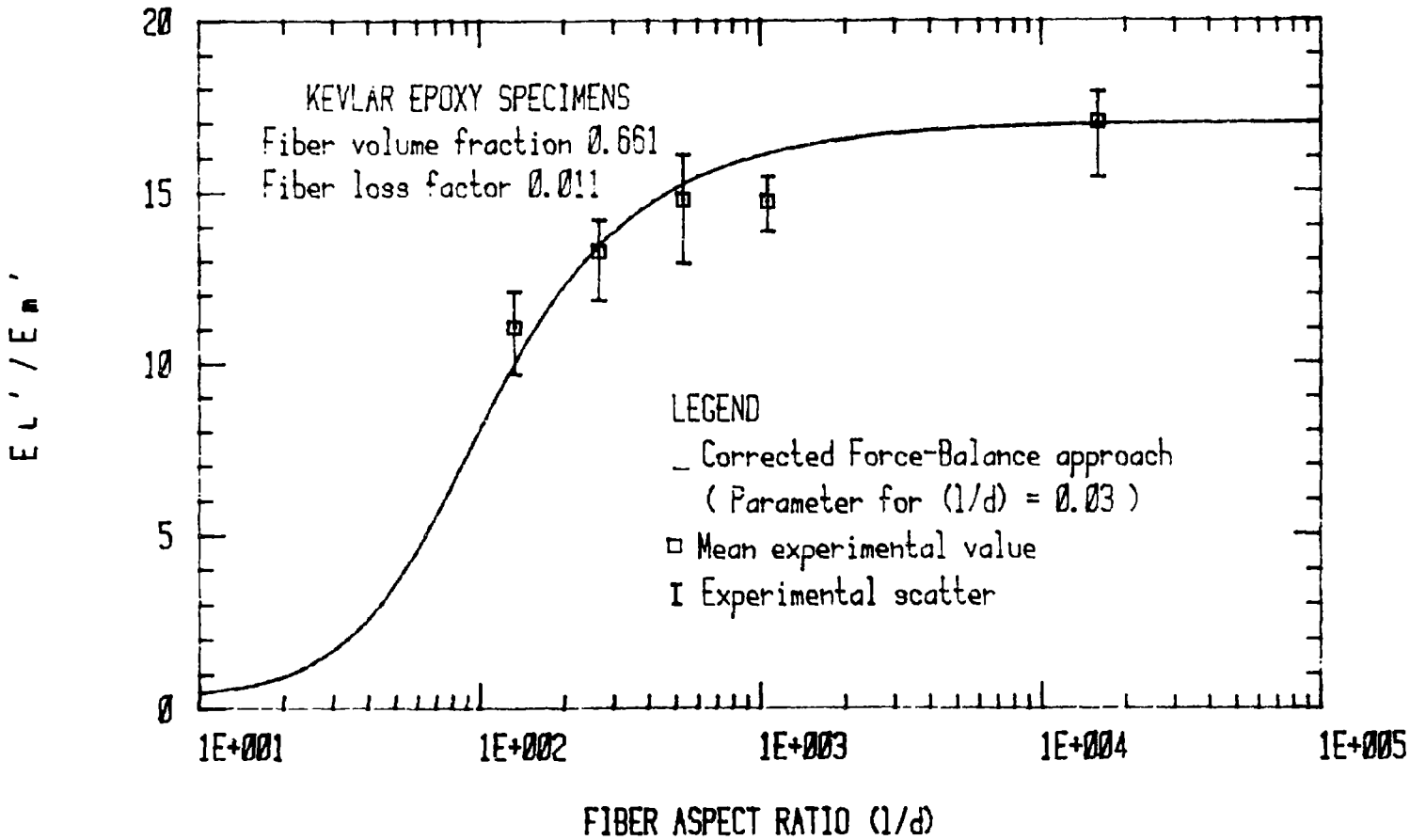

Figure 5.17. E_L'/E_m' vs. fiber aspect ratio for Kevlar/epoxy with curve fitting [E_f' = 14.48 x 10^6 psi (99.767 GPa), Z=0.03, f=38.75 Hz].

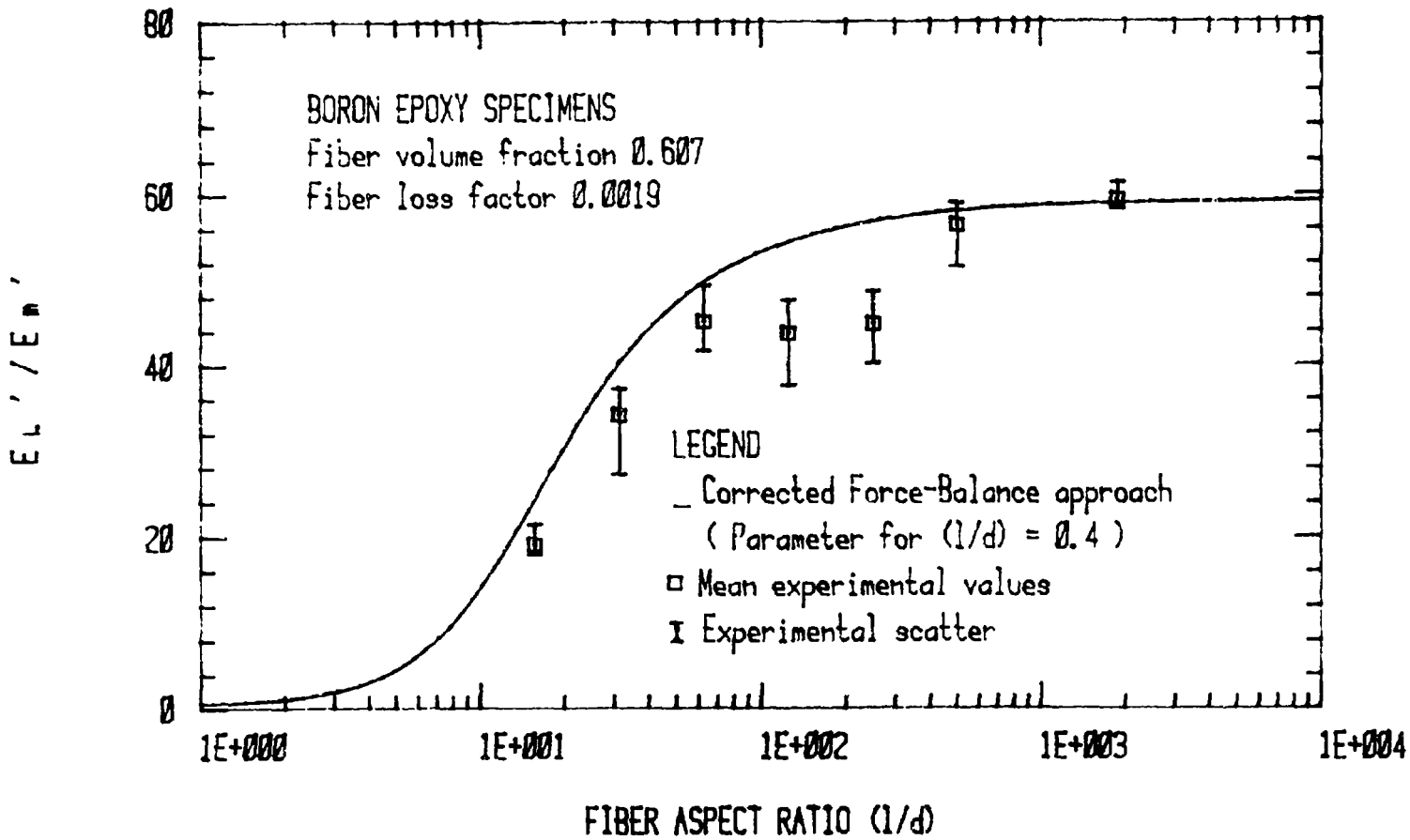

Figure 5.18. E_L'/E_m' vs. fiber aspect ratio for boron/epoxy with curve fitting [E_f' = 55.43 x 10^6 psi (381.913 GPa), Z=0.4, f=51.62 Hz].

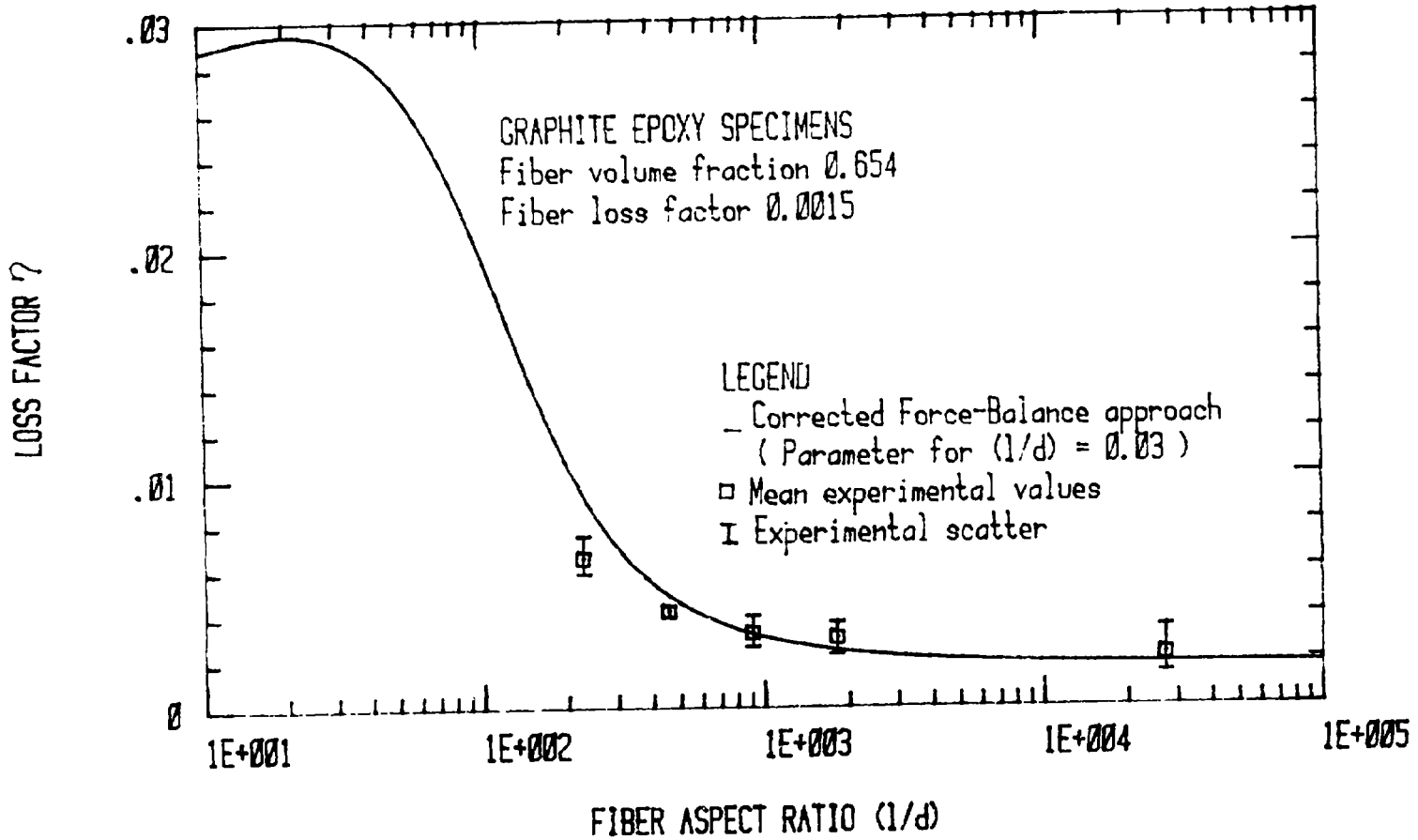

Figure 5.19. Loss factor vs. fiber aspect ratio for graphite/epoxy with curve fitting [E'_f = 25.51 x 10^6 psi (175.76 GPa), Z=0.03, f=54 Hz].

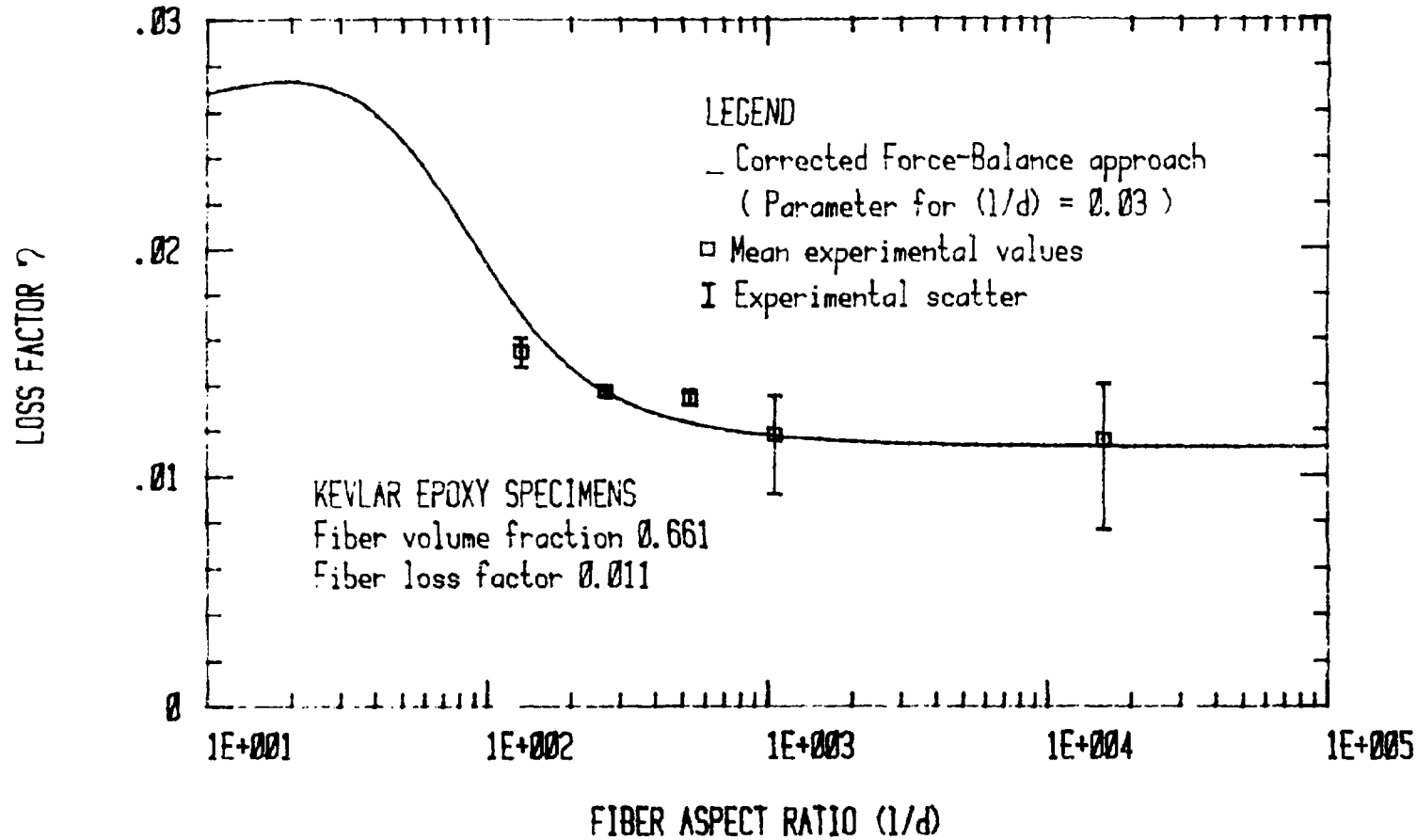

Figure 5.20. Loss factor vs. fiber aspect ratio for Kevlar/epoxy with curve fitting [E_f^1 = 14.48 x 10^6 psi (99.767 GPa), Z=0.03, f=38.75 Hz].

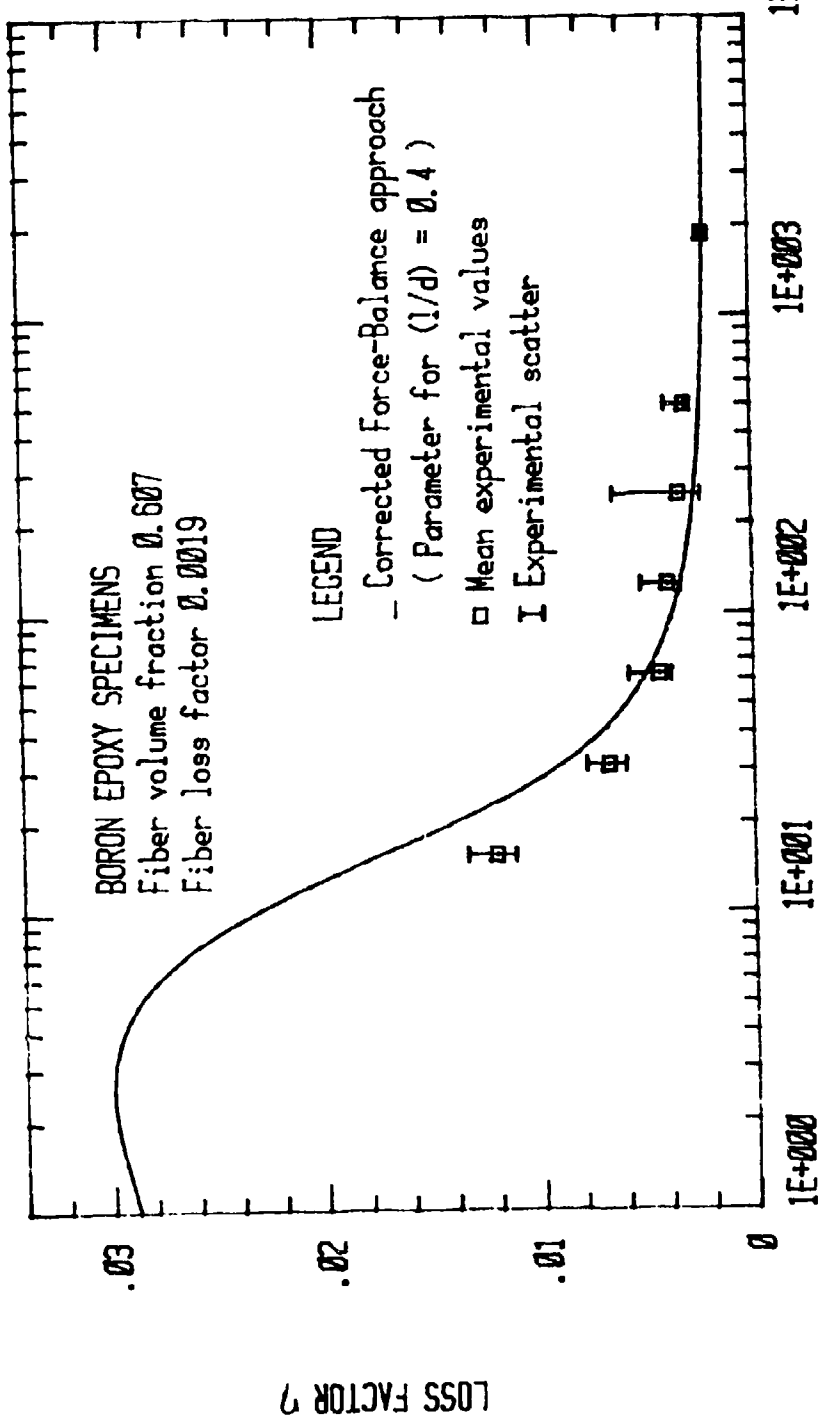

Figure 5.21. Loss factor vs. fiber aspect ratio for boron/epoxy with curve fitting [E_f' = 55.43 x 10^6 psi (381.913 GPa), Z=0.4, f=51.62 Hz].

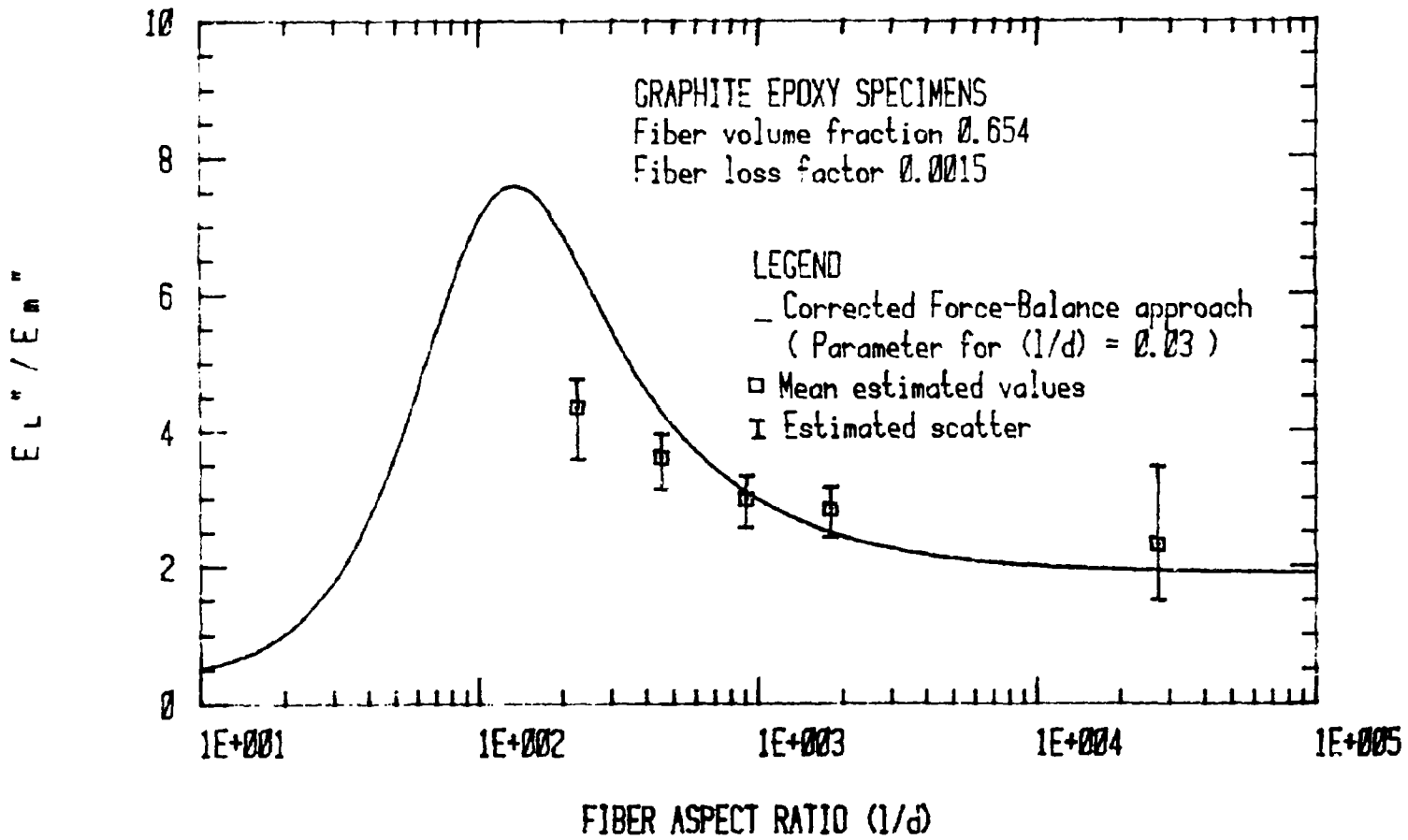

Figure 5.22. E''_L/E''_m vs. fiber aspect ratio for graphite/epoxy with curve fitting [E'_f = 25.51 x 10^6 psi (175.76 GPa), Z=0.03, f=54 Hz].

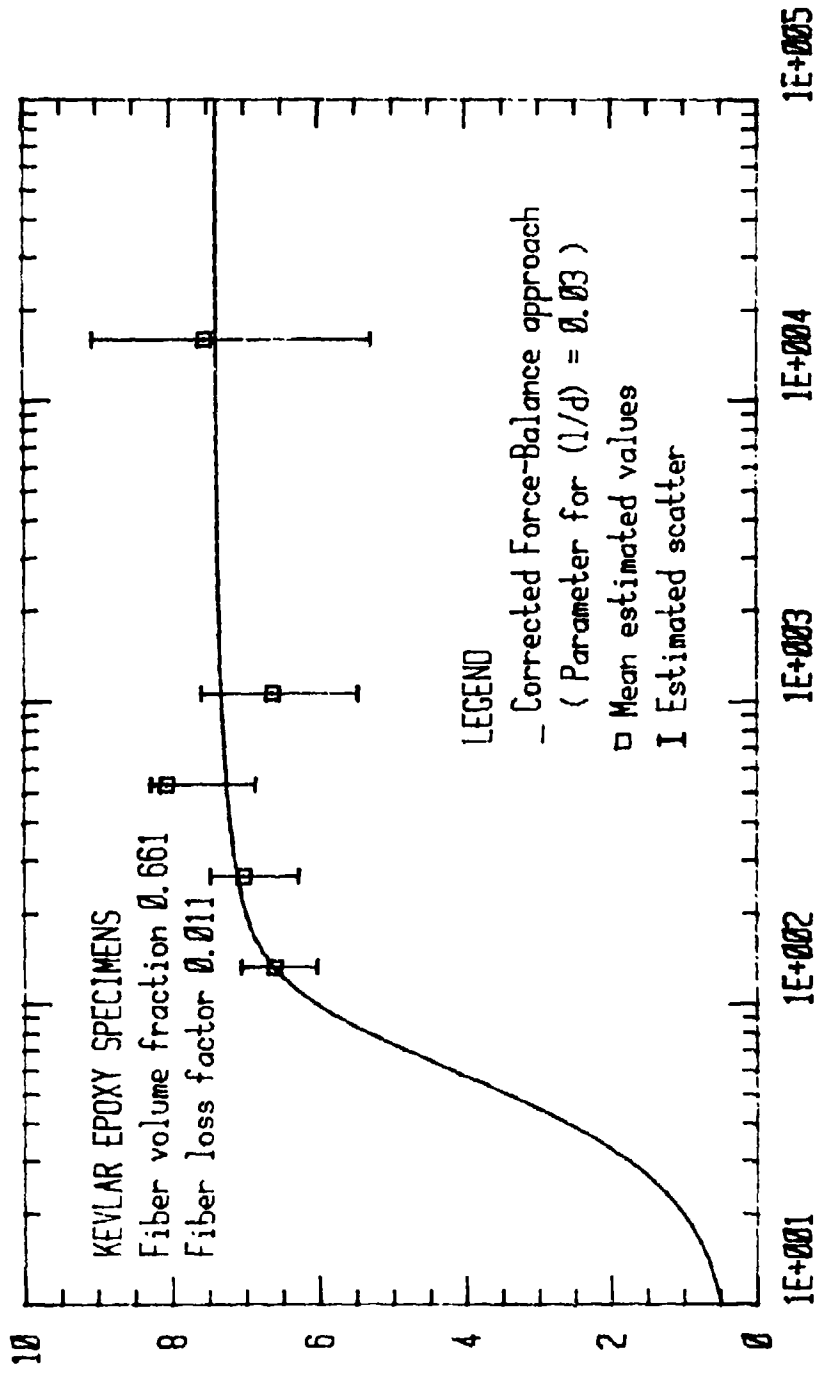

Figure 5.23. E''_L/E''_m vs. fiber aspect ratio for Kevlar/epoxy with curve fitting [E'_f = 14.48 x 10^6 psi (99.767 GPa), Z=0.03, f=38.75 Hz].

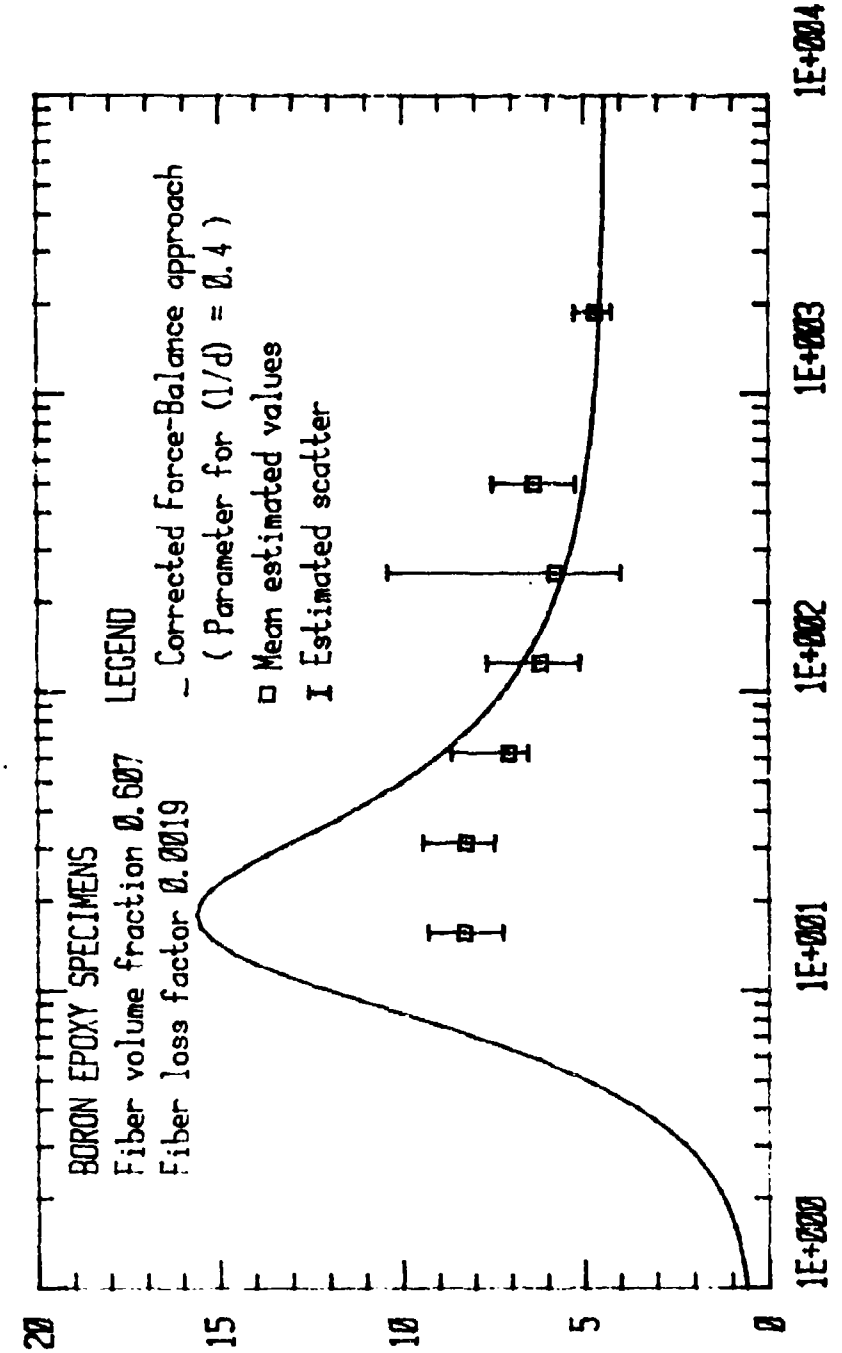

Figure 5.24. E_L''/E_m'' vs. fiber aspect ratio for boron/epoxy with curve fitting [E_f' = 55.43 x 10^5 psi (381.913 GPa), Z=0.4, f=51.62 Hz].

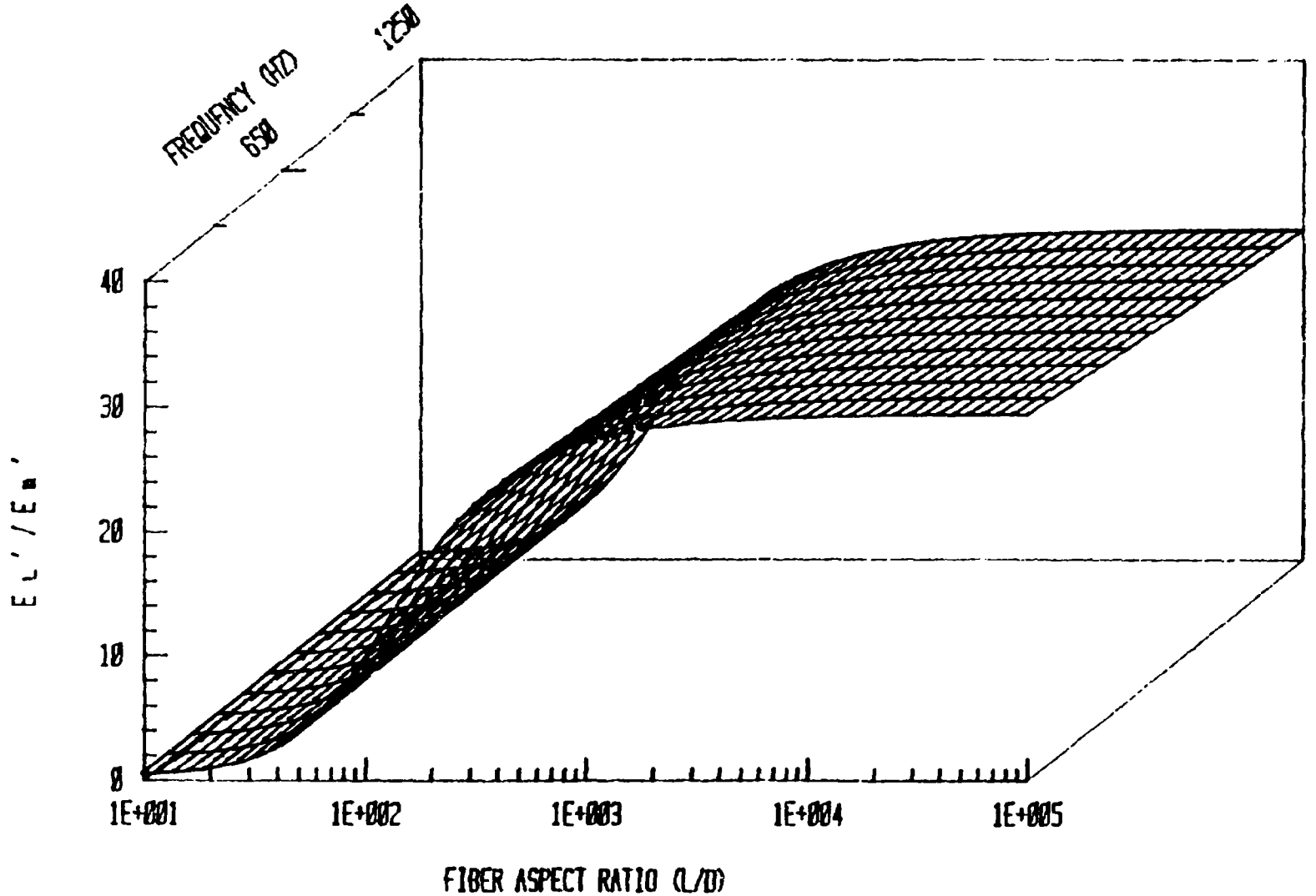

Figure 5.25. Tridimensional plot of E_L'/E_m' vs. fiber aspect ratio and frequency, for grahite/epoxy composite.

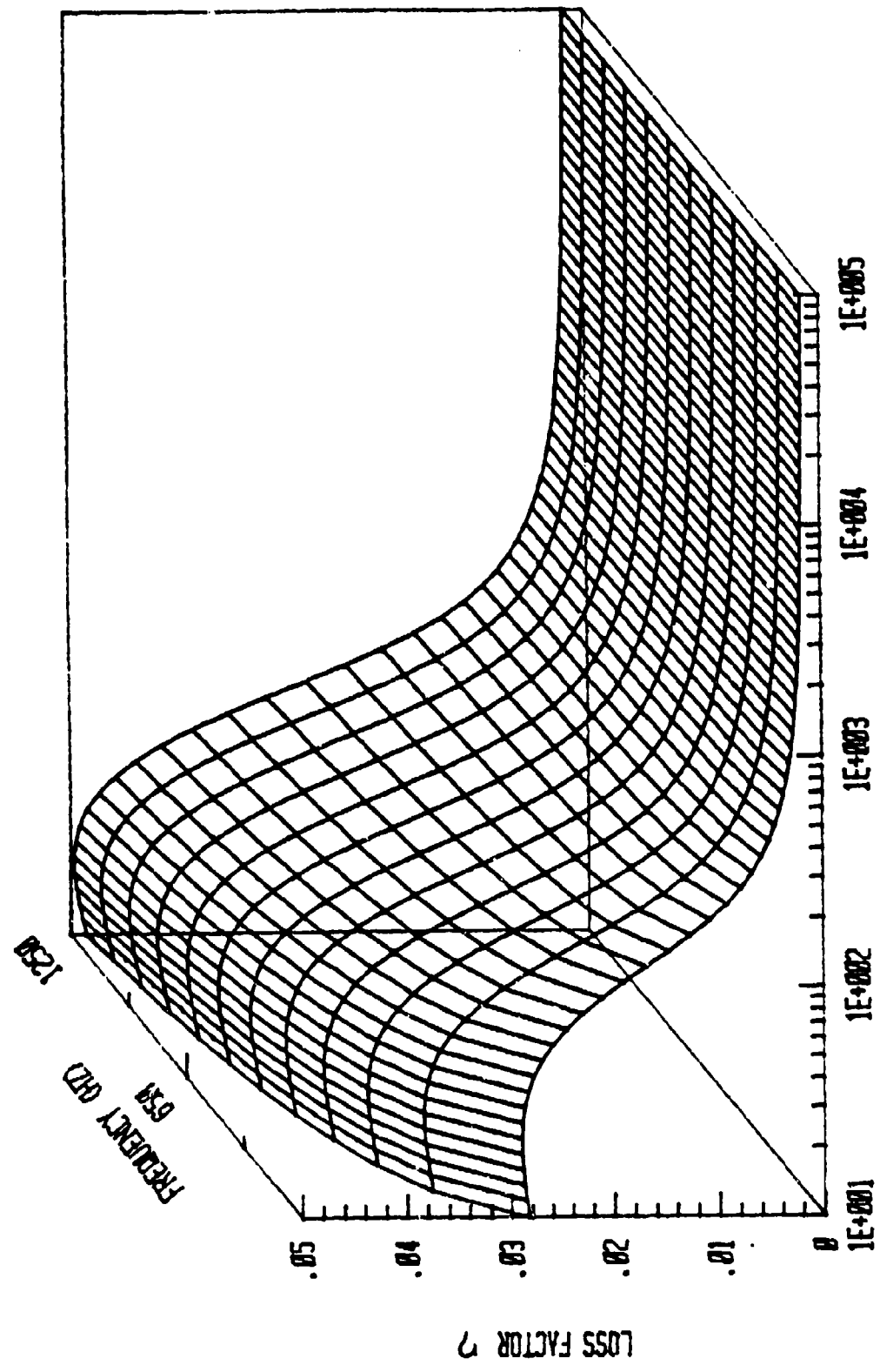

Figure 5.26. Tridimensional plot of loss factor vs. fiber aspect ratio and frequency, for graphite/epoxy composite.

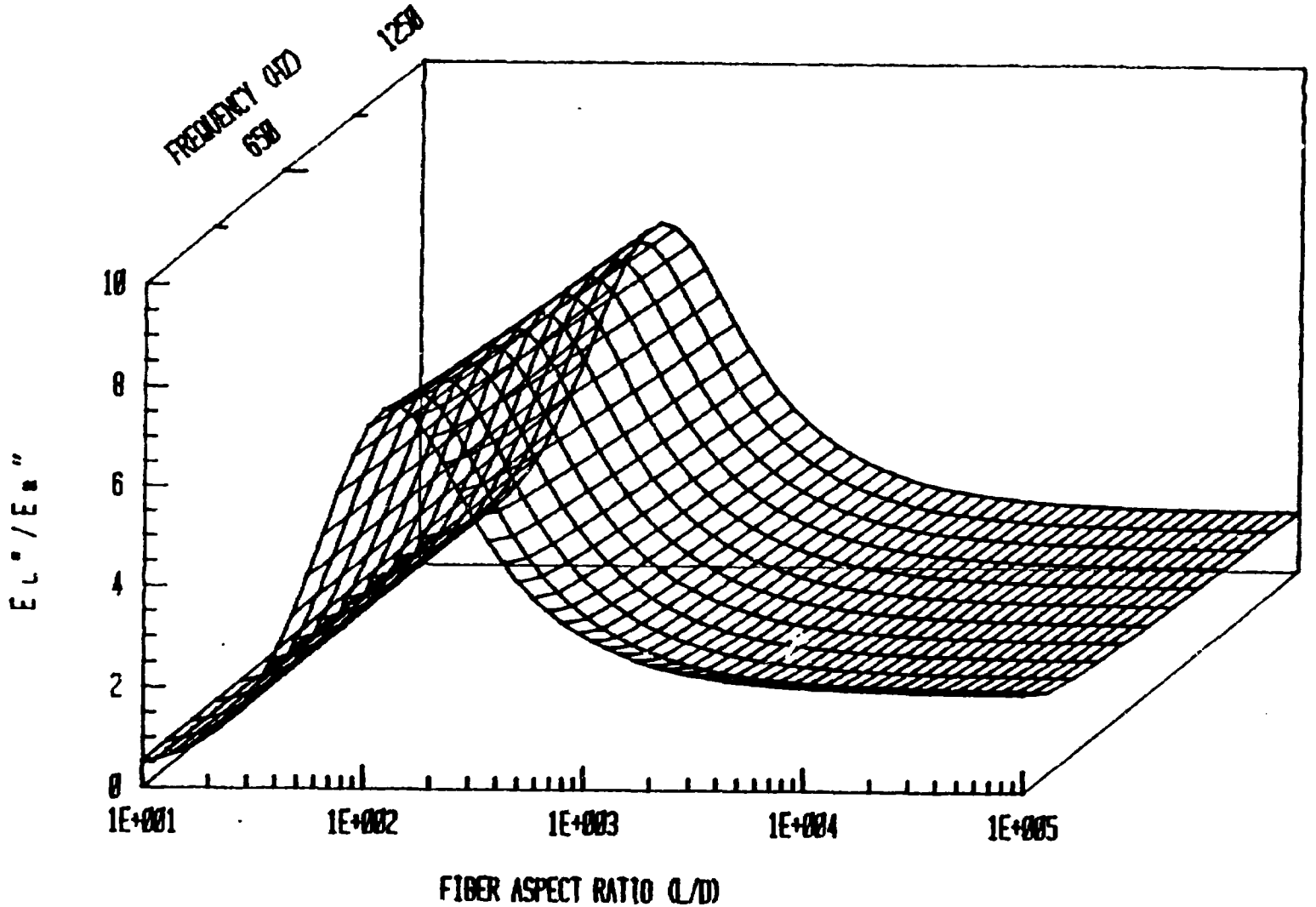

Figure 5.27. Tridimensional plot of E''_L/E''_m vs. fiber aspect ratio and frequency, for graphite/epoxy composite.

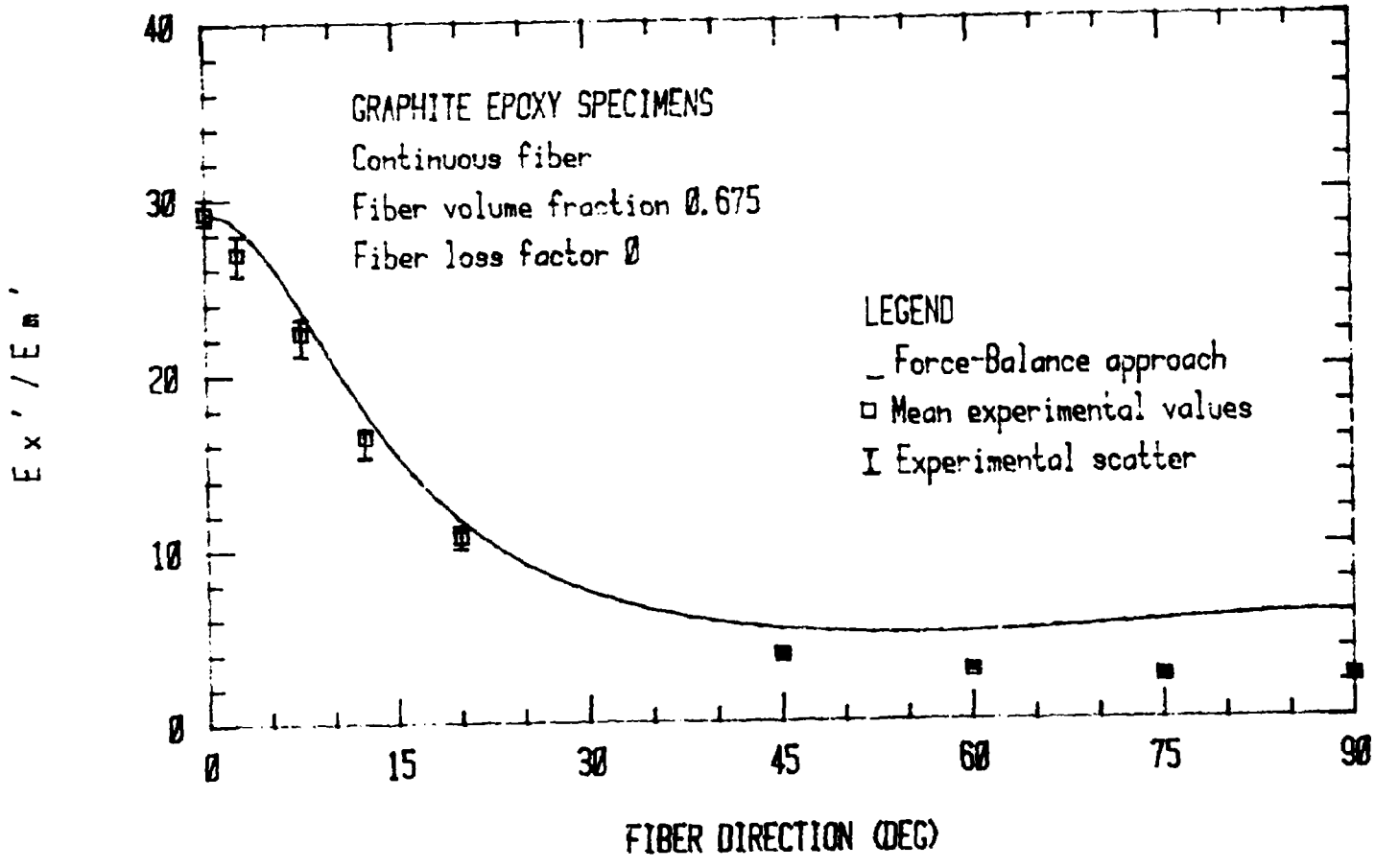

Figure 6.1. E_x'/E_m' vs. fiber direction for continuous graphite/epoxy, without curve fitting [isotropic fiber, E_f' = 33 x 10^6 psi (227.38 GPa), ξ_1=2, ξ_2=2, Z=1, f=1152.5 Hz].

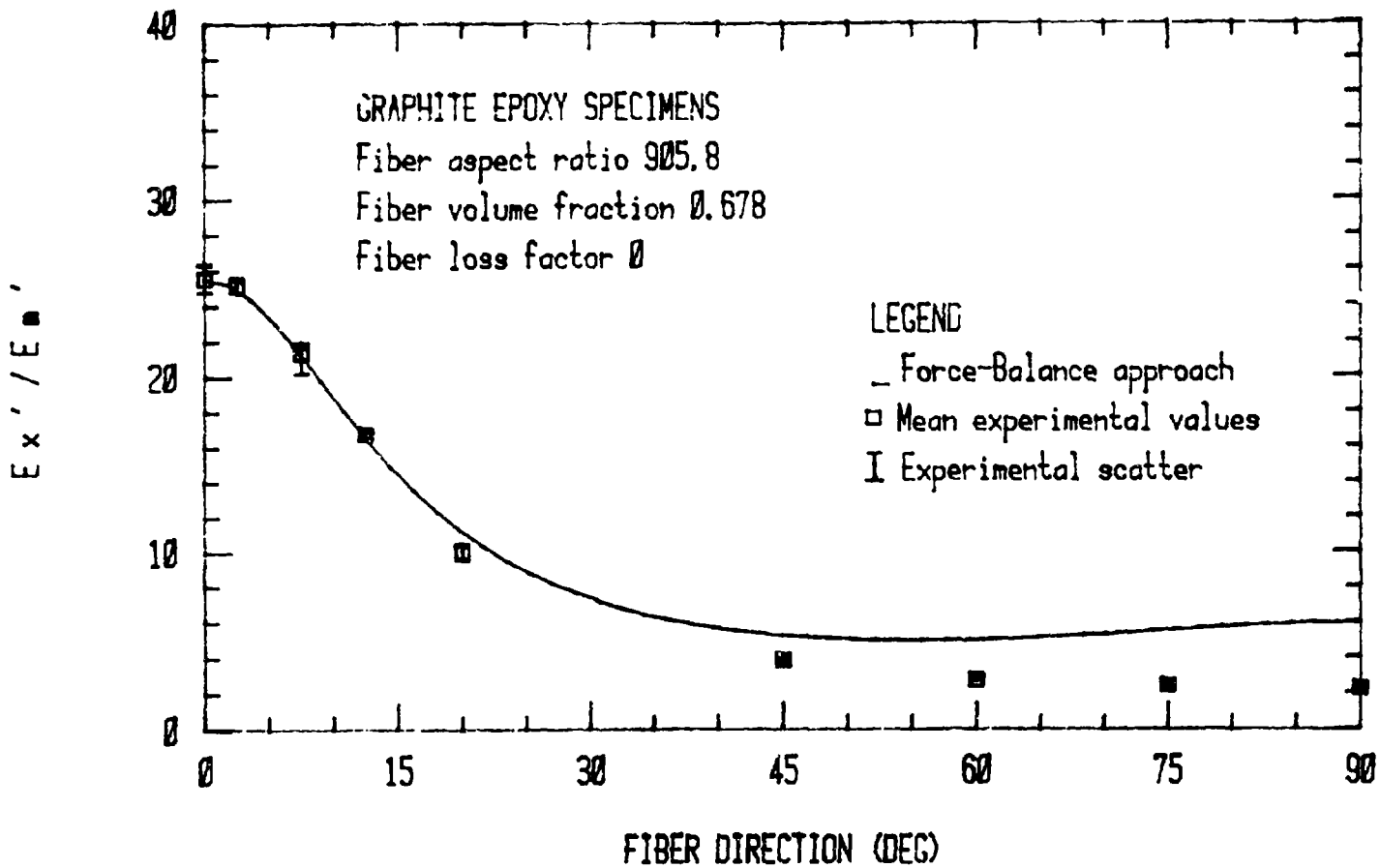

Figure 6.2. E'_x/E'_m vs. fiber direction for discontinuous graphite/epoxy, without curve fitting [isotropic fiber, E'_f = 33x 10^6 psi (227.38 GPa), ε_1=2, ε_2=1, Z=1, f=1206.15 Hz].

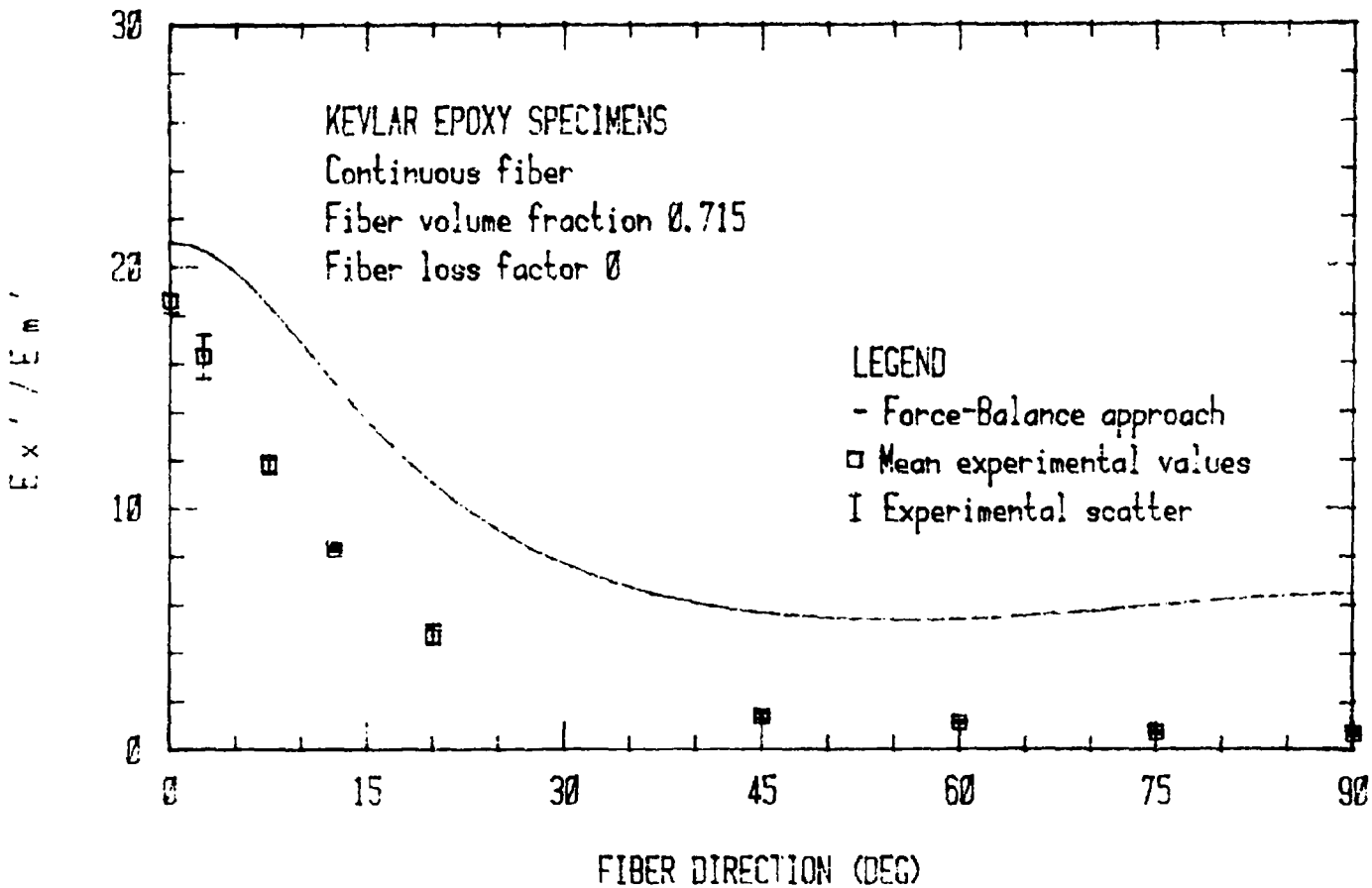

Figure 6.3. E_x'/E_m' vs. fiber direction for continuous Kevlar/epoxy, without curve fitting [isotropic fiber, E_f' = 18 x 10^6 psi (124.02 GPa), ξ_1=2, ξ_2=1, Z=1, f=895.1 Hz].

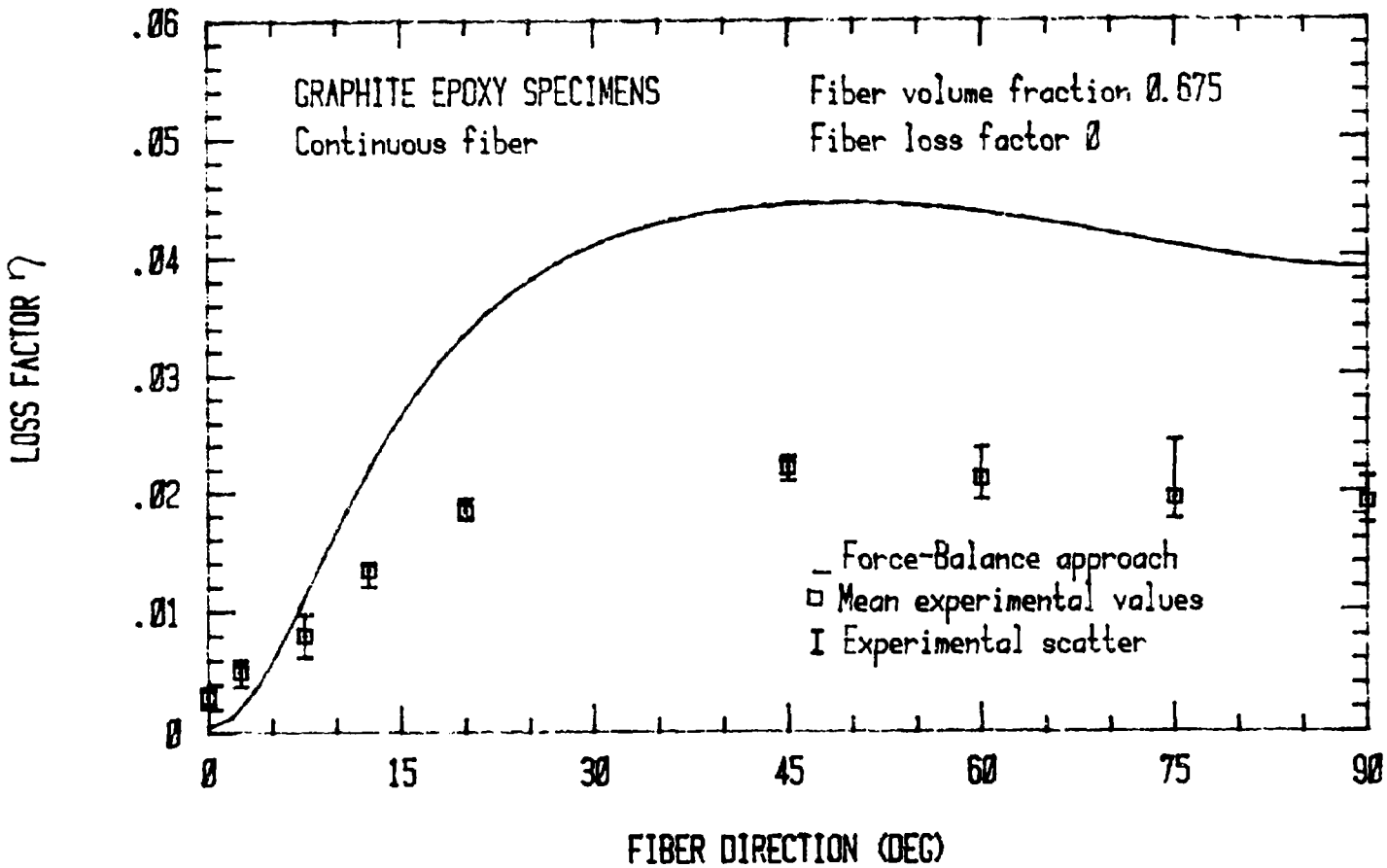

Figure 6.4. Loss factor vs. fiber direction for continuous graphite/epoxy, without curve fitting [isotropic fiber, E_f = 33 x 10^6 psi (227.38 GPa), ε_1=2, ε_2=1, Z=1, f=1152.5 Hz].

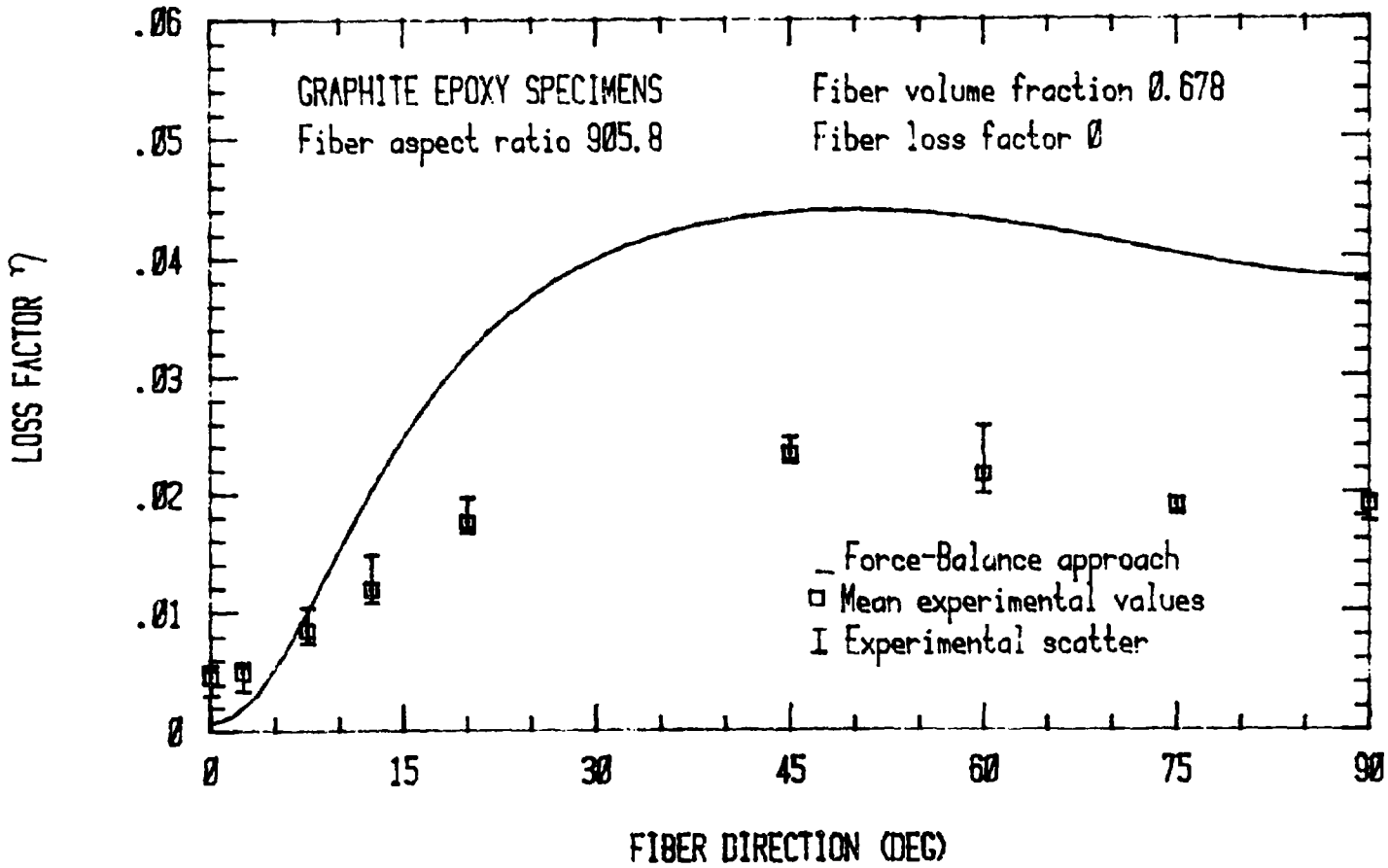

Figure 6.5. Loss factor vs. fiber direction for discontinuous graphite/epoxy, without curve fitting [isotropic fiber, $E_f' = 33 \times 10^6$ psi (227.38 GPa), $\xi_1=2$, $\xi_2=1$, Z=1, f=1206.15 Hz].

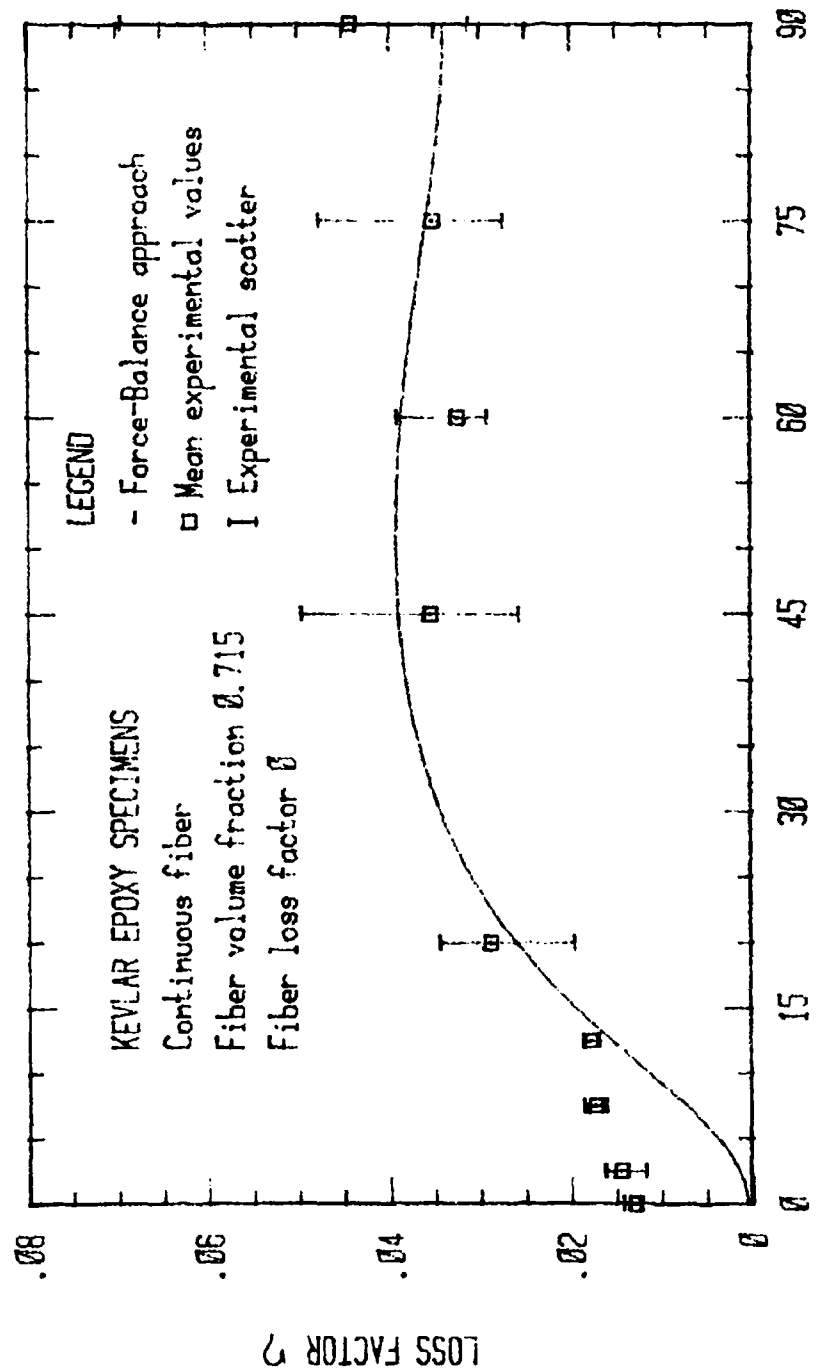

Figure 6.6. Loss factor vs. fiber direction for continuous Kevlar/epoxy, without curve fitting [isotropic fiber, $E_f' = 18 \times 10^6$ psi (124.02 GPa), $\xi_1=2$, $\xi_2=1$, Z=1, f=895.1 Hz].

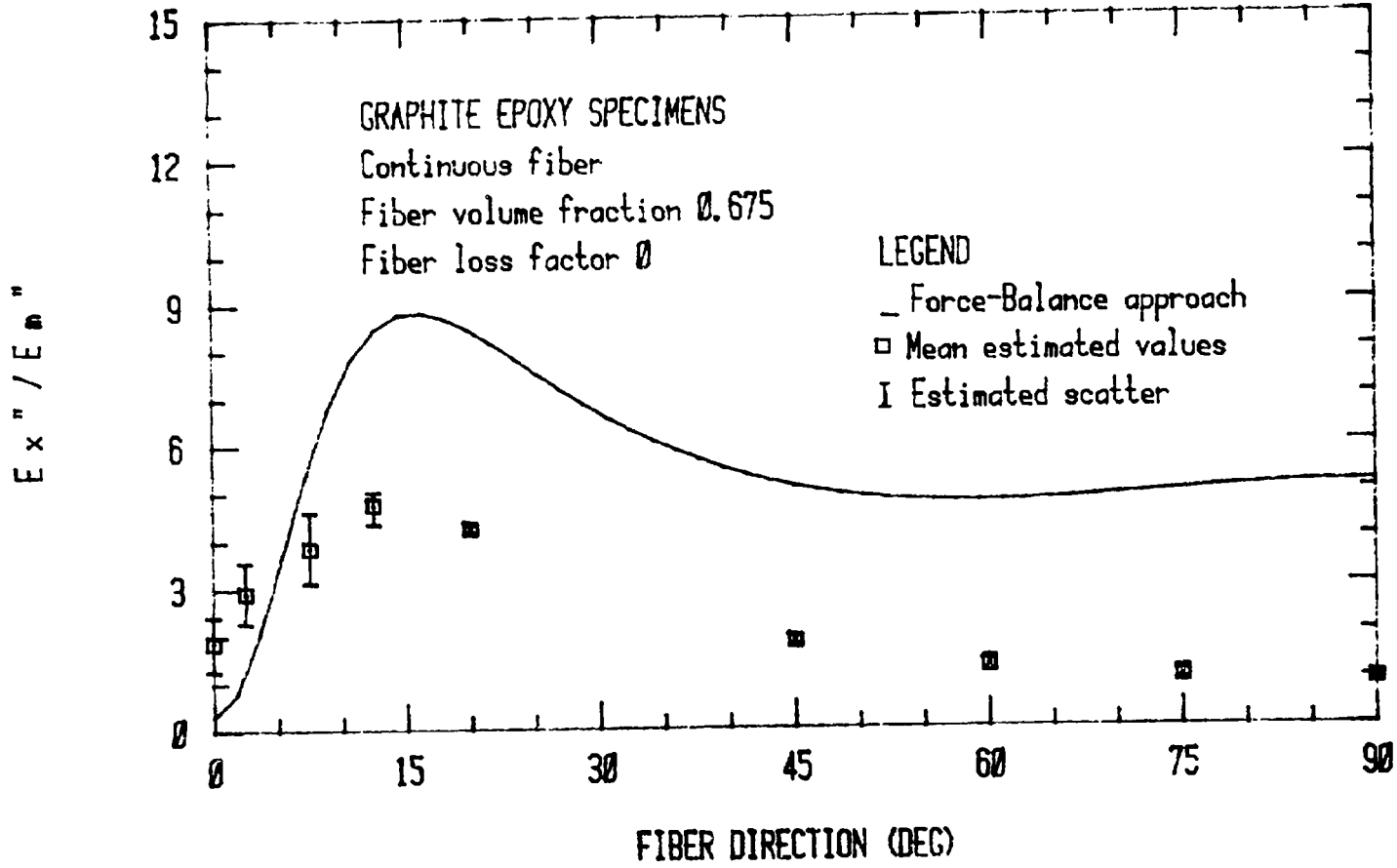

Figure 6.7. E''_x/E''_m vs. fiber direction for continuous graphite/epoxy, without curve fitting [isotropic fiber, E'_f = 33 x 10^6 psi (227.38 GPa), ξ_1=2, ξ_2=1, Z=1, f=1152.5 Hz].

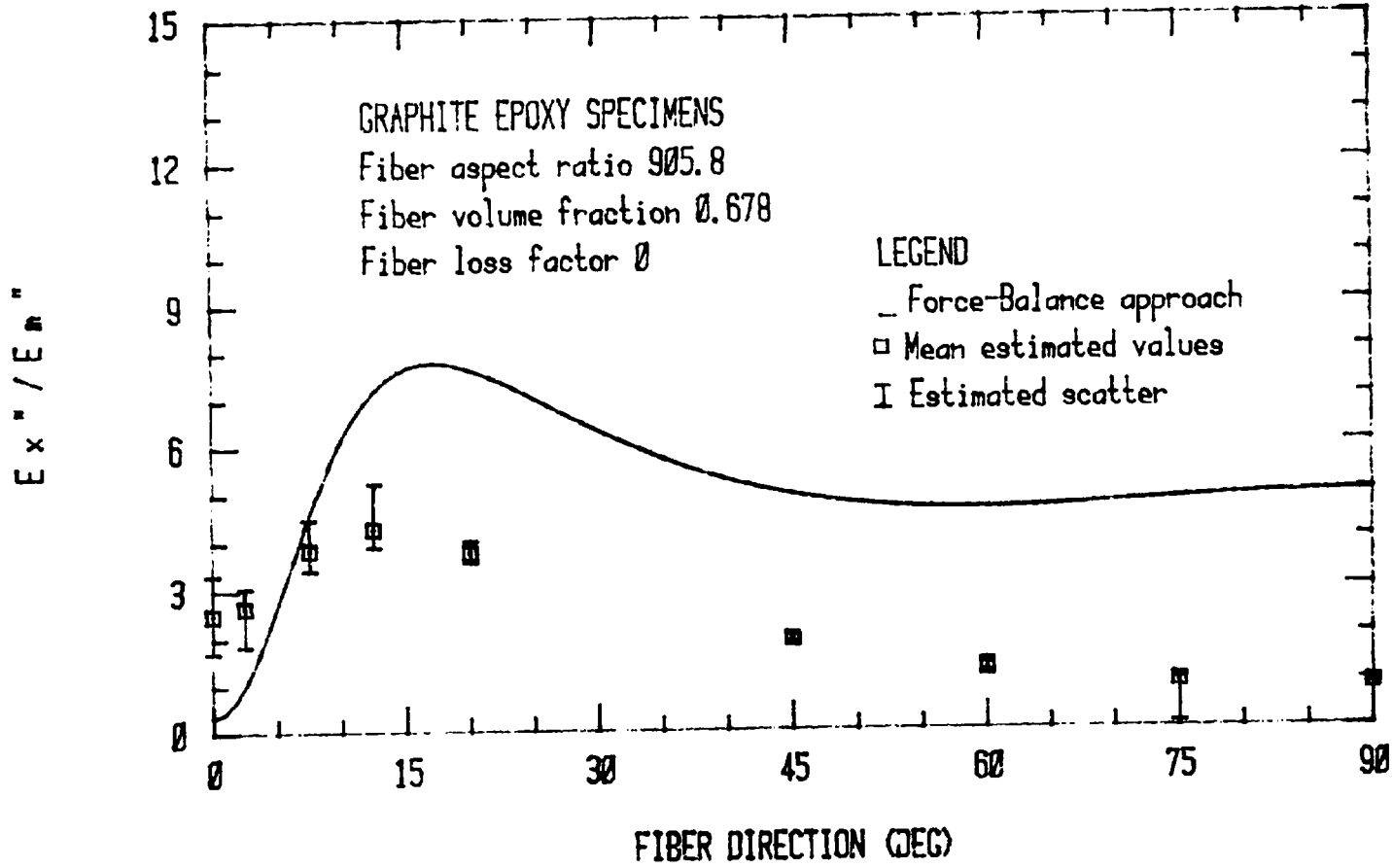

Figure 6.8. E_x''/E_m'' vs. fiber direction for discontinuous graphite/epoxy, without curve fitting [isotropic fiber, E_f' = 33 x 10^6 psi (227.38 GPa), ξ_1=2, ξ_2=1, Z=1, f=1206.15 Hz].

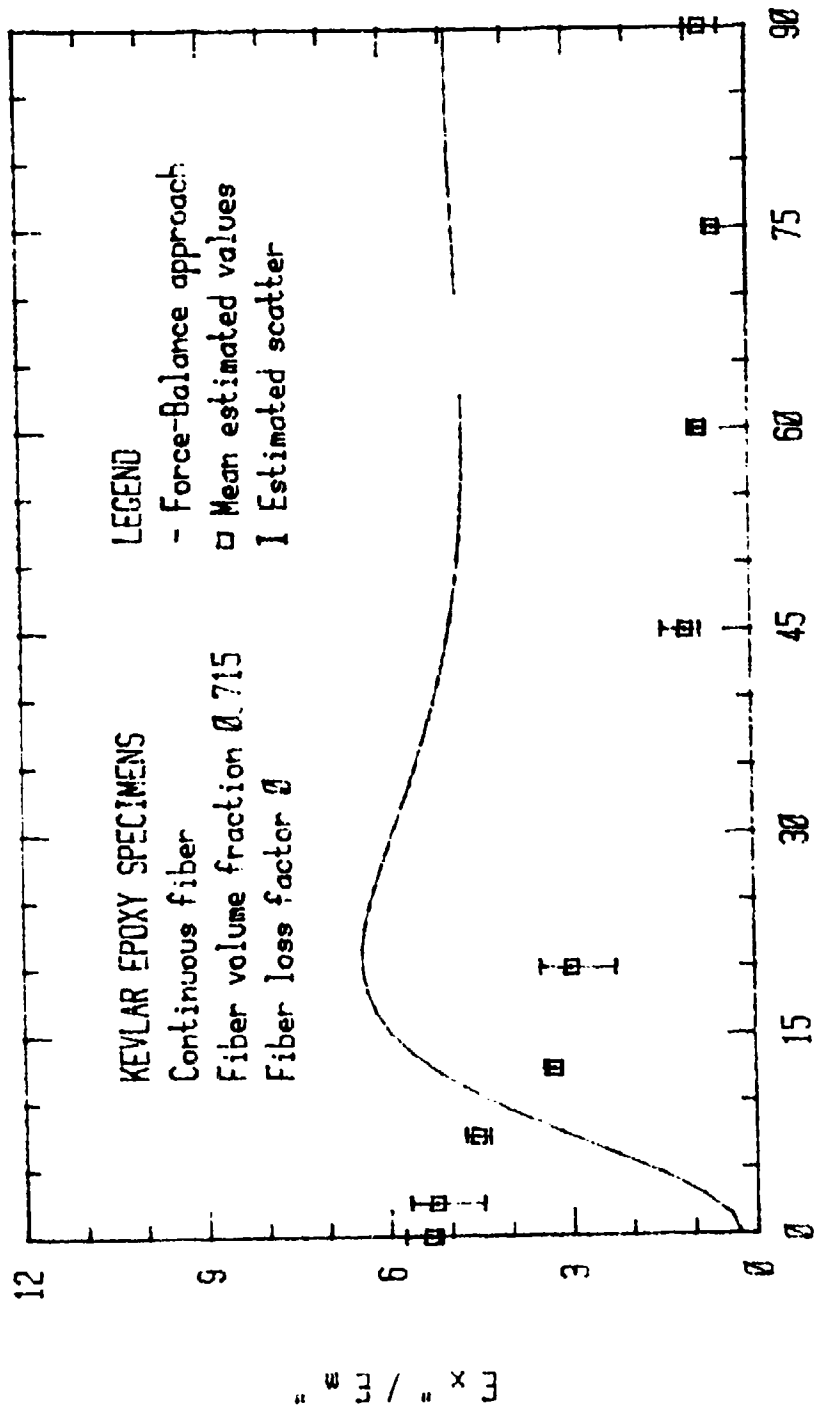

Figure 6.9. E''_x/E''_m vs. fiber direction for continuous Kevlar/epoxy, without curve fitting [isotropic fiber, $E'_f = 18 \times 10^6$ psi (124.02 GPa), $\xi_1=2$, $\xi_2=1$, Z=1, f=895.1 Hz].

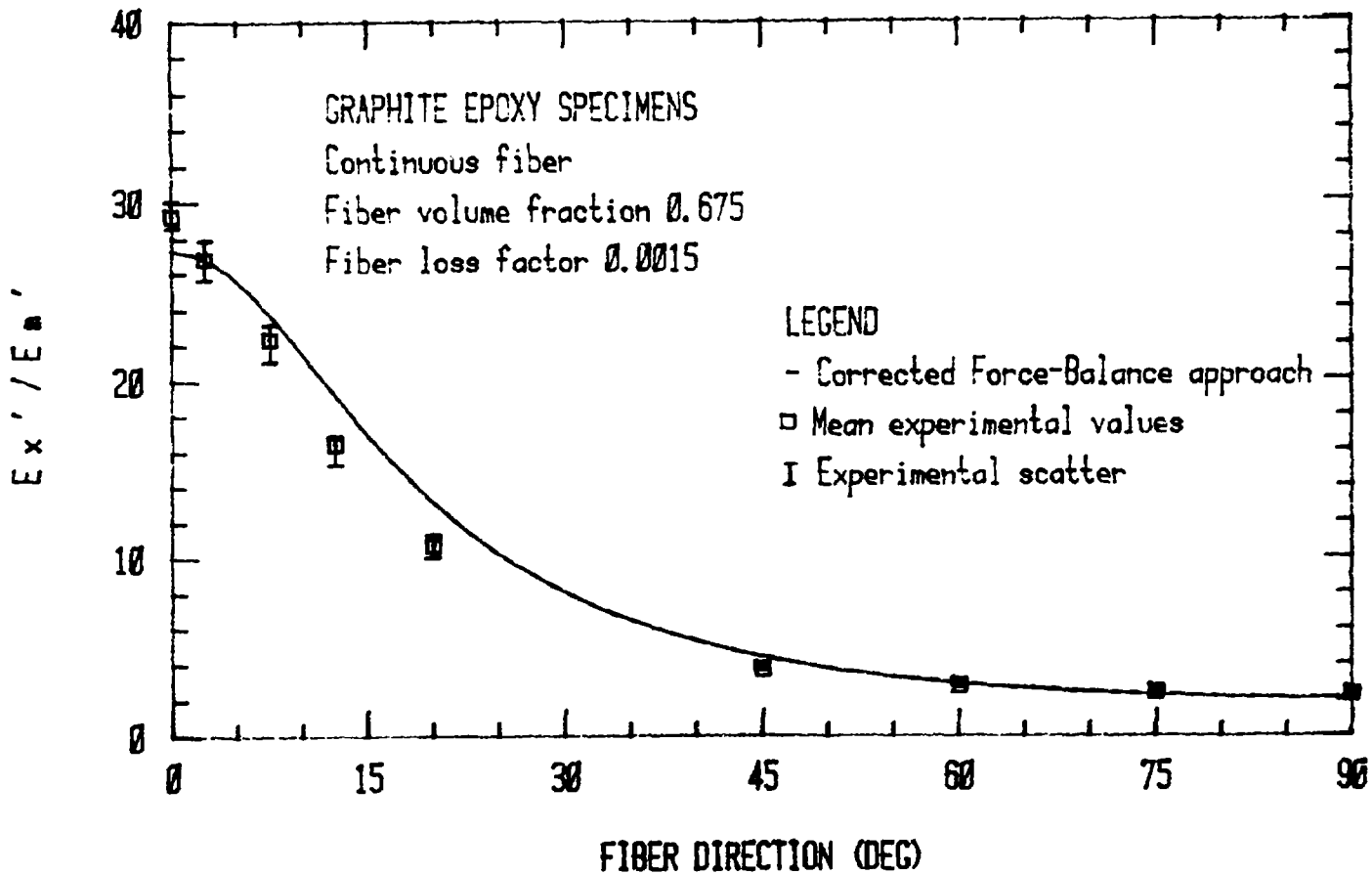

Figure 6.10. E_x'/E_m' vs. fiber direction for continuous graphite/epoxy, with curve fitting [$E_{fL}' = 25.51 \times 10^6$ psi (175.76 GPa), $E_{fT}' = 2 \times 10^6$ psi (13.78 GPa), $G_{fLT}' = 4 \times 10^6$ psi (27.56 GPa), ζ_1=2, ζ_2=4, Z=0.03, f=1152.5 Hz].

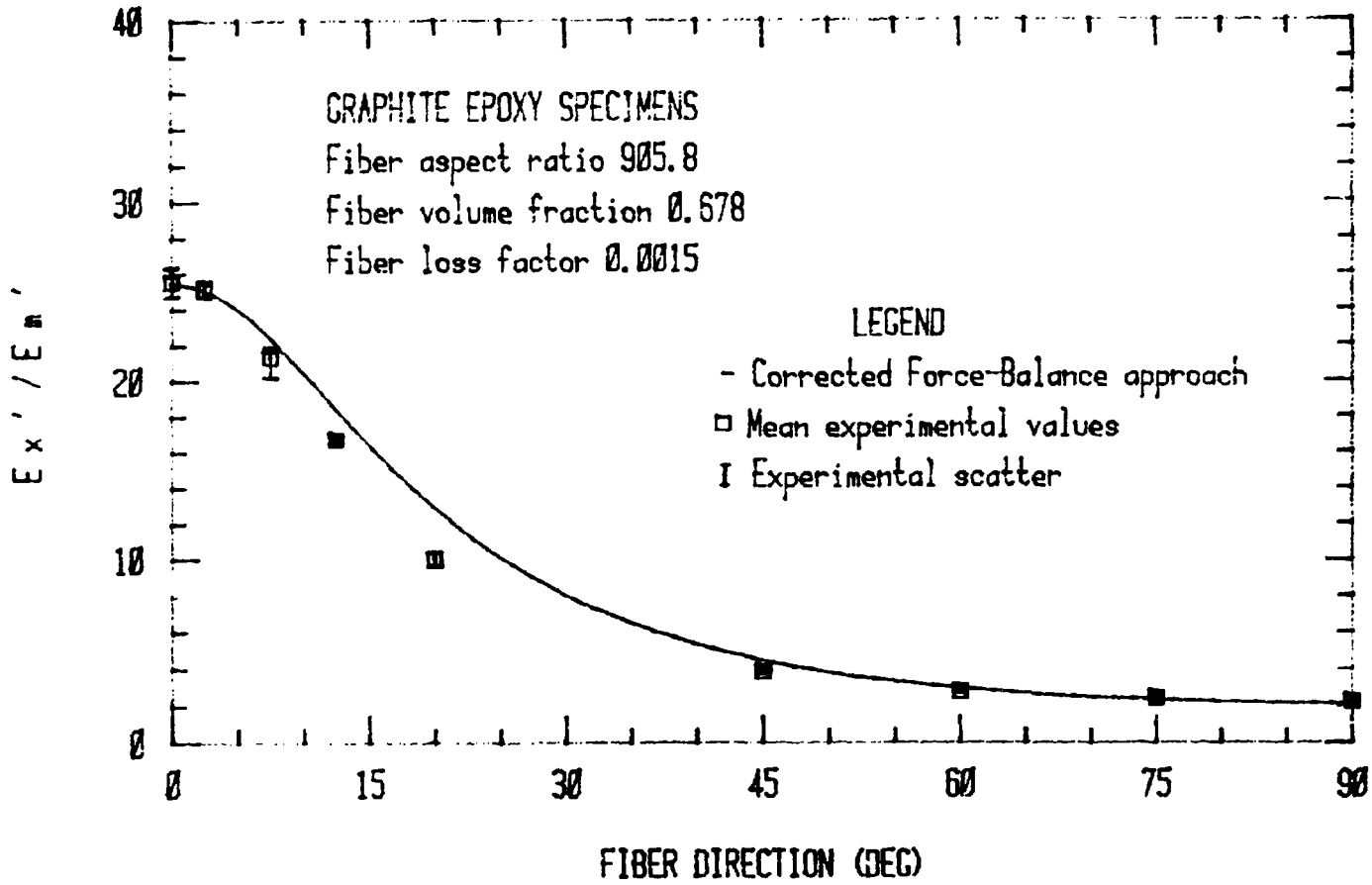

Figure 6.11. E'_x/E'_m vs. fiber direction for discontinuous graphite/epoxy with curve fitting [E'_{fL} = 25.51 x 10^6 psi (175.76 GPa), E'_{fT} = 2 x 10^6 psi (13.78 GPa), G'_{fLT} 4 x 10^6 psi (27.56 GPa), ζ_1=2, ζ_2=4, Z=0.03, f=1206.15 Hz].

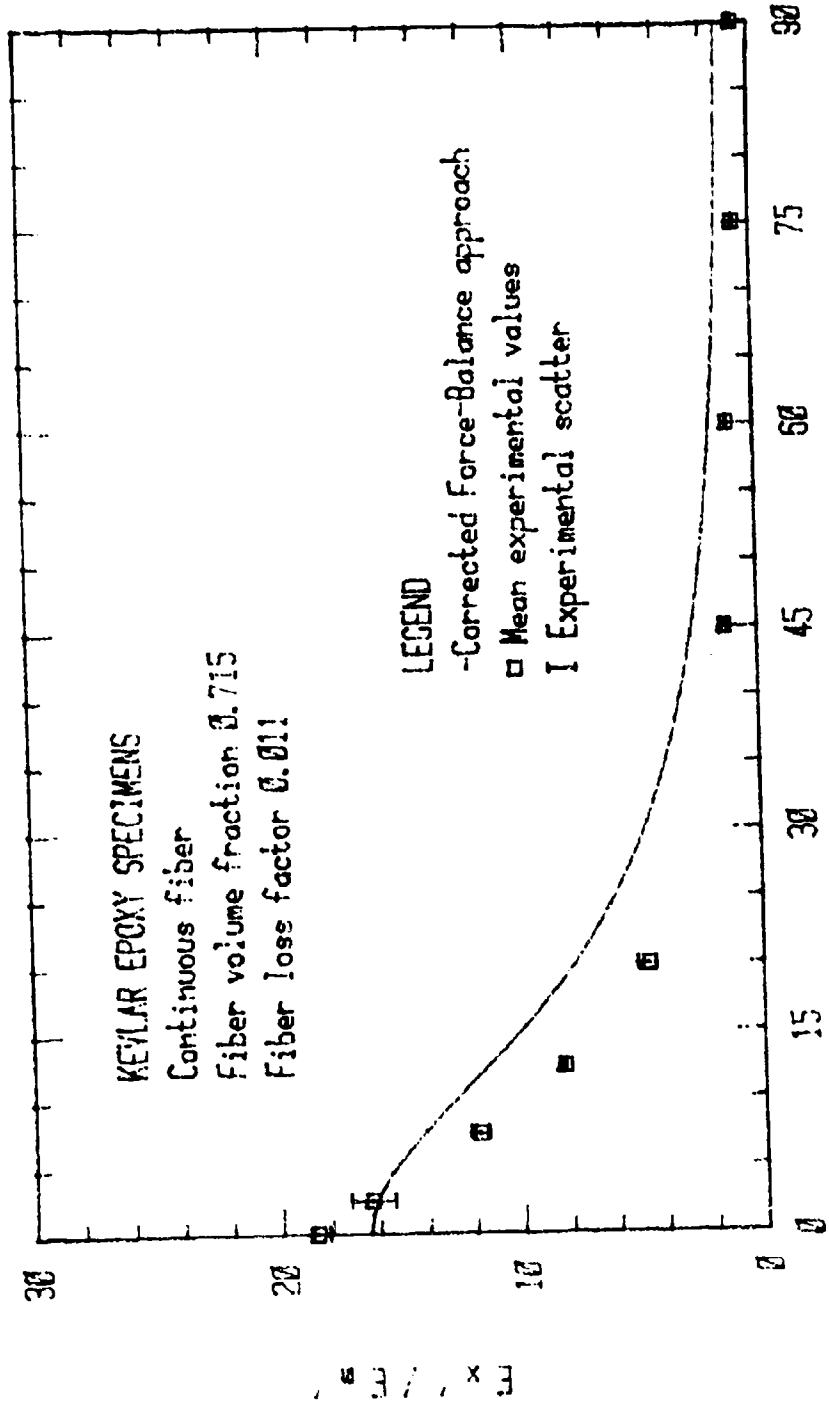

Figure 6.12. E'_x/E'_m vs. fiber direction for continuous Kevlar/epoxy, with curve fitting [E'_{fL} = 14.48 x 10^6 psi (99.767 GPa), E'_{fT} = 1 x 10^6 psi (6.89 GPa), G'_{fLT} = 2 x 10^6 psi (13.78 GPa), ξ_1=2, ξ_2=1, Z=0.03, f=895.1 Hz].

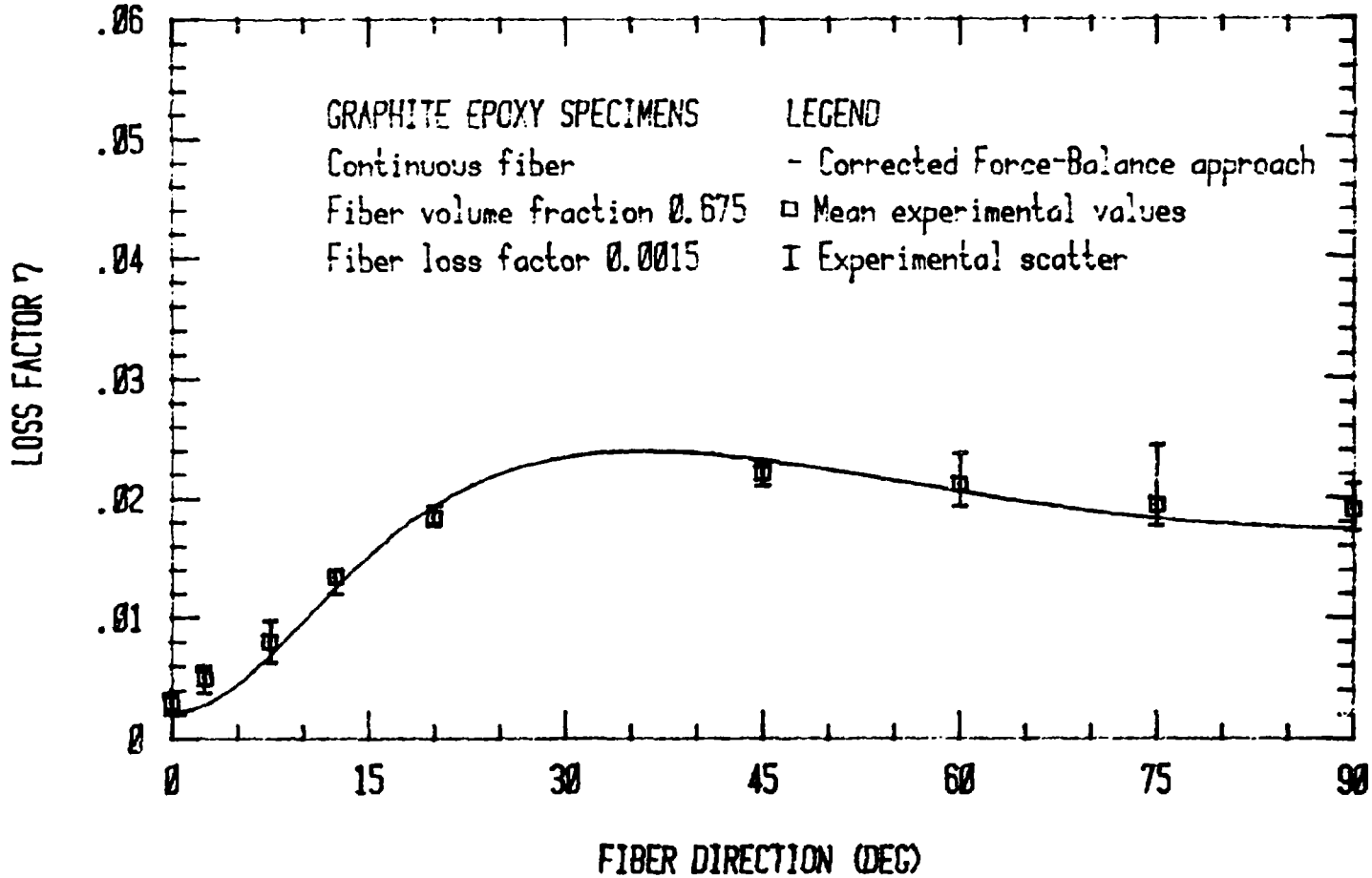

Figure 6.13. Loss factor vs. fiber direction for continuous graphite/epoxy, with curve fitting [E'_{fL} = 25.51 x 10^6 psi (175.76 GPa), E'_{fT} = 2 x 10^6 psi (13.78 GPa), G'_{fLT} = 4 x 10^6 psi (27.56 GPa), ε_1=2, ε_2=4, Z=0.03, f=1152.5 Hz].

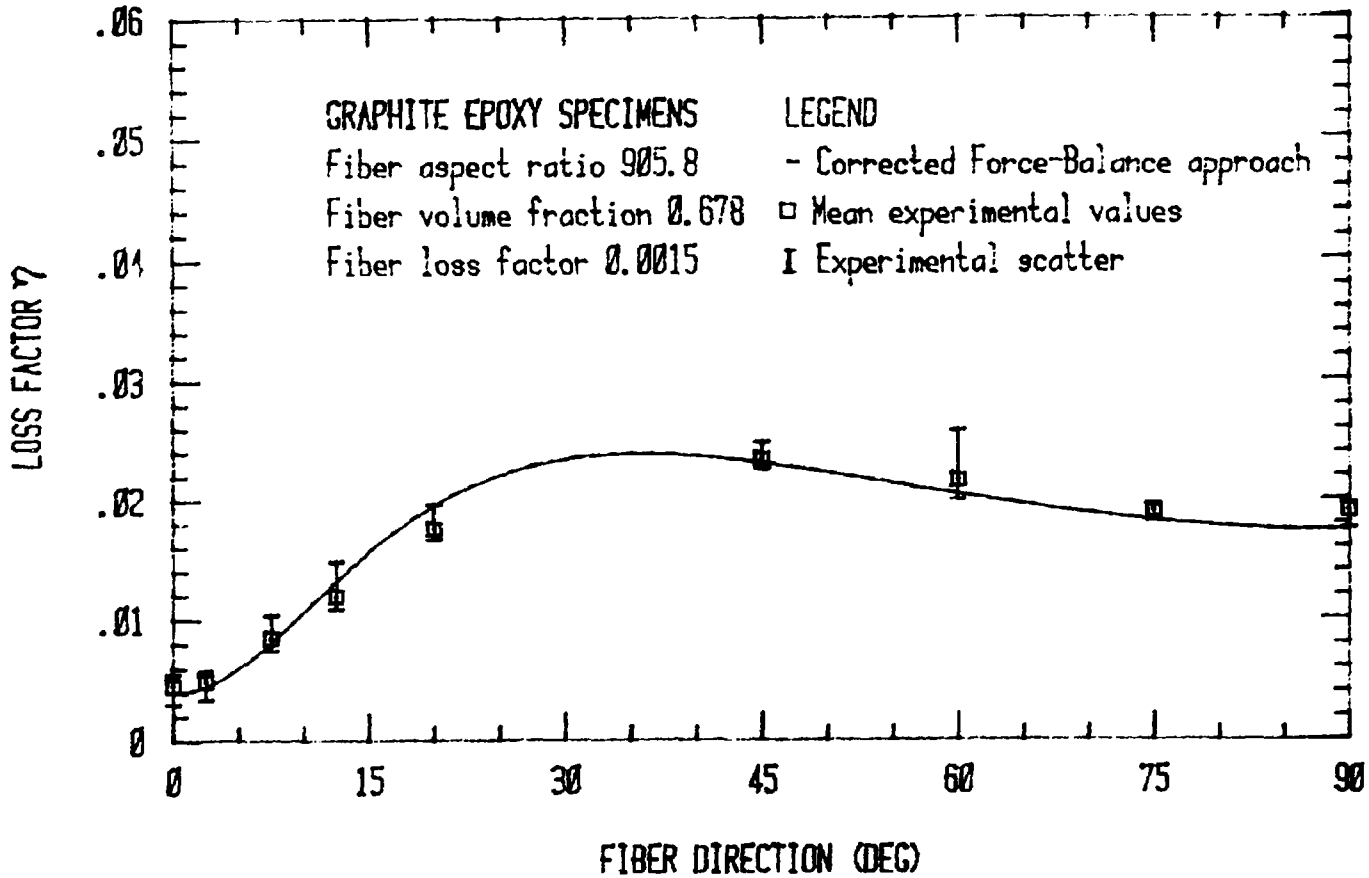

Figure 6.14. Loss factor vs. fiber direction for discontinuous graphite/epoxy, with curve fitting [E'_{fL} = 25.51 x 10^6 psi (175.76 GPa), E'_{fT} = 2 x 10^6 psi (13.78 GPa), G'_{fLT} = 4 x 10^6 psi (27.56 GPa), ϵ_1=2, ϵ_2=4, Z=0.03, f=1206.15 Hz].

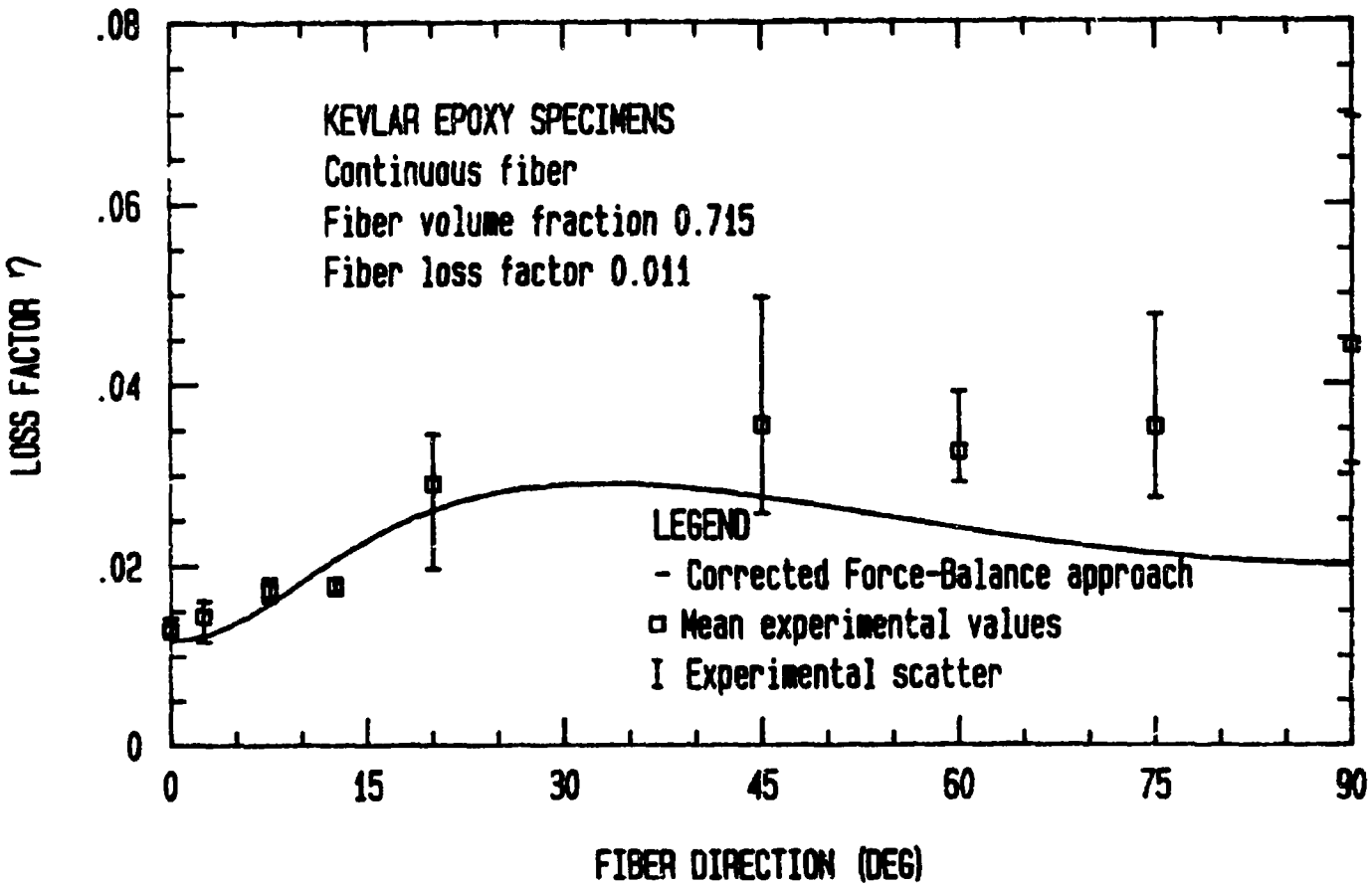

Figure 6.15. Loss factor vs. fiber direction for continuous Kevlar/epoxy, with curve fitting [E'_{fL} = 14.48 x 10^6 psi (99.767 GPa), E'_{fT} = 1 x 10^6 psi (6.89 GPa), G'_{fLT} = 2 x 10^6 psi (13.78 GPa), ε_1=2, ε_2=1, Z=0.03, f=895.1 Hz].

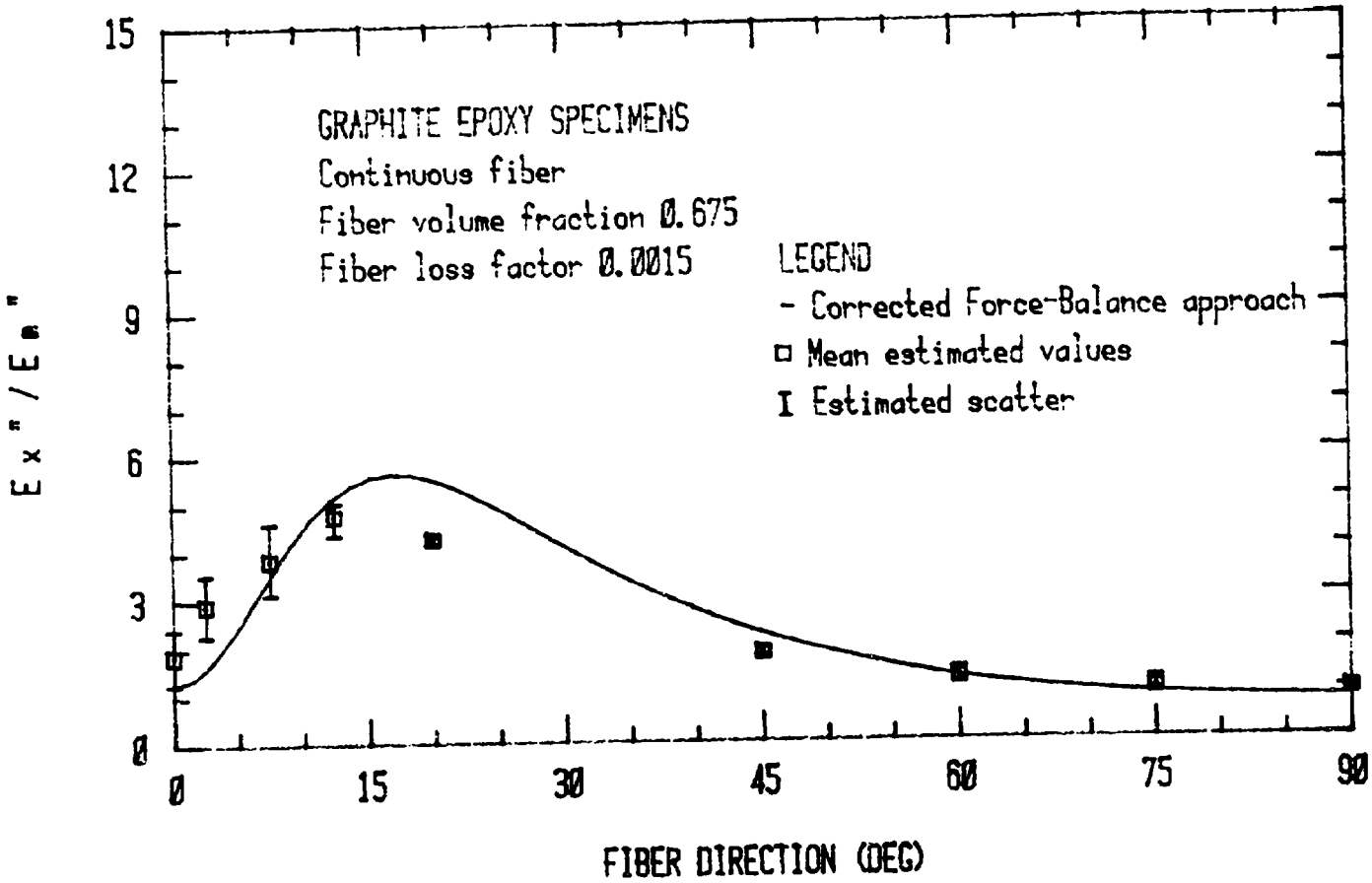

Figure 6.16. E_x''/E_m'' vs. fiber direction for continuous graphite/epoxy, with curve fitting [illegible] E'_{fL} = 25.51 x 10^6 psi (99.767 GPa), E'_{fT} = 1 x 10^6 psi (6.89 GPa), G'_{fLT} = 2 x 10^6 psi (13.78 GPa), ξ_1=2, ξ_2=1, Z=0.03, f=895.1 Hz].

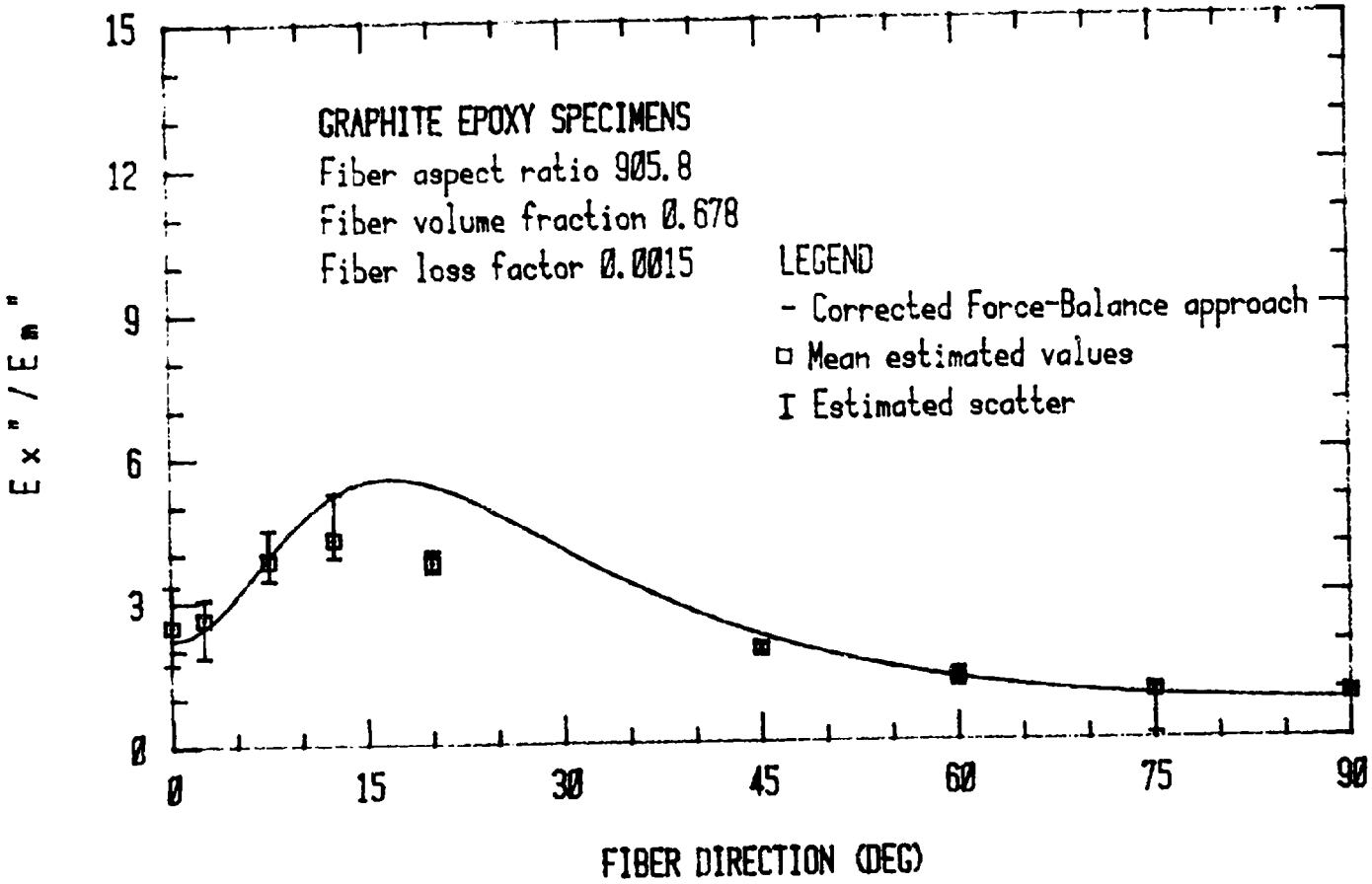

Figure 6.17. E_x''/E_m'' vs. fiber direction for discontinuous graphite/epoxy with curve fitting [E'_{fL} = 25.51 x 10^6 psi (175.76 GPa), E'_{fT} = 2 x 10^6 psi (13.78 GPa), G'_{fLT} = 4 x 10^6 psi (27.56 GPa), ϵ_1=2, ϵ_2=4, Z=0.03, f=1206.15 Hz].

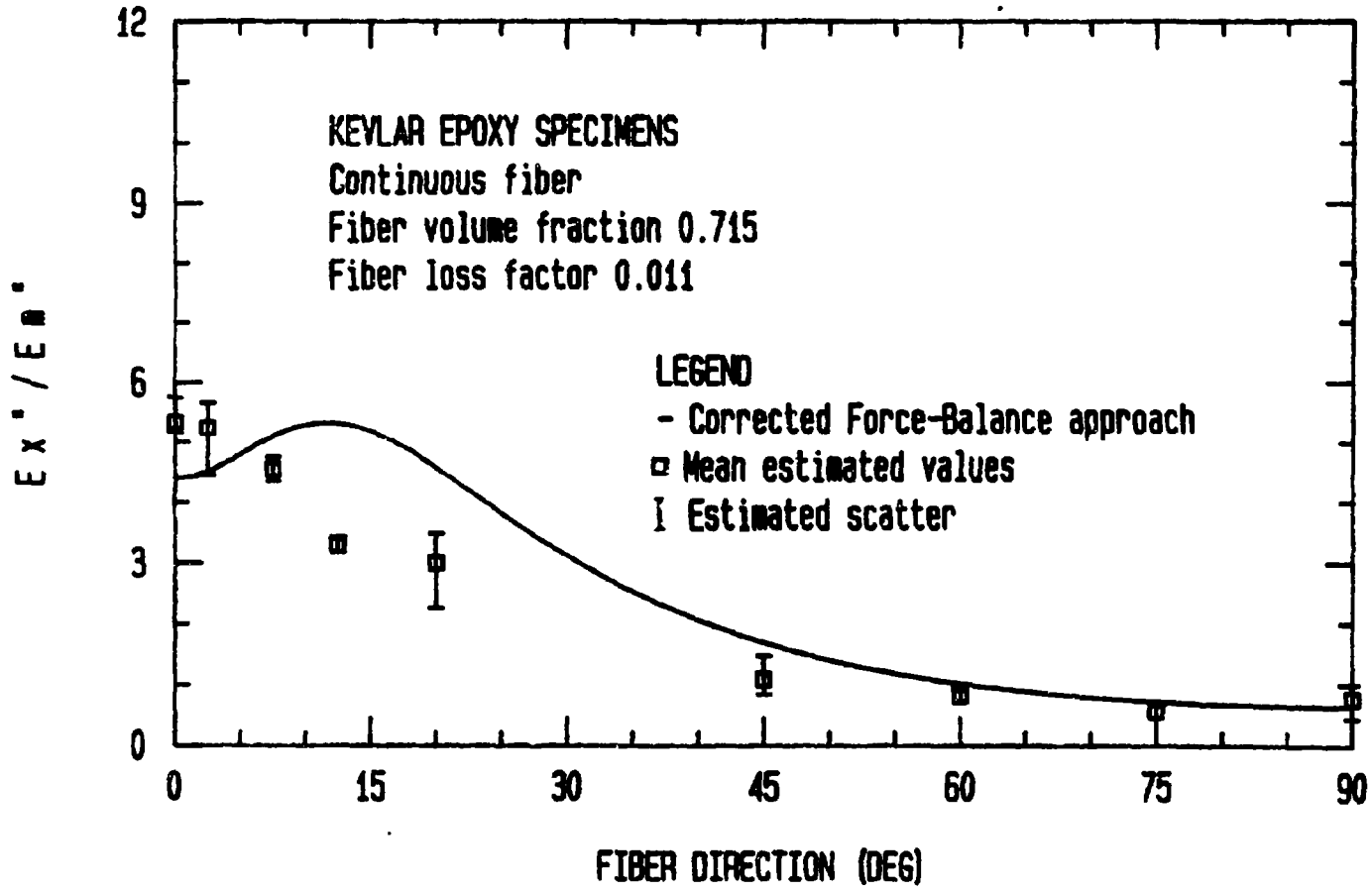

Figure 6.18. E_x''/E_m'' vs. fiber direction for continuous Kevlar/epoxy, with curve fitting [E_1' = 14.48 x 10^6 psi (99.767 GPa), E_{fT}' = 1 x 10^6 psi (6.89 GPa), G_{flT}' = 2 x 10^6, ξ_1=2, ξ_2=1, ν=0.03, f=895.1 Hz].

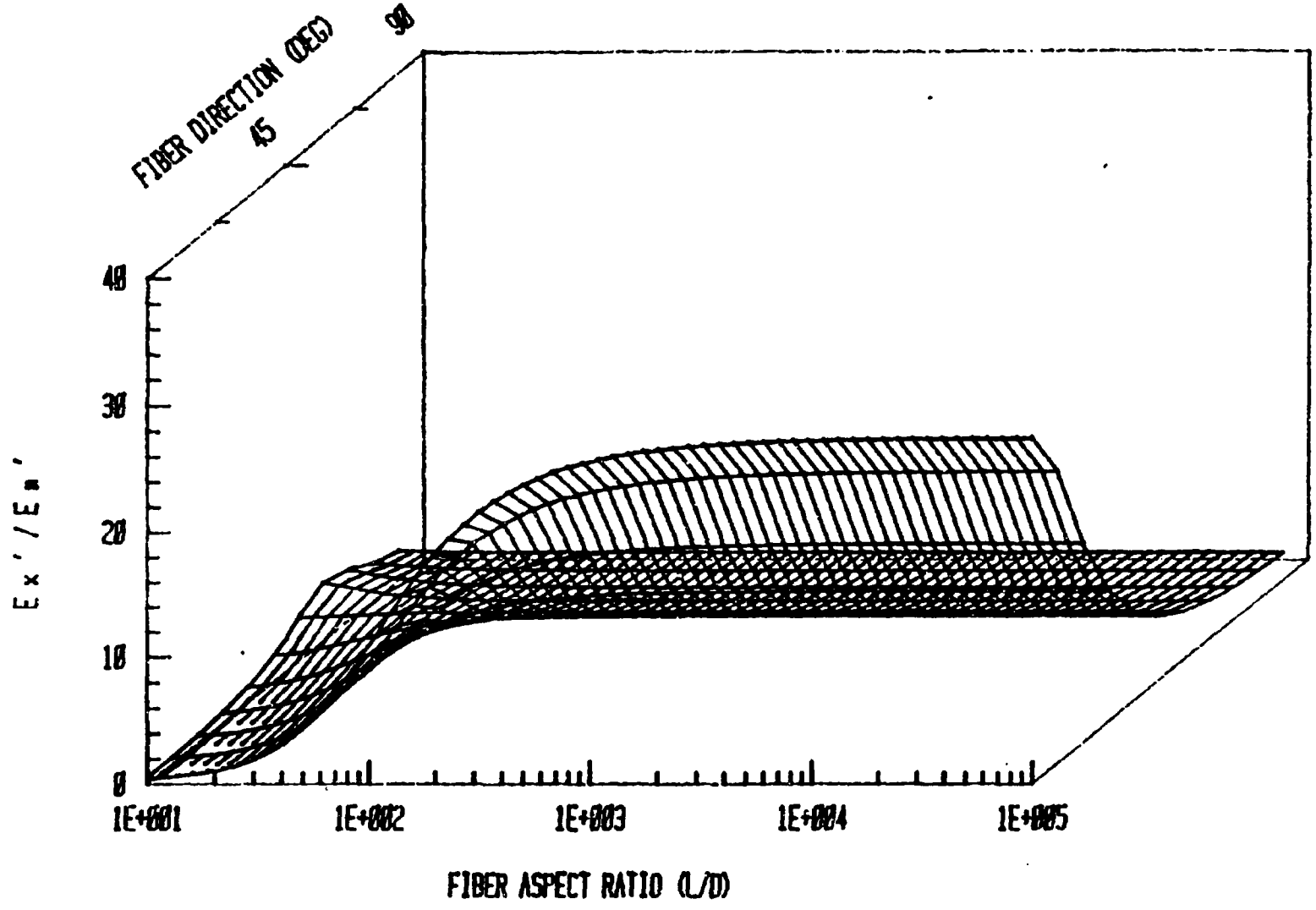

Figure 6.19. Tridimensional plot of E'_x/E'_m vs. fiber aspect ratio and fiber direction, for graphite/epoxy composite.

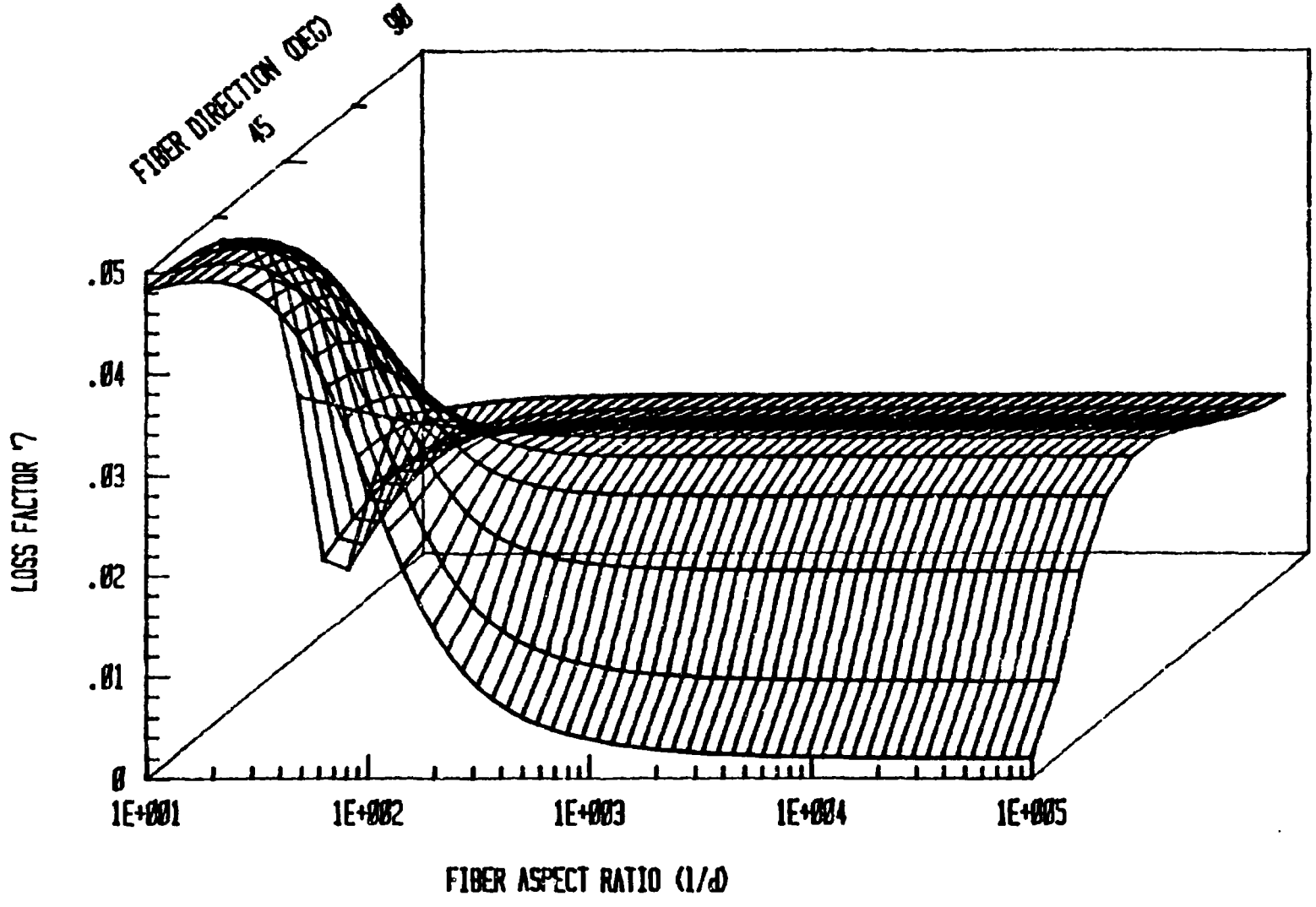

Figure 6.20. Tridimensional plot of loss factor vs. fiber aspect ratio and fiber direction, for graphite/epoxy composite.

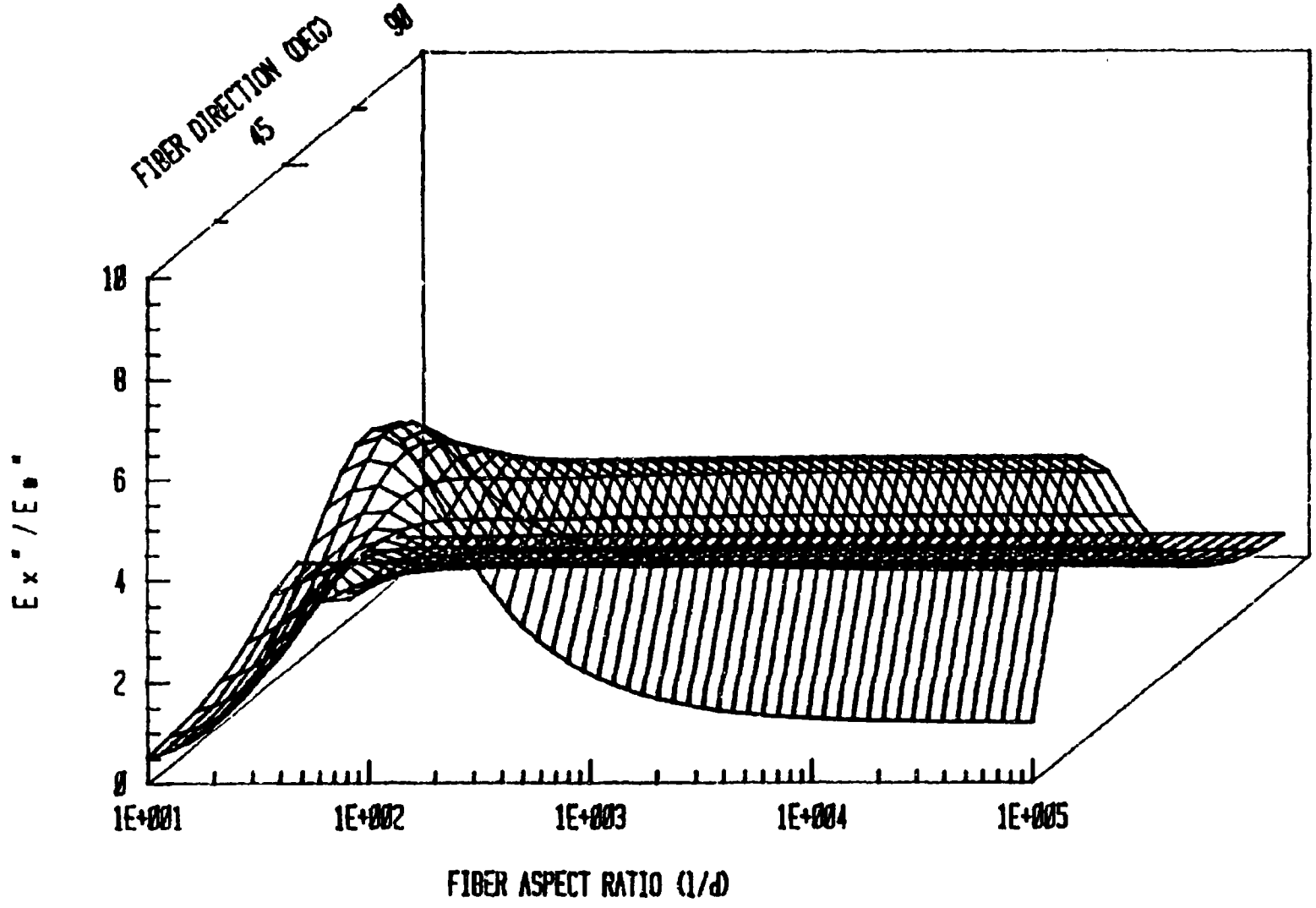

Figure 6.21. Tridimensional plot of E''_x/E''_m vs. fiber aspect ratio and fiber direction, for graphite/epoxy composite.